De Montfort University

Department of Health and Life Sciences

Synthesis, characterisation and biological activity of FITC-insulin for the development of an artificial pancreas.

Vu Ngoc Minh Tam

January 2021

First Supervisor: Dr Tarsem Sahota

Second Supervisor: Professor Joan Taylor and Dr Harprit Singh

Submitted by Vu Ngoc Minh Tam, to De Montfort University as a thesis for the degree of Doctor of Philosophy in specialised drug delivery.

Author’s declaration

To the best of my knowledge I confirm that the work in this thesis is my original work undertaken for the degree of Doctor of Philosophy in specialised drug delivery in the Faculty of Health and Life sciences, De Montfort University. I confirm that no material of this thesis has been submitted for any other degree or qualification at any other university except where due reference has been made clearly in the text.

Acknowledgements

Firstly, I would like to express my sincere gratitude to my greatest mentor, Dr Tarsem Sahota for his continuous support during my study. His guidance and motivation have always led me to the right path throughout my research journey and enabled me to achieve many great things. Also, I would like to thank Prof. M Joan Taylor for her valuable suggestions and immense knowledge to help me in all the time of need during my research and writing of this thesis. My sincere thank also goes to Dr Harprit Singh for his helpful insights and expert guidance in the biological activity study.

I would like to thank my research team, Dr Krishan Chauhan for his motivating discussions and constant supports with all the technical issues I have encountered, and Jay Bilimoria who have provided training and supports with the cell culture techniques that are fundamental to conduct part of my *in-vitro* study. Also, I thank my friend, Dr Chi Tran from Queen Mary University for her assistance in using Excel.

I would like to take this opportunity to acknowledge and thank Dr Mark Wyatt from Swansea University (EPSRC UK National Mass Spectrometry Facility), Dr Andrew Bottrill and Dr Cleidi Zampronio from Warwick University (Proteomics Research Technology Platform) for their analytical support in performing Mass Spectrometry analysis.

Finally, I would like to thank my extended family in Vietnam and the UK who have always remembered me in their prayers. Without their encouragements and support, the fulfilment of this thesis would have been more challenging and incomplete.

Posters and publications

“Fluorescently labelled insulin for specialised drug delivery “poster at the Royal Society of Biology Postgraduate Poster Symposium 2019.

Synthesis and identification of mono-labelled FITC-insulin conjugate (Tam Vu et al., 2021) *submitted for peer review.*

Abstract

In advanced drug development and delivery, fluorescence studies have clarified and improved aspects such as biodistribution, stability and metabolism with respect to the complexities imposed by the biological systems. The ultimate aim of this study was to assess the delivery kinetics of a synthesised fluorescently labelled insulin in an implantable artificial pancreas (INsmart device) developed by Taylor et al, 2016, which is currently being tested *in-vivo.*

The first objective of this thesis was to produce a fluorescein isothiocyanate (FITC)-insulin conjugate which shows equivalent biological activity to native insulin under novel reaction conditions without the need for using protecting groups and multi-step synthetic conditions. Secondly, the stability and solubility profiles of the synthesised FITC-insulin conjugate in solution will be investigated for long-term storage and future applications. Thirdly, physiologically relevant glucose concentrations will be used to assess the performance of FITC-insulin delivery from an INsmart device. Lastly, other dyes such as eosin isothiocyanate (EITC) and rhodamine B isothiocyanate (RBITC) will be assessed as labelling candidates to produce other derivatised insulin conjugates.

Mono-labelled FITC-insulin conjugate was successfully synthesised using a molar ratio of 2:1 (FITC: insulin) with short reaction times (up to 18h) at pH7 after studies were conducted to examine the effects of reaction time, molar ratio and pH. The labelling position of this mono-labelled species was identified by MS-Orbitrap Fusion at the B1 residue (MonoB1). However, during synthesis, MonoB1conjugate always contains some trace amounts of unlabelled insulin that required further purification by RP-HPLC using a gradient method. This HPLC method could identify four FITC-insulin conjugates including two mono-labelled species (labelled at the A1 or B1 position), di-labelled species (labelled at the A1 and B1) and tri-labelled species (labelled at the A1, B1 and B29). Further analysis was performed using MALDI-MS to confirm the molecular weight of each conjugate produced.

The biological activity of four FITC-insulin conjugates was assessed in human umbilical vein endothelial cells (HUVEC) and skeletal muscle cells (C2C12) via the insulin signalling pathway by examining the levels of AKT phosphorylation (pAKT) and cell surface GLUT4. There was no significant difference in pAKT and the GLUT4 cell surface levels observed for synthesised MonoB1 compared to native insulin, highlighting that this conjugate was as biologically active as native insulin.

The enhanced stability and solubility of FITC-insulin conjugate using diluting fluid containing m-cresol, glycerol and zinc oxide, which is typically contained in most commercial insulin formulations are beneficial for setting up the *in-vitro* delivery study of the INsmart device. Because it allows a concentrated depot of FITC-insulin in the device for release over an extended time. Improvement in the smart gel formulation with diluting fluid and the use of correct membrane pore size showed promising and reproducible results in the extended experiments where the INsmart device has been set up and triggered multiple times with glucose and other dietary saccharides which act as controls to show the specificity of the gel to glucose challenges. The results indicated that the device is capable of delivering basal insulin dose which can be boosted in response to multiple (11x) mealtime glucose surges over a 5-day period.

EITC and RBITC were used as fluorescent candidates to assess whether the same synthetic methodology of fluorescently labelled insulin was applicable to different dye sizes. Mono-labelled insulin conjugate with EITC was achieved using the same reaction conditions as in FITC-insulin synthesis. Further development is still needed to remove unreacted RBITC during the synthesis of RBITC-insulin conjugate.

Contents

Lists of figures

Lists of Tables

Abbreviations and Nomenclature

%RSD	percentage relative standard deviation
~	approximately
ACN	acetonitrile
Acry/Bis	Acrylamide/Bis-acrylamide
ADA	American Diabetes Association
Alex647-HI	Alexa Fluor 647 labelled human insulin conjugate
Alex680	Alexa Fluor 680
AMPK	5’-AMP-activated protein kinase
ATP	adenosine triphosphate
AS160	AKT substrate of 160kDa
BBB	blood-brain barrier
BG	blood glucose
BINP	bio-mineralised insulin nanoparticle
BSA	bovine serum albumin
Ca2+	Calcium ion
cAMP	cyclic adenosine Monophosphate
CASFISH	Cas9-mediated FISH
CGM	continuous glucose monitor
CHO	carbohydrates
CID	covalent insulin dimers
CIO	covalent insulin oligomers
con A	Concanavalin A

con A-MA	methacrylated concanavalin A (concanavalin A methacrylamide)
CPE	carboxypeptidase E
CR	cysteine-rich region
CVD	cardiovascular diseases
dexMA	methacrylated dextran (dextran methacrylamide)
Di	Di-labelled FITC-Insulin analogues/ Actrapid® conjugate
DKA	diabetic ketoacidosis
DMSO	anhydrous dimethyl sulfoxide
DTT	dithiothreitol
EC	extinction coefficient
EDTA	ethylenediaminetetraacetic acid disodium salt
EITC	eosin isothiocyanate
EqC	Equilibrium Concentration
eNOS	endothelial nitric oxide synthase
FA	fatty acids
FBS	fetal bovine serum
FITC	fluorescein isothiocyanate
FITC-HI	fluorescein isothiocyanate -labelled human insulin
FISH	fluorescence in situ hybridisation
Fn-1	fibronectin type III domains-1
Fn-2	fibronectin type III domains-2
Fn-3	fibronectin type III domains-3
FRP	Fluorescent Reporter Proteins

FSC	fluorescein
GAPs	GTPase-accelerating proteins
GDM	Gestational Diabetes Mellitus
GEFs	guanine nucleotide exchange factors
GFP	Green fluorescence protein
GLUT4	insulin-dependent glucose transporter 4
GLUTs	facilitated diffusion glucose transporters
GVS	glucose transporter 4 storage vesicles
HbA1c	glycated haemoglobin (HbA1c
HCl	hydrochloric acid
HI	human insulin
HMWT	higher molecular weight transformation
HNF-1 α	hepatocyte nuclear factor-1 alpha
HPLC	High-Performance Liquid Chromatography
HUVEC	Human Umbilical Vein Endothelial Cells
IAA	autoantibodies to insulin
ICG	Indocyanine Green
ID	insert domain
i.e.	that is
IP	intraperitoneal
INS-647	human insulin labelled with AlexaFluor 647
IR	insulin receptor
IRS	Insulin receptor substrate

ICT	Isothiocyanate
IV	Intravenous
JM	juxtamembrane
K_{ATP}-channels	ATP-sensitive K^+-channels
KBs	ketone bodies
L1	leucine-rich repeat domain 1
L2	leucine-rich repeat domain 2
LADA	Latent Autoimmune Diabetes in Adults
LCT	long-chain triglyceride
LSGS	Low Serum Growth Supplement
LOD	Limit of detection
LOQ	Limit of quantitation
MAPK	mitogen-activated protein kinases
MCA	7-methoxycoumarin-4-acetic acid
m-cresol	meta cresol
MCT	medium-chain triglyceride
MDI	multiple-dose injection
MI	myocardial infarction
min	minutes
mL	millilitre
MODY	Maturity-Onset Diabetes of the Young
Mono	singly labelled FITC-insulin conjugate
MonoA1	singly labelled FITC-insulin or Actrapid® conjugate at the A1 position

MonoB1	singly labelled FITC-insulin or Actrapid® conjugate at the B1 position
MS	mass spectrometry
Na_2HPO_4	disodium hydrogen phosphate
NaCl	sodium chloride
NDM	Neonatal Diabetes Mellitus
NaH_2PO_4	sodium dihydrogen phosphate
NaOH	sodium hydroxide
NBD	4-chloro-7-nitrobenz-2-oxa-1,3-diazole
NCVIN	National Cardiovascular Intelligence Network
NICE	National Institute for Health and Care Excellence
NO	nitric oxide
pAKT	Phosphorylated AKT
PBS	Sterilised phosphate buffer
PD	pharmacodynamic
PDA	Photo Diode Array detector
PDE5	Phosphodiesterase 5
PDK1	3-phosphoinositide-dependent protein kinase 1
PI3K	phosphatidylinositol 3 kinase
PIP2	phosphatidylinositol 4,5- diphosphate
PIP3	phosphatidylinositol 3, 4, 5 triphosphates
PK	pharmacokinetic
QY	quantum yield (QY)
RBCs	red blood cells

RBITC	rhodamine B isothiocyanate
rDNA	recombinant-DNA
rpm	rotation per minute
PR-HPLC	Reverse Phase High-Performance Liquid Chromatography
RT	retention time
RTKs	receptor- tyrosine kinases
SA	Solvent Addition
SC	subcutaneous
SDS	Sodium Dodecyl Sulphate
SGLTs	Sodium-glucose linked transporters
smRNA-FISH	Single-molecule RNA FISH
SNEDDSs	self-(nano)-emulsifying drug delivery systems
SPC	soybean phospholipid
T1DM	Type 1 diabetes mellitus
T2DM	type 2 diabetes mellitus
t-boc	tert-butyloxycarbonyl
TBS	Tris buffered saline
TBST	Tris buffered saline containing Triton-X
TEMED	N, N, N′, N′-Tetramethyl ethylenediamine
TFA	trifluoroacetic acid
TM	transmembrane
Tri	Tri-labelled FITC-insulin or Actrapid® conjugate
TRITC	tetramethylrhodamine isothiocyanate

TV	Temperature Variation
VDCCs	voltage dependent $Ca2^{+}$ channels
WFI	Water for injection
WHO	World Health Organisation

Chapter 1. Introduction

The main objectives of the thesis were to:

- produce a biologically active fluorescein isothiocyanate (FITC)-insulin conjugate by modifying certain reaction conditions such as molar ratio, reaction time and pH.
- confirm FITC labelling position on the insulin molecule by fragmentations of the modified insulin for mass spectrometry (MS) analysis.
- examine the biological activity of FITC-insulin candidates by investigating their stimulation effect in HUVEC and skeletal muscle cells via the insulin signaling pathways.
- investigate the stability and solubility profiles of FITC-insulin conjugate in solution for long-term storage and future application in both *in-vitro* and *in-vivo* testing as well as optimising mast production.
- assess other dyes such as eosin isothiocyanate (EITC) and rhodamine B isothiocyanate (RBITC) as labelling candidates to produce further coloured insulin conjugates.
- investigate the performance and kinetics of insulin delivery from an implantable closed-looped insulin delivery device (INsmart) using FITC-insulin conjugate.

The thesis begins with a general introduction chapter about diabetes mellitus and the development of a closed-loop insulin delivery system. Chapter 2 presents the synthesis and identification of FITC-insulin conjugates from commercially available insulin preparations, followed by chapter 3 which studies the biological activity of FITC-insulin species synthesised inhouse. Chapter 4 investigates the stability and solubility profiles of FITC-insulin while chapter 5 examines the drug delivery mechanism of FITC-insulin from the INsmart device. Chapter 6 looks at the synthesis and identification of EITC-insulin and RBITC-insulin conjugates. Lastly, there will be a summary chapter including suggestions for future work.

This introductory chapter provides a basic understanding of diabetes mellitus, its current management guidelines and the disease-associated complications. An insight into insulin structure, the evolution of clinically used insulin pharmaceutical preparations and routes of insulin delivery will also be discussed. The main focus is to understand the insulin structure and the properties behind it to be fully engaged in its labelling process. The development of an artificial pancreas as a possible treatment option for insulin users will also be summarised with details about the *in-vivo* study for the performance of an implantable INsmart device developed by Taylor et al., 2016. Lastly, fluorescent labelling technique and its applications will be discussed, highlighting the use of fluorescently labelled insulin in biochemical research and drug delivery.

1.1 Diabetes mellitus

1.1.1 Overview of glucose homoeostasis

Generally, all living organisms require energy which comes from different sources such as sunlight, food, drinks, or supplements to maintain life (growing and reproducing). For instance, carbohydrates (CHO) nutrition like glucose is the most fundamental source of energy for survival in mammalian cells. At the cellular level, glucose is rapidly metabolised to produce a high energy end product known as ATP (adenosine triphosphate). In the body, glucose is continuously used as the primary energy source to carry out daily activities, including movements, balancing, thinking and even sleeping. Glucose homeostasis can be defined as a process of maintaining intercellular glucose concentrations at a steady-state level within a living cell, organism and to a larger scale, the human body. Cellular processes of glucose uptake during CHO ingestion, peripheral glucose consumption and hepatic glucose production are tightly regulated by specific hormones, namely insulin and glucagon released from the pancreatic cells to maintain glucose homeostasis. (O'Brien et al., 2020; Dunn and Grider, 2020; Aronoff et al., 2004). While glucagon is responsible for increasing blood glucose (BG) level, insulin reduces it (Error! Reference source n ot found.). Therefore, their antagonistic effects help maintain BG level within an acceptable range of 4.0 to 5.9 mM pre-prandial (before meal) and under 7.8 mM at least 90 minutes (min) postprandial (after meal) (National Institute for Health and Care Excellence (NICE),2016).

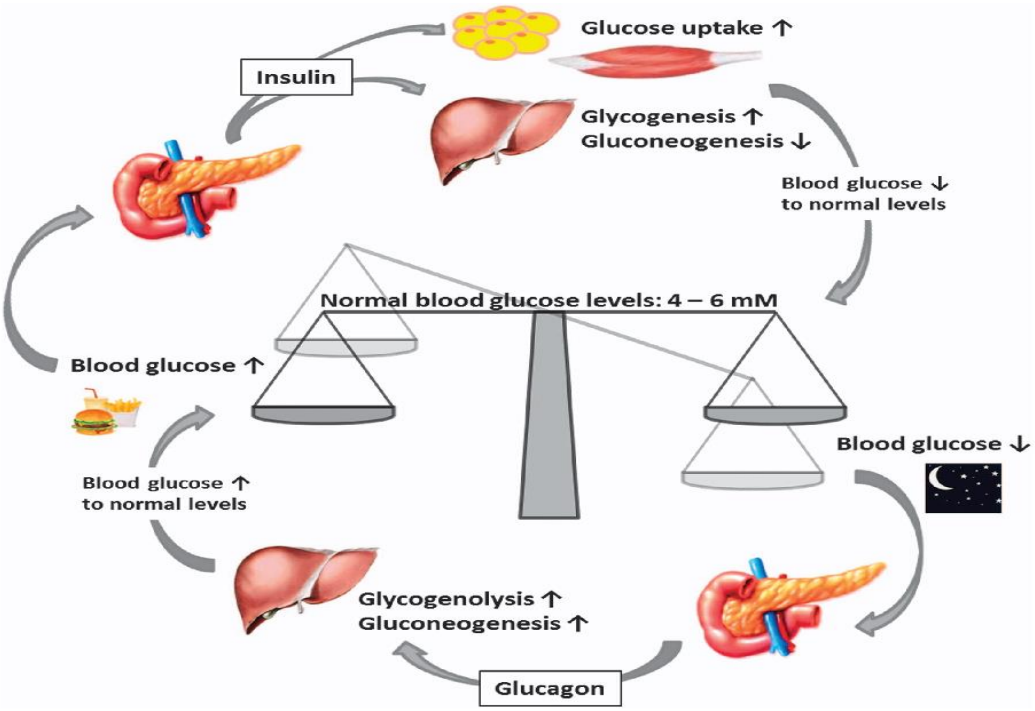

Figure 1-1: The maintenance of glucose homeostasis. (Taken from Röder et al. 2014)

Hypoglycaemia can result in seizures, unconsciousness and even death, whereas long-lasting hyperglycaemia eventually can lead to blindness, cardiovascular disease (CVD), renal failure, and neuropathy. Glucose homeostasis is crucial for both healthy individuals and people with diabetes to maintain long-term health. In addition to the tightly regulation of insulin and glucagon hormones, glucose homeostasis is also maintained by the body performance of various contribution factors. These include the rate of dietary CHO consumption and intestinal absorption, the rate of glucose utilisation by peripheral tissues as well as rate of glucose elimination or release by the liver and the rate of glucose reabsorption by the kidney (Röder et al., 2016a; Szablewski, 2011). These cellular activities in glucose homeostasis are defined into five phases namely phase I (Well-fed state), II (Glycogenolysis), III (Glucogenesis), IV (Glucose, Ketone bodies oxidation) and V (Fatty acid, Ketone bodies oxidation) as summarised in **Table 1-1.**

Table 1-1: Phases of glucose homeostasis (Information is summarised mainly from the original work of George F Cahill, 1959)

	Phase I	Phase II	Phase III	Phase IV	Phase V
Stimuli	Food intake	when dietary glucose supply is exhausted (During early fasting)	When glycogen stores in the liver are exhausted (<20h)	Several days of fasting	Prolonged fasting/ starvation
Source of blood glucose	Dietary CHO	Glycogen (75%) Hepatic gluconeogenesis	Hepatic gluconeogenesis Glycogen	Hepatic and renal gluconeogenesis	Hepatic and renal gluconeogenesis
Cellular activities	The liver removes ~70% glucose load after a CHO meal. Glucose absorbed from the gut is supplied to all cells, signalling insulin released from pancreatic β-cells. Some glucose is converted to glycogen for storage in the liver (glycogenesis) - Excess glucose is converted to fatty acids (FA) and triglycerides in the liver in response to insulin secretion. Gluconeogenesis is inhibited	Hypoglycaemia signals glucagon released from pancreatic α-cells. Hepatic glycogenolysis (break down of glycogen into glucose) and gluconeogenesis (synthesis of glucose from non-carbohydrate sources) maintain the blood glucose level	Hepatic gluconeogenesis from lactate, pyruvate, glycerol and alanine maintains blood glucose level The glucose-alanine cycle becomes activated.	Gluconeogenesis starts to decrease. The peripheral cells switch to using alternative fuels. FA oxidation increases ketone bodies (KBs) accumulation. Glycerol and amino acids released form adipose and muscle tissues respectively are used for glucose production. KBs enter the brain and muscle for energy production. The brain uses both glucose and KBs for energy.	Less dependence on gluconeogenesis. Energy production for all body tissues usage mainly from FA and KBs oxidation. High levels of KBs and glucose inhibit proteolysis in the muscle (conservation of muscle) When all FA and KBs are used up, the body uses muscle protein (alanine and glutamine) to maintain blood glucose level (the last stage)
Tissues using glucose	All	All (Utilisation rate is slower in hepatic, muscle and adipose tissue)	All (Utilisation rate is slower in hepatic, muscle and adipose tissue)	Brain, red blood cells (RBCs), Renal medulla and small amount used by muscles cells	Brain at a slower rate, RBCs and Renal medulla
Major fuel of the brain	Glucose	Glucose	Glucose	Glucose KBs	KBs Glucose

In healthy individuals, there is a constant release of insulin from the pancreatic β-cells to maintain glucose homeostasis during the basal state of fasting and 3-5h after a meal when food absorption has ceased, this endogenous level of insulin is referred to as basal insulin (Home, 2015; Navale and Paranjape, 2016). Physiologically, an increase or decrease in the level of insulin release would match higher or lower BG concentrations. For instance, the insulin secretory response at 10 mmol/L glucose is reported to be twice as high the response at 5 mmol/L glucose (Rorsman and Ashcroft, 2018). Notably, it is highlighted that insulin secretion is detectable in the human pancreas at glucose concentrations as low as 3 mmol/L (Henquin, Dufrane and Nenquin, 2006; Doliba et al., 2012; Braun et al., 2010; Rorsman and Ashcroft, 2018).

Figure 1-2 demonstrates the cellular activity in pancreatic cells that resulted in insulin and glucagon secretion in response to low and high BG levels.

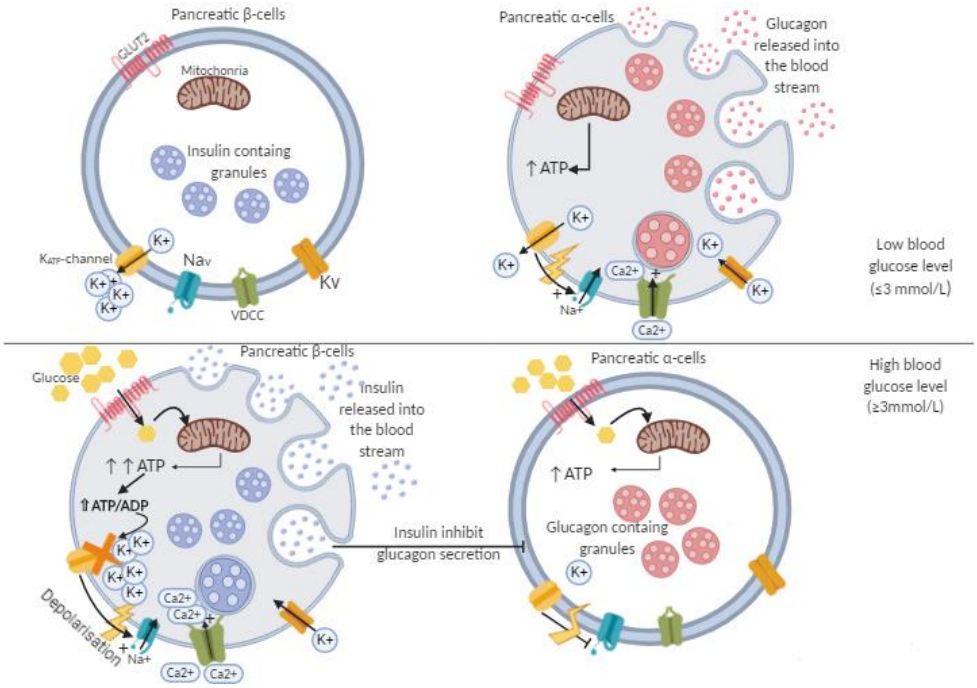

Figure 1-2:Illustration of insulin and glucagon secretion in response to the change in blood glucose levels (Adapted from Gaisano, MacDonald and Vranic, 2012)

Typically following a meal, increased insulin secretion from the pancreatic β-cells is stimulated by elevated BG level. Initially, a high influx of circulating glucose into the pancreatic β-cells is facilitated by the glucose transporter GLUT2 (or SLC2A2) located on the surface of β-cells. Once inside the cells,

these intracellular glucose molecules then undergo glycolysis, thereby generating ATP from the breakdown of glucose (Nicholls, 2016; Perego et al., 2019; Aronoff et al., 2004; Das et al., 2020)(Detailed process of glucose metabolism via a glycolytic pathway and Kreb cycle can be found from recent reviews by (Marchetti et al., 2020; Roma and Jonas, 2020; Westermeier et al., 2019). The resulting ATP production leads to an increased ATP/ADP ratio, thereby inducing the closure of ATP-sensitive K^+-channels (K_{ATP}-channels). Under non-stimulated conditions, these channels are open to transport K^+-ions down their concentration gradient out of the cell, therefore, securing the maintenance of resting potential. Upon closure, the subsequent reduction of K^+ efflux leads to an increase in the inward current of the membrane resting potential thereby depolarising the bilayer. The resultant membrane depolarisation causes the opening of voltage-dependent Ca^{2+}channels (VDCCs), which facilitates extracellular Ca^{2+} influx to the pancreatic β-cells. The increasing intracellular Ca^{2+} concentration eventually triggers the fusion of insulin-containing granules stored in the pancreatic β-cells with the membrane for subsequent releasing of their content (Rorsman and Braun, 2013; Rorsman and Ashcroft, 2018; Skelin Klemen et al., 2017). Meanwhile, in response to elevated glucose levels, the pancreatic β-cells will increase the production of insulin to maintain homeostasis. Notably, the secretion of insulin can be understood as a two-phased process that is (i.e) the initial rapid release of preformed insulin and an increase in insulin synthesis and release in response to elevated BG level. Once released into the bloodstream insulin is picked up mainly by insulin-responsive tissue such as skeletal muscle, adipose and hepatic (Marchetti et al., 2020; Jones et al., 2018; Röder et al., 2016b). Here, insulin can be understood to act as a facilitator for glucose transportation from the blood into tissues where glucose can be utilised for instant energy source, while excess glucose can be stored as glycogen or fat via glycogenesis and lipogenesis processes respectively. In order to reduce circulating glucose level, insulin also acts on the liver to decrease glucose production and increase glycogenesis (Tokarz, MacDonald and Klip, 2018; Patel and Goyal, 2019; Westermeier et al., 2019). Overall, following insulin secretion in response to

elevated BG level, there will be a high influx of glucose into tissues for energy usage/storage and low output of glucose from the liver leading to a decline in BG level and thereby maintain glucose homeostasis (Podobnik et al., 2020; Gerich, 1993; Tokarz, MacDonald and Klip, 2018; Röder et al., 2016)

Conversely, when BG levels fall below a critical threshold (<3mmol/L), the pancreatic α-cells respond by releasing glucagon. This counter-regulatory hormone stimulates hepatic glucose production and promotes the breakdown of glycogen and lipids to release more glucose to the bloodstream to bring back normal BG level. The autonomic nervous system activation and the glucose action at the islet levels are responsible for the stimulation of glucagon secretion to correct hypoglycaemia (Marty, Dallaporta and Thorens, 2007; Cryer, 2012; Gilon, 2020; Gromada, Chabosseau and Rutter, 2018). However, the overall physiology of glucagon secretion by pancreatic α-cells in response to low BG level is still a debatable research area mainly due to the scarce population of α-cells. Its lack of functional identification patterns and the technical limitations of conventional methods have also rendered α-cells more challenging to study than β-cells (Briant et al., 2016; Gilon, 2020; Gaisano, MacDonald and Vranic, 2012). Nevertheless, in the past decade, remarkable progress has been made in the study of pancreatic α-cell function at the cellular level. It is documented that K_{ATP} channels also play a fundamental role in the releasing of glucagon by the α-cells because they contribute to the variations of extracellular glucose level and the alterations of membrane action potential. As in pancreatic β-cells, α-cells are also electrically excitable since they are furnished with specific ion channels that generate action potentials of Na^+ and Ca^{2+} in the absence or at low levels of glucose. Glucagon exocytosis is also triggered by Ca^{2+} entry through VDCCs except that voltage-dependent Na^+ channels (Na_V) are thought to play a more prominent role in glucagon secretion (Briant et al., 2016; Gilon, 2020; Bankir et al., 2018; Gaisano, MacDonald and Vranic, 2012; Gylfe and Gilon, 2014).

In general, the pancreas plays vital roles in the regulation of macronutrient digestion by releasing various digestive enzymes and pancreatic hormones and therefore is important in the control of metabolism/energy homeostasis. The

body maintaining glucose homeostasis is primarily regulated by glucagon and insulin hormones released from the pancreatic α and β-cells respectively in response to change in BG levels. For individuals with diabetes mellitus, which is a lifelong metabolic disease, there is a disruption in the balance action of these two opposing regulatory hormones leading to persistent high BG level (Ajmera et al., 2013; Padhi, Nayak and Behera, 2020a; Nath et al., 2018). Since insulin is the main hormone that is responsible for reducing the BG level, defects in insulin secretion or/and action would result in impaired glucose metabolism and eventually lead to chronic hyperglycaemia (Szablewski, 2011; Gerich, 1993; Röder et al., 2016c; Kharroubi and Darwish, 2015)

1.1.2 Prevalence of diabetes mellitus

Diabetes mellitus is one of the most common endocrine disorders that is on the rise, affecting 4.7 million people in the UK, of whom 90% have type 2 (Whicher, O'Neill and Holt, 2020; Magliano et al., 2019) and 442 million adults around the world (World Health Organisation (WHO),2016). According to WHO report 2016, the global prevalence of diabetes (most of which is type two) in the adult population has almost doubled since 1980, rising from 4.7% to 8.5%. Although this dramatic increase was partly due to the population growth and ageing (accounting for 40%), other contributing factors include age-specific prevalence and changes in how people eat or drink and live.

Besides the economic burden on the health-care system and the wilder global economy, diabetes also largely affects the quality of life in those who have the disease and their families in terms of health-care cost; reduction in family income associated with disability and premature loss of life. Moreover, it was also recorded in 2012 that there were 1.5 million deaths directly caused by diabetes worldwide with the addition of 2.2 million deaths due to the consequence of prolonged high BG level leading to increased risks of cardiovascular and other diseases, making diabetes the eighth leading cause of death in 2012 (WHO,2016; Taverna, 2018).

Currently, in the UK, it is proposed that 1 in 15 people (both diagnosed and undiagnosed) are living with this disorder, mainly type 2. Every year, owing to

the complications of having diabetes, at least 10,350 people in the UK have end-stage kidney failure while more than 1,700 people have had their sight severely affected. Every week diabetes also leads to more than 169 amputations, 530 heart attacks, 680 strokes and almost 2,000 cases of heart failure (Diabetes UK facts and stats,2019). Additionally, there are even more than 500 premature deaths every week in the UK due to diabetes. It is predicted in the next decade there will be 5.5 million people in the UK who have diabetes. These figures are highly alarming and still on the rise, marking diabetes one of the biggest health challenges not only in the UK but also worldwide. Although there is no cure for diabetes, type 2 diabetes is reversible and both types can be treated and well-controlled by specific pharmacological medications in conjunction with appropriate diet and exercise However, early diagnosis especially in type 2 is vital since complications from diabetes can begin five to six years before a confirmed diagnosis (Diabetes UK facts and stats,2019).

1.1.3 Classification of diabetes mellitus

Diabetes mellitus is classified according to each aetiology of the disease characteristic. The severity of symptoms is dependent on the type and duration of diabetes. It is important to classify different types of diabetes to establish appropriate treatment strategies tailored to individual need. Generally, there are two main types of diabetes, namely, type 1 and type 2 as proposed by the American Diabetes Association in 1997 (American Diabetes Association, 2020) Besides these two main types, Gestational Diabetes Mellitus (GDM) is also classified in the UK. Other rarer specific types of diabetes include Maturity-Onset Diabetes of the Young (MODY), Neonatal diabetes mellitus (NDM), and Latent Autoimmune Diabetes in Adults (LADA) (Ke et al., 2020; Maniruzzaman et al., 2017).

Type 1 diabetes mellitus

Type 1 diabetes mellitus (T1DM), also known as insulin-dependent diabetes is an autoimmune disease that causes destruction to the insulin-secreting pancreatic β-cells, preventing them from being able to produce insulin, thus resulting in an absolute deficiency of insulin. Besides the apparent lack of insulin secretion, another key feature of T1DM is the presence of autoantibodies

against the pancreatic islet cells. These include islet cell autoantibodies, autoantibodies to insulin (IAA), glutamic acid decarboxylase (GAD, GAD65), protein tyrosine phosphatase (IA2 and IA2β) and zinc transporter protein (ZnT8A). These markers can be detected in the serum of people with T1DM months or years before the onset of the disease. The autoimmune destruction of pancreatic β-cells is also proposed to involve responses from T-cell mediated inflammatory (insulitis) as well as humoral (B-cell) (Norris, Johnson and Stene, 2020; Jean-Baptiste et al., 2017; Kharroubi and Darwish, 2015). Although the exact cause of T1DM is unclear, the complex interlinks between genetic predisposition and several environmental factors such as viral infections, allergic pollutants, early infant cow milk nutrition or other autoimmune disease have been considered to involve in the aetiology of the disease. However, no specific environmental risk factor has been linked to the significant number of cases (WHO, 2016). Notably, other pieces of evidence seem to support the causative effect of virus infections contributing to T1DM (Sabouri et al., 2020; Wernroth et al., 2020; Morse et al., 2020; Principi et al., 2017; Jean-Baptiste et al., 2017).

The majority of T1DM cases manifest in children and adolescents before the age of 20. T1DM accounts for 8% of all diabetes mellitus cases in the UK (Diabetes Facts and Stats updated, 2019). The condition often develops suddenly and rapidly resulting in minor to severe symptoms including excessive thirst, polyuria, involuntary urination, lethargy, fatigue, polyphagia, sudden weight loss, slow wound healing, recurrent infections, vision changes and possibly severe dehydration (Casu et al., 2020; Lucier and Weinstock, 2020). As the BG level is affected by daily dietary intake and physical activity, insulin is crucial for the regulation of how the body uses glucose for energy and storage (Gonzalez and Betts, 2019a; Murphy, Watt and Febbraio, 2020; Brown et al., 2020). However, in patients with T1DM, pancreatic β-cell destruction would prevent insulin secretion, therefore, leading to insulin deficiency. The resultant accumulation of circulating glucose causes extreme high BG level because there is no insulin available to aid the intracellular absorption of glucose for energy usage and storage. This condition needs urgent medical attention to

avoid further complications and possibly loss of life. The complete lack of insulin means that patients with T1DM are dependent on exogenous administration of insulin for survival; (Sims and DiMeglio, 2019; Tan et al., 2019; Lucier and Weinstock, 2020; Khursheed et al., 2019).

Type 2 diabetes mellitus

Type 2 diabetes mellitus (T2DM), is by far the most prevalent form of diabetes that accounts for almost 90% of all cases (Diabetes Facts and Stats updated, 2019). In T2DM there is a relative deficiency of insulin due to either the pancreatic β-cells inability to secrete sufficient insulin to cope with the body's demands or a decline in tissue's responsiveness to the hormone, referred to as insulin resistance. Some insulin-responsive tissues, including skeletal muscle, adipose and to a lesser extent, hepatic lose their sensitivity to the hormone as a result of insulin resistance in the initial development stage of T2DM. The reduction in glucose transport into muscle, liver and fat cells leads to the breakdown of other energy sources such as fat while hyperglycaemia occurs (Marchetti et al., 2020; Kahn, Cooper and Del Prato, 2014; Weir, Gaglia and Bonner-Weir, 2020). In the presence of prolonged insulin resistance, the pancreatic β-cells are incapable of producing sufficient insulin to overcome the resistance and correct high BG level, thereby resulting in chronic hyperglycaemia. This incapability could lead to a decline in insulin production and eventually fails in pancreatic β-cell function (Marchetti et al., 2020; Sampath Kumar et al., 2017; Vandana Saini, 2010). Recently, the impairment of pancreatic α-cells function has also been recognised to be involved in the pathophysiology of T2DM. Following a meal, pancreatic α-cells dysfunction fails in the suppression of glucagon released and hepatic glucose production, which normally occurs during the fasting stage. Given that BG level rises following a meal, the continuous glucagon secretion in addition to increased insulin resistance and inadequate levels of insulin secretion would lead to persistent hyperglycaemia eventually leading to T2DM (Grubelnik et al., 2020; Moon and Won, 2015; Roncero-Ramos et al., 2018; Olokoba, Obateru and Olokoba, 2012).

This condition is usually but not exclusively associated with obesity which is a contributing factor to the development of insulin resistance. According to Diabetes UK,2019 obesity is held responsible for up to 85% of someone's risk to develop T2DM. In the obese state, the amount of triglyceride intake exceeds the storage capacity in adipose tissue. Further CHO overload causing excess adipose build-up eventually lead to fat accumulation in ectopic tissues such as liver, heart and skeletal muscle (Longo et al., 2019; Ferrara et al., 2019). This disturbed fat distribution is proposed to interfere with the insulin signalling pathway (refer to section 3.1.1) and reduce the ability of insulin receptor substrates to propagate the insulin signal, thereby making tissues resistant to insulin (Guilherme et al., 2019; Guo, 2014; Dai et al., 2013). Meanwhile, in an attempt to bring back insulin activity to correct hyperglycaemia, the pancreatic β-cells respond by releasing even more insulin (hyperinsulinemia). During this pre-diabetic stage, the high level of amylin co-secretion with insulin results in the formation of amyloid through aggregation in the vicinity of the pancreatic β-cells. This triggers β-cells apoptosis and leads to long-term damage to the pancreatic islet, thereby reducing its capability to release insulin (Brannick and Dagogo-Jack, 2018; Kiriyama and Nochi, 2018; Verma et al., 2020). The impairment of insulin secretion develops progressively over a sustained period and if continued, will eventually result in T2DM. Notably, T2DM was formerly referred to as non-insulin-dependent diabetes in contrast to T1DM where there is a complete dependence on exogenous insulin administration. However, there is a significant number of patients with T2DM requiring insulin as the condition progresses, the terminology of non-insulin-dependent diabetes can be misleading and is therefore no longer applicable (Boarder et al. 2017).

Gestational diabetes mellitus

GDM as its name suggests, refers to a condition of glucose intolerance develops during pregnancy. Although it is a temporary condition that usually ends shortly after giving birth, it also carries long-term risk of developing diabetes and cardiovascular diseases (CVDs) (Johns et al., 2018; Szmuilowicz, Josefson and Metzger, 2019; Walker, Flannery and Mackillop, 2020). In the UK, GDM affects up to 10% of pregnant women with no previous diagnosis of

diabetes mellitus (Stacey et al., 2019). Women with GDM as well as their babies could be at increased risks of developing complications during pregnancy and giving birth if the condition is not well managed (Bordin et al., 2020 and Li, Y.,et al 2020). GDM can happen at any stage of pregnancy; however, during the second and third trimester, it is more common. GDM does not usually cause any symptoms and is diagnosed during antenatal screening when there are one or more risk factors determined (Stacey et al., 2019; Kachikis et al., 2017; Bordin et al., 2020; Johns et al., 2018). There are several risk factors and markers for GDM including mainly age; overweight or obesity (IBM > 30) and excess glucose in urine or excessive weight gain during pregnancy or previously gave birth to babies who weighed ≥ 4.5kg(10lb). Other history factors contributing to the risk include a family history of diabetes, ethnicity, GDM during a previous pregnancy and a history of stillbirth or giving birth to an infant with congenital abnormalities (Stacey et al., 2019; Ménard, Sotunde and Weiler, 2020; Li, Y. et al., 2020; Sweeting et al., 2019). Diabetes in pregnancy or GDM also increase the risk of future obesity and T2DM in offspring (WHO,2016). Although the exact cause remains uncertain, the hormonal changes during pregnancy are proposed to play a role in the development of GDM by putting some pregnant women at a higher risk of insulin resistance (Plows et al., 2018; Johns et al., 2018; Egan, Dow and Vella, 2020). Infants born to mothers who have suffered from GDM usually have additional fat resulting from the excessive circulating glucose that crosses the placenta, therefore, explaining the heavier weights that are normally seen in those infants (Prentice et al., 2019; Andersson-Hall et al., 2019; Stacey et al., 2019). In most cases, GDM can be well managed by the appropriate diet and physical activity. Some rare cases will require insulin to ensure good BG control (NICE, 2015a; Laredo-Aguilera et al., 2020; Egan, Dow and Vella, 2020).

Other specific types of diabetes mellitus

MODY is a group of monogenic disorders categorised by an autosomal dominant inherited non-insulin-dependent form where hyperglycaemia occurs at an early age. The most common gene defect concerns a mutation in the hepatocyte nuclear factor-1 alpha (HNF-1 α) gene on chromosome 12 (MODY

3). Another defect is caused by mutations in the glucokinase gene on chromosome 7p. These mutations account for a small number of people with diabetes (1%) but are important in determining therapeutic approaches (Oliveira et al., 2020; Aarthy et al., 2020).

NDM is another form of monogenic disorders that occurs in the first 6 to 12 months of life. However, it is very rare, occurring in around 1 in 300,000 to 400,000 births. NDM may or may not require insulin treatment so, diagnosis by genetic testing is recommended (Habeb et al., 2020; Dahl and Kumar, 2020).

LADA is another different form of autoimmune diabetes which occurs during adulthood rather than in childhood and adolescents as seen in T1DM. It is distinct from T1DM by the older age of onset and slower destructive progression of pancreatic islet towards insulin requirement. However, there is a substantial proportion of people with LADA who have an initial clinical diagnosis of T2DM as they also show some degrees of insulin resistance. It is therefore important to identify LADA features to ensure appropriate treatment for good glycaemic control (Maddaloni et al., 2020; Verma, Sharma and Rangari, 2019).

1.1.4 Disease management

Currently, there are two main groups of pharmacological medications used for diabetes treatment, including insulin and antidiabetic drugs (Stubbs, Levy and Dhatariya, 2017; Feingold, 2020). As previously discussed, exogenous insulin administration is essential for survival in patients with T1DM. The ultimate goal for T1DM management is the lifelong control of normal BG level. This is achievable through a carefully combined strategy of insulin replacement therapy to closely mimic the standard release of insulin in healthy people and dietary intake with adequate exercise for an individual patient (Neupane and Evans, 2019; Subramanian et al., 2016; Khardori and Griffing, 2017). Most clinically used insulin formulations nowadays are manufactured using genetic engineering and recombinant DNA technologies. They are generally classified following their speed of onset or duration of action (Vajo, Fawcett and Duckworth, 2001; Baeshen et al., 2014; Khan et al., 2016). There are four main groups of insulin preparations, namely short-acting, rapid-acting, intermediate

and long-acting (detailed in section 2.1.1). The most common method of exogenous insulin administration is by subcutaneous (SC) injection. The intravenous (IV) route of delivery is mainly used in an emergency to achieve a rapid response.

The initial treatments for T2DM tailored to individual patient usually involve a good lifestyle and diets control in addition to a single oral antidiabetic drug if lifestyle intervention alone cannot achieve good glycaemic control. It is highly encouraged to have non-pharmacological management, including weight loss, smoking cessation and regular exercise which can help to reduce hyperglycaemia and reduce cardiovascular risk. There are several classes of oral antidiabetic drugs with a wide-range mechanism of action available for the treatment of T2DM as summarised in **Table 1-2**. The choice of drug is generally based on effectiveness, safety and tolerability. The patient's comorbidities and concomitant medication with co-existing diseases should also be considered. However, as the disease progresses, insulin therapy becomes typically necessary owing to the decline in pancreatic β-cells function (Seidu et al., 2020; Feingold, 2020; Padhi, Nayak and Behera, 2020b; NICE, 2015b)

Table 1-2: Summary of antidiabetic drugs used in the treatment of Type 2 Diabetes Mellitus. (The information is taken mainly from the BNF online and Boarder et al. 2017)

Therapeutic class	Drugs	Mechanism of action	Common adverse drug reactions
Biguanides	Metformin	Decrease gluconeogenesis and increase peripheral glucose ultilisation; since it acts only in the presence of endogenous insulin it is effective only if there are some residual functioning pancreatic islet cells	Gastrointestinal (GI) disturbances Decreased vitamin B12 absorption Lactic acidosis (discontinue)
Sulfonylureas	Glibenclamide, Tolbutamide Gliclazide, Glimepiride, Glipizide,	Block ATP-dependent K^+ channels on pancreatic β-cells to cause depolarisation, leading to an influx of Ca^{2+} through VDCCs, thereby increasing insulin secretion. They are effective only when some residual pancreatic β-cell activity is present; They also show an extra-pancreatic action in long-term use.	Abdominal pain; Diarrhoea; Hypoglycaemia; Nausea
Meglitinides	Nateglinide, Repaglinide	Stimulates insulin secretion similar to sulfonylureas	Diarrhoea; GI discomfort; hypoglycaemia; nausea
Thiazolidinedione	Pioglitazone	Reduces peripheral insulin resistance, leading to a reduction of blood-glucose concentration.	Bone fracture; increased risk of infection; numbness; visual impairment; weight increased
α-glucosidase inhibitors	Acarbose	Reversible inhibition of α-glucosidase; Reduce post-prandial peak of glucose by slowing intestinal glucose absorption.	Bloating, Flatulence, Diarrhoea
Dipeptidylpeptidase-4 (DPP-4) inhibitors	Alogliptin, Linagliptin, Sitagliptin, Saxagliptin, Vilda gliptin	Competitively inhibits DPP-4 to increase insulin secretion and reduce glucagon secretion.	Headache, Nausea, Infections
Sodium-glucose co-transporter 2 (SGLT2) inhibitors	Canagliflozin, Dapagliflozin, Empagliflozin	Reversibly inhibits SGLT2 in the renal proximal convoluted tubule to reduce glucose reabsorption and increase urinary glucose excretion.	Hypotension Urinary tract infection
Glucagon-like peptide-1(GLP-1) receptor agonists (Incretin mimetics)	Dulaglutide, Exenatide, Liraglutide, Lixisenatide	Mimic action of GLP-1, enhancing glucose-dependent insulin secretion from pancreatic β-cells while inhibiting glucagon released from pancreatic α-cells, and slows gastric emptying.	Abdominal pain; Nausea; Vomiting Diarrhoea; Dyspepsia

1.1.5 Diabetes mellitus-associated complication

When diabetes is not treated or well managed, short and long-term complications can develop that threaten the health and even endanger life. Maintaining good glycaemic control is therefore essential in the management of diabetes mellitus to achieve better health outcome. Abnormally low BG level may lead to seizures or unconsciousness. It could happen after skipping a meal or exercising more than usual, or if the dosage of insulin /anti-diabetic medication is too high, resulting in a dramatic drop in BG level. Persistently high BG level over time owing to poorly controlled diabetes can also result in damage to the heart, blood vessels, eyes, kidneys and nerves, increasing the risk of cardiovascular diseases (CVD) and stroke. Diabetic complications are the leading cause of mortality and morbidity associated with the disease. The high healthcare cost to manage these associated complications has also been a huge burden not only to the patients and their family but also to the healthcare system providers (Aarthy et al., 2020; Papatheodorou et al., 2018).

Acute complications of diabetes mellitus are commonly associated with T1DM and are often metabolic emergencies that can be life-threatening. Diabetic ketoacidosis (DKA) is a dangerous complication that can lead to coma or even death if it is not treated quickly. DKA mainly occurs in T1DM as a result of the uncontrolled breakdown of fats and proteins due to the body lacking sufficient insulin to allow enough glucose to enter cells. Since energy is essential for the body to function when there is a shortage of glucose, the body switches to burning fatty acids to compensate the energy need, resulting in accumulation of acidic KBs. A high level of KBs in the blood can cause nausea, vomiting and seriously disturb the body acid-base balance, leading to acidosis. In an attempt to correct acidosis, hyperventilation may occur while the breath may smell of acetone due to the excreted ketones. A decrease in plasma pH in addition to dehydration can lead to a coma that requires urgent medical attention (Duca et al., 2019; Kreider, 2018). In the UK, nearly 4.3% of people with T1DM experience DKA each year during their hospital stay (National diabetes audit

2019). Treatment of DKA requires IV fluids administration to correct dehydration and to replace any salts that could be lost from excessive urine excretion during ketoacidosis. Insulin is also required via IV administration to suppress the KBs that the body produces instantly. Although people with T2DM that produce very little of their insulin may also be affected by DKA, it is very rarely observed since sufficient insulin is usually available to prevent excessive lipolysis in adipose tissue and the liver (Diabetes UK, 2019; Boarder et al. 2017)

Long-term complications of diabetes mellitus due to uncontrolled hyperglycaemia mainly associated with macrovascular and microvascular diseases that can result in visual loss, kidney failure, lower limb amputation and several other long-term consequences leading to significant impacts on the quality of life (Visaria et al., 2020; Hippisley-Cox and Coupland, 2016). Sustained hyperglycaemia can cause damage to a wide range of organs and cells via various mechanisms, including RBC, blood vessels, nerves, the liver and kidney, and the lens of the eye (Lotfy et al., 2017a; Yaribeygi, Atkin and Sahebkar, 2019). The elevated glucose level inside these cells can cause non-enzymatic binding of glucose with other molecules such as FA, proteins and nucleic acids to produce advanced glycation end-products. These can lead to altered functions underlying many of the pathological changes and characteristic of the chronic diabetic state (Yang et al., 2019; Park et al., 2019; Yaribeygi, Atkin and Sahebkar, 2019). Haemoglobin in RBC and structural proteins like collagen and elastin are some important examples (Szablewski and Sulima, 2017; Yang et al., 2019). In particular, collagens become cross-linked by the transformed glucose groups, disturbing turnover and function. The glycated molecules thicken basement membranes, leading to alterations in permeability and transport mechanism of cells. Especially, cells of the kidney are particularly at high risk to these structural alterations, resulting in deflective filtration and kidney damage (nephropathy) (McKay, Priyadarsini and Karamichos, 2019; Amorim et al., 2019; Hippisley-Cox and Coupland, 2016). Accumulation of the advanced glycation end-products can also increase risk of inflammation while glycation of the α-crystalline protein in the lens of the eye can result in cataract formation (Zhu, Titone and Robertson, 2019; Giri et al.,

2018). An altered affinity for oxygen is usually seen in glycated haemoglobin (HbA1c), resulting in reduced oxygen supply to many tissues; thus, may compromise their body function. Similarly, vascular endothelium is also affected at an early stage. The key features include an increase in vascular permeability and the loss in the vasodilatory influence of nitric oxide, which contributes to the pathogenesis of both microvascular and macrovascular complications associated with diabetes (Lotfy et al., 2017b; Forbes and Cooper, 2013).

Meanwhile, damage to smaller blood vessels (microvascular disease) caused by hyperglycaemia can lead compilations involving the eye, kidneys and nerves (Mauricio, Alonso and Gratacòs, 2020; Lotfy et al., 2017; Chawla, Chawla and Jaggi, 2016). Diabetic retinopathy is the leading cause of blindness in people aged under the 60s in developed countries. It is estimated that over 80% of patients who have had diabetes mellitus for more than 20 years are also affected by this condition (Saleh et al., 2018; Rabiu et al., 2020; Zhu, Titone and Robertson, 2019). Chronic renal failure (nephropathy) is the most common consequence of diabetes mellitus. Although the exact mechanism of hyperglycaemia resulting in kidney damage has not yet been fully understood, the obvious outcome is the compromised glomerular filtration and the presence of protein in the urine. High blood pressure also significantly contributes to this kidney damage which in turn is associated with an increased risk of CVD. Prolonged high BG level also predisposes to nerve damage, leading to the progressive loss of peripheral nerves fibres that include autonomic, sensory and motor nerves, referring to as diabetic neuropathy. Patients who suffer from diabetic neuropathy can sometimes experience numbness and profound pain which often does not respond to conventional analgesia, causing considerable morbidity (Anders et al., 2018; Braunwald, 2019; Amorim et al., 2019). Unfortunately, there is no specific treatment for diabetic neuropathy despite the availability of various drugs to relief their symptoms. The primary goal for management is to control symptoms and prevent worsening of neuropathy by improving glycaemic control. Furthermore, the combined effects of neuropathy and macrovascular damage can result in diabetic foot problems owing to the development of foot ulcers which can easily become infected without the

patients noticing due to nerve damaged and can even necessitate amputation (Braunwald, 2019; Lotfy et al., 2017; Hippisley-Cox and Coupland, 2016).

Most importantly, complications associated with damage to large blood vessels owing to high levels of circulating glucose has accounted for the significant increases in mortality related to diabetes mellitus (Visaria et al., 2020; Dal Canto et al., 2019). Macrovascular complications of diabetes can develop from uncontrolled hyperglycaemia, excess free FA, and insulin resistance, leading to CVD such as heart attacks, strokes and insufficiency in blood flow to legs, genitals, feet and toes. CVD is the major cause of mobility and mortality in patients who suffer from diabetes mellitus (Glovaci, Fan and Wong, 2019; Anders et al., 2018). The early stage of the macrovascular disease is associated with atherosclerotic plaques in the vasculature supply of blood to the heart, brain or limbs. Later disease stage involves the complete obstructions of these vessels that can contribute to the risk of myocardial infarction, stroke, claudication and foot gangrene. The process of atherosclerosis (built-up of plaque inside the arteries) resulting in the narrowing of arterial walls is believed to be the main pathophysiology in macrovascular disease. In addition to the formation of plaque, there is strong evidences of increased platelet adhesion and hypercoagulability in T2DM patients where compromised production of nitric oxide, altered calcium regulation and the increase in free radical formation of platelets could promote platelet aggregation. Elevated levels of plasminogen activator inhibitor type 1 may also impair fibrinolysis in these patients. The combined effects of hypercoagulability and impaired fibrinolysis are, therefore, likely to further escalate the risk of vascular occlusion and CVD in T2DM (Fowler, 2008; Raghavan et al., 2019).

1.2 Insulin

1.2.1 Insulin discovery and structure

Before the discovery of insulin in the 1920s, the prognosis for people with diabetes mellitus requiring insulin replacement was very poor. There were hardly any treatment options available and therefore, usually resulted in high morbidity and mortality, particularly in children. In general, once the diagnosis of

diabetes had been confirmed, eventual complications and subsequent deaths were usually observed within two years at the most. At that time, the condition had to be managed through dietary modification alone, meaning that some affected individuals were restricted to a diet with an almost negligible CHO intake with the hope of controlling their BG levels. In those circumstances, the benefit of repeated fasting and prolonged undernourishment, was relatively short-lived since it was only a modest extension of life. Furthermore, there was little or no evidence in supporting the longer-term efficacy of undernourishment therapy, yet it more likely resulted in poorer health accompanied by a risk of infection, exhaustion from lack of nourishment, and poor quality of life (Hilgenfeld et al., 2014; Vecchio et al., 2018; Didangelos, 2011). Undoubtedly, the discovery of insulin as an injected therapeutic agent by Banting and Best in 1922 for the treatment of insulin-requiring diabetes mellitus has been the most important and controversial breakthroughs in modern medical history. Their research groups successfully isolated a concentrated pancreatic secretion from crude extracts of cow, pig and sheep pancreas. This product demonstrated a reduction of BG level with relatively low toxicity firstly in animals and under careful control in humans with diabetes. Following its discovery, insulin has remained as an indispensable mainstay of treatment for T1DM and GDM for almost a century later. There are also many more people with T2DM requiring insulin treatment as their diabetic condition progresses (Nwaneri, 2015; Flier, 2019; Vecchio et al., 2018).

In addition to its key role in the regulation of human metabolism, the insulin polypeptide with all the structural features of a large protein is an ideal model molecule for studying the structure, properties and characteristic of proteins. Insulin, therefore, remains one of the most extensively studied molecules of biochemistry for nearly a century (Yaribeygi et al., 2019a; Vecchio et al., 2018; Didangelos, 2011; Quianzon and Cheikh, 2012). Although, the first insulin preparations were originated from porcine (pig) - and/or bovine (cow), the continuous evolution of insulin had progressively developed after the 1980s when semi-synthetic human insulin (HI) production became clinically available. The primary structure of insulin comprising A chain and B chain differs among

animal species in their amino acid sequences. However, the folding and packing of the two chains into their three-dimensional (3D) conformation are essentially similar. HI has the closest structure and function to bovine or porcine insulin (Jacob, 2015). The difference in their amino acid residues is summarised in **Table 1-3**.

Table 1-3: Difference in the amino acid residues between human insulin, bovine insulin and porcine insulin (Taken from Jacob 2015).

Residue	Human insulin	Bovine insulin	Porcine insulin
A8	Threonine	Alanine	Threonine
A10	Isoleucine	Valine	Isoleucine
B30	Threonine	Alanine	Alanine

Figure 1-3: Insulin structure from (a) the initial insulin synthesis to its final structure of insulin monomer and (b) amino acid sequences of connecting C-peptide (grey) as well as insulin A&B chains (blue) (taken from Chhabra 2012).

presents the overall changes in the insulin structure from its initial synthesis as pre-proinsulin to its monomer form of insulin (a) and the detailed amino acid sequences of C-peptide and insulin monomer of A and B chains (b).

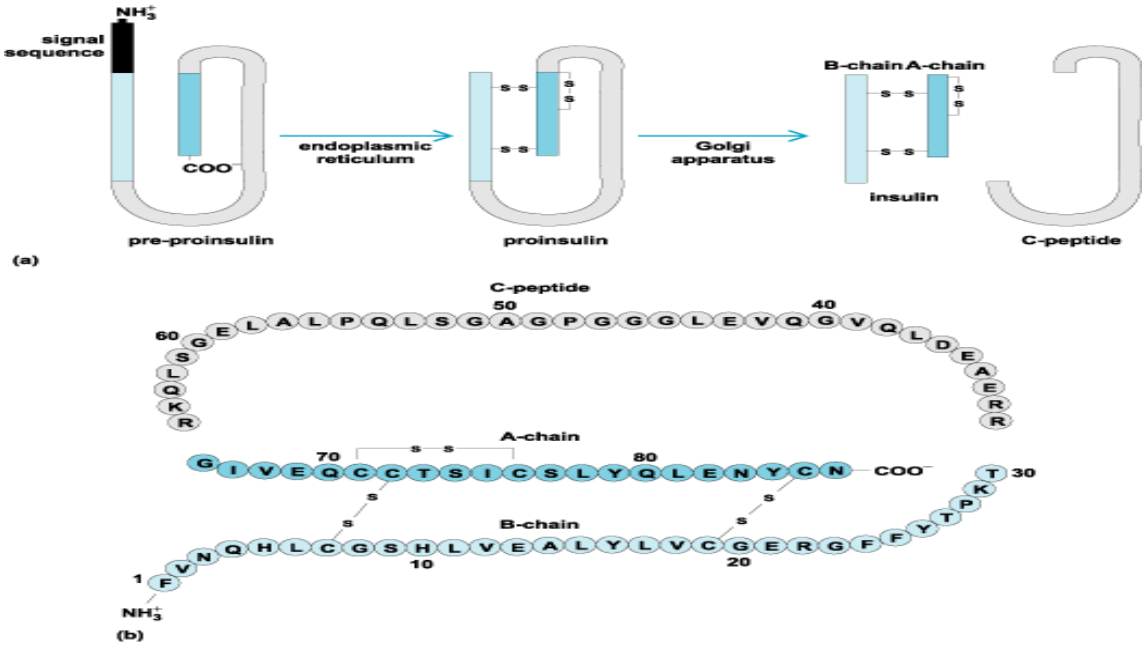

Figure 1-3: Insulin structure from (a) the initial insulin synthesis to its final structure of insulin monomer and (b) amino acid sequences of connecting C-peptide (grey) as well as insulin A&B chains (blue) (taken from Chhabra 2012).

The insulin hormone is originally produced by the pancreatic β-cells in the form of a single polypeptide chain called preproinsulin, which is composed of 110 amino acids. The ‘signal peptide’ (in black, Figure 1-3a) of 24 amino acids is removed from one end of the chain by enzymatic action when it passes through the endoplasmic reticulum, leaving pro-insulin behind. Further two amino acids are removed by another enzyme carboxypeptidase E (CPE). The pro-insulin has the middle C-peptide consisting 33 amino acids which connect the amino terminus (NH2-) of the A chain to the carboxyl terminus (-COOH) of the B chain. This connecting peptide section is then removed by the action of prohormone convertase 1 and 2 enzymes, leaving the final primary structure of the insulin molecule consisted of the A and B chains (in blue, Figure 1.3) (Vasiljević et al., 2020; Liu et al., 2014; Liu et al., 2018).

Principally, biologically active insulin exists as a monomer, comprising A and B polypeptide chains. The two chains are linked to each other by two disulphide bonds linking two sulfhydryl groups of cysteine between A7 and B7 as well as

A20 and B19. Chain A has 21 amino acid residues with an additional disulphide loop between A6 and A11, whereas the longer B chains consist of 30 residues. (Weiss, Steiner and Philipson, 2014; Liu et al., 2018; Xiong et al., 2020).

Figure 1-4: Insulin monomer 3D structure of the A chain (blue), highlighting the two parallel α- helices (A2-A8 and A13-A20) and the B chain (grey) with the large α-helix (B9-B19). Three disulphide bridges are shown in yellow (Adapted from Lierop et al., 2017).

shows the 3D version of the insulin monomer.

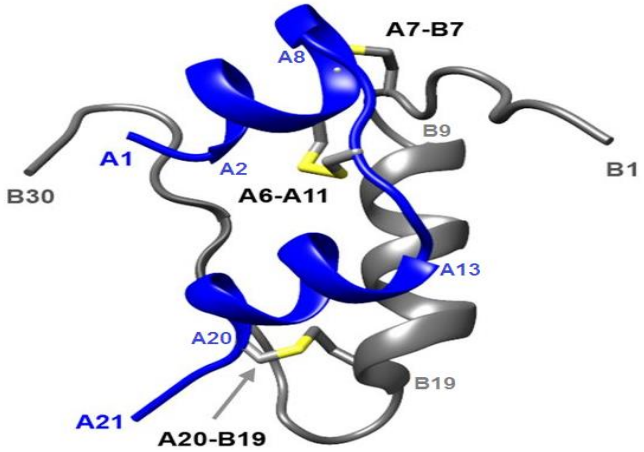

Figure 1-4: Insulin monomer 3D structure of the A chain (blue), highlighting the two parallel α-helices (A2-A8 and A13-A20) and the B chain (grey) with the large α-helix (B9-B19). Three disulphide bridges are shown in yellow (Adapted from Lierop et al., 2017).

Insulin can adopt different structures depending on its concentration. At a low concentration of <10μM, insulin only exists as a monomer of a compact globular structure with a hydrophobic core.Within the insulin folding of its secondary structure, the A chain forms a compact unit containing two sections (A2 - A8 and A13 – A20) of the α-helix in between presenting a fairly flat ribbon. This allows each α-helix section to lie alongside one another, and thereby brings the side chains of A2 and A19 close enough to allow Van der Waals contact. The B chain, which wraps around the A chain comprises a more extensive section of α-helix (B9 - B19) and the smaller glycine residues at B20 and B23, enabling it to fold into a V shape. The resulting V-folding brings the C terminal residues B24 and B26 into Van der Waals contact with B15 and B11 of the α-helix to

form the globular structure of the insulin monomer. At higher concentration (> 10 µM) relevant for pharmaceutical formulations, each insulin monomer joins in two to form a dimer, as shown in **Figure 1-5 A** (Weiss, Steiner and Philipson, 2014; Hilgenfeld et al., 2014; Liu et al., 2018; Hjorth et al., 2016a)**.**

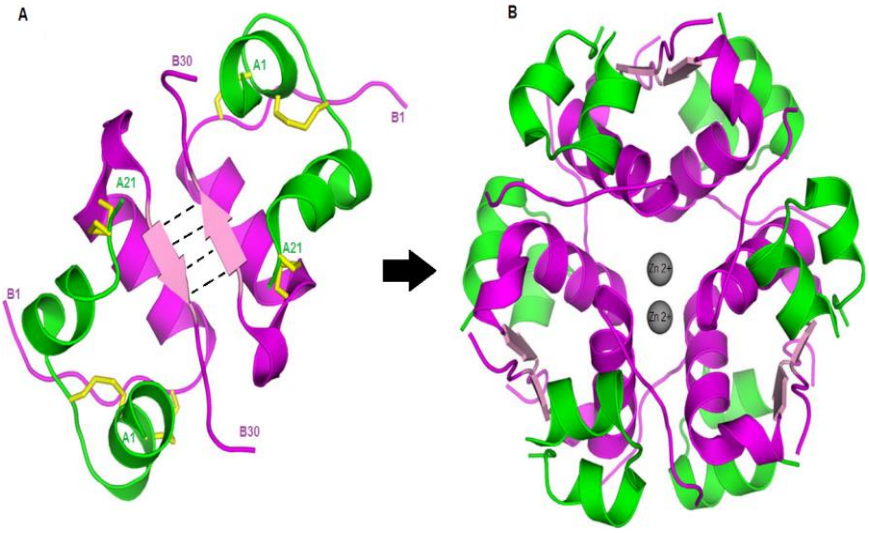

Figure 1-5: 3D illustration of insulin dimer (A) showing antiparallel β-sheet in black dotted line with the A chain coloured in green, B chain in magenta and disulphide bridges in yellow. In the presence of zinc ions, the three dimers then associate to form a hexamer (B) (Adapted from Hilgenfeld et al. 2014).

Each insulin dimer consists of two insulin molecules held together by nonpolar forces and four hydrogen bonds (between B24 and B26 residues). They are arranged as an antiparallel β-sheet structure (**Figure 1-5A**) between the two COOH-terminal strands of the B chain. The arrangement of the chains buries the nonpolar cysteine A6-A11 and the aliphatic side chains of residues A2, A16, B11 and B15 in the hydrophobic core contributing to its stability, which is also lent by the disulfide bridges. While B25-B30 and B1-B8 segments can vary in conformation, the A-chain and the B9-B19 helix form a stable structure unit of insulin. Furthermore, within the pH range of 4-8 and at 10 to 200 µM concentrations, three insulin dimers then assemble in the presence of two zinc ions located above and below the 2-fold axis to form an insulin hexamer, a globular protein structure (**Figure 1-5B**). Meanwhile, at ≥ 2mM concentration, the hexamer can be formed at neutral pH without the assistance of zinc ions

(Weiss, Steiner and Philipson, 2014; Hilgenfeld et al., 2014; Liu et al., 2018; Banerjee, Mondal and Bagchi, 2018).

Generally, there are three structural families of insulin hexamers (T_6, T_3 R^f_3, and R_6) formed, as shown in **Figure 1-6** when insulin exists in crystals and solution (Weiss, Steiner and Philipson, 2014).

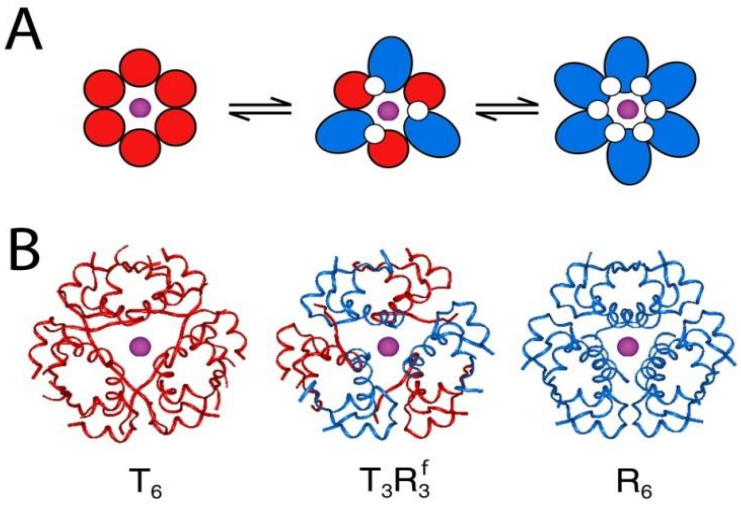

Figure 1-6: Structural families of insulin hexamers showing (A): Schematic representation of the three types of zinc-insulin hexamers, designated T_6, T_3 R^f_3, and R_6 and their corresponding ribbon representation of wild-type crystal structures (B) with zinc ions coloured in magenta and phenol molecules in white (Taken from Weiss et al.,2014).

Insulin hexamer is also referred to as an allosteric protein, which possesses ligand-mediated cooperative binding sites. The presence or absence of specific ligands would result in different conformational states namely T_6, $T_3R^f_3$, and R_6 hexamers. These states are differentiated by the change in conformation of the B-chain residues, in which fully extended form of B1-B8 residuals results in the conformation of T state. Whereas, the long B1-19 helix continuation to the N-terminus leading to a helical structure is responsible for R^f or R state (Březina et al., 2018; Weiss, Michael A., 2009; Lierop et al., 2017). The frayed R^f state presents B1-B3 in extended conformation and B4-B8 in helical conformation which is similarly observed in the conformation of the R state (Palmieri et al., 2013; Weiss and Lawrence, 2018).

The equilibrium of the R_6, T_6 and R^f arrangements of insulin hexamers are modulated by the interaction between the allosteric ligands (favours the T state) such as lyotropic anions ($Cl^{-1,}$ SCN^{-1}) or bivalent metal ions (Zn^{2+}, Co^{2+}) and the binding of phenolic ligands (favours the R state or frayed R^f state) (Gast et al., 2017a; Maikawa et al., 2020; Weiss, 2009; Wollmer et al., 1987). The T_6 insulin hexamer comprises six insulin molecules associated into three dimeric units that are connected by a threefold symmetry axis. Each dimeric unit holds a pseudo twofold symmetry axis, which rotates perpendicularly to the threefold axis. Although each insulin monomer within the dimers shares the same amino acid sequence of the A and B chain structure, they are not identical in the arrangement of certain side chains, thereby, breaking the twofold symmetry. In particular, the most apparent difference is that in one monomer the B25 side chain is folded in towards the hydrophobic core while the other has it folded outwards. Within the polar central axis of the hexamer, two axial zinc ions situate on the threefold symmetry, each of which is coordinated by three B10 residues (histidine) and three water molecules in an octahedral arrangement (Weiss, Steiner and Philipson, 2014; Liu et al., 2018; Weiss and Lawrence, 2018; Rege et al., 2018).

Meanwhile, high concentrations of sodium chloride would result in the classical "rhombohedral transition" of zinc insulin crystals, referred to as $T_3R^f_3$ hexamers or 4-Zn insulin. Proposed that each dimeric unit consists of two monomer molecules (monomer I and monomer II). Within the hexameric unit, monomer I trimer (T_3) shares the same octahedral zinc-ion coordination as in the T_6 hexamer whist monomer II trimer (R^f_3) displays substantially more structural reorganisation, especially at the N-terminal of the B-chain residues. The $T_3R^f_3$ hexamers can also be induced at lower salt concentrations in the presence of phenolic ligands in which three bound phenolic molecules are contained in the R^f_3 trimer. Whereas, high concentrations of phenolic ligands would lead to the conformational change of the R_6 hexamers (Fili et al., 2015; Palivec et al., 2017; Palmieri et al., 2013; Weiss, Steiner and Philipson, 2014). There are usually six (or uncommonly seven) bound phenolic ligands assembled within the R_6 hexamer (Weiss, Steiner and Philipson, 2014). At each

dimer-dimer interphase, phenol molecules bind to a largely hydrophobic pocket which is made up by the side chains of B5 and B11 residuals from each different dimer in addition to A6 and A11 residuals. The orientations of phenol molecules in these pockets usually vary within one hexamer as well as from various insulin analogues. However, in all cases, it is the basic formation of two hydrogen bonds between the phenolic hydroxyl groups and cysteine residues at A6 and A11 positions, in combination to the hydrophobic contact with the B5 side chain that holds each phenol molecule in position (Weiss, Steiner and Philipson, 2014; Berchtold and Hilgenfeld, 1999; Palivec et al., 2017).

In general, the T_3 R^f_3 hexamer and R_6 hexamer have a similar arrangement to the classical T_6 hexamer. The equilibrium of these three structural families is largely affected by the concentration gradients of salts and phenolic ligands (Brange et al., 1997; Berchtold and Hilgenfeld, 1999; Weiss, Michael, Steiner and Philipson, 2014a). More importantly, in the presence of phenolic ligands, the R_6 hexamer of insulin in solution was reported to be the most thermodynamically stable structure (Gast et al., 2017; Maikawa et al., 2020; Derewenda et al., 1989; Wollmer et al., 1987). Whereas, the T_6 hexamer resembles the solution structure of insulin as a monomer in solution (Fili et al., 2015; Maikawa et al., 2020; Hua et al., 1996). T_6 insulin hexamer has widely been employed as the prototypic insulin structure owing to its defined structural characters of hydrophobic, solvent-exposed, and potential binding surfaces of insulin (Mukherjee et al., 2018a; Liu et al., 2018; Weiss, Steiner and Philipson, 2014). Commercially available insulin preparations are formulated at high concentration of 100Unit/mL (0.6mM) to 500Unit/mL (3mM), with the addition of allosteric ligands, such as Zn^{2+} and phenolic compounds or at neutral pH, thus promoting insulin to exist in its hexameric state. The standard structural unit of insulin hexamer is, therefore, typically present in all clinically used insulin injections to ensure sufficient shelf life for long-term storage (Rege et al., 2018; Maikawa et al., 2020; Gast et al., 2017). However, it is emphasised that the monomeric state is essential for the instantaneous action of insulin. Consequently, maintaining high stability of insulin in formulations and the rate

of dissociation to monomer insulin after SC injection are two key features in the development of clinically used insulin formulation.

There are various types of clinically used insulin pharmaceutical preparations (namely rapid-acting, short-acting and long-acting) that exhibit different dissociation rate and thus onset of insulin action owing to their excipient contents such as phenol or meta cresol (m-cresol), zinc oxide, glycerine, and protamine sulphate. It was reported that T_6 and R_6 insulin hexamers exhibit different dissociation rate, which is known to be the rate-limiting step for SC absorption thus determining the onset of insulin action (Gast et al., 2017; Banerjee, Mondal and Bagchi, 2018; Liu et al., 2018). For instance, many rapid-acting insulin analogues such as Novorapid® and Humalog® are formulated in excess Zn^{2+} to promote the T_6 hexameric state (Maikawa et al., 2020; Gast et al., 2017). Whereas the addition of phenol or m-cresol stabilises the R_6 insulin hexamer by forming hydrogen bonds between dimers (Maikawa et al., 2020). Phenolic ligands were traditionally employed in insulin formulations for their bacteriostatic properties. However, they were also found to facilitate the stability of insulin hexamer against deamidation and intermolecular cross-linking reactions (Weiss, Steiner and Philipson, 2014; Derewenda et al., 1989; Hilgenfeld et al., 2014; Maikawa et al., 2020). Besides having modifications to the insulin amino acid sequence, the content of zinc ions and phenolic ligands (phenol or m-cresol) also contributes to different onset of actions for each insulin analogue. For example, Apidra® (insulin glulisine) has asparagine at B3 replaced by lysine and glutamic acid substituted for lysine at B29 to aid rapid absorption from the SC tissue. It is also formulated without Zn^{2+} to facilitate monomeric insulin formation and has been found to demonstrate slightly faster onset and peak of action than Novorapid® and Humalog®, but overall similar control of glucose levels (Donner and Sarkar, 2019a; Home, 2012; Maikawa et al., 2020). Nevertheless, since insulin binds to its receptor and imparts its biological effects as a monomer, the presence or adoption of the monomeric state of insulin (rate of dissociation) after SC injection is the most essential factor in the use of insulin replacement therapy for the treatment of diabetes mellitus. The overall goal of insulin pharmaceutical preparations, whether alone

or in combination, is to help patients with diabetes mellitus to mimic the physiologic pattern of insulin secretion by pancreatic β-cells and thereby achieving at least approximately (~) metabolic homeostasis (Donner and Sarkar, 2019; Weiss, Steiner and Philipson, 2014; Hilgenfeld et al., 2014).

1.2.2 The evolution of clinically used insulin pharmaceutical preparations

Soon after the first use of isolated insulin extraction from the animal pancreas by Banting and Best for the administration of insulin replacement in a patient with T1DM in 1922, tremendous efforts were carried out to obtain pure and crystalline insulin preparations. Although the first administration resulted in a slight reduction in BG levels, no clinical benefits and severe local reactions, including abscesses were also observed owing to the insulin extract impurities. Thanks to Collip, who subsequently provided a better extract of insulin with higher purity for further testing. It was reported that frequent administration to the same patient over the first 24h of insulin treatment resulted in immediate improvement, with BG levels dropping from 28.9 mmol/L to 6.7 mmol/L and glucose excretion reducing from 71.1 to 8.7 g. Ketonuria was also eliminated, following improvements in associated symptom. This purer and more consistent extract of insulin resulted in fewer injection-site reactions, emphasising the importance of purification to obtain an insulin extract as pure as possible (Vecchio et al., 2018; Wright Jr, 2020; Zimmerman, Forlenza and Schatz, 2020). Since then, there has been a high demand in the manufacturing of insulin worldwide owing to its life-saving properties for the treatment of T1DM, thereby urging the development of improved large-scale production and purification techniques. The initial approach was to establish the manufacture of bovine and porcine insulin. However, the scaling up in productions of insulin has encountered numerous challenges owing to the heating process for alcohol evaporation. This process often destroyed some of the insulin products thus, leading to a reduction in yields and potency comparing to the original extract. As a result, the production of insulin during this time was inconsistent, with wide batch-to-batch variation in potency, meaning a close monitor of the treatment was crucial. The problem was overcome in 1922 when both Walden and Shaffer's research team independently discovered the isoelectric precipitation

method of insulin purification under mildly acidic conditions. By adjusting the solution to insulin's isoelectric point, the production of insulin at a higher purity with reduced batch-to-batch potency variation has been successful. By 1925, there were 12 different pharmaceutical companies producing insulin, highlighting the enormous global demand for insulin (Karamitsos, 2011; Didangelos, 2011; Hilgenfeld et al., 2014; Heinemann et al., 2019).

After the achievement of crystallised insulin on a large-scale production, it was understood for several years that many pharmaceutical companies could produce principally pure insulin formulated in pharmaceutical preparations from the animal pancreas. Meanwhile, HI extract from human cadaveric pancreases had been available in small quantities since the 1960s. However, due to the limited availability in quantity, it was mainly used as reference material in insulin radioimmunoassay or physicochemical identity tests. Alternatively, it was also used clinically in a restricted manner for skin-testing of insulin-allergic individuals, pharmacokinetic studies and short-term clinical studies (Hilgenfeld et al., 2014). By the late 1960s as many important analytical methods such as partition chromatography and gel filtration were developed, it became progressively clear that insulin purified solely by crystallisation also contained impurities. Steiner et al.,1968 later identified these impurities with a higher molecular weight than that of insulin to be mainly proinsulin, proinsulin intermediates and a covalent insulin dimer. For many years after the identification of impurities in animal insulin pharmaceutical preparations, great efforts were commenced to produce a synthetic version of HI in the belief that HI was preferable to animal insulin (Heinemann et al., 2019; Baeshen et al., 2014; Brange and Volund, 1999; Vecchio et al., 2018).

Figure 1-7 highlights important timeline in the development of pharmaceutical HI preparations.

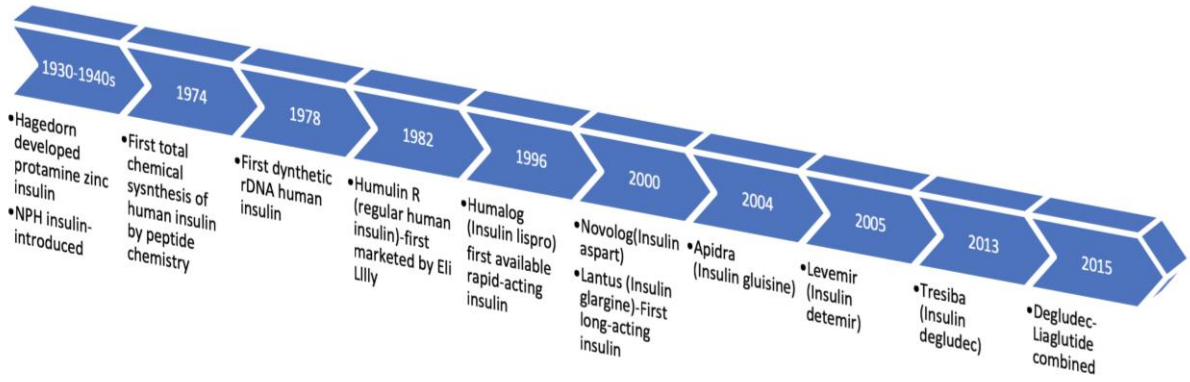

Figure 1-7: Timeline development of clinically available human insulin injections.

Newer generations of insulin analogues have been developed to further improve on many features of an ideal basal insulin regime. These include protracted duration of action beyond 24h without possessing an action peak, having little intra-individual and inter-individual day-to-day variability of action, and minimal risk for inducing hypoglycaemia and incurring weight gain. However, the inherent ability of insulin therapy to cause hypoglycaemia is still recognised as a major drawback in achieving tight glycaemic control in most insulin-requiring patients. Hypoglycaemia is an important adverse event that can potentially impair the patient's quality of life while imposing other burdens such as costly complication. Moreover, nocturnal hypoglycaemia, which occurs during sleep, is particularly dangerous since patients (especially children) are unlikely to recognise symptoms or awake during an episode (Eliaschewitz and Barreto, 2016; Standl and Owen, 2016a).

Table 1-4 summarises different types of clinically used insulin preparations that are currently available in the UK for the treatment of insulin-dependent patients. The details of structural changes will be further discussed in chapter 2.

Table 1-4: Summary of clinically used insulin preparation currently available on the NHS, UK (The information was largely taken from online BNF, EMC and NICE guideline NG17)

Insulin types		Generic/Brand	Peak action	Onset of action	Duration of action	Clinical use & comments
Bolus insulin (prandial) (Short-acting)	Soluble insulin	Human insulin (Actrapid®; Humulin S®; Humulin R®)	Between 1 and 4h	30 to 60min	Up to 9h	For maintenance regimens Administration 15 to 30min before meals
	Rapid-acting insulin	Insulin lispro (Humalog®) Insulin aspart (Novorapid®) Insulin glulisine (Apidra®)	1-3h	Within 10-20min	~ 2–5h	For maintenance regimens Administration immediately before meals. Avoiding routine use of *post-meal* injections Associated with poorer glucose control, increased risk of high postprandial-glucose concentration, and subsequent hypoglycaemia.
	Ultra-rapid-acting insulin	Insulin aspart (Fiasp®) Insulin lispro (Lyumjev®)	30min-2h	Within 10min	3-5h	For maintenance regimens Administration up to 2min before meals or up to 20min after staring the meal. Fiasp® has a quicker onset of action and shorter duration, therefore, is not interchangeable with Novorapid®
Basal insulin	Intermediate-acting insulin	NPH or isophane insulin (Insulatard®; Humulin® M3; Novolin® NPH)	3–12h	~ 1–2h	12-18h and up to 24h depending on the ratio mixed with rapid-acting insulin	Maybe given as one or more daily injections alongside separate meal-time short-acting insulin injections, or mixed with a short-acting (soluble or rapid-acting) insulin in the same syringe
	Long-acting insulin	Insulin glargine (Lantus®) Insulin detemir (Levemir®)	No peak	90min	Up to 24h 16-24h	Both provide insulin cover for 24h, independent of mealtime. Given once or twice daily according to individual requirements.
	Ultra-long acting insulin	Insulin degludec (Tresiba®) Insulin glargine U300 (Toujeo®)	No peak	90min Up to 6h	Up to 24h Up to 36h	Both provide insulin cover for 24h, independent of mealtime. Lower risk of hypoglycaemia

Overall, after the introduction of insulin replacement therapy nearly a century ago for insulin-requiring patients, improvements for this therapy remain a major attention to achieve good glycaemic control. Despite continuous efforts and improvements in the development of various insulin analogues serving as bolus and basal insulin to mimic the normal physiological activity of endogenous insulin, the risk of hypoglycaemia remains the most challenging obstacle for the evolution of insulin therapy to overcome. Nevertheless, the introduction of insulin glargine and insulin detemir as long-acting insulin analogues has showed notable improvement with a significant reduction in the risk of hypoglycaemia, especially nocturnal, compared with earlier-developed intermediate-acting insulin analogues (Swinnen et al., 2010; Standl and Owen, 2016b; Ratner et al., 2013; Rosenstock et al., 2013). The most recently available new ultra-long-acting basal insulin analogues namely insulin degludec and the more concentrated insulin glargine U300 both exhibit superior pharmacokinetic/pharmacodynamics (PK/PD) properties with an even more prolonged action lasting beyond 24h and a much lower variability compared with other clinical used basal insulin preparations (Riddle et al., 2014; Mathieu, Gillard and Benhalima, 2017; Tambascia and Eliaschewitz, 2015). In addition, the development of a more concentrated formulation of soluble HI (Humulin R® 500Unit/mL) has also been beneficial for patients with severe insulin resistance that might require significantly higher insulin dose than others (Dashora et al., 2016; Heinemann et al., 2019). The main clinical benefits of these recently developed basal insulin including the flexibility of insulin administration timing and the lack of weight gain or even weight loss have contributed to an overall improvement in health-related quality-of-life for numerous insulin-dependent patients.

1.2.3 Insulin routes of delivery

Because gastrointestinal enzymes can quickly inactivate insulin, the ideal route of insulin administration has always been to bypass this effect while still mimicking the normal physiological delivery of endogenous insulin and so far, insulin delivery directly into the systemic circulation, i.e., by injection is the most appropriate method (Shah et al., 2016; Matteucci et al., 2015). Currently, SC

administration is the most common and standard route of delivery for exogenous insulin injections. In general, insulin is injected into a body area with plenty of SC fat, usually the abdomen which has the fastest absorption rate or outer thighs/buttocks. Insulin absorption from a limb site can vary considerably (20–40% in both inter- and intra-day), particularly in children. In addition to the effect of various insulin formulations, the rate of insulin absorption is also affected by numerous environmental factors including local tissue reactions, injection site and depth, blood flow, changes in insulin sensitivity and the amount of insulin injected. Furthermore, increased blood flow around the injection site due to exercise can also increase insulin absorption (Taylor et al., 2016; Donner, 2015; Shah et al., 2016; Zhang et al., 2018; Matteucci et al., 2015). There is an increasingly high demand for delivering insulin in the least invasive or non-invasive way with most physiologically acceptable method while still maintaining accuracy and preciseness to reduce patient burden. **Table 1-5** summaries different approachable routes for insulin delivery that are currently used and under investigation for the treatment of diabetes mellitus in insulin-required patients.

Table 1-5: Characteristics of different routes for insulin delivery (Information was largely collected from Shah, R. B. et al., 2016; Matteucci et al., 2015; Zhang et al., 2018; Mikhail, 2016)

Routes of insulin delivery		Advantages	Disadvantages	Clinical remarks
SC	Vial and syringe	Instant delivery of insulin when required	More pain; Patient unfriendly Psychological issues Inconvenient to carry around Reduce accuracy compared with pen	Most frequently used methods.
	Insulin pen	Convenient, easier to use, shorter needle; Reduce pain, more accurate and precise compared with the syringe.	More expensive than the syringe Two insulin types cannot be mixed	No superiority of pen use over syringe for glycaemic control
	Insulin pumps	Greater flexibility with meals, exercise, and daily schedule improved physical and psychological well-being continuous delivery of insulin for smoother glycaemic control	Risk of infection More frequent hypoglycaemia Higher risk of developing DKA Constant physical reminder of diabetes The computerised device can be faulty	Certain criteria need to be met before commencing insulin pump treatment. Need patient education and motivation Better glycaemic control, however, requires contentious CGM (continuous glucose monitor)
Oral		Most preferred form; Non-invasive Delivered directly to the liver via the portal circulation.	Extremely low bioavailability due to GI degradation of insulin. Unpredictable and inconsistent absorption. Variable bio-efficacy.	No oral insulin formulation is commercially available. Very few clinical trial reports with human data
Buccal		Patient-friendly Bypass GI degradation of insulin Non-invasive Increase portal insulin concentration	Poor bioavailability	Oral-lyn approved by FDA in 2009 under the Treatment Investigational New Drug program. Data still lacking appropriately designed and performed phase II and III trials
Intranasal		No interfere with pulmonary function Non-invasive Increase portal insulin concentration	Nasal & local irritation Reduced bioavailability (15-25%)	Nasulin is still undergoing phase 3 trial
Inhale		Rapid absorption due to the large surface area (~145 m^2) and the close proximity of the air and blood compartments Non-invasive	Reduced bioavailability Inhalational device issues Transient cough Reduced lung function	Exubera was withdrawn from the market in 2007 due to low cost-effectiveness. Technosphere insulin (Afrezza) was approved by the FDA in 2014. Uncertainties about efficacy and safety remain in addition to considerably higher cost may result in termination
Intraperitoneal		Direct delivery to the portal vein More physiological	Invasive; Increased cost, risk of infection and portal vein thrombosis.	Long-term data not available
Transdermal		Non-invasive, needle-free	Inefficient passive insulin absorption through the skin Skin irritation, blister formation and redness	No long-term trials Safety not established

1.3 Development of an artificial pancreas as a possible treatment option for people with T1DM and T2DM.

Although it is generally accepted that there is no cure for diabetes mellitus especially in those require exogenous insulin at present, significant time and efforts have been put in all over the world with an attempt to bring insulin replacement therapy as close as possible to mimic the normal endogenous insulin release profile and action to achieve good glycaemic control. To date, the overall development of insulin treatment covering various types of insulin analogues and route of delivery has been targeted to minimise hypoglycaemia episodes experienced by patients while maintaining a good PK/PD profile of exogenous insulin equivalent to normal physiology (Owens and Bolli, 2020; Kovatchev, 2019). Principally, the type of control provided and the site at which insulin is delivered would indicate different methods of insulin delivery classified as open-loop and closed-loop. The open-loop insulin delivery relies on patients administering insulin to themselves at different times of the day whereas the involvement of patients in maintaining glucose control is minimised in the closed-loop method. Although the SC insulin injection remains the most common method of open-loop insulin delivery, further improvement involves the development of the external insulin pump that can provide a basal insulin throughout the day. Notably, all open-loop delivery systems require the involvement of patients or physicians to take BG measurements and consider meal consumption in order determine an empirical estimate of the insulin requirement (Owens and Bolli, 2020; Farmer Jr, Edgar and Peppas, 2008a; Taylor, Sahota and Chauhan, 2019).

One of the most cutting-edge technology in the development of insulin replacement therapy is the introduction of a closed-loop delivery system, referred to as an artificial pancreas. As its name suggests, this system uses man-made technology to mimic the way a pancreas works so that insulin is released in response to changing BG levels as similar to normal physiology. Ideally, this system would be able to determine the insulin requirement in real-time and deliver the proper insulin dosage (Boughton and Hovorka, 2019;

Donner, 2015). Currently, there are three main artificial pancreas systems being studied as summarised in **Table 1-6**

Table 1-6: Summary of currently studied artificial pancreas systems (Information is taken from Diabetes UK, 2019)

Artificial pancreas systems	Academic group/ Company	Latest developments	Insulin delivery mechanism
Closed-loop artificial pancreas	Cambridge University (Hovorka et al.)	European Commission's Horizon 2020 trial to assess the efficacy of the device in children.	The system includes an externally worn insulin pump communicating wirelessly to a CGM worn as a patch on the skin. The CGM measures BG levels and the result is fed into a small computer which calculates the required dose of insulin to be delivered into the body by the insulin pump.
Bionic pancreas	Dr Edward Damiano's Beta Bionics firm	FDA approval in 2018 to begin recruitment for home-use studies testing the insulin-only configuration of its iLet bionic pancreas system in a series of ground-breaking trials in adults and children with T1DM	This automatic BG control system comprises two pumps which deliver insulin and glucagon respectively. The pumps connect with an iPhone app via Bluetooth enabling communication between the CGM device that help make automated dosing decisions about insulin and glucagon every five minutes based on the patient body weight and the updated CGM readings.
Implanted artificial pancreas	De Montfort University (Taylor et al.)	Satisfying performance in glycaemic control has been achieved in diabetic rats and pigs. Human trials are still waiting to be commenced.	The implantable insulin delivery device features a smart gel as part of the insulin reservoir that is responsive to changes in BG levels. When BG levels are elevated, the viscosity of this glucose-sensitive gel drops to enable a rapid release of insulin; during low BG levels, the gel remains intact to prevent insulin being released. The implantable system could be refilled with insulin regularly.

Two of the artificial pancreas systems represented commercially and in clinical studies comprise an electronic sensor and pump for SC insulin delivery. However, the implantable artificial pancreas developed by Taylor et al. represents a different innovative system wherein the sensor and delivery system are principally the same component. This device, namely the INsmart, was developed based on a reservoir that insulin can deliver through a smart gel as a function of changing glucose environment. The smart gel is formulated to exhibit a fast gel-sol transition with a response specifically to glucose (detailed in chapter 5). The device is completely implantable in the peritoneal region between the lowest rib and the hip and can be refilled with insulin every few weeks via SC ports accessible on the skin surface. The closed-loop device is proposed to respond rapidly to the presence of glucose in the blood and allow accurate administration of insulin dose, providing that the fast equilibration between glucose from blood to peritoneal fluid and insulin from peritoneal fluid to blood is achieved. Other advantages of this device include no electronic or moving parts; simple to implant and easily refillable; without the need for additional immunosuppressant therapy; not visible externally therefore socially preferable over the external portable pump (Taylor et al., 2016; Jacob, 2015).

The *in-vivo* performance of this intraperitoneal (IP) implantable artificial pancreas was first assessed in induced-diabetic rats using a simpler version of the device. The performance of this closed-loop insulin delivery system was compared over time in diabetic rats against a control system following a protocol that involves the introduction of several glucose challenges and daily assessments of blood glucose level and body weight. Following daily assessment and challenging with large glucose doses, successful glycaemic control was observed in the device containing active gel compared with an inactive gel analogue which served as a control. It was estimated that the outputting response every hour from the device was ~ 0.5 Unit/kg for basal level with 2 Unit/kg to match the demand of high glucose challenges. Notably, this apparently high dose rate was tolerated because the metabolic rate in rats is higher than humans. Eventually, the device was exhausted of insulin, thus emphasising the need for fill and refill mechanism. In addition, in this *in-vivo*

study, the rats were implanted and recover post-operatively with a low insulin output from the device when the diabetic stage had not yet been introduced, whereas insulin delivery should ideally start after recovery when the rats were rendered diabetic. However, since the rats would have normal BG which would not result in a significant drop in the gel viscosity to trigger high insulin release from the device (Taylor, Tanna and Sahota, 2010)

Moving forward, it was necessary to scale up the device to apply to human trials. Consequently, the improved device engineered with filling circuit was surgically implanted to the IP region of domestic pig. In this case, the weight-to-weight insulin requirement of the pigs was essentially the same as for humans. The surgery was developed and diabetes in pigs was induced using streptozotocin on day 4 of the observed period, and BG levels were ensured to reach at least 33 mmol/L on day 15 before filling the device in situ with insulin solution via the subcutaneous ports. There was normal access to food and water with the addition of several oral glucose challenges at weekly intervals while the animals were observed for over 60 days (Taylor et al., 2016).

Preliminary data for insulin delivery to induced-diabetic pigs using IV multiple-dose injection (MDI) in both fasted and fed state were initially collected to investigate the basal dose needed and the boost dose requirement for 60g oral glucose challenges. It was reported that a fasted pig of 35 kg would need a dose of 40–50 Unit/day (loading dose, then 2 Unit every hour) of soluble insulin to reduce BG from >30 mmol/L to between 5 and 10 mmol/L while exposing to hypoglycaemia before the glucose challenge. Whereas in the freely fed pig, 60 to 170 Unit/day doses (2.5–7 Unit/h) was insufficient for basal needs. An additional 3–5 Unit dose prior to the boost doses (in non-fasted animals) given before or at the time of the glucose challenge was insufficient to control the eventual glucose-induced surge, even in the higher basal dose (7 Unit/h) regimen. Furthermore, the timing was critical in which a 5 Unit boost dose given 50min before glucose challenge produced profound hypoglycaemia, whereas a similar dose given immediately before the glucose aggravated a hyperglycaemic state. Despite much surgical practice, only one successful kick was reported. This preliminary study illustrated the difficulties of implementing a

successful open-loop regimen with insulin. However, the same pigs were not used subsequently for the assessment of the closed-loop system (Taylor et al., 2016).

Meanwhile, the results from the implanted pig illustrated that BG levels were successfully reduced from over 33 to under 10 mmol/L within five and a half days after filling the device with regular HI (Humulin® R 500Unit). Glucose challenge responses also demonstrated progressively well glycaemic control in which the increased BG levels observed after introducing high oral glucose challenges (60g) were normalised within 35 min. It was also highlighted that hypoglycaemia was less likely with IP dosage compared to IV injection because of the short half-life in the peritoneal and hepatic environment. After the removal of residual insulin solution on day 11 of good glycaemic control, the occurrence of diabetic BG levels above 33mmol/L was observed only after a further 24 days. This implies that a depot of insulin had remained after insulin reservoir removal, most likely due to insulin precipitation in the smart gel, which was released over time until complete exhaustion. Based on the assumption that about 3 Unit/h were delivered over the seven loading dose days, an average dose of ~ 62.5 Unit every 24h was required to control diabetes from day 21 to day 52, including the increased output necessary to meet the high demand of large oral glucose challenges. This highlights the successful performance of the automatic bolus system without the need for manual insulin injection intervention. The study showed that the implantable artificial pancreas adequately controlled the basal and bolus needs for more than four weeks without any manual insulin adjustment (Taylor et al., 2016; Jacob, 2015). It could be arguable that there was still some pancreatic input from the tested pigs to support their basal and bolus needs, not just from the exogenous insulin held in the device. This can be justified by doing a C-peptide test to confirm if there was any endogenous insulin produced. However, since the BG levels went soaring up again when the device was empty, it was confirmed that the pigs were indeed fully diabetic and would have to rely on the device to meet their basal and bolus needs (Taylor et al., 2016).

1.4 Fluorescent labelling in bioanalytical applications

1.4.1 Fluorescence process and detection

Along modern technology evolution, there has been a wide range of analytical tools developed to gain an understanding of intracellular dynamics and function at a molecular level. Some analytical methods widely used in various applications include absorption spectrometry, fluorescence spectrometry and chemical luminescence. In particular, fluorescence spectrometry offers highly sensitive and straightforward analysis of non-fluorescent biological molecules of interest. Fluorescent probe has become an indispensable tool in biotechnology laboratories as it can offer high sensitivity and selectivity in the detection of specific components from complex bio-molecular assemblies, such as live cells (Suzuki and Yokoyama, 2015). Generally, fluorescent molecules can be used directly or labelled onto other molecules of interest to investigate the locations or structural changes of certain assemblies within the cells. They can also be used to visualise the presence of individual membrane constituents on the cell exterior for the identification purpose. Alternatively, they are also utilised for the verification of various cellular activities such as enzyme action (Crivat and Taraska, 2012; Yue et al., 2019; Wang et al., 2017; Prakash and Rajeswari, 2014; Jensen, 2012).

Fluorescence is usually described as an event where certain molecules referred to as fluorophores or fluorescent dyes absorb, then emit light.as a result of a three-stage process as demonstrated in Error! Reference source not found.

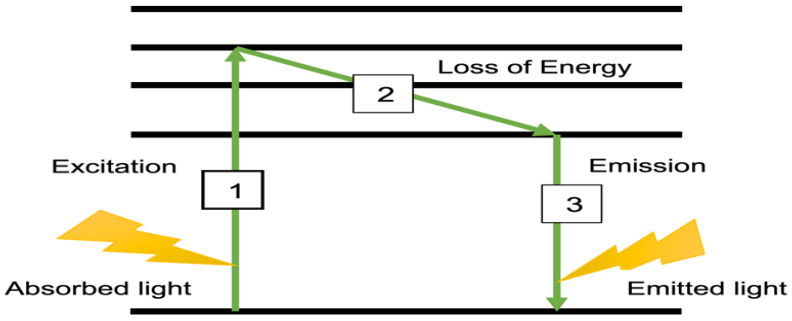

Figure 1-8:Fluorescence process showing the energy difference of excitation state (1) when a molecule absorbs light as energy and remains as its excited state (2) then emits light in the form of fluorescence in the emission state (3).

Within the excitation stage, the fluorophore absorbs a photon of energy from an external source such as an incandescent lamp or a laser, thus raising the energy level of the fluorophore (its electron) to an excited state. Interestingly, this process enables the distinction between fluorescence and chemiluminescence, in which the excited state is stimulated by a chemical reaction. The excited state then exists for a finite time typically 1–10 nanoseconds. During this short period, some of the energy gained from the fluorophore is dissipated by interactions with its molecular environment or transferred to a proximal molecule. A photon is then emitted from the remaining lower energy to bring the excited fluorophore back to its ground state. This associated energy release is known as fluorescence emission (Lakowicz, 2013; Bernard Valeur and Mario Berberan-Santos, 2012). Due to the higher energy relaxation mechanism, the energy of this emission photon is lower, and of longer wavelength than the excitation photon absorbed by the fluorophore in the first stage. For example, if the absorbed light was blue (shorter wavelength) then green light (longer wavelength) will be emitted. Fluorescence emission, therefore, represents the loss of energy from excited state back to ground state that accompanied by the output of radiation such as light. The resultant energy/wavelength difference between the excitation and emission states is described as Stokes shift, which affects the sensitivity of fluorescence detection. This is because it allows the detection of emission photons against a low background, distinct from excitation photons. Notably, a massive Stokes shift can prevent the reabsorption of emitted photons, allowing higher contrast in fluorescent imaging. (Haugland, 2002; Gan et al., 2020; Lakowicz, 2013; Fu and Finney, 2018). Principally, the same fluorophore can repeatedly be excited and detected (a cyclical fluorescence process) providing that it is not irreversibly destroyed (Detail in the next section). It is, in fact, the ability of a single fluorophore to emit numerous detectable photons through this cycle of excitation and emission that gives fluorescence detection its high sensitivity and repeatability in various research applications (Limpouchová and Procházka, 2016; Jameson, 2014; Santos et al., 2020).

Generally, fluorescence spectral data are shown as emission spectra (plots of the fluorescence intensity against wavelength or wavenumber). They can vary widely depending on the chemical structure of the fluorophore and the dissolving solvent (Lakowicz, 2013). Beside those definable factors including the intensity of excitation source and the instrument efficiency for fluorescence collection, the brightness (fluorescence output) of a given fluorophore is also affected by its chemical properties. These include the efficiency of how it absorbs and emits photons, as well as its ability to undergo repeated excitation/emission cycles. Absorption and emission efficiencies are therefore the most useful quantifications for determining fluorescence output.
Fluorescence quantum yield (QY) presents the number of emitted photons by a fluorophore relative to the number of absorbed photons. Fluorophores with a large QY, approaching unity, such as rhodamine will display a bright emission (Wang et al., 2019; Lv et al., 2020; Lakowicz, 2013). The value of molar extinction coefficient (EC) for absorption efficiency indicates how effectively the fluorophore absorbs light, specifically at a single wavelength (usually the absorption maximum). It is defined by the Beer-Lambert law as $A = EC \cdot c \cdot l$, where A = absorbance, c = molar concentration, l = optical pathlength. Overall, fluorescent intensity/brightness of a given dye, which is an important feature for the selectivity of suitable fluorescent probes, is determined by the product of EC (at the relevant excitation wavelength) and fluorescence QY (Thorn, 2017; Villamena, 2017).

1.4.2 Fluorescent labelling methods and choice of fluorescent probes

Fluorescent labelling is a process in which biomolecules of interest such as proteins are covalently tagged by fluorescent probes so that they can be visualised by fluorescence imaging. Here, the fluorescent signal represents the position of the tagged molecules as the label is covalently bonded and does not detach easily. Nowadays, fluorescent labelling method is widely used for detection purpose in many bioanalytical applications and often supersedes the use of radiolabelling. This is because it can offer a more stable, highly sensitive (even at low concentrations), safer, easier and inexpensive alternative over radiolabelling. It also enables multiple detections of many molecules at the

same time (Santos et al., 2020; Man, Gawne and de Rosales, 2019; Fu and Finney, 2018). Furthermore, its additional properties such as sensitivity to the environment i.e. pH, visibility against a dark background and fluorescence lifetime also offer many more applications. One most significant advantage of fluorescent labelling over radiolabelling is that it does not damage the targeted molecule's structure and is therefore preferable in many live-cell studies (Jameson and Ross, 2010; Wysocki and Lavis, 2011).

Another key consideration is the brightness of the fluorescent tag, which is typically assessed based on its fluorescent intensity as detailed in section 1.4.1. In general, a larger value indicates a brighter fluorescence output. In addition, the fluorescent intensity can also be affected by the surrounding environment of the tagged protein (pH or salt concentration). It is well established that the fluorescent tag of many proteins is quenched at low pH, thus can cause problems when analysing in acidic environments (Shinoda, Shannon and Nagai, 2018; Stoddard and Rolland, 2019; Thorn, 2017). Another related issue is the photo-stability of the fluorescent tag. All fluorescent molecules can undergo side reactions when repeatedly excited that may result in the destruction of a fluorophore, leading to loss of fluorescence over time, described as photobleaching. How rapidly this occurs is nonlinearly dependent on the excitation light intensity and the illuminated period of a fluorophore, thus the experimental design is equally important for consideration. Furthermore, the effects of the tag on the protein including size, solubility, biological activity or partition coefficient must also be considered to ensure the normal activity of native proteins is minimally affected. (Thorn, 2017).

The first-ever used fluorophore synthesised in 1871 was fluorescein (FSC) which exhibits excitation at 490 nm and emission at 514 nm. It is made up from two xanthene moieties, each of which contains two benzene rings joined together by a pyran ring (Nishi et al., 2015; Ikeno, Nagano and Hanaoka, 2017). To improve its biological, chemical and fluorescent properties and especially its stability, various forms of FSC derivatives have been synthesised such as Oregon Green, FITC, fluorescein diacetate and carboxyfluorescein (Zheng et al., 2013; Rajasekar, 2020). There is also the family of FSC-like dyes such as

eosin Y, erythrosin and rose bengal (Zhang, Zhang and Liu, 2014). FSC and its derivatives have been the most commonly used reagents for covalently labelling proteins via their amine-reactive groups owing to their availability for several decades and relatively cheap and straightforward labelling methods. Another remarkable point for these labelling candidates is that their conjugates are not exceedingly susceptible to precipitation at physiological pH and can be prepared in high purity. However, in addition to their excellent water solubility and fluorescent quantum yield as well as relatively high absorptivity, FSC-based dyes and their conjugates are highly pH-dependent and prone to photobleaching. Regardless, their applications are broadly limitless in various bioassays/biomaterials and life science. These include cell assays such as flow cytometry or fluorescent microscopy, FRET-based assays, probing (fluorescent hybridisation) as well as microarray/biochip assays (Crivat and Taraska, 2012; Prakash and Rajeswari, 2014; Sahoo, 2012; Aderinto, 2020).

Similarly, alternative fluorophores like rhodamine and its derivative such as tetramethylrhodamine isothiocyanate (TRITC) were also extensively used in various bioassays/biomaterials including cell assays (fluorescent cytomics), probing and microarray/biochip assays (Zheng et al., 2013; Nishi et al., 2015). To improve photo-stability and increase brightness, newer candidates such as AlexaFluor and DyLight Fluor dyes were also developed. In addition to having greater photostability and brightness, they are also more advantaged with lower pH sensitivity than conventional dyes while maintaining comparable excitation/emission profiles. However, they are relatively more expensive. These newly developed AlexaFluor dyes have been used in various bioassays/biomaterials, such as biosensing (magnetic modulation biosensing), probing (small molecule fluorochrome assay) and microarray/biochip assays (Kobayashi et al., 2009; Li, Tebo and Gautier, 2017; Sabnis, 2015). Overall, the availability of various fluorescent probes and improving properties of newly developed probes have enabled great flexibility in selecting a fluorophore of choice for specific bioanalytical applications which are increasingly growing along with new technology and worldwide research in life science.

1.4.3 The use of fluorescent probes for detection techniques in bioanalytical applications

Fluorescence-based assays have become increasingly useful for the study of numerous biological processes down to single cellular level since the first use in the early 1900s to stain tissues, bacteria, and other pathogens for various biological investigations. The movement of individual proteins in real-time can also be visualised through the fluorescent assay. Nowadays, there have been numerous applications of fluorescence-based technology such as metabolic enzymes and DNA sequencing as well as investigation of biomolecule dynamics cell signalling and adaptation (Alam, Vedaei and Wahid, 2020; Khan, Fortunato and Leiknes, 2019). For example, the use of fluorescence in situ hybridisation (FISH) has enabled the identification of specific DNA sequences in cells to detect numerical and structural abnormalities of chromosome (Cui, Shu and Li, 2016) or the use of genetically encoded fluorescent probes (GEFPs) to investigate metabolic alterations in cancer (Depaoli et al., 2019). All of these have contributed greatly towards the understanding of various disease stages like in neurodegenerative diseases and liver metastasis, thus providing data to help with possible treatment (Zhou et al., 2020; Werner et al., 2019; Lavaud et al., 2020).The high selectivity of fluorescent probes to target specific organisms has also led to new paths for resolving many industrially and medically related problems in areas like public health, the safety of foods and environmental monitoring. For instance, fluorescence imaging is particularly useful in tracking drug delivery both *in-vitro* and *in-vivo* for advanced drug development as well as diagnosis of disease including cancer (Zavvar et al., 2020; Dong et al., 2020). Due to its preferably non-invasive approach, the use of fluorescent technology for molecular imaging is widely considered the future for medical imaging (Sano et al., 2012; Kobayashi et al., 2009; White and Errington, 2005; Thorn, 2017). Overall, the increasingly indispensable use of fluorescent molecule as a tool for detection techniques has become the standard in many bioanalytical applications especially those of interest in biomedical research. **Table 1-7** summaries some of those remarkable applications using fluorescent-based technology.

Table 1-7: Summary of some remarkable applications of fluorescent-based technology.

Applications	Fluorophores used	Labelled conjugates	Remarks	References
Medical diagnostic imaging	AlexaFluor680 (Alexa680) Indocyanine Green (ICG)	Alexa680-panitumumab ICG-trastuzumab	Two-colour activable fluorescent probes administered as a cocktail enabled multi-colour target-specific fluorescence breast cancer imaging. The images have visualised a specific receptor expression in each breast tumour without post-image processing. It is useful for in-vivo characterisation of breast cancers.	(Sano et al., 2012)
In-vivo imaging of the blood vessels	3-Azido-7-hydroxycoumarin	Hydroxycoumarin-dextran 70 kDa (HCD-70K)	The development of a bright blue fluorescence dextran has been proven to be advantageous for stable vascular visualisation and detection of blood leakage, especially in combination imaging with red- and green-labelled pathogens and immune cells.	(Lee et al., 2019)
Molecular Neurobiology	FITC	FITC-Ghrelin	The use of FITC labelled ghrelin has enabled the visualisation of ghrelin uptake by cells of the blood-cerebrospinal fluid (CSF) and the quantification of ghrelin diffusion onto the periventricular tissue of the brain where it can mediate rapid effects.	(Uriarte et al., 2019)
Investigation of biochemical processes at a molecular level in living cells	Rhodamine B	Rhodamine B-pentacyclic triterpenes	Achievement of a direct visualisation of the antiviral mechanism (by targeting influenza HA protein) of pentacyclic triterpenes and the confirmation of their accumulated location after being taken up by MDCK cells.	(Li, M. et al., 2020)
In-vitro and *In-vivo* study of drug delivery system for cancer treatment	Indocyanine green (ICG)	ICG labelled aptamer (AS1441) ICG labelled AS1441-C_8 ligand conjugate.	AS1441-ICG complexes were used as fluorescent tracers to track their accumulation in tumoral cells and a melanoma mouse model to investigate the biodistribution of anticancer C_8 ligands. AS1441-ICG is promising drug delivery agents for targeting tumoral cells in melanoma cancer models.	(Lopes-Nunes et al., 2020)
Cell-Based Genetic Diagnostic	FISH	Cas9-mediated FISH (CASFISH) Oligopaint-FISH Single-molecule RNA FISH (smRNA-FISH)	The use of FISH technology enabled the detection genetic disorders from chromosomal abnormalities to sub-microscopic copy number variants (CNVs) and the extension of the cell-based analysis from metaphases to interphases	(Cui, Shu and Li, 2016)

1.4.4 The use of fluorescently labelled insulin in biochemical research and drug delivery

Since the discovery of insulin over a century ago, insulin remains as one of the most intriguing molecules of interest and has been studied extensively owing to its indispensable role. It has a small molecular weight yet possessing the typical structural features of many larger proteins. Various approaches have been carried out worldwide to study insulin at molecular and cellular levels. These include insulin structural configurations, its synthesis and release from the pancreatic β-cells, the binding mechanism to its receptors, its biological activity as well as the delivery of exogenous insulin by various routes (Asthana et al., 2019; Wasko et al., 2020; Iannuzzi et al., 2017; Ferri et al., 2019). Fluorescently labelled insulin was used back in the 1960s to investigate the localisation of insulin in different tissues (Tietze, Mortimore and Lomax, 1962; Maggi, 1966). Up to now, it still plays an indispensable role in the study of insulin biodistribution and pharmacokinetics for advanced insulin delivery via various routes (Caprifico et al., 2020; Sudhakar et al., 2020). Moreover, in advanced drug development and delivery, fluorescence studies have clarified aspects such as biodistribution, stability and metabolism with respect to the complexities imposed by the biological systems. These include cell/tissue penetration, drug-target interaction, and the pharmacodynamic consequences, thus emphasising the usefulness of fluorescently labelled insulin in research and drug delivery (Sudhakar et al., 2020; Pandey et al., 2018; Lochhead et al., 2019).

There have been several studies that use fluorescently labelled insulin to investigate the advanced delivery of insulin through various routes including oral, intranasal, transdermal and implanted artificial pancreas (Lee et al., 2020; Lochhead et al., 2019; Chen, Shyu and Chen, 2018; Jacob, 2015). For instance, FITC- insulin was used to investigate the intracellular localisation of insulin in vitro through the delivery of bio-mineralised insulin nanoparticle (BINP) in a liver cell line. Interestingly, the intracellular delivery test showed that there was no detectable intracellular FITC signal in the control group (free FITC-insulin not formulated as bio-mineralised insulin nanoparticle) using insulin resistance induced human hepatoma (R-HepG2) cells, suggesting that free FITC-insulin in its molecular form was not able to enter cells. In contrast, intense green fluorescence was observed intracellularly when BINP solution was applied to the insulin-resistant cells. Also, the uptake kinetics of

BINP were further quantified using flow cytometry and the result showed that 96% of the cells contained insulin within its intracellular fluid only after 30min of insulin stimulation. This value gradually reached 100% after 2h, suggesting that the cellular uptake of BINP in insulin-resistant cells was rapid and highly efficient. Although a therapeutic effect of BINP via the intraperitoneal route of delivery on long-term improvement of glucose metabolism was further confirmed in mice, it is still in question for the reason behind the inability of R-HepG2 cells to uptake any free FITC-insulin molecules despite showing 50% glucose metabolism of normal cells. Overall, the study offered an alternative strategy for T2DM treatment with insulin by introducing mineralisation of insulin with calcium ions to improve its intracellular delivery (Xiao et al., 2017).

Lochhead et al.,2019 also used FITC-insulin to investigate the distribution of insulin in trigeminal nerve and brain via intranasal (IN) administration to rats. Although details in the production and identification of FITC-insulin species were not given, their fluorescent signal data suggested that insulin can be delivered to the brain via the nasal passages along the perineural spaces of the trigeminal nerve. Insulin distribution along cerebral perivascular spaces was also visualised after 30mins of IN administration. Their data suggested that insulin administrated via the IN route can reach the brain areas with high expression of insulin receptors (IR) like the cortex. Interestingly, the FITC-insulin conjugate used in the study was also confirmed by SDS-PAGE electrophoresis to be primarily monomeric, which is the biologically active form of insulin. However only native insulin was used to examine the activation of IR in brain cells and their Western Blot data illustrated significantly higher level of phosphorylated IR in the brains compared to the saline control. The study also indicated the uncertainty of using fluorescently labelled insulin to investigate the biological activity of insulin as certain modifications to the insulin molecule by the fluorophore may affect how labelled insulin bind to the IR.

FITC-insulin has also been used to determine the different degree of labelling effect on the hydrophilicity and lipophilicity of the insulin molecule that may alter its permeability through a cell monolayer. They found that the unlabelled insulin and its mono-labelled conjugate with FITC demonstrated significantly higher transport than tri-labelled conjugate. It is proposed that the slight increase in permeation of mono-conjugates could be due to the lipophilicity induced by FITC molecule, whereas the

decreased permeability of tri-conjugates may be contributed by the size increase by over 1000Da in molecular weight of tri-labelled FITC-insulin conjugate (Shah et al., 2019). However, it is important to highlight that the low purity of the conjugates produced could jeopardise the interpretation of the results.

Not only applied in insulin drug delivery, but a recent study also demonstrated the use of Alexa488- insulin to investigate the cellular behaviour and intracellular signalling properties of insulin with ageing. For the first time, the cellular journey of insulin has been fully explored in the liver cells of young and aged pigs from insulin signalling response, its internalisation dynamics (nuclear localisation), endocytosis pathway down to post-endocytic sorting of insulin and insulin receptor. It was justified from a medical point of view that pigs would be a better model to study the role and cellular biology of insulin compared to the rodent model, especially for insulin resistant with ageing. In addition, porcine insulin can also be used for human diabetes treatment and it only has one amino acid difference to HI. There are three key points highlighted in the study including the inability of insulin to enter the recycling endosome or translocate into the nucleus in aged pig hepatocytes, which suggested that their mechanism of insulin clearance is different compared to the young pig hepatocytes. The second point was the significant reduction in insulin signalling response with age. Lastly, there was a series of changes in the cell behaviour of insulin between the young pigs and the aged pigs, which could contribute to insulin resistance with ageing. The study has suggested a potential contribution to insulin resistance with ageing from a cellular level perspective (Li, S. et al., 2020).

Overall, the use of fluorescently labelled insulin in research and drug delivery has become increasingly useful in the understanding of insulin kinetics profiles for advanced drug development because it can offer high sensitivity, ability to visualise high contrast image and reasonably inexpensiveness. Despite its numerous applications in advanced drug delivery development, there were very little studies addressing the quality and characterisation of the fluorescently labelled insulin being used. Chapter 2 covers important aspects of labelling modification to investigate the quality of FITC-insulin conjugate produced in-house. It is emphasised that the degree of labelling can affect the overall structure and activity of native insulin depending on the number of labels and their tagged position.

Chapter 2. Synthesis and identification of FITC-insulin analogues conjugate

2.1 Introduction

In this chapter, the use of FITC as the fluorescent probe of choice for labelling insulin will firstly be discussed, followed by a general overview of insulin receptor structure and binding sites. Different commercial insulin products will also be presented with details about changes in their structure and formulation. There will also be a summary of key findings from previous studies on the synthesis of fluorescently labelled insulin conjugates. The practical work will involve screening most of the clinically used commercially available insulin preparations that have modifications in their amino acid sequences to select the best candidate for synthesising the desired Mono labelled FITC-insulin conjugate. The process of synthesis, purification and identification of FITC-insulin conjugate will also be described. The objective is to modify specific reaction conditions such as molar ratio, reaction time and pH to produce the most biological active FITC-labelled insulin at the B1 position.

2.1.1 FITC– the fluorescent probes of choice

FITC is still the fluorophore of choice to label proteins and other biomolecules because of its relatively high absorptivity and excellent fluorescence quantum yield in aqueous media. Furthermore, its covalent conjugation with protein is not susceptible to precipitation. FITC is the derivative of FSC with an isothiocyanate (ITC) reactive group, which is reactive towards amine and sulfhydryl groups commonly found in biomolecules. FITC isomer I is more easily isolated in pure form and is, therefore, less expensive than the isomer II with the thiocyanate group on the 5-carbon atom of the benzene ring instead of 4 (Yan et al., 2017), as shown in **Figure 2-1**.

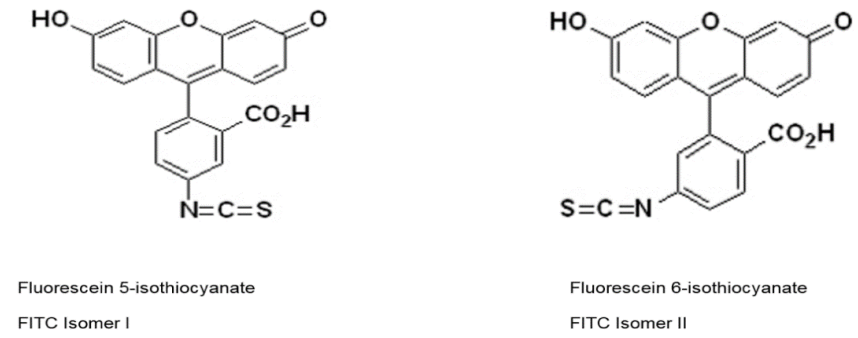

Figure 2-1: Structure of Fluorescein isothiocyanate isomers (Taken from Fluorescent probes G.T. Hermanson 2013)

FITC exists as a fine yellow-orange powder which is quite hygroscopic with a molecular weight of 389.4 Da. It is highly soluble in acetone (1mg/mL), in anhydrous dimethyl sulfoxide (DMSO) at 5 mg/mL and to a lesser extent at 9 mg/ml in 2-methoxy ethanol and 20 mg/mL in ethanol. Although FITC is soluble in water at 0.1mg/mL, it rapidly decomposes; therefore, an organic solvent is preferable. Its ITC group reacts with amino-terminal and primary amines in proteins, forming covalently bonded conjugates (**Figure 2-2**)

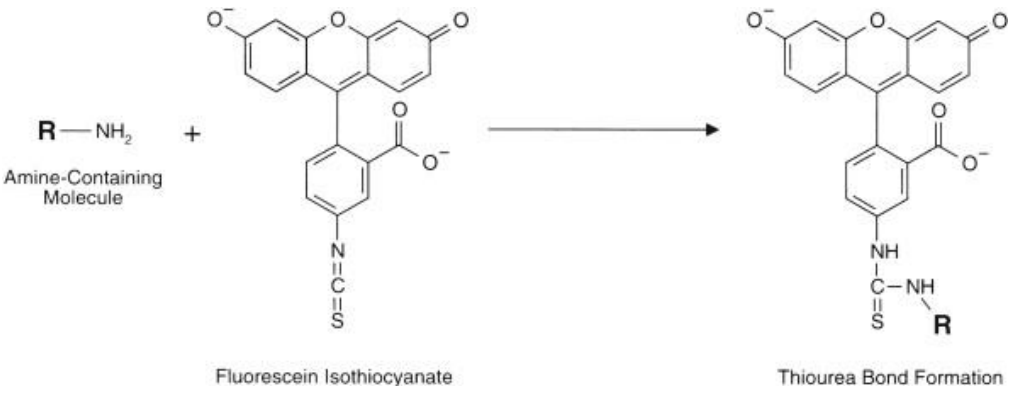

Figure 2-2: FITC reacts with amine-containing compounds (Taken from Fluorescent probes G.T. Hermanson 2013)

FITC displays a maximum absorption excitation at 494 nm and emission at 519 nm in the visible range of the spectrum. Owing to its closely matching maximum excitation with the 488 nm spectral line of the argon-ion laser, FITC is indeed an important fluorophore for flow cytometry applications and confocal laser-scanning microscopy (Haugland, 2002; Johnson, 2019). It is widely applicable to fluorescently label proteins via the amine group in various biological research

such as protein tracing and micro-sequencing of proteins. It is also used as a reagent in fluorescent antibody techniques for the rapid identification of pathogens as well as in medical practices like FSC angiography and FSC-guided surgery (Rodríguez-Sáinz et al., 2013; Yeo et al., 2016; Lepore et al., 2018; Acerbi et al., 2018).

Despite being the most common fluorophore to covalently label proteins, FSC-based dyes and their conjugates do have some drawbacks. Especially the high rate of photobleaching and pH sensitivity spectra between pH5 and pH8 could cause a problem to quantitative measurements. There have been no new dyes available that can completely solve photobleaching problems seen by FSC dyes although newer alternatives such as AlexaFluor 488 or Oregon green 488 are much more photostable and have less pH sensitivity in the physiological pH range. Nevertheless, FITC has remained as one of the most useful reactive dyes partly due to its well-established applications in research and medical practice but also because of the low cost and widespread availability of optical filter sets designed to efficiently excite and detect its fluorescence (Warrier and Kharkar, 2014; Yan et al., 2017).

FITC conjugation with antibodies, proteins and clinical drugs have been widely used in many biological applications and research. However, their stability profiles have not been fully investigated and therefore it is difficult to establish how stable they are in various biological applications (Broadwater et al., 2019; Icha et al., 2017). So far, an extensive study by Reeves et al. 2012 was one of the very few that investigated the stability, safety and suitability of FITC-labelled conjugates using both *in-vitro* and *in-vivo* models. There was very little or no photobleaching (irreversible loss of fluorescent property) and phototoxicity (cellular damage caused by prolonged illumination with high laser power) observed *in-vitro* using their synthesised FITC-BSA conjugate compared to commercial products. A dorsal microcirculatory chamber implanted in rats was also used to examine whether varying the illumination duration and repeated administration of the synthesised FITC-BSA conjugate in conscious animals would lead to microvascular instability. The results showed that de-conjugation would occur after 4h causing fluorescence leakage into the interstitium.

Repeated administration studies indicated that the FITC-BSA conjugate synthesised inhouse can be repeatedly administered to conscious animals at weekly interval without resulting in damage to the microcirculation. There was also no sight of long-term side effects reported (Reeves et al., 2012). Meanwhile, a more recent study by Salari et al. 2019 has examined the potential cytotoxic level of FITC-labelled nano-cellulose using a cellular gut epithelium model. The results showed that the FITC-tagged materials were not cytotoxic, and they also have comparable bioactivity to their native counterparts hence making them suitable for biological studies (Salari et al., 2019).

Overall, the fluorophore probe of choice should ideally be small, stable, bright, non-toxic, reasonably inexpensive and do not interfere with the biological property of the tagged molecule. The chosen fluorophore should also be selectively specific, able to label multiple proteins at the same time and have no tendency to oligomerise (Toseland, 2013). However, it may not always be possible to achieve all criteria of an ideal label for a specific experiment. Despite some drawbacks in photobleaching and pH sensitivity, FITC is the best compromise for this project, considering it is relatively cheap and widely applicable in various studies, therefore providing adequate background information to its suitability.

2.1.2 Insulin receptor structure and binding sites on the insulin molecule.

Many studies of insulin analogues have enabled mapping of the interactive residues on the surface of the molecule. These demonstrated how the authenticity of insulin folding could affect its activity. It is necessary to highlight the importance of certain insulin residues involved in insulin-insulin receptor recognition and binding for understanding the impact of fluorescent labelling on specific sites of the insulin molecules and therefore affecting its activity.

Insulin receptor (IR) belongs to a family of receptor- tyrosine kinases (RTKs), which phosphorylate their substrate proteins on tyrosine residues. There are primarily two subunits within an IR: the extracellular α-subunit containing the ligand-binding site where insulin molecules can bind to and the transmembrane β-subunit, which is involved in intracellular signaling. The IR comprises two

monomers (αβ), also known as a homodimer that are linked together by disulphide bonds. The extracellular portion of each IR monomer consists of six domains, including the first leucine-rich repeat domain (L1), a cysteine-rich region (CR) followed by a second leucine-rich repeat domain (L2) and three fibronectin type III domains (FnIII-1, Fn-III2, and FnIII-3), with FnIII-2 containing a large (~120 residues) insert domain (ID). The ID contains the furin (α/β) cleavage site yielding the α-chain and β-chain (IDα and IDβ) of the mature receptor monomer. Ending the α-chain component of the ID is the carboxy-terminal α-chain (α-CT) segment. The intracellular C-terminal region of the IR monomer contains the tyrosine kinase (TK) catalytic domain bordered by two regulatory regions of the trans- and juxta-membrane domains (TM/JM) and lastly the C-terminal tail region (Menting et al., 2013; De Meyts, 2016; Scapin et al., 2018). The layout of the IR domains (from the N-terminal α chain to the C-terminal β chain) is illustrated in **Figure 2-3**.

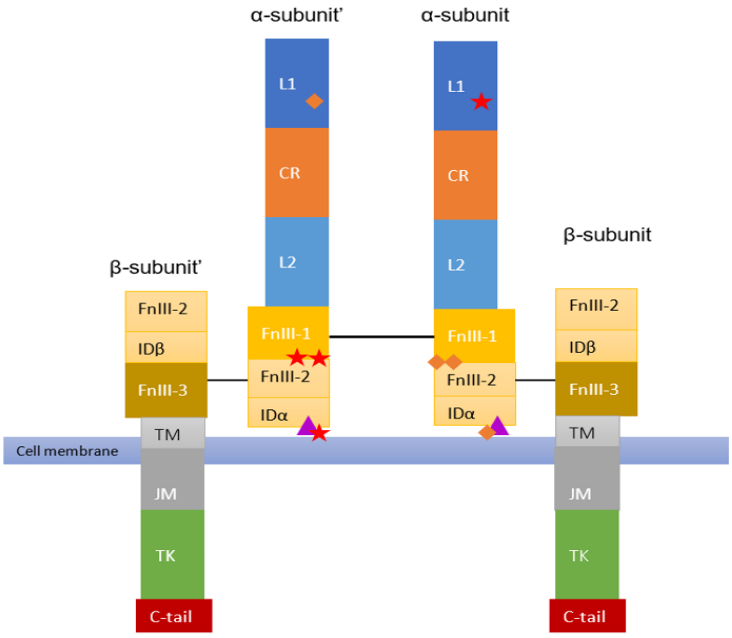

Figure 2-3: Insulin receptor homodimer domains layout showing the disulphile bonds in black, the α-CT segment in purple triangles, the first binding site pair in red stars (1 star for IR-site1 and 2 stars for IR-site2) and the second binding site pair in orange diamonds (1 diamond for IR-site1' and 2 diamonds for IR-site2'). (Adapted from Menting et al,.2013)

According to De Meyts et al. 2015 and Lawrence et al. 2014, the current model for insulin molecule binding surfaces of the IR homodimer involves two different

binding sites, located on separated regions of each alternate IR monomer**.** The first site also referred to as the low-affinity site (IR-site1), involves residues within the L1 domain of α-subunit and the α-CT segment on the other α-subunit' (marked as red star in **Figure 2-3**)**.** The second site (IR-site2) involves residues at the FnIII-1/ FnIII-2 junctions (marked as two red stars in **Figure 2-3**) of the α-subunit' opposite to that contributing to the L1 region of IR-site1 (they are distinguished by α-subunit and α-subunit' in **Figure 2-3**). It is highlighted that within an IR homodimer, there are two pairs of IR binding site from each alternate IR monomer. One composes the IR-site1 of the α-subunit and the IR-site2 of the opposite α-subunit' and vice versa (the other pair is marked as orange diamond in **Figure 2-3**). Furthermore, the ectodomain IR homodimer is also understood to show a two-fold symmetric inverted "V" conformation. One strand of each monomer consists of the FnIII-1, -2, -3 modules extended in a linear arrangement from the cell membrane upwards and the L1-CR-L2 modules folding over downwards. Within an IR dimer, the L1-CR-L2 modules of one monomer are packed against the FnIII-1, -2, -3' modules of the alternate monomer (De Meyts, 2015; Diwanji, Thaker and Jura, 2019; Ye et al., 2017) as illustrated in **Figure 2-4**.

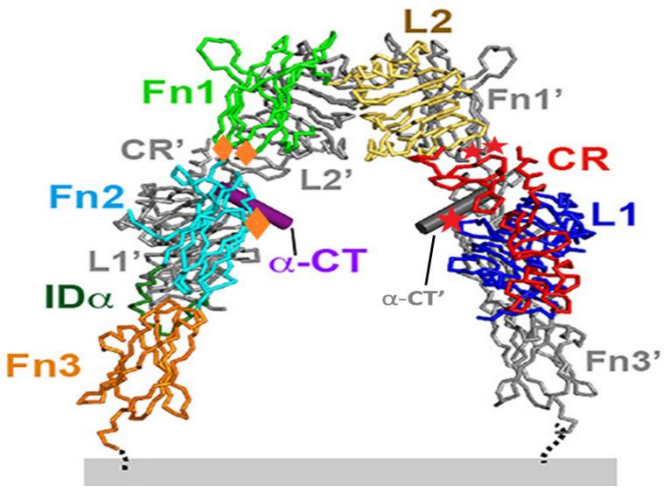

Figure 2-4: Structure of the ectodomain IR homodimer in a two-fold symmetric inverted "V" conformation showing the binding site pairs in red stars (one star indicates IR-site1 and two stars indicate IR-site2) and orange diamond (one diamond shows IR-site1' and two diamonds represent IR-site2') (adapted from Diwanji, Thaker and Jura, 2019)

Menting et al. 2015 also described that there are two surfaces of an insulin molecule interacting with the two IR binding sites. The first surface mainly involves residues derived from insulin's dimerised conformation that contact IR-site1. While the residuals predominantly drew from insulin's hexameric surface are proposed to interact with residues of IR-site2. Once insulin binds to the IR-site1 on either side of the α-subunits, a second binding event occurs between the bound insulin and the IR-site2 of the opposite IR α-subunit. It is understood that two insulin molecules cannot bridge both IR-site1 and IR-site2 pairs on one side of the IR homodimer and the corresponding pairs on the alternate side simultaneously hence resulting in negative co-operativity. This is because high-affinity binding can only occur between either single pair within one IR dimer or the corresponding pair of the alternate side (Xu et al., 2018; Weis et al., 2018; Menting et al., 2013; De Meyts, 2016).

Figure 2-5 shows two surfaces of insulin molecule that involve in IR binding region.

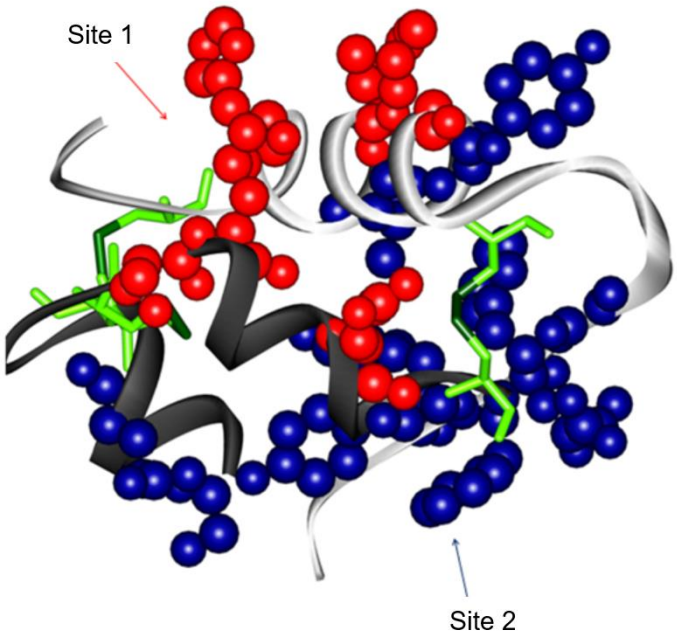

Figure 2-5: Two binding surfaces on insulin molecule: The red residuals represent binding site 1 and residuals from binding site 2 are in blue. Note that binding site 1 is partially covered by the C-terminus of the B chain (Taken from Correial et al., 2012)

The classical binding surface, referred as site 1, comprises several residues in the dimer-forming surface including both A-chain residues A1(Gly), A5(Gln), A19(Tyr), A21(Asn) and B-chain residues B24(Phe), B25 (Phe), B26(Tyr), B12(Val), B16(Tyr) with some of the hydrophobic residues buried beneath the C-terminus of the B chain. Site 2 includes A12 (Ser), A13(Leu), A17(Glu), B10(His), B13(Glu) and B17(Glu) residuals which contribute to the hexamer surface of insulin molecule. Notably, the primary binding motif that links between site 1 and site 2 was the central helix of B-chain insulin. Upon receptor engagement of the insulin molecule to the ectodomain of IR**,** insulin would rearrange itself by displacing the C-terminal B chain residues B20-B30 from its helical core**,** thereby inducing structural changes in the β subunit of the IR intracellular domains. This change removes the inhibitory effect on the intracellular TK domains, thus allowing them to trans-phosphorylate each other and initiate the insulin signalling pathways (Uchikawa et al., 2019; Menting et al., 2013; De Meyts, 2016)**.** The overall receptor binding and activation process highlights the importance of certain sites of the insulin molecule for the IR recognition and the receptor compatibility to initiate insulin response. It is stressed that the degree and position of FITC substitution at particular sites on the insulin molecule would affect its structural conformation as well at its interaction with the IR binding sites and therefore the biological activity of insulin.

2.1.3 Different types of clinically used commercially available insulin preparations based on human insulin

HI was successfully made using recombinant-DNA (rDNA) technology in the early 1980s. Nowadays, clinically used insulin preparations are either neutral or low-pH solutions. These insulin analogues have modified amino-acid sequences (except for Humulin® S and Actrapid® which are essentially the same as HI but do not originate from human) with improved pharmacokinetic properties according to general principles of protein folding and assembly. However, they all have the insulin hexamer as a typical structure unit (Berenson et al., 2011; Nagel et al., 2019). It is essential to recognise the primary structural modifications between different insulin analogues on understanding the impact

of fluorescent labelling on specific sites of the insulin molecule. The production of short-acting insulin analogues (Humulin® S and Actrapid®) uses rDNA technology with the same structure as natural HI thus have similar absorption profile and mode of action (refer to **Table 1-4**). Apidra®, NovoRapid® and Humalog® containing insulin glulisine, insulin aspart and insulin lispro respectively have been produced with reduced self-association properties or accelerated hexamer dissociation properties leading to rapid absorption than regular insulin hence classified as rapid-acting insulin analogues (Danne, Heinemann and Bolinder, 2019; Jacob, 2015). Newer generation of rapid-acting insulin analogues include Fiasp® and Lyumjev®. They have the same active molecules as in NovoRapid® and Humalog® respectively. However, the formulation of Fiasp® also contain niacinamide (Vitamin B3) to increase the initial absorption rate of insulin aspart and L-arginine to aid in stabilising effect. Meanwhile, Lyumjev® utilises treprostinil and citrate excipients to accelerate the absorption of insulin lispro from the administration site. The improved formulation of Fiasp® and Lyumjev® to increase the absorption of their active molecules results in a faster insulin time-action profile and in earlier glucose lowering when compared to NovoRapid® and Humalog® (Davis, Kuriakose and Clements, 2019; Shiramoto et al., 2020). Long-acting insulin analogues include insulin detemir (Levemir®), insulin glargine (Lantus®). They have been synthesised either by introducing changes in amino acid sequence that reduce its solubility at physiological pH (Lantus®) or by covalent acylation (Levemir®). Insulin glargine has asparagine at A21 position replaced by glycine (to prevents deamidation and dimerisation that would occur with acid-sensitive asparagine) and two arginines added to the C-terminus of the β-chain (**Figure 2-6**), resulting in a shift of isoelectric point to neutrality. After SC injection, the insulin glargine acidic solution (pH 4) is neutralised; leading to the formation of micro-precipitates from which insulin glargine is slowly released. This results in a relatively constant concentration /time profile over 24hrs with no pronounced peak, allowing once-daily dosing as basal insulin (Nagel et al., 2019) . Meanwhile, insulin determir has threonine in position B30 omitted and replaced with acylation of a C14 fatty acid chain (myristic acid) to the lysine residue at

B29 (**Figure 2-6**). This modification allows a delayed absorption of insulin determir from the SC tissue due to increased self-association into hexameric form at the injection site and high degree of reversible albumin binding by a fatty acid chain. Slightly different to Lantus®, Levemir® can be administrated once or twice daily for basal insulin need (Noorden, Knopp and Chase, 2019). The ultra-long acting insulin analogues including Tresiba® (insulin degludec) and Toujeo® (insulin glargine U300) have an extended duration of action of up to 42 hours and 36 hours respectively. Insulin degludec has threonine at B30 position removed and the addition of 16-carbon fatty acid to lysine at B29 via a γ-L-glutamic acid linker (**Figure 2-6**). It is formulated as a soluble di-hexamer which forms stable soluble multi-hexamers after SC injection. The gradual separation of degludec Monomers from the multi-hexamers enables a slow and continuous delivery of insulin degludec from the SC tissue into the circulation (Shimoda et al., 2016; Sharma et al., 2019). The glargine U300 formulation in Toujeo® has a more extended time-action profile than Lantus® because it forms a more compact subcutaneous depot with smaller surface area and volume, thus achieving a prolonged dissolution from the SC tissue (Standl and Owen, 2016c; Hemmingsen, Richter and Metzendorf, 2019).

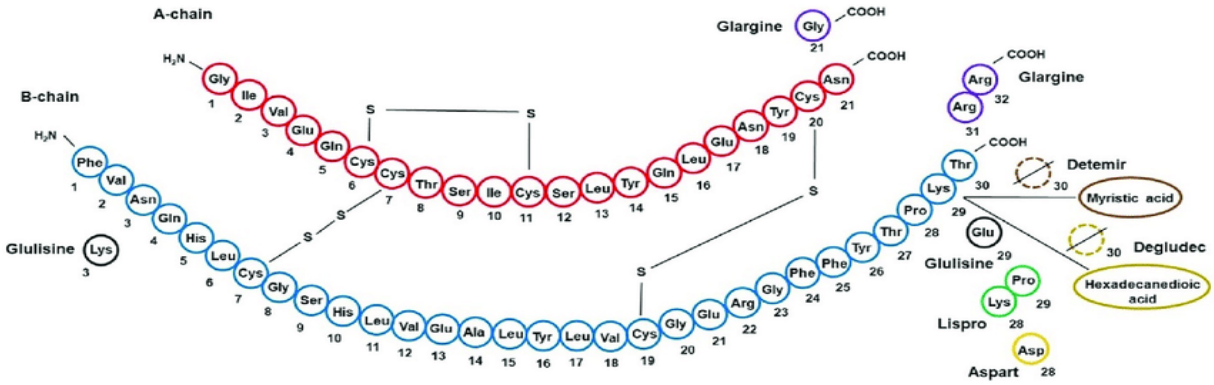

Figure 2-6: Modifications of pharmaceutical insulin analogues compared to human insulin primary structure (taken from Nagel et al,.2019)

Table 2-1 summarises the main differences of some insulin analogues that are used for FITC labelling in this study (the information was primarily taken from product monographs and Jacob, 2015).

Table 2-1: Different types of commercially available rapid-acting and short-acting insulin analogues

Insulin types	Insulin, brands, manufacturer	Differences from natural HI and mode of action	Molecular formulation & mass	Formulation details
Short-acting	HI Humulin S® Eli Lilly	Structurally identical to natural HI thus have similar absorption profile and mode of action	$C_{257}H_{383}N_{65}O_{77}S_6$ 5807.57Da	Colourless, clear aqueous solution. Each mL contains 100 Units of HI (produced by rDNA technology in a special non-disease-producing laboratory strain of *Escherichia coli* bacteria,16mg glycerol, 2.5mg m-cresol, 0.005mg zinc oxide & Water for injection (WFI), pH 7.0-7.8 (adjusted with HCl and/or NaOH).
	HI Actrapid® Novo Nordisk			Neutral, clear, colourless solution containing 100 Units/ mL HI corresponding to 3.5mg of anhydrous HI /mL produced by rDNA technology using *Saccharomyces cerevisiae;* glycerol, m-cresol, zinc chloride and WFI, HCl and/or NaOH for pH 7.0-7.4
Rapid-acting	Insulin aspart NovoRapid® Novo Nordisk	Insulin aspart has proline in position B28 replaced by aspartic acid (**Figure 2-6**) creating charge repulsion and steric hindrance due to local conformational change at the B-chain C-terminus. Reduced tendency to self-associate due to electrostatic repulsion at the dimer interface resulting in rapid absorption→ earlier peak & shorter duration of action than soluble insulin.	$C_{256}H_{381}N_{65}O_{79}S_6$ 5825.8Da	Clear, colourless aqueous solution. Each mL contains 100 Units of insulin aspart produced by rDNA technology using *Saccharomyces cerevisiae,*16mg glycerol, 1.5mg phenol, 1.72 mg m-cresol, 0.0196mg zinc chloride, 1.25mg disodium phosphate dehydrate, 0.58ng sodium chloride (NaCl) & WFI, pH 7.2-7.6 (adjusted with HCl and/or NaOH).
	Insulin glulisine Apidra®, Sanofi-Aventis	The asparagine at position B3 is replaced by lysine while glutamic acid is substituted for lysine at position B29 which is involved in FITC covalently binding site. Glucose lowering activities of Apidra® & regular HI are equipotent when administered by IV route, however after SC administration; the effect of Apidra® is more rapid in onset & for a shorter duration of action as it does not contain zinc ions.	$C_{258}H_{384}N_{64}O_{78}S_6$ 5823Da	Clear, colourless solution. Each mL contains 100 Units (3.49mg) of insulin glulisine produced by rDNA technology using a non-pathogenic laboratory strain of *Escherichia coli* (K12), 3.15mg m-cresol, 6mg tromethamine, 5mg NaCl, 0.01 mg polysorbate 20 & WFI, pH 7.3 (adjusted with HCl and/or NaOH).
	Insulin lispro Humalog® Eli Lilly	The amino acid proline at position B28 and lysine at B29 are swapped over in insulin lispro (**Figure 2-6**) creating steric hindrance and reducing the ability to self-associate so is absorbed more rapidly than regular soluble insulin from SC injection site and also has a shorter duration of action.	$C_{257}H_{383}N_{65}O_{77}S_6$ 5807.57Da	Clear, colourless solution. Each mL contains 100 units (3.5mg) insulin lispro produced by rDNA technology using a non-pathogenic laboratory strain of *Escherichia coli* 16 mg glycerol, 1.88 mg dibasic sodium phosphate, 3.15 mg m-cresol, zinc oxide to provide 0.0197mg zinc ion, trace amounts of phenol & WFI, pH 7.0-7.8(adjusted with HCl and/or NaOH).

2.1.4: The synthesis of fluorescently labelled insulin conjugates from previous studies and key findings

Initial work on the synthesis of FITC-insulin conjugates yielded mixtures with reduced biological activities (Maggi, 1966; Gök and Olgaz, 2004). Fluoresceinthiocarbamyl insulin derivatives of bovine insulin were first prepared in aqueous solution in 1967 by Bromer and his team. However, the products yielded mixtures of mono, di and tri substituted species where the mono-labelled fraction only retained 40% of native insulin activity.

The synthetic method described by Hentz et al. 1997 can be regarded as the seminal work in the production, separation and identification of FITC-labelled insulin but none of the commercially available insulin injections was studied. HI was labelled with FITC by employing four different reaction conditions. These comprised FITC: HI molar ratio of 3:1 and 1:1 at both pH7 and 8.5. These reactions were monitored at different time intervals by HPLC over 20h.The 3:1 reaction carried out at pH 8.5 for 20h had the highest number of FITC-HI species so was chosen by Hentz for further characterisation. The four isolated species were labelled at A1(Gly), B1 (Phe), A1(Gly)B1(Phe) and A1(Gly)B1(Phe)B29(Lys) positions on the amino acid sequence. **Figure 2-7** illustrates the binding site of FITC molecule to insulin.

Figure 2-7:Human insulin structure with yellow stars indicating possible positions for FITC label (adapted from Jacob 2015)

Based on their biological activity measurements using a TK phosphorylation assay, the FITC-HI conjugate labelled at B1(MonoB1) had an equivalent activity to native insulin while the rest showed a decreased biological activity. Hentz proposed that the structure conformational changes and hence the activity of FITC-HI species differ concerning the degree and position of substitution. Consequently, he hypothesised that the B1 position was not considered to be involved in binding to the IR while the A1 site plays a role in forming part of the classical binding site for the receptor since the conjugates labelled at A1(MonoA1) and A1B1(di-labelled) show a ten-fold decrease in biological activity compared to native insulin. Furthermore, the conjugate labelled at A1B1B29 (tri-labelled) have almost 100-fold reduction in activity. This significant reduction suggested that the B29 site has a vital role in receptor binding in which the conformation of the tri-labelled molecules must be altered in such a way that the receptor-binding region on the insulin molecule is no longer recognisable therefore, reducing its biological activity. This work has formed the most fundamental research on the synthesis and characterisation of FITC-HI conjugates for bioanalytical analysis. However, their synthesis methods produced a mixture of mono-, di- and tri-labelled species which are not all the desirable due to the variation in their biological activity.

A recent extended study on fluorescently labelled insulin with FITC by Jacob et al. 2015 built on Hentz synthesis method produced several mono-labelled and di-labelled products whose biological activity was not assessed. In Jacob's work, the effects of varying reaction time and adding phenolic compounds to FITC-HI conjugate produced were studied and compared to the commercially available FITC-insulin product manufactured by Sigma Aldrich, which was found by Jacob to contain a mixture of conjugates, predominantly the biologically inactive tri-labelled species. The results showed that at a short reaction time of up to 5h, mono-labelled conjugate was successfully produced but the product also contained unlabelled HI. Besides, this work has not specified the labelling position of the mono-labelled species to be at A1 or B1 and their biological activity were not determined. Meanwhile, increasing reaction time over a 45h period showed no unlabelled HI, however, di- and tri-labelled species was also

produced after 20h reaction time. Furthermore, there was a 10% decrease in the amount of mono-labelled species produced at a short reaction time of 2h in the presence of phenol or m-cresol. This observation could occur because the phenolic compounds promote the stable R-state of insulin monomer in which the A1 residue is in an extended form and is more readily available for labelling at both A1 and B1 positions. Commercially available insulin preparations ranging from short-acting, rapid-acting to long-acting were also fluorescently labelled with FITC by Jacob et al 2015 for future biomedical applications. This recent work produced a mixture of mono- and di-labelled conjugate whose biological activities were not examined. Despite trying a wide range of insulin preparations and adding phenolic compounds, Jacob et al 2015 still has not successfully synthesised FITC-labelled insulin conjugate at the desired B1 position that showed by Hentz to have similar biological activity as native insulin.

A more recent work on the development of a fully bioactive fluorescent-labelled insulin has been described by Williams et al. 2018. This study has greatly emphasised the indispensable role of fluorophores in contributing to the finding of how insulin from the interstitial fluid enters the skeletal muscle cell cytoplasm. This group successfully synthesised fluorescently labelled HI at the B1 position whose biological activity has also been fully confirmed via IR-binding assay and insulin tolerance test *in-vivo*. However, their fluorophore of choice was AlexaFluor 647 and only biosynthetic HI was used in the study. The use of tert-butyloxycarbonyl (t-boc) protection chemistry to block the activity of free amines at the A1 and B29 position, consequently leaving the B1 position free for AlexaFluor 647 labelling has successfully produced the desired mono-labelled species. However, the lengthy process of synthesising the insulin protected t-boc intermediates is very time-consuming. Furthermore, the intermediates also required purification by RP-HPLC before they could undergo another synthesis for the desired conjugates labelled at the B1 position, which also required further HPLC purification. Moreover, the high cost of materials used, and the low yield of the desired product have also rendered this method less reproducible.

Overall, the insulin binding sites including residues A1, A13, A21, B12, B17 and B-chain residues B20-B30 play an essential role in the binding of insulin to IR, therefore, are crucial for insulin biological activity. Meanwhile, the labelling of FITC to insulin involves A1, B1 and B29 residues. However, only FITC label at the B1 position could maintain the biological activity of insulin whereas the A1 and B29 positions showed a reduction (~10-100 fold) in insulin activity, thus emphasising the importance of A1 and B29 in the binding of insulin to IR (Hentz et al., 1997; Jacob et al., 2016; Williams et al., 2018). The objective of this current study is to synthesis the desired biologically active FITC-insulin conjugate labelled at the B1 position merely by modifying certain reaction conditions including molar ratio, pH and reaction time. However, it is also understood that the use of protecting group on specific sites of the insulin molecules may be required to target B1 specific binding site in future research.

2.2 Materials and Methods

2.2.1 Chemicals and Reagents

FITC isomer I (F-7250, CAS: 3326–32-7) and Sephadex TM-G25 were purchased from Sigma-Aldrich (St. Louis, MO). Actrapid®, NovoRapid® and Insulatard® manufactured by Novo Nordisk; Humalog® and Humulin S® by Eli Lilly and Apidra® by Sanofi-Aventis were used. HPLC grade acetone, HPLC grade acetonitrile (ACN), HPLC grade trifluoroacetic acid (TFA), sodium dihydrogen phosphate (NaH_2PO_4), disodium hydrogen phosphate (Na_2HPO_4) glycerol, m-cresol and zinc oxide were purchased from Fisher Chemicals (Loughborough, UK). Ethylenediaminetetraacetic acid disodium salt (EDTA) was from Hopkins & Williams. Milli-Q water obtained from a Milli-Q UF Plus water purification system was used throughout for all HPLC analysis while the use of distilled water was for other preparation processes such as the making of buffers; 0.1M NaOH and 0.1M HCl were used for pH adjustment.

2.2.2 Synthesis of FITC-insulin analogues conjugates

The protocol for the synthesis of clinically used commercially available insulin injections labelled with FITC conjugate is detailed below:

2.2.2.1 Preparation of FITC stock solution

A 25mg/mL solution of FITC in acetone was freshly prepared just before use in a 5mL volumetric flask. It was protected from light by covering with foil and kept in the dark at 2-8°C until use.

2.2.2.2 Preparation of 0.1M Sodium Phosphate buffer pH 7.0

6.6g of NaH_2PO_4 and 10.27g of Na_2HPO_4 were dissolved in ~ 500mL of distilled water. After dissolution, the solution was made up to 1L in a volumetric flask with distilled water and pH was adjusted to 7.0 with 1M NaOH or 1M HCl.

2.2.2.3 Synthesis of FITC-Actrapid® (Human Insulin) conjugate

5mL of Actrapid® solution (equivalent to 17.5mg HI) was measured and transferred into a clean glass jar. This is equivalent to 0.003 millimoles of HI (Number of mole of HI=17.5mg/5808Da). For a 2:1 molar ratio, 0.006 millimoles of FITC is required, which is equal to 2.34mg of FITC (Mass of FITC=0.006x389.382Da). Therefore, 94 µL of 25mg/mL FITC stock solution is required for conjugation.

0.44mg EDTA (200mM) was added to the Actrapid® solution. The volumes of FITC stock (25mg/mL) solution added according to each molar ratio of FITC and Actrapid® being synthesised are shown in **Table 2-2** with the pH of the mixture being adjusted to pH7 to yield a bright yellowy-orange solution.

Table 2-2: Volumes of FITC solution corresponding to each molar ratio of FITC and Actrapid®

The molar ratio (FITC: Actrapid®)	Volume of FITC stock solution (25mg/mL) added (**µL**)
3:1	141
2:1	94
1.5:1	70
1:1	47
0.5:1	23

The mixture was left to react in the dark on a magnetic stirrer for the allocated reaction time (For the molar ratio study, the reaction time was 4h; For the reaction time study at 2:1 molar ratio, the reactions were stopped after 2h,17h,18h,19h,20h & 23h)

Similarly, to study the effect of pH on the synthesis of FITC-Actrapid® conjugates at 2:1 molar ratio and 2h reaction time, each set of FITC-Actrapid® preparations was adjusted to pH 7.5; pH8.5, pH9 and pH9.5

2.2.2.4 Synthesis of FITC- Apidra® (Insulin glulisine)/ NovoRapid® (Insulin aspart)/ Humalog® (Insulin lispro)/ Humulin S® (Human insulin)/ Insulatar ® conjugates

The protocol to label other commercially available insulin injections with FITC at pH7 using 2:1 molar ratio was following the synthesis of FITC-Actrapid ® conjugate as summarised in **Table 2-3**

Table 2-3:The protocol to label other pharmaceutical insulin injections with FITC.

Conjugates	Volumes of FITC stock solution (25mg/mL) added (**µL**)	Volumes of pharmaceutical insulin injection used (**mL**)/ tradename
FITC-Apidra®	93	5/ Apidra®
FITC-NovoRapid®	94	5/ NovoRapid®
FITC-Humalog®	94	5/ Humalog®
FITC-Humulin S®	94	5/ Humulin S®
FITC-Insulatar ®	94	5/ Insulatar ®

2.2.3 Purification of FITC-insulin conjugates

Once the allocated reaction time has been reached, the synthesised FITC-insulin conjugates were separated by gel permeation chromatography (GPC). The GPC equipment consists of a Buchii apparatus chromatography pump B-688, peak detector B-686, fraction collector B-684 and a gel permeation column, which was composed of a borosilicate plastic-glass column containing Sephadex™ G25.

To pack the column, ~ 15g of dry Sephadex-G25 (bead size: dry 50–150 µm) was swollen with 100mL of distilled water for 3h at 20°C and the resulting slurry was packed vertically into the column to provide a continuous bed for separation.

2.2.4 Analytical procedures for identification of FITC-insulin conjugates

The fractions collected from GPC were analysed using Reversed-Phase High-Performance Liquid Chromatography (RP-HPLC) and Mass Spectroscopy (MS) to identify the species produced.

RP-HPLC chromatographic analyses

A Shimadzu Prominence HPLC system consisting of an in-line DGU-20AS Prominence degasser, LC-20 AD Prominence quaternary pump, SIL-20A Prominence autosampler, CTO-20 AC Prominence column oven and SPD-M20A Prominence diode array detector was used to analyse the conjugation products. A Luna (3 µ) C18(2), 150 × 4.60 mm column from Phenomenex, Cheshire UK was used for the separation preceded by a 0.5 mm in-line filter and a widepore C18, 4 × 3 mm guard column. Elution was achieved using a gradient method with a flow rate of 1.0 mL/min, a column temperature of 40 °C and a sample injection of 50 µL. The following gradient was used in HPLC determinations: 0–15 min (85 % to 65% A), 15–25 min (65%to 35% A), and 25–32 min (35% A) where A was mobile phase A containing 0.1 % trifluoroacetic acid (TFA) in Milli-Q water and B was mobile phase B containing 90% Acetonitrile, 10 % Milli-Q water and 0.1% TFA. SIL-20A Prominence autosampler performed the sampling and the sample volume used throughout was 50µL. The peaks were monitored by fluorescence detection where the excitation and emission wavelengths were set at 494 and 518 nm, respectively. The Photo Diode Array (PDA) detector was also set to scan from 190 to 400 nm and had a channel set at 215 nm to detect the presence of unlabelled native insulin.

MS analyses

MS to determine the mass and labelling position of FITC-insulin conjugates produced was performed using an MS-Orbitrap Fusion with UltiMate 3000 RSLCnano System (Thermo Scientific) consisting of a TriVersa Nanomate nanospray source (Advion, NY) which was set to electrospray the samples directly using a flowrate of 300 nL per minute voltage of 1.4 kV and gas

pressure of 0.3 psi.MS analyses were performed by the Proteomics Research Technology Platform at the University of Warwick.

2.2.5 FITC- insulin conjugate storage conditions and lyophilisation process

All fresh FITC-insulin conjugates collected after GPC purification would be protected from light and kept at -20°C for lyophilisation no later than a week after being synthesised. The samples were placed inside a round bottom flask and sharp frozen using liquid nitrogen. The frozen flask was then placed on the Heto drywinner freeze dryer for 48h to ensure no aqueous solution remained in the flask. Once achieving the yellow powder of FITC-insulin conjugate, it is ready for storage at 4°C in an amber bottle until further use.

2.2.6 Validation procedures for HPLC analysis

The qualification parameters assessed for the validation of FITC-insulin RP-HPLC methods were set out in **Table 2-4** according to FDA guidance documents Q2B Validation of Analytical Procedure.

Mono-labelled FITC-Actrapid® conjugate (Mono) synthesised inhouse was used throughout the validation study.

Table 2-4: Validation Procedures

Parameters	Samples	Criteria
Selectivity/specificity	Milli-Q water and diluting fluid containing m-cresol, glycerol, zinc oxide excipients as present in Actrapid® both adjusted to pH7.0 with 0.1M NaOH	There should be no peaks present in Milli-Q water or diluting fluid interfering with the peak area response from Mono.
System suitability	The integral system (including the equipment, electronics, analytical operations and sample to be analysed) suitability was assessed by a minimum of six replicate analyses of Mono at 1mg/mL	An acceptance criterion of ±2% for percentage relative standard deviation(%RSD) for the peak areas and retention times (RT) of Mono
Linearity and range	A minimum 5-point curve generated over a range of 80-120% of the test standard. A series of 10 concentrations (0.07-0.08-0.09-0.1-0.11-0.12-1-2-3-4 mg/ml) of Mono standard solutions were analysed. Calibration plots from at least six replicate experiments were constructed	R^2 ≥0.990 Achieving an acceptable degree of linearity within and at the extremes of the concentration ranges studied
Accuracy	Analysing three replicates of four different concentrations (0.05-0.1-0.5-1 mg/ml of the standard Mono sample) Area under the peak (AUP) for each sample was recorded [mean AUP for 3 replicates +/- SD] and the Recovery percentage was calculated using the regression equation.	Determined concentration at each level must be 97.0%–103.0% of theoretical concentration
Precision/repeatability intra-day and Inter-day	The precision of the assay was determined by Intra-day (repeatability, testing the sample on the same day) and Inter-day (intermediate precision, testing the sample on different days with freshly prepared mobile phase and different FITC- Actrapid® standard) Data collected using three replicates of three different concentrations from low (0.01mg/ml) to medium(10mg/ml) and high(100mg/ml) of Mono.	%RSD at each level ≤3.0%
Detection and Quantitation limits (sensitivity) LOD and LOQ	Limit of detection (LOD) and quantitation (LOQ) were calculated based on the standard deviation of the analytical response represented by AUP (lowest concentration used 0.5 %) and slope of the calibration curve. The following equations were used: $\text{LOD} = 3.3\frac{SD}{s} \quad and \quad \text{LOQ} = 10\frac{SD}{S}$ Where SD is the standard deviation of the response and S is the slope of the calibration curve. The regression data obtained from the linearity studied were used.	Report LOD and LOQ results

2.3 Results and Discussions

2.3.1 Validation of RP-HPLC method used to analyse FITC-insulin for the determination of Mono

Selectivity/Specificity

The RP-HPLC method used to analyse FITC-Actrapid® conjugate under chromatographic conditions had a run time of 45min with elution of mono-labelled species at 21.9min retention time (RT), di-labelled species at 22.6min RT and tri-labelled species at 23.7min RT as shown in **Figure 2-8**

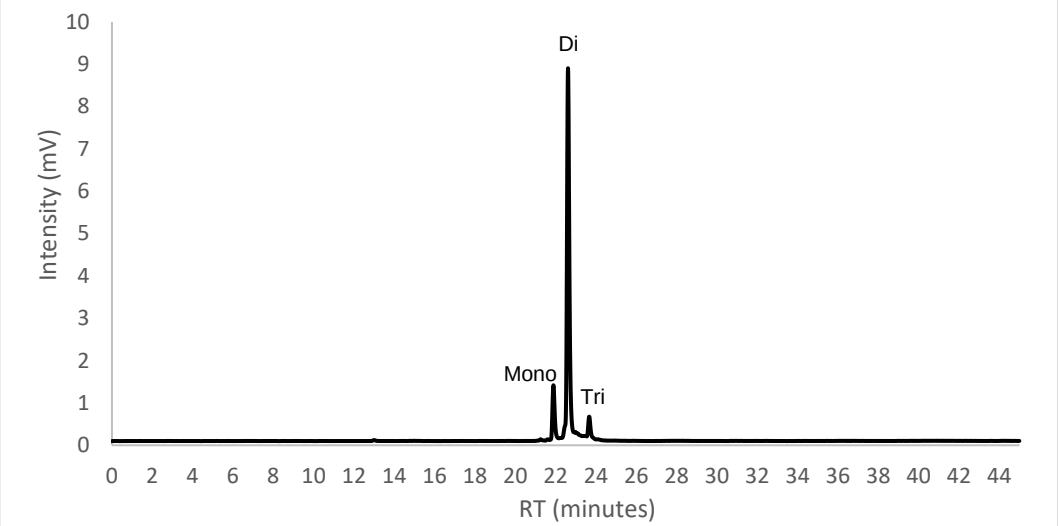

Figure 2-8: RP-HPLC fluorescence chromatogram of FITC-Actrapid® conjugate in water showing peaks at RT 21.9min (mono-labelled species); 22.6min (di-labelled species) and 23.7min (tri- labelled species)

Comparisons of the fluorescent chromatograms for placebo (diluting fluid) and FITC-Actrapid® conjugates revealed no additional peak co-eluting with the peaks corresponding to each conjugated species.

System suitability

System suitability for FITC-insulin method with 1mg/mL Mono showed an RT of 21.9min for mono-labelled species with a %RSD = 0.04 (n=6) and %RSD for peak areas was 1.57. Both results are within ±2% acceptance criteria indicating the suitability of the RP-HPLC system. The capacity factor and resolution were both >2 and the tailing factor was <2 within accepted criteria. The data suggested that the chromatographic system and conditions used in this FITC-insulin method are suitable for the samples analysed.

Linearity

Figure 2-9 shows the linear relationship of Mono concentrations over the range of 0.07-4 mg/mL and their AUP. The calibration curves constructed for the six replicate experiments were evaluated by their correlation coefficient where R^2 equal to 0.9997 and the Pearson correlation coefficient, r is 0.9998.

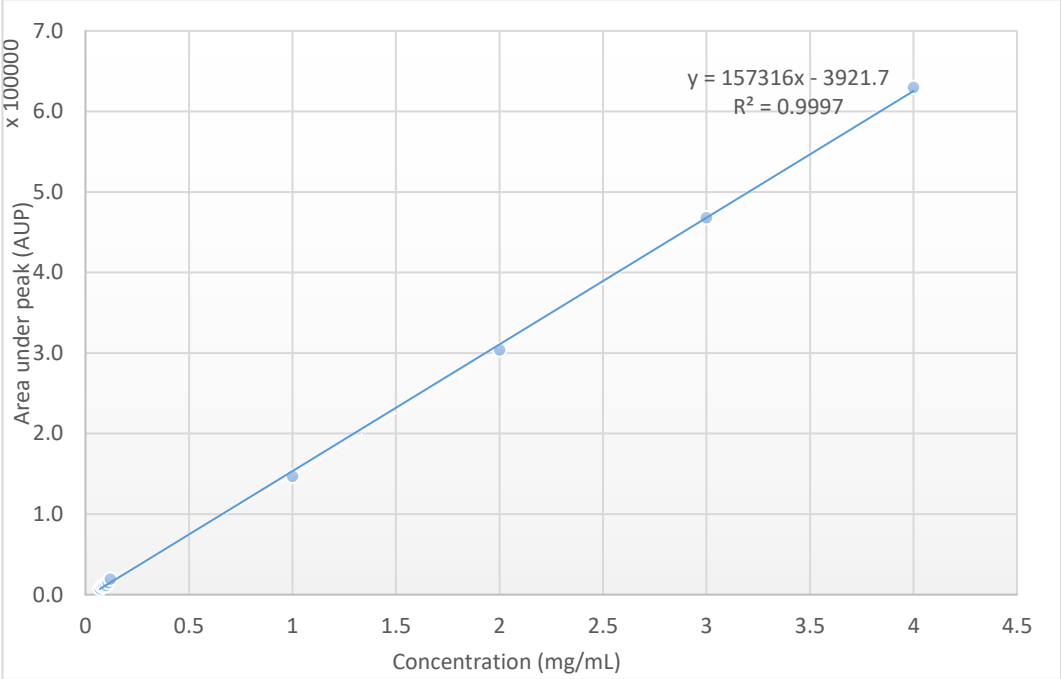

Figure 2-9: Parameters of the regression equation for Mono against analytical response (AUP) using the RP-HPLC method for FITC-insulin.

Range

The linearity results demonstrated in **Figure 2-9** suggest that the FITC-insulin analytical method provide an acceptable degree of linearity within and at the extremes of the concentration ranges studied.

Accuracy

The AUPs corresponding to four concentrations of 0.05,0.1,0.5,1 mg/mL of Mono from two different sets of four solutions were used to calculate the recovery percentage of each samples using the regression equation. The average recovery was 98.6 ± 1.02% which is within the acceptable range of theoretical concentration of 97-103%.

Precision

Table 2-5 shows precision data for Mono samples prepared at three different concentrations of 0.01,1 and 10 mg/mL during intra- and inter-day runs. The

%RSD for intra- and inter-precision was ≤1.0% except for the lowest concentration of 0.01mg/mL.

Table 2-5: Precision of FITC-insulin method for determination of Mono.

Standard concentrations	Intra-day		Inter-day		Overall RSD %
mg/mL	AUP Mean ±SD	RSD %	AUP Mean ±SD	RSD %	
0.01	1594±60	3.73	1359±57	4.00	3.85
1	148761±724	0.49	145206±1819	1.25	0.87
10	1651035±9262	0.56	1636451±5319	0.33	0.45

Precision studies demonstrated the repeatability and intermediate precision of the FITC-insulin method used for 1 and 10 mg/mL concentrations. The results suggest that 0.01 mg/mL concentration was below the limit of detection for the sample to be analysed because the %RSD for intra- and inter-precision was greater than 3.

Detection and Quantitation limits (sensitivity)

Limit of detection (LOD) and quantitation (LOQ) were calculated based on the standard deviation of the analytical response represented by AUP (lowest concentration of 0.07mg/mL used in the linearity study) and slope of the calibration curve shown in **Figure 2-9**. The calculated LOD and LOQ was 0.055mg/mL (1.57 Units/mL) and 0.167mg/ml (4.77 Units/mL), respectively. The result showed the sensitivity of FITC-insulin analytical method used to determine Mono.

2.3.2 Purification of FITC-insulin conjugates by GPC

After the required reaction time, the FITC-insulin sample was injected directly onto the GPC to achieve three separated fractions as showed in **Figure 2-10** . Band 1 showed the larger molecules of FITC-insulin conjugates, and Band 3 indicated unreacted FITC.

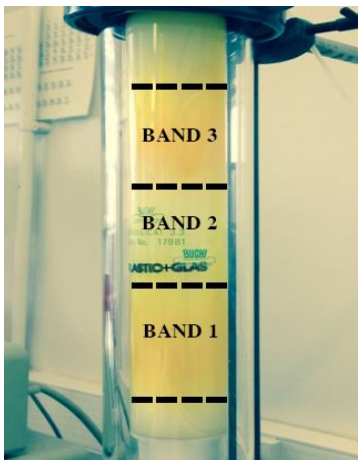

Figure 2-10: Picture showing separated bands corresponding to FITC-insulin conjugates and unreacted FITC molecules purification by GPC.

2.3.3 The screening of commercially available insulin preparations to select the desired mono-labelled conjugate.

Before identifying which species of FITC-insulin was produced using PR-HPLC system; it is necessary to confirm complete removal of unreacted FITC by GPC from fluorescent conjugates as well as the presence of any unlabelled insulin in the final conjugated products. **Figure 2-11** shows FITC peaks observed at RT of 13min, 24min and 28.1min.

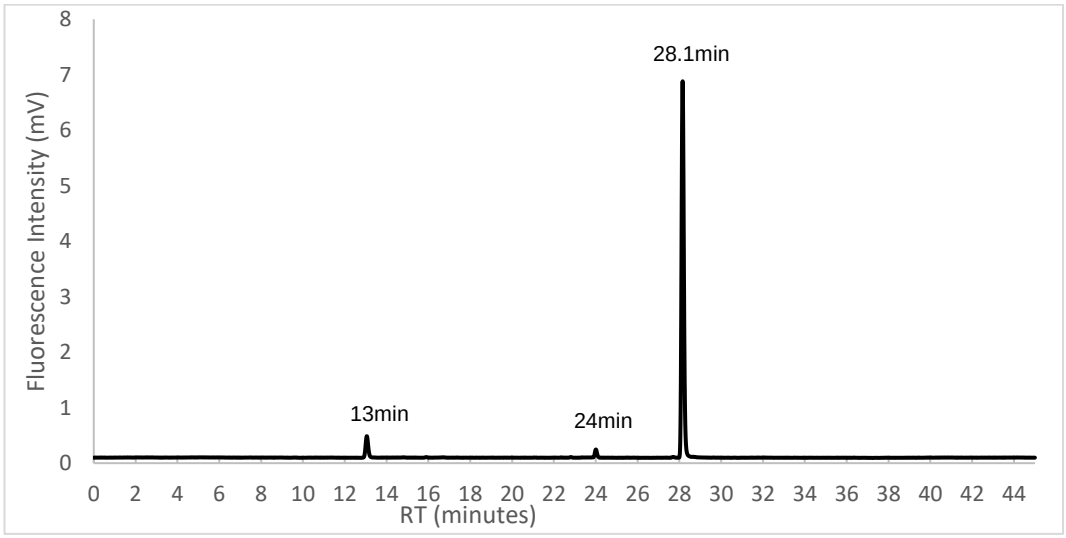

Figure 2-11: RP-HPLC fluorescence chromatogram of FITC in acetone showing peaks at RT 13min, 24min and 28.1min

Figure 2-12 shows the PDA UV chromatogram detected at 215nm for Actrapid® with peaks at 16.8min RT and 20.4min RT corresponding to m-cresol and native insulin respectively.

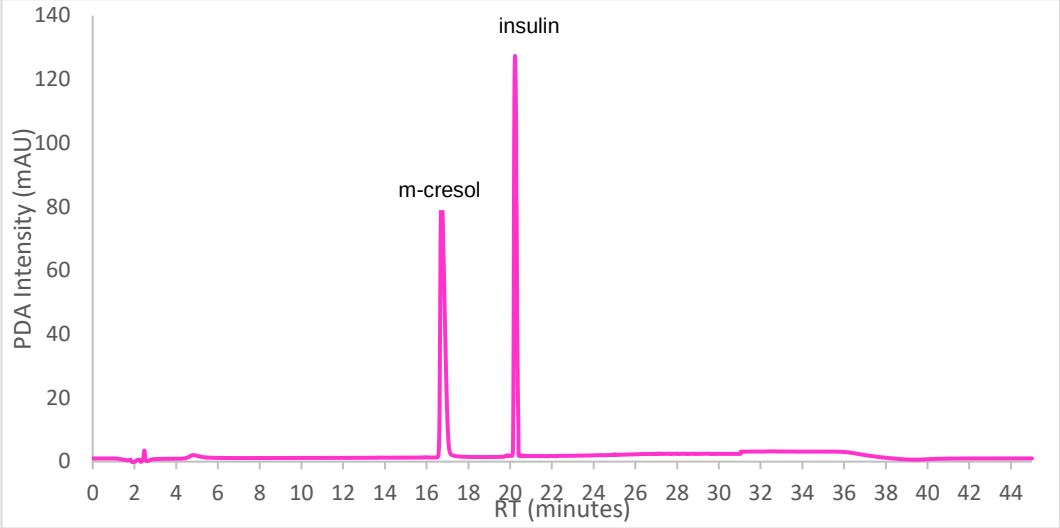

Figure 2-12: PDA UV chromatogram of native insulin (Actrapid®) showing peaks at 16.8min RT for m-cresol and 20.4min RT for Actrapid®

The detection of these identified peak for FITC and insulin in subsequent chromatograms would indicate that unreacted FITC and unlabelled insulin are still present after GPC purification.

The initial approach was based on previous findings by Jacob 2015 where the conjugates were produced with a 3:1 FITC: insulin ratio. In this work, the ratio was reduced to 2:1 and FITC conjugation with Actrapid®, Humulin S®, Apidra®, Humalog®, NovoRapid® and Insulatard® at pH 7 will be assessed after 2h and 20h. The long-acting insulin analogues Levermir® and Lantus® were excluded from this study because of their distinct structural differences at the B29 positions and low pH formulation that make it difficult for FITC conjugation following the usual synthesis method. The low yield achieved in Jacob 2015 study using these two analogues also suggested that they are unsuitable

Error! Reference source not found. summarises the overall yield of FITC-insulin c onjugates as a percentage AUP corresponding to each insulin analouges labelled with FITC obtained from the chosen reaction conditions

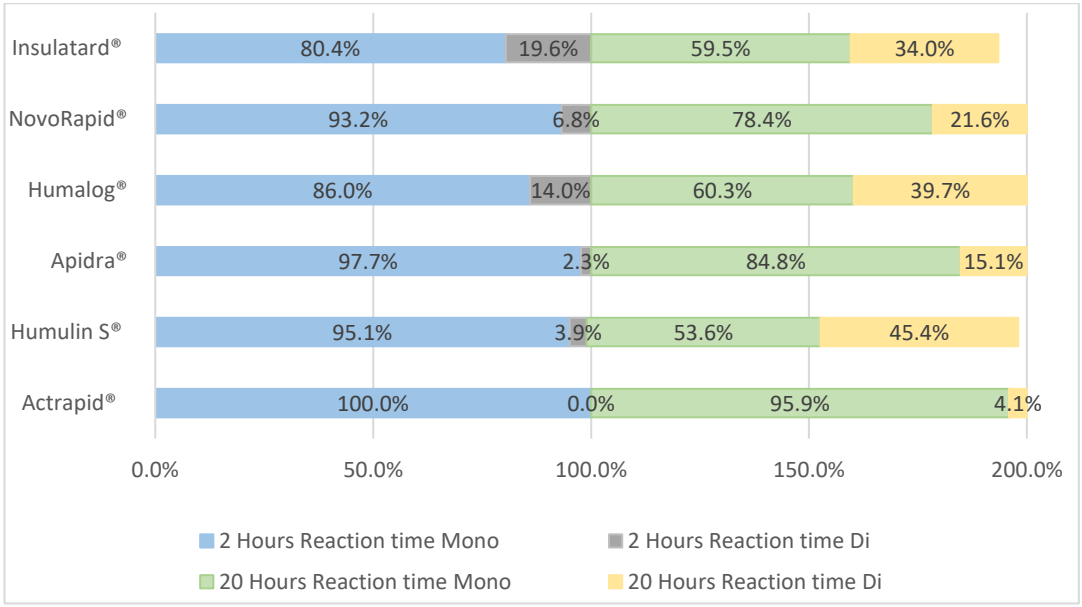

Figure 2-13:Charts showing various percentage AUP of Mono and Di produced at 2h and 20h reaction time for Actrapid®, Apidra®, NovoRapid®, Humalog®, Humulin S® and Insulatard®

All conjugates synthesised at a reaction time of 2h had unlabelled insulin peak at 20.4 min (PDA). This peak was not present in those synthesised at a reaction time of 20h, suggesting that with a lower amount of FITC used, 2h is still not long enough to allow complete FITC-insulin conjugation. The absence of unreacted FITC was also confirmed from HPLC fluorescence chromatograms, indicating that GPC purification was successful in removing all the unreacted dye from the conjugated product.

At a short reaction time of 2h, the FITC conjugates produced with the chosen insulin analogues were predominantly Mono with a considerably smaller amount of di-labelled FITC-insulin conjugate (Di). Actrapid® showed the highest Mono yield (100%) while the rest produced a mixture of Mono and Di. Apidra®, Humulin S® and NovoRapid® showed a similar yield of more than 93-98% Mono with less than 7% Di. Insulatard® and Humalog® had the lowest yield of Mono with only 80-86%.

Meanwhile, at a longer reaction time of 20h, there was also a mixture of Mono and Di produced with a higher percentage yield of Di than the synthesis at a short reaction time. Actrapid® maintained the highest yield (96%) of Mono while the rest showed a much lower amount of Mono. As there was an increased

amount of Di being produced, the percentage yield of Mono was reduced to 85% for Apidra® and 78% for NovoRapid®. Insulatard® and Humalog® showed a similar yield of 60% Mono while Humulin S® had the lowest amount of 54%.

It was anticipated that the short-acting insulins such as Actrapid® and Humulin S® should have a similar production of conjugates with FITC because they share the same structure as HI. However, this similarity in the synthesis of FITC-insulin conjugates was only observed at a short reaction time of 2h while there was a 41% reduction in the yield of Mono at 20h reaction using Humulin S®. The longer reaction time of 20h did not seem to largely affect the synthesis of Mono using Actrapid®. It is possible that other excipients formulated in Actrapid® might contribute to the structural configuration of insulin in such a way that FITC labelling to more than one site is more challenging.

Similar to Actrapid®, the rapid-acting insulin analogues including Humulin S®, Apidra® and Novorapid® also produced predominantly Mono. However, only Actrapid®, Humalog® and Novorapid® had a single peak in their fluorescent chromatogram that represented one species of Mono at 21.9min RT while Apidra® and Humulin S® had two mono-labelled peaks at 21.3min RT (although at a much lower percentage of less than 2%) and 21.9min RT, which could indicate labelling at both A1 and B1 positions; refer to Error! Reference s ource not found. and Error! Reference source not found. for illustrations of FITC-Actrapid® and FITC-Apidra® conjugates.

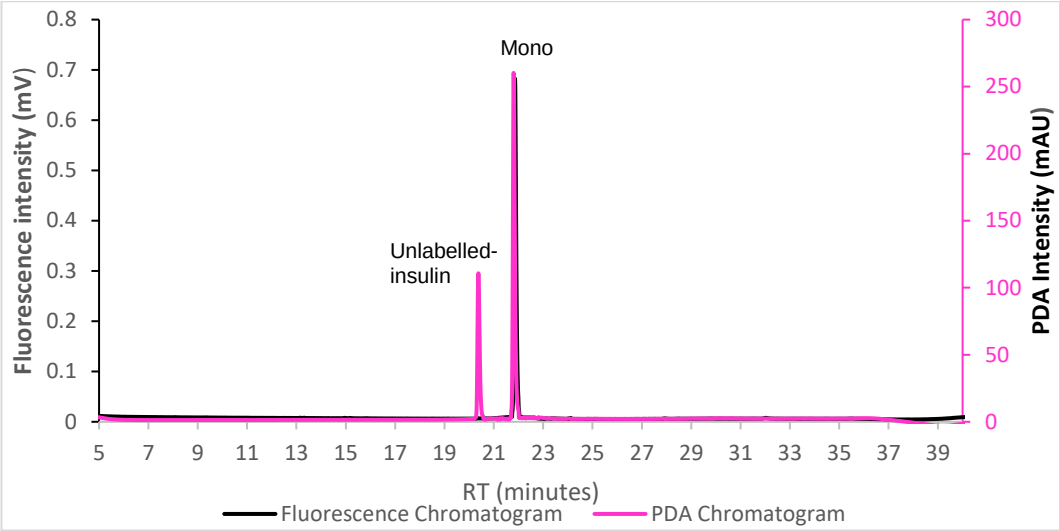

Figure 2-14: Combined Fluorescence (black) and PDA UV chromatograms (pink) of Actrapid®-FITC synthesised at 2:1 molar ratio (FITC: Actrapid®) after 2h reaction showing a single Mono peak at 21.9min RT (100% AUP) and PDA peak at 20.4min RT for unlabelled insulin.

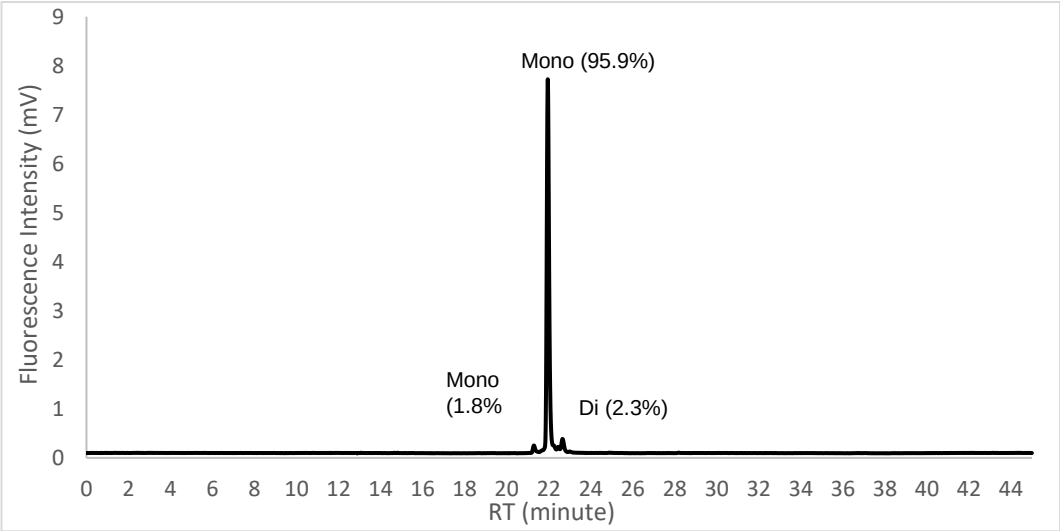

Figure 2-15: RP-HPLC fluorescence chromatogram of Apidra®-FITC conjugate synthesised at 2:1 molar ratio (FITC: Apidra®) after 2h showing two Mono peaks at RT 21.3min (1.8% AUP) and RT 21.9min (95.9% AUP) and one Di peak at RT 22.6min (2.3% AUP).

It is possible that the modifications in the amino acid sequences of these analogues and the differences between the equilibrium of the R- and T- state of the insulin hexamer could both contribute to the production of two mono-labelled species. This is because the B1 binding site for FITC is fully exposed regardless of the insulin molecule being in the R- or T-state, thus is more

accessible for FITC binding. On the other hand, the A1 binding site is folded inward in the T-state and shielded from FITC by the α-helix, whereas in the R-state it is facing outward and more expose, hence enabling FITC binding at the A1 position (refer to **Figure 2-16**) (Kosinová et al., 2014).

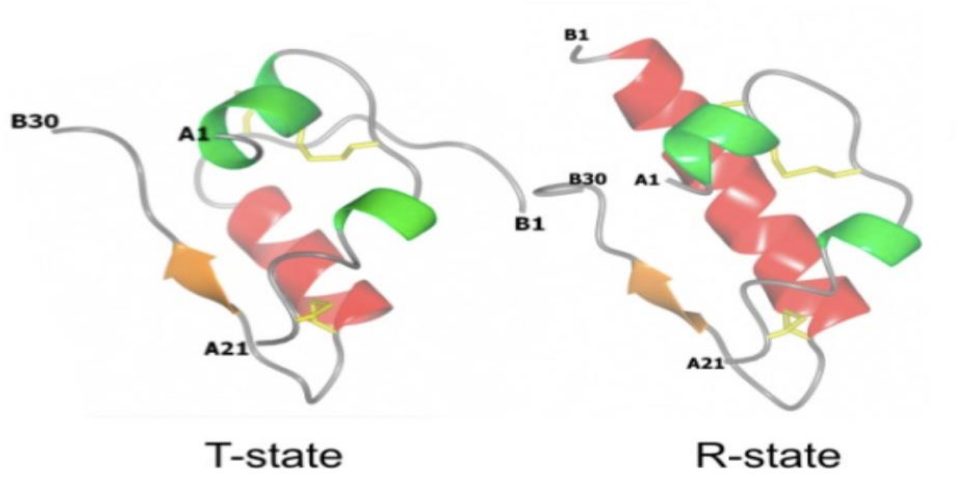

Figure 2-16: Structure of the T/R state transition (Taken from Kosinová et al., 2014)

The production of two Mono at both B1 and A1 position using Apidra® is likely because it is formulated without zinc ions but still contains m-cresol. Therefore, the T/R transition would be subjected to the phenolic induced R-state in which the A1 is also exposed for FITC label. Notably, the slightly higher pH in Humulin S® formulation may have contributed to the higher production of Di at 20h reaction times. This observation could be due to the initial high pH formulation of Apidra favouring the R-state of hexameric insulin which allows more accessibility to the A1 position for FITC labelling. Although there was 13-15% reduction in Mono production using Apidra® and NovoRapid® at 20h reaction time; this was only a quarter of the reduction observed for 3:1 molar ratio at 20h reaction time by Jacob 2015. The results indicated that excessive amount of FITC in addition to longer reaction time could result in a higher production of Di and possibly tri-labelled FITC-insulin analogue conjugate (Tri) produced.

Interestingly, Insulatard® containing HI with prolonged duration of action produced the lowest yield of Mono at both short and long reaction time. This is because Insulatard® formulation is a suspension containing protamine

sulphate, which precipitate the insulin at its isoelectric point. The results suggested that HI formulated for protracted action like Insulatard® would have a higher tendency to produce a mixture of conjugates that is undesirable. Considering the lower yield of conjugates synthesis at 3:1 ratio reported by Jacob 2015 for long-acting insulin including Lantus® and Levermir® in addition to the observed data for Insulatard®, it is concluded that insulin analogues formulated for protracted action are not suitable for FITC label.

The overall results showed that reducing the amount of FITC is beneficial in lowering the production of Di at both long and short reaction time of 2h and 20h and so far, Actrapid® is the best analogue for producing the highest yield of Mono.

2.3.4 Molar ratio study using Actrapid® after 4h reaction time and at pH7

Table 2-6 summarises the synthesis of FITC-Actrapid ® conjugates at pH7 using various mole of FITC to 1 mole of Actrapid® analysed by RP-HPLC after 4h reaction. Two main species Mono and Di were identified with their corresponding percentage AUP and the presence of unlabelled insulin (PDA).

Table 2-6: Molar ratio study between FITC and Actrapid® showing the synthesis of different FITC-Actrapid® conjugates and their corresponding AUP percentages analysed by RH-HPLC and the presence of unlabelled insulin identified from their PDA chromatogram.

Molar ratio FITC: Actrapid®	RP-HPLC Peaks RT (min) (AUP %)	Theoretical molecular mass (Da) (No of FITC)	Identity of conjugates
0.5:1	20.4 (PDA 6.4%)	5807.6(0)	Unlabelled Actrapid®
	21.9 (100%)	6197.0(1)	Mono-labelled species
1:1	20.4 (PDA 4.8%)	5807.6(0)	Unlabelled Actrapid® (Confirmed by MS raw data peaks at 1162.3354 z5 and 1452.6674 z4)
	21.9 (100%)	6197.0(1)	Mono-labelled species (Confirmed by MS raw data peak at m/z 1555.4228 z4)
1.5:1	20.4 (PDA 3.2%)	5807.6(0)	Unlabelled Actrapid®
	21.9 (100%)	6197.0(1)	Mono-labelled species
2:1	20.4 (PDA 1.7%)	5807.6(0)	Unlabelled Actrapid® (Confirmed by MS raw data peaks at 1162.3364 z5 and 1452.9185 z4)
	21.9 (100%)	6197.0(1)	Mono-labelled species (Confirmed by MS raw data peaks at m/z 1244.7402 z5 and 1555.6726 z4)
3:1	20.4 (PDA 0.5%)	5807.6(0)	Unlabelled Actrapid®
	21.3 (2.88%)	6197.0(1)	Mono-labelled species
	21.9 (94.69%)		
	22.6 (3.7%)	6586.3(2)	Di-labelled species

As anticipated from previous studies by Jacob 2015, synthesis using 3:1 molar ratio produced a mixture of two mono-labelled species in addition to Di while other lower molar ratios yielded 100% Mono. Unfortunately, unlabelled insulin was still present in all conjugates despite the increase in reaction time from 2h to 4h. However, the PDA peaks detected for unlabelled Actrapid® was highest for 0.5:1 (6.4% AUP) and lowest for 3:1 (0.5%) molar ratio, suggesting that having FITC in excess could enable complete labelling of insulin but also increase the chance of producing more Di and Tri. The higher amount of unlabelled insulin presence from the synthesis at a lower molar ratio indicated that longer reaction time is necessary for achieving complete labelling of Actrapid® with FITC. However, increasing reaction time may lead to the production of other undesired conjugates as previously reported by Jacob et al 2015.

Overall, the synthesis of FITC-Actrapid® requires a compromised reaction condition between choosing a suitable molar ratio and appropriate reaction time. Ideally, if choosing 2:1 molar ratio then the reaction time should not be longer than 20h because this resulted in the production of Di. However, the reaction time should also not be shorter than 4h due to the presence of unlabelled insulin. Labelling at longer reaction time than 20h may be necessary for lower molar ratios of 1.5:1 or 1:1 in which the availability of FITC molecules could be limited for selective labelling at a single site on each insulin molecule while there still is sufficient time for achieving a complete conjugation and leaving no unlabelled insulin left.

2.3.5 The effect of pH on the conjugation of FITC and Actrapid®

Hentz et al. 1997 demonstrated that the synthesis of FITC-insulin conjugates at pH8.5 would result in a mixture of two mono-labelled species at both A1 and B1 positions. It was also found from their study that the mono-labelled at the A1 position had an RT of 22.6min while the one labelled at the B1 position exhibited a slightly longer RT of 23.1min, i.e. MonoA1 would elute from the RP-HPLC column first. Although there are several factors governing the degree of labelling, the nucleophilicity of the amino acid side chains and thus their pK_a seem to contribute to the selective labelling of FITC at a particular site on the

insulin molecule. For instance, at a neutral pH of 7, the ITC reactive group of FITC would have a tendency to react more readily to the α-amino groups of insulin having a similar pK_a range around 7 rather than the ϵ-amino groups that have pK_a value >9. Notably, several findings also reported that the pK_a of the two N-terminal α-amino groups on insulin molecule was 8.4 for the aliphatic neutral Glycine at the A1 position and 7.1 for the aromatic hydrophobic neutral Phenylalanine at the B1 position while the ϵ-amino group of Lysine with a polar hydrophilic charge at the B29 position had a pKa above 9.8 (Wong, 1991; Bothelho and Gurd,1989; Hentz et al. 1997). It is therefore of interest to investigate the effect of changing pH on the labelling selectivity towards a particular amino acid group of Actrapid®, preferably where it can retain the biological activity of FITC-Actrapid® conjugate as well as native insulin.

Error! Reference source not found. shows the combined RP-HPLC fluorescence c hromatograms of FITC-Actrapid® conjugates produced with changing pH from pH7-9.8 at a 2:1 molar ratio of FITC: Actrapid® after 2h and **Table 2-7** summarises the identification of each conjugate according to their RT and the corresponding percentage AUP.

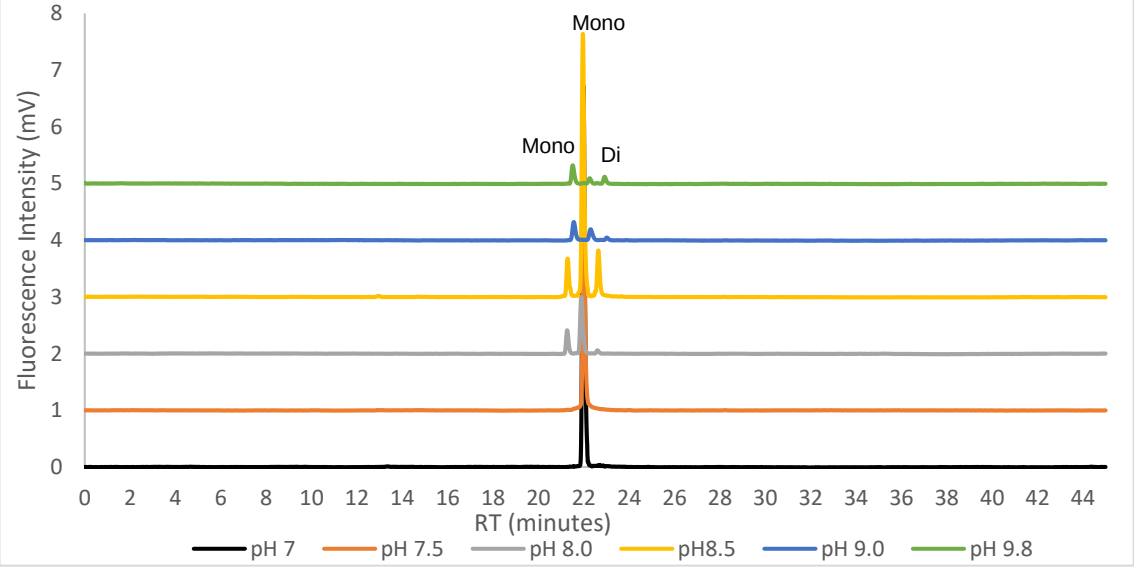

Figure 2-17: RP-HPLC Fluorescence chromatograms showing the effect of pH on the synthesis of FITC-Actrapid® conjugates at 2:1 molar ratio after 2h at pH7(black), pH7.5(orange), pH8(grey), pH8.5(yellow), pH9(blue) and pH9.8(green). The first and second peak at 21.3min and 21.9min RT indicate Mono. The third peak at 22.6min RT indicates Di.

Table 2-7: The peaks identified by RP-HPLC analysis for FTIC-Actrapid® conjugates and their corresponding yield in percentage AUP from the above fluorescence chromatograms.

pH	RP-HPLC fluorescence Peaks RT (min) (AUP %)	Theoretical molecular mass (Da) (No of FITC)	Identity of conjugates
7	21.9 (100%)	6197.0(1)	Mono-labelled species (Confirmed by MS raw data peak at m/z 1555.4228 z4)
7.5	21.9 (100%)	6197.0(1)	Mono-labelled species
8	21.4 (3.2%)	6197.0(1)	Mono-labelled species
	21.9 (94.9%)		
	22.6 (1.9%)	6586.3(2)	Di-labelled species
8.5	21.4 (4.9%)	6197.0(1)	Mono-labelled species (Confirmed by MS peak at m/z 6198)
	21.9 (89.2%)		
	22.6 (5.9%)	6586.3(2)	Di-labelled species (Confirmed by MS peak at m/z 6586)
9	21.6 (60.2%)	6197.0(1)	Mono-labelled species
	22.5 (39.8%)	6586.3(2)	Di-labelled species
	23.2 (Trace)	6975.6(3)	Tri-labelled species (Confirmed by MS peak at m/z 6972)
9.8	21.6 (73.8%)	6197.0(1)	Mono-labelled species
	22.5 (Trace)	6586.3(2)	Di-labelled species
	23.2 (26.3%)	6975.6(3)	Tri-labelled species

Although it was not possible to collect all the mass spectra data for each FITC-Actrapid® conjugate synthesised from different conditions, **Figure 2-18** illustrates the confirmation of three conjugated species identified by MS analysis according to their corresponding MS peaks at m/z 6198 ;6586 and 6972 for Mono, Di and Tri respectively.

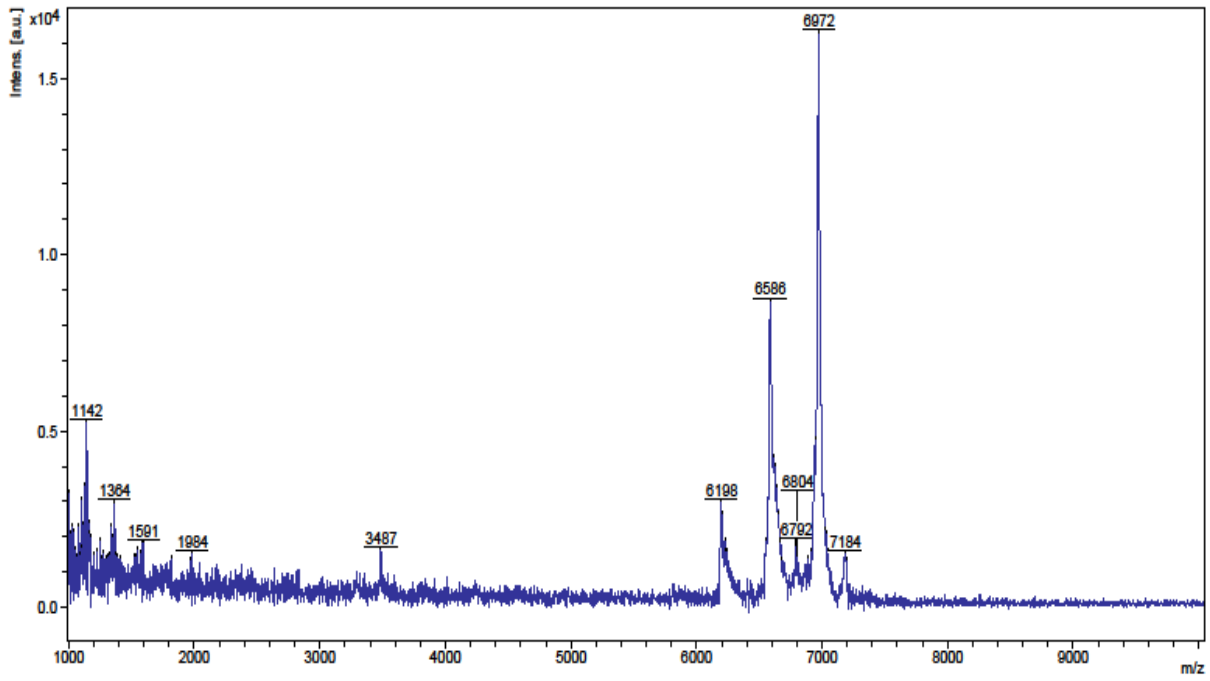

Figure 2-18: Mass Spectrum of FTIC-Actrapid conjugate mixture synthesised at pH9 shows a peak at 6198 m/z corresponding to mono-labelled species; peak at 6586 m/z for di-labelled species and peak at 6972m/z for tri-labelled species.

The reactions at pH7-7.5 successfully produced 100% Mono identified by a single peak at 21.9 min RT (refer to Error! Reference source not found.). Notably, as the pH i ncreased to 8.0 and 8.5, there was a mixture of two different mono-labelled species (peaks at 21.4min RT and 21.9min RT) as well as Di, however the predominant species was still the mono-labelled peak at 21.9min RT. Based on previous chromatographic data obtained from Hentz et al. 1997, the detection of another mono-labelled peak with slightly shorter RT from the conjugation at pH8-8.5 highly suggested that the 100% Mono (peak at 21.9min RT) produced at pH7-7.5 was labelled at the B1 position and the earlier peak at 21.4min RT observed for pH8-8.5 would indicate MonoA1. The reaction at pH 8.5 also yielded the highest mixture of Mono and Di while pH>9 showed a considerably lower production of Mono. Interestingly, ITC labelling was found by Hermanson, 2013 to occur optimally at a pH

range of pH9-9.5, and the general protocol for FITC labelling of protein, particularly immunoglobulins also recommends that the reaction should occur at pH9 for maximal labelling (Hermanson, 2013). However, this pH study illustrated that FITC labelling of insulin was best optimised at pH7-7.5 rather than the highly alkaline pH of 9-9.8. Although the change in pH alone was not successful in selectively labelling FITC at a single site of the insulin molecule, increasing the pH to ≥8 produced a mixture of FTIC-Actrapid® conjugates (MonoA1, monoB1 and Di); while keeping the pH at 7-7.5 has achieved only one mono-labelled species. This observation could be due to the microenvironmental effects of Actrapid® where there may be overlap in the nucleophilicity of the two N-terminal α-amino groups on insulin molecule at pH>8 thus allowing covalent coupling to occur at both groups (A1 and B1 positions). Besides, the structural conformation of the insulin molecule may enable the exposure of one N-terminal α-amino group, proposed to be the phenylalanine at the B1, more than the other. Therefore, the production of Mono identified by the peak at 21.9min RT was predominant at pH7-8.5. Similarly, reaction condition at pH 9.8 could not selectively target the labelling at the ϵ-amino group of lysine (B29) possibly due to competitive covalent coupling of other preferable amino acid groups at the B1 and A1 position. However, it is anticipated that by increasing the reaction time (as observed in Jacob,2015 study) or having twice the amount of FITC, the production of Di and Tri could have increased.

Despite having some degree of selectively labelling for all three amino acid targeting sites with increased pH, pH7-7.5 offers the best compromise for achieving only one mono-labelled species. Meanwhile, the distinct difference in the pK_a of Glycine at A1 position (8.4) and Phenylalanine at B1 position (7.1) in addition to a single mono-labelled species produced at pH7 compared to two species at pH8.5 also supported the hypothesis that the Mono predominantly synthesised so far was labelling at the B1 position. According to Hentz et al. 1997, the FITC-insulin conjugate labelled at B1 is the most biologically active species. However, the presence of unlabelled insulin in the final conjugated product is still suggesting that either optimised labelling conditions would require more adjustment perhaps at a higher temperature for short reaction time or the conjugated product would need to undergo further purification.

2.3.6 Reaction time study

As explained, some pH conditions with short reaction times at 2:1 molar ratio could produce a single species of Mono. However, the presence of unlabelled insulin in the FITC-Actrapid® conjugates is still undesirable. It is, therefore, necessary to further investigate at which time point there will be no unlabelled insulin left while still achieving only the desired Mono. Observation from the previous study indicated that for 2:1 molar ratio (FITC: Actrapid®) at pH7, a 4h reaction time was not long enough to achieve this while at a 20h reaction time although there was no unlabelled insulin left, 5% of Di was also produced. The synthesis of FITC-Actrapid® conjugate at 2:1 molar ratio and pH7 was further investigated at a reaction time of 17h,18h and 19h to determine the balance of producing only Mono without any Di or unlabelled insulin.

Error! Reference source not found. shows the combined fluorescence c hromatograms of FITC-Actrapid® conjugates analysed by RP-HPLC for the effect of 4h,17h,18h,19h and 20h reaction times on achieving only the desired Mono.

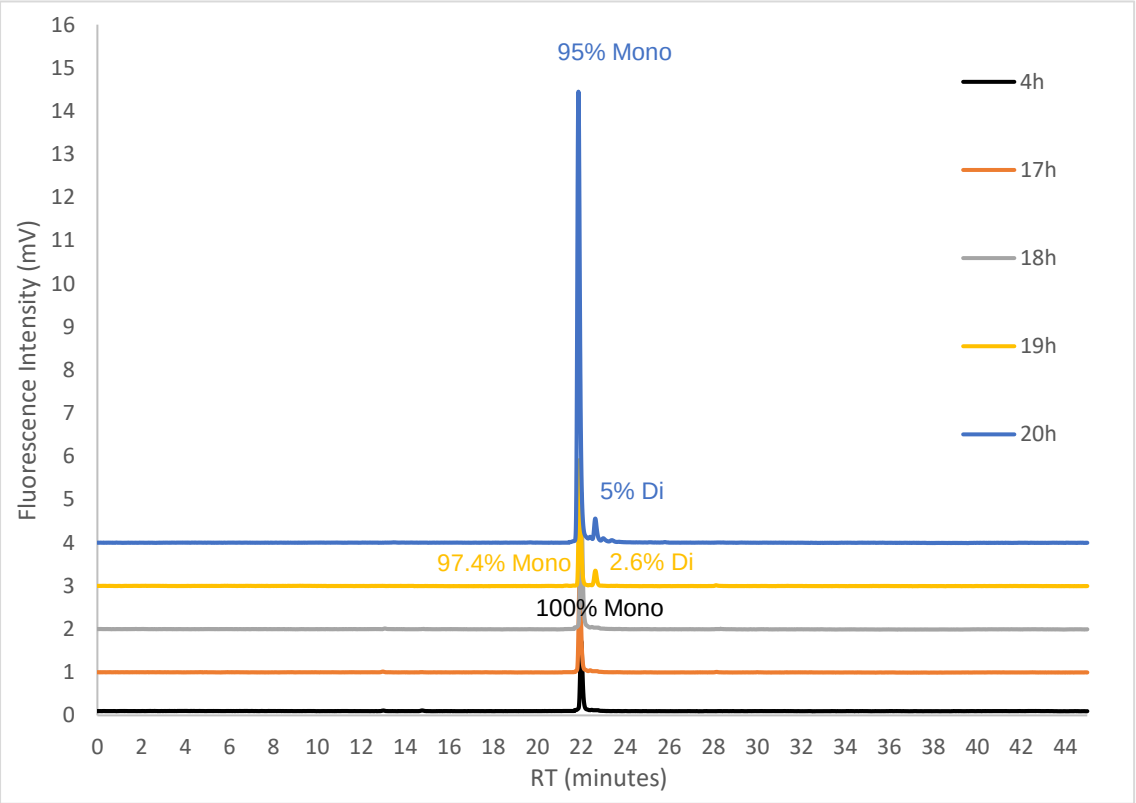

Figure 2-19: Fluorescence chromatograms showing the effect of reaction time on the synthesis of FITC-Actrapid® using 2:1 molar ratio at pH7 for 4h(black); 17h (orange);18h(grey);19h (yellow) and 20h (blue). Peak at 21.9min RT indicates Mono and peak at 22.6min RT is Di.

Notably, the cut-off points for producing Di seemed to occur at the 19h reaction time in which Di accounted for ~ 3% of the total conjugates produced; however, there was also a trace amount of unlabelled insulin detected from the PDA chromatogram at this reaction time, suggesting that reaction times of shorter than 20h would result in under-labelling of FITC to Actrapid®. Furthermore, any reaction time of ≤18h could achieve 100% Mono production. However, unlabelled insulin is also present, suggesting that further purification is necessary. In general, mono-labelling of Actrapid® with FITC is still achievable at longer reaction time (≥20h) to ensure sufficient time for all insulin molecules to become covalently coupled to FITC. However, this would produce a mixture of conjugates (predominantly Mono and some Di). To achieve the desired balance, a reaction time of 18-19h is needed but further synthesis development necessary.

To examine the biological activity of the desired conjugate, it is necessary to ensure there is no unlabelled insulin or any other conjugated species. The isolation of FITC-Actrapid® conjugate using RP-HPLC has been successful in achieving a 100% yield of the desired Mono without any unlabelled insulin. Mono was pooled from its synthesis of 2:1 molar ratio at pH7 and 18h reaction time. The resultant lyophilised Mono was further analysed by HPLC to confirm its purity as shown in **Figure 2-20**.

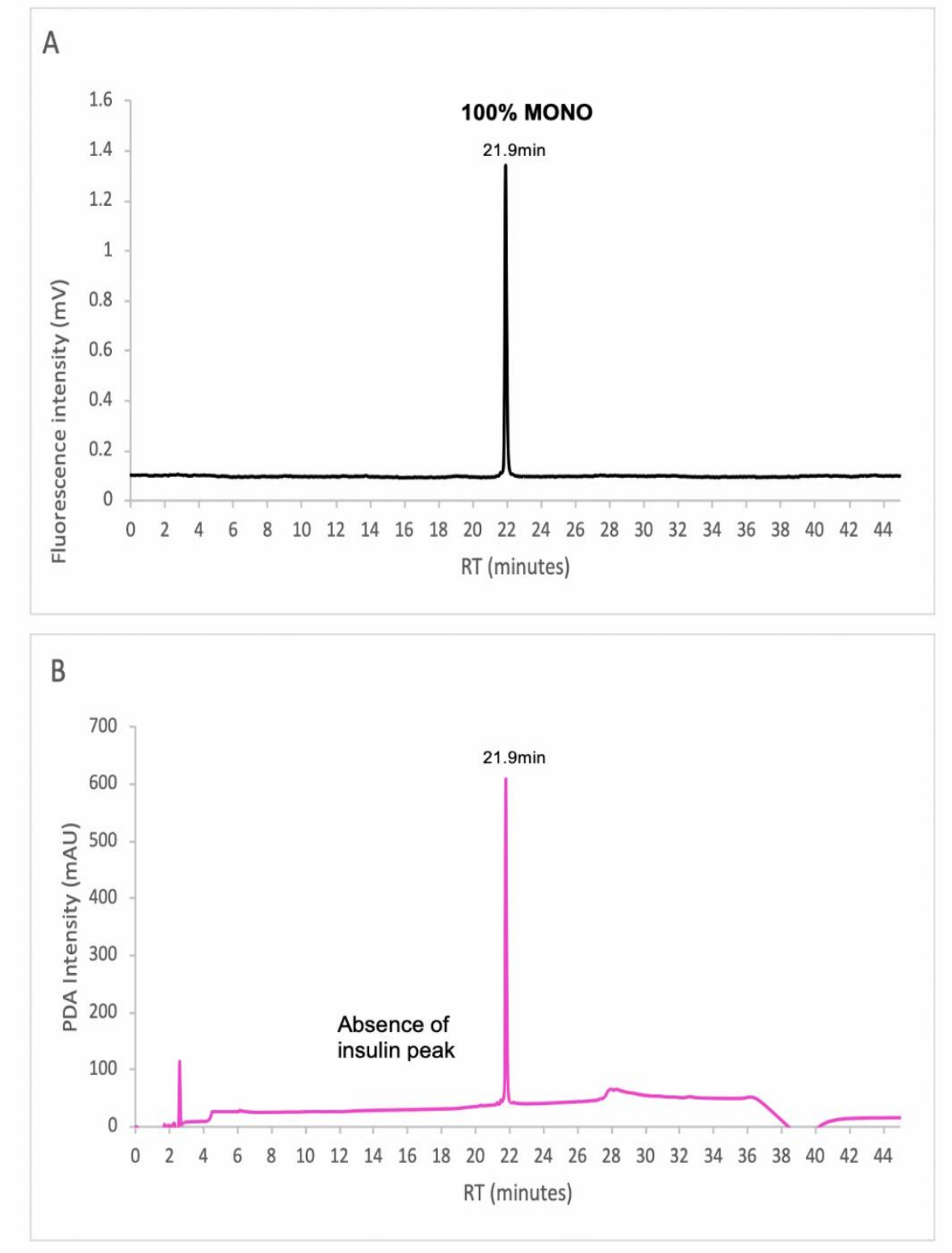

Figure 2-20: RP-HPLC fluorescence chromatogram (A) of the isolated FITC-Actrapid® conjugate showing Mono peak at 21.9min RT and the PDA chromatogram (B) indicating the absence of unlabelled insulin peak at 20.4min RT.

Figure 2-21 shows the mass spectrum data for the isolated Mono sample identified by HPLC, confirming its molecular mass of 6192.7Da and the absence of unlabelled insulin.

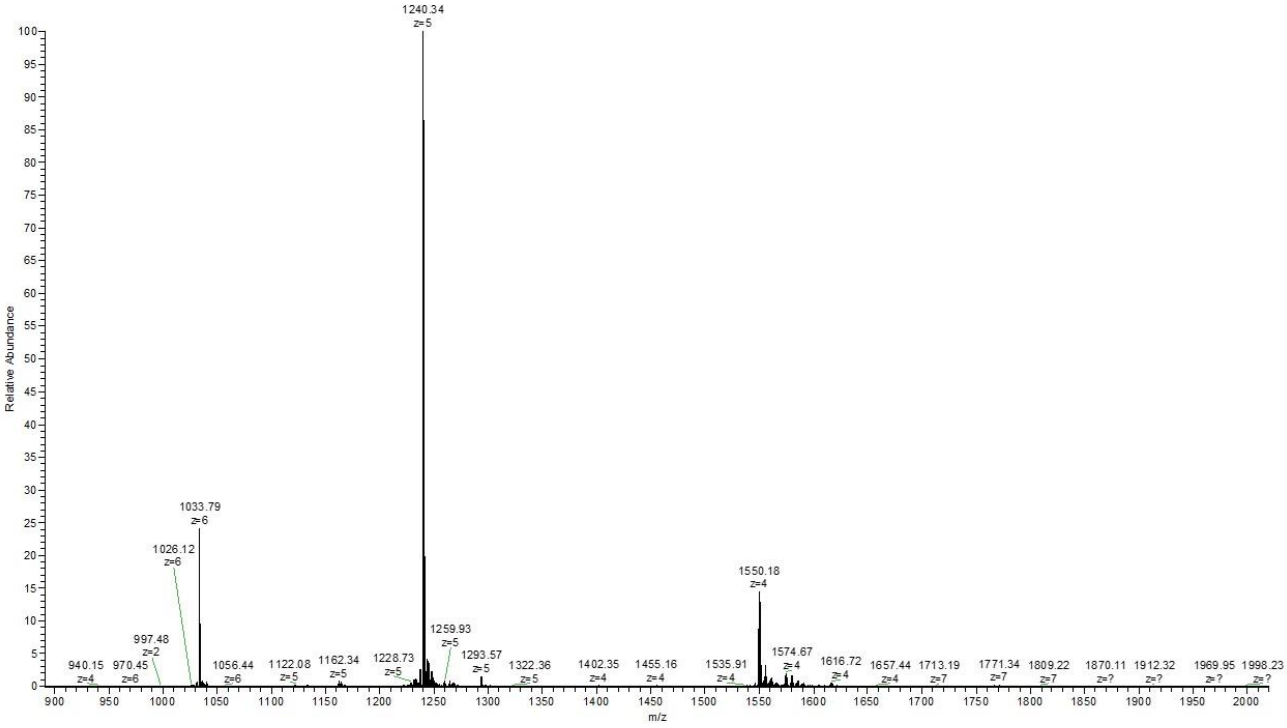

Figure 2-21: Mass Spectra for the isolated FITC-Actrapid® conjugate showing peak corresponding to Mono at m/z of 1240.34/5 and the absence of insulin molecular mass of 5808Da

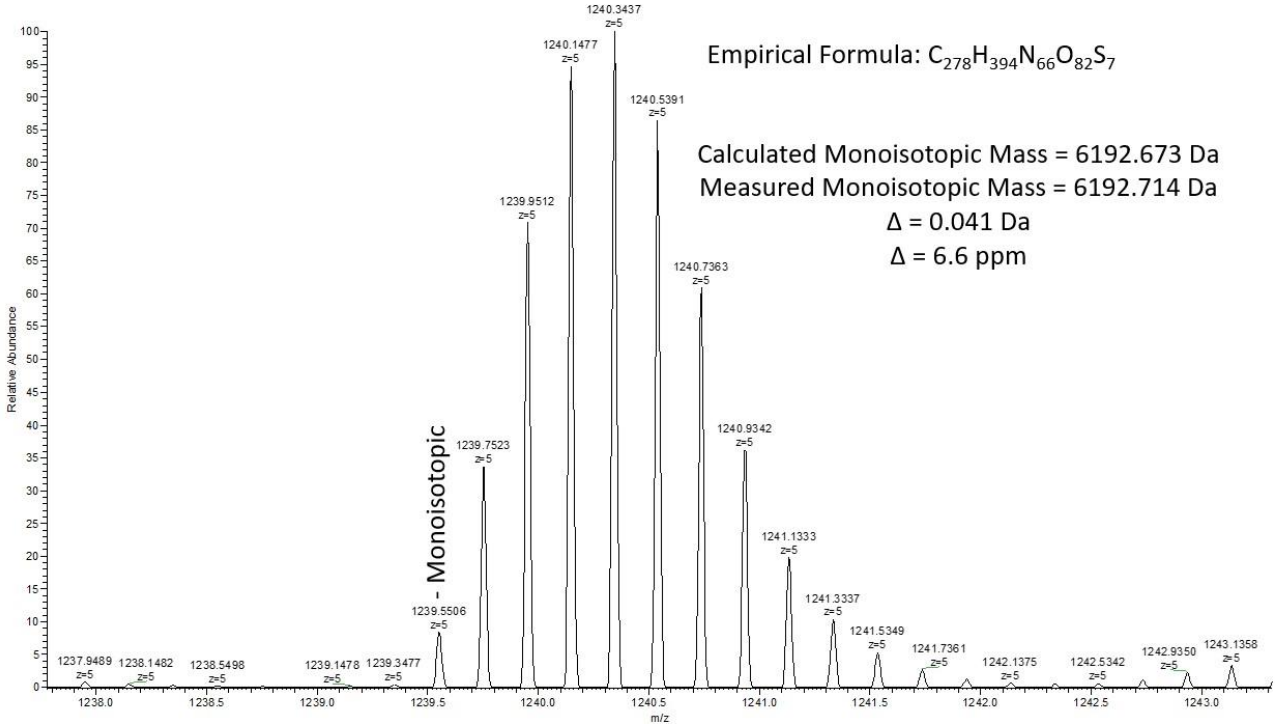

Figure 2-22: Monoisotopic data obtained from the Mass Spectra of Mono at peak 1240.34/5 m/z

Both HPLC and MS analyses confirmed the isolated Mono was in its purest form. To further confirm its labelling position on the insulin molecule, an additional HCD MS2 fragmentation spectrum of 1240.40 (5+) was also obtained. **Figure 2-23** indicates that FITC (peak at 390.0427/1 m/z) was labelled at the B1 position (peak at 537.1112/1 m/z which is the amino acid Phe).

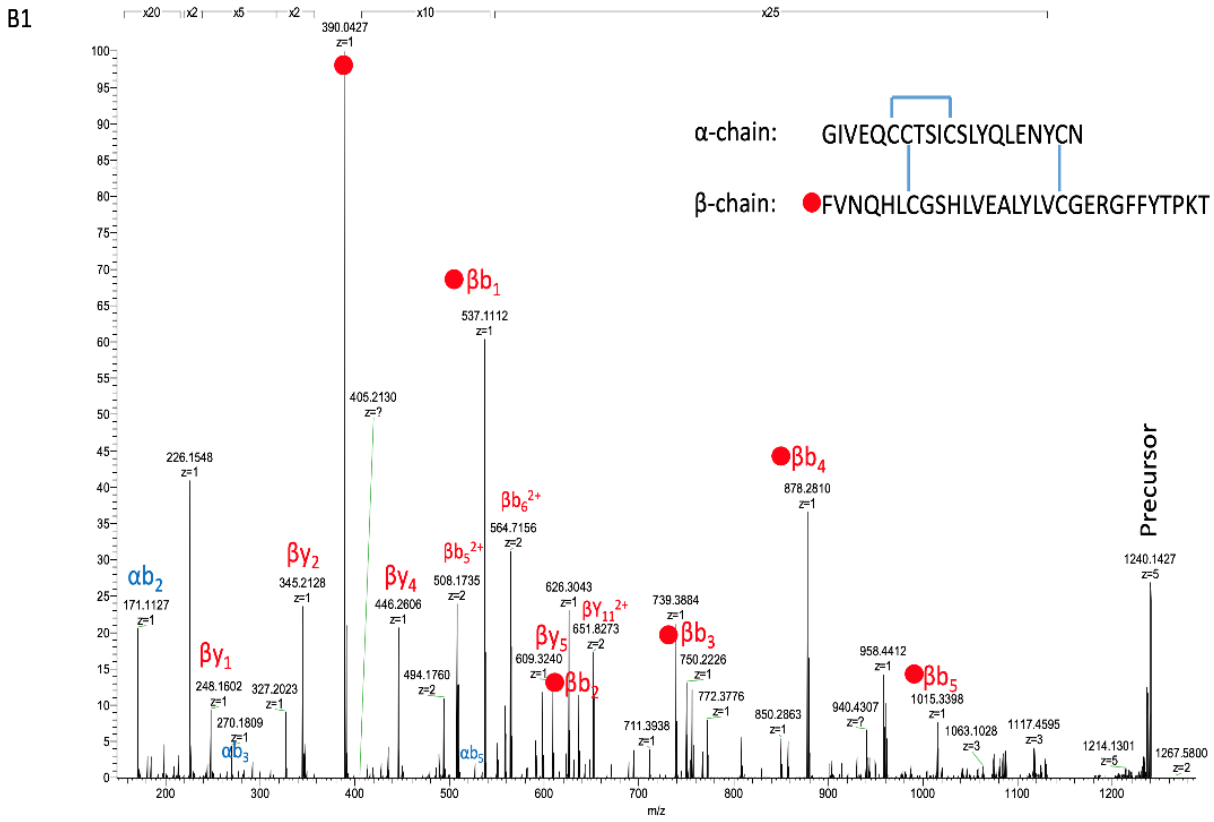

Figure 2-23: HCD MS2 fragmentation spectrum of 1240.40 (5+) with red dots indicating FITC containing fragments. Noting that the m/z peak at 390.0427/1 for FITC was present at the first amino acid of the β-chain which is B1(Phe)

Generally, a quick and robust synthesis protocol by merely adjusting specific reaction conditions to achieve the desired MonoB1 production would be preferred without having to consider the use of protecting group, involving multiple steps of synthesis and purification of intermediates. Modification of pH, molar ratio and reaction time have been successful in producing a single species of mono- labelled FITC-insulin conjugate. However, it is necessary to compromise a balance between obtaining the highest degree of labelling that is consistent with the preservation of activity, which according to Hentz et al. 1997 is MonoB1and minimising nonspecific

binding that can result in labeling of other species with reduced activity. Despite the production of a single entity (MonoB1) using 2:1 molar ratio (FITC: Actrapid®) at pH7 with all reaction time lower than 18h, the compromise leaves unlabelled insulin in the final conjugated products and this is undesirable. However, this problem was overcome by further removal of unlabelled insulin using RP-HPLC method to isolate only the desired MonoB1 from the synthesis with the highest yields.

2.4 Chapter summary

The need to synthesise fluorescently labelled insulin inhouse was first because commercially available FITC-insulin was expensive and not readily available. Secondly, labelling insulin randomly may result in insulin losing its biological activity and thus is not practically ideal for studying the cellular activity of insulin. In our particular work, large amounts of fluorescently labelled insulin will be necessary for further *in-vitro* diffusion experiments to investigate the release profile of insulin from the closed-loop insulin delivery (INsmart) device developed within our group. FITC-bovine insulin and FITC-HI available from Sigma Aldrich were both found to contain a mixture of Mono, Di and Tri as analysed by Jacob 2015. The commercial FITC-bovine insulin also contained unlabelled bovine insulin and unreacted FITC while Tri were the main products identified in the commercial FITC-HI. Each of these is undesirable for representing the *in-vitro* rate of insulin release from our INsmart device since the diffusion rate of FITC alone compared to FITC-HI gives an overestimate due to the big differences in molecular weight. In addition, unlabelled insulin cannot be analysed by fluorescence detection, therefore the diffusion rate analysed from FITC-HI alone may represent only a fraction of the total insulin released from the INsmart device. Moreover, fluorescence detection offers highly sensitive and specific quantification at significantly lower concentration compared to UV absorbance of insulin alone, which could be compromised by the protein absorbance of the smart gel components in the device. Therefore, FITC-labelled insulin was chosen as an improved analytical tool for fluorescence quantification to understand the release profile of insulin from the INsmart delivery device.

The synthesis protocol according to previous studies by Hentz et al.1997 and Jacob 2015 was adopted and further developed to produce the most biologically active FITC-Actrapid® conjugate, which is mono-labelled at the B1 position. Previously, the diffusion study by Jacob 2015 used FITC-HI conjugates that were produced at a

molar ratio of 3:1 after 25h reaction. This conjugate was predominantly di-labelled species (75%). However, the synthesis was successful in confirming the absence of unlabelled insulin. It is anticipated that using further modification of these reaction conditions, it would be possible to synthesise only MonoB1. This desired conjugate is ideal for retaining the biological activity of native insulin as well as offer a more realistic release of insulin from the closed-loop insulin delivery device. The following summaries key findings and achievements:

- Clinically used insulin analogues synthesised for commercially available insulin injections often have modifications to their amino acid sequences which may be of interest to selectively target FITC labelling at a certain site. Screening of short-acting, rapid-acting and intermediate-acting insulin preparations for the production of FITC-insulin conjugates using 2:1 molar ratio at both short and long reaction time has selected Actrapid® as the best candidate for achieving the desired mono-labelled species. Besides, the quick onset of action exhibited by Actrapid® also makes it the most preferable product for future biological applications in tracing and receptor binding essay using both *in-vitro* and *in-vivo* study.
- Reducing the molar ratio of FITC/insulin to 2:1 has successfully prevented the production of Tri while minimising the yield of Di at a reaction time of 20h however the conjugates synthesised at a shorter reaction time than 20h always contain some unlabelled insulin. The result suggested that having a high amount of FITC would increase the chance of producing more di- and tri-labelled species, especially at a long reaction time of ≥ 20h. In another way, lowering the molar ratio of FITC has selectively inhibited the labelling of FITC at the B29 position that results in the production of Tri, however, reducing the amount of FITC also limits the degree of insulin labelling and therefore there would be a higher amount of unlabeled insulin at shorter reaction time. A fine balance of FITC: insulin molar ratio and sufficient reaction time are therefore required to achieve optimal labelling.
- Having a low amount of FITC as in 0.5:1 molar ratio (FITC/Actrapid®) also produced only Mono. However, there was more unlabelled insulin present in the conjugates. Longer reaction time at this low molar ratio was not studied in this current work as it could take several days to overcome the presence of

unlabelled insulin however it might be of interest to find out if the production of Di can be prevented even at longer reaction time than 20h using this low ratio. Overall, 2:1 molar ratio has been chosen for further synthesis to produce the desired Mono

- Adjusting the pH of the reaction mixture close to the pK_a of the individual amino acid at A1 (pK_a of 8.4); B1(pK_a of 7.1) and B29 (pK_a>9.8) could not selectively target labelling to a specific amino acid. There was some degree of selective labelling at pH≥8 which resulted in the production of two mono-labelled species at A1 and B1 positions with some Di (6%) even at a short reaction time of 2h. Reaction at pH≥9 resulted in a mixture of conjugates including Mono, Di and Tri. Meanwhile, only the reactions at pH7 and 7.5 have successfully produced a single Mono (100%). However, unlabelled insulin was also present at 2h reaction time. Based on the chromatographic data presented by Hentz et al., the production of mixed conjugates at pH≥8 highly supported the hypothesis that the Mono produced at pH7-7.5 could be labelling at the B1 position, which according to Hentz et al. is also the most biologically active species.
- Several reaction times of less than 19h at pH7 using 2:1 molar ratio (FITC/Actrapid®) are capable of producing only the desired Mono. However, optimise labelling of FITC to Actrapid® is not yet achieved due to the presence of unlabelled insulin in the final conjugated product. Further HPLC purification of the highest Mono yield produced at 2:1 molar ratio, pH 7 after 18h has successfully removed any unlabelled insulin to achieve 100% pure Mono. This was confirmed by RP-HPLC and MS to only contain mono-labelled species labelled at the B1 position. Further examination of this conjugate activity in different cell-line will be done to conclusively confirmed its biological activity.

Chapter 3. The biological activity study of FITC-insulin species synthesised in-house

3.1 Introduction

The experimental work presented here provides one of the first investigations into the biological activity of four different FITC-Actrapid® conjugates synthesised inhouse using HUVEC. The insulin signalling pathway for the regulation of glucose metabolism has been well studied both *in-vitro* and *in-vivo* using insulin-responsive models such as skeletal muscle, adipose and liver cells (Karlsson et al., 2005; Titchenell et al., 2016; Honka et al., 2018). The use of HUVEC has also been used as a model for insulin signalling studies, however the specific effect of insulin stimulation on glucose metabolism has not yet been investigated (Maeno et al., 2012). Besides, there is also very little research on the expression of insulin-dependent glucose transporter (GLUT4) in HUVEC. More investigation into the regulation of insulin, especially glucose transport, in HUVEC is, therefore, necessary to address this gap in the existing literature. This chapter covers a basic overview of the insulin signalling pathway; its specific role for glucose uptake; introduction to endothelial cells and their use to investigate the biological effect of insulin. The main objective is to assess the biological activity of Actrapid® and its fluorescent labelled conjugate with FITC by measuring the level of serine/threonine AKT phosphorylation and GLUT4 translocation via the insulin signalling pathway in HUVEC and skeletal muscle cells C2C12 respectively. The outcome of the study would confirm if the mono-labelled FITC-Actrapid® conjugate synthesised inhouse has similar or equivalent biologically activity as native insulin.

3.1.1 Insulin signalling pathway overview

Principally, cells communicate and function via a specific biochemical signalling pathway which involves three essential elements: the substrate/stimuli, a receptor type on the cell membrane and a cascade of events that triggers series of cellular activities once the substrate/stimuli binds to its receptor. The insulin

signalling pathway is one of the most important mechanisms of biological action, which regulates many fundamental functions of the cells. Cellular responses to insulin involve regulation of glucose homeostasis, stimulation of glycogenesis, lipogenesis and protein synthesis, modification of gene expression leading to cell proliferation, cell differentiation and apoptosis (Kolb et al., 2020; Hatting et al., 2018). The signalling pathway of insulin is also one of the most attractive research areas not only because of its fundamental roles in cellular activity but also due to its complex yet impressive cascade of cellular events that help maintain normal cell functions. Besides, these cascades of events stimulated by insulin are also famous as a targeting site for the treatment of diabetes mellitus and other related diseases (Kerru et al., 2018; Artasensi et al., 2020; Yaribeygi et al., 2019b). Although the activity and function of insulin involve complex signalling cascades, one keynote is that these series of events would occur in a chronicle cascade, most of which is via phosphorylation of several substrate proteins and disruptions to these events would result in abnormal cell function or disease (Di Camillo et al., 2016).

Initially, insulin hormone released to the bloodstream by beta cells from the islets of Langerhans in response to high blood glucose level arrives at the extracellular fluid and are recognised by its insulin receptor (IR) on the cell surface of target tissues. As detailed in chapter 3, IR is a glycoprotein dimer consisting of two extracellular (α) and two transmembranes (β) subunits that also project inside the cell. The signalling begins when insulin, the primary messenger, binds to the alpha subunit of IR of target cells on the extracellular membrane, resulting in dimerisation of the receptor to form the $\alpha_2\beta_2$ complex in the cell membrane. This complex, in turn, activates the beta subunit of the IR by auto-phosphorylation of its activating loop. Here, the three tyrosine kinase residues on each beta subunits are phosphorylated (**Figure 3-1**), leading to the phosphorylation of several substrates that provide specific docking sites for the recruitment of other downstream signalling proteins (Hall, Yu and Choi, 2020; De Meyts, 2016)

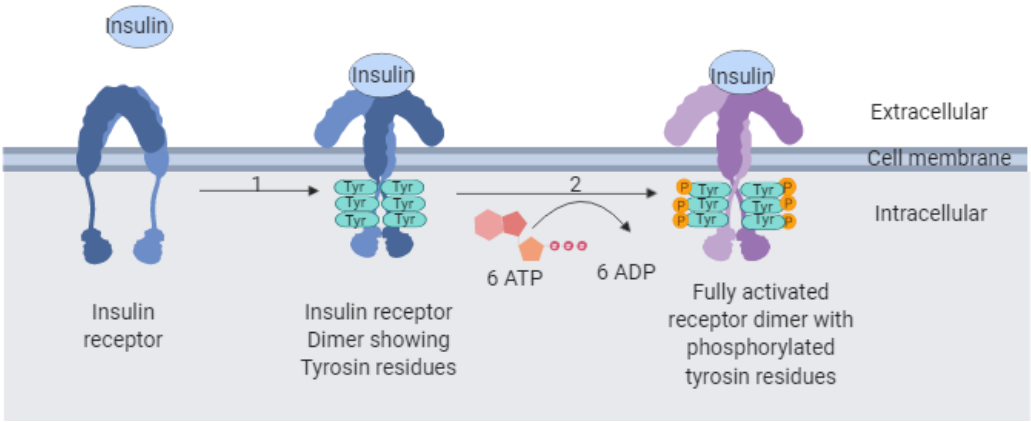

Figure 3-1: Initial activation of the insulin receptor. Insulin binds to insulin receptors triggering its dimerisation (1) and intracellular autophosphorylation of their tyrosine residues (2) (Adapted from Chapman 2013)

The subsequent result from a fully activated IR then leads to the activation of two major signalling cascades of events: the mitogen-activated protein kinases (MAPK) pathway and phosphatidylinositol 3 kinase (PI3K)/ AKT pathway. The MAPK pathway which is also known as the extracellular signal-regulated kinase mainly involves in the regulation of genes expression and therefore has a role in mitogenic functions of cell growth (Hall, Yu and Choi, 2020; Zhao and Zheng, 2017). Meanwhile, the PI3K/ AKT pathway is regulated exclusively by the insulin receptor substrate (IRS) and is responsible for the metabolic action of insulin throughout the body (Madhunapantula, Mosca and Robertson, 2011; Rai et al., 2019; Świderska et al., 2018)

The metabolic action of the insulin-dependent cascade is carried out by most cell types in the body yet is more specific to cells of the muscle tissue, vascular endothelium, heart, adipose tissue and liver. Initially, glucose metabolism via glucose uptake into cells of adipose tissue, skeletal muscle, and the heart is one of the essential responses generated by insulin's effects to maintain glucose homeostasis (Zatterale et al., 2020; Chadt and Al-Hasani, 2020; Rai et al., 2019). In the liver, insulin exerts its metabolic effect on the reduction of gluconeogenesis (production of glucose) and increases in glycogenesis (conversion of glucose to glycogen). Insulin also stimulates the synthesis of fat as a source of energy storage and protein synthesis as well as conversely

inhibits lipolysis and protein degradation. Vasodilation via the production of nitric oxide (NO) is also observed in the vascular endothelium and heart as a result of insulin stimulation (Bahadoran, Mirmiran and Ghasemi, 2020; Vargas and Carrillo Sepulveda, 2019).

Although the full pathway of insulin signalling is far too complex to be discussed in detail as it involves several signal-transduction steps and consequential series of responses. The need to understand the effect of insulin stimulation that leads to the phosphorylation of AKT is important for the investigation of insulin biological activity in fluorescently labelled insulin candidates. A more detailed account for the mechanism of insulin action through the PI3K/AKT signalling pathway is discussed in the next section.

3.1.2 Insulin stimulates PI3K/AKT signalling pathway

The following description mainly focuses on the mechanisms of PI3K/AKT signalling that regulates metabolism in normal physiology in response to insulin stimulation (refer to **Figure 3-2)**.

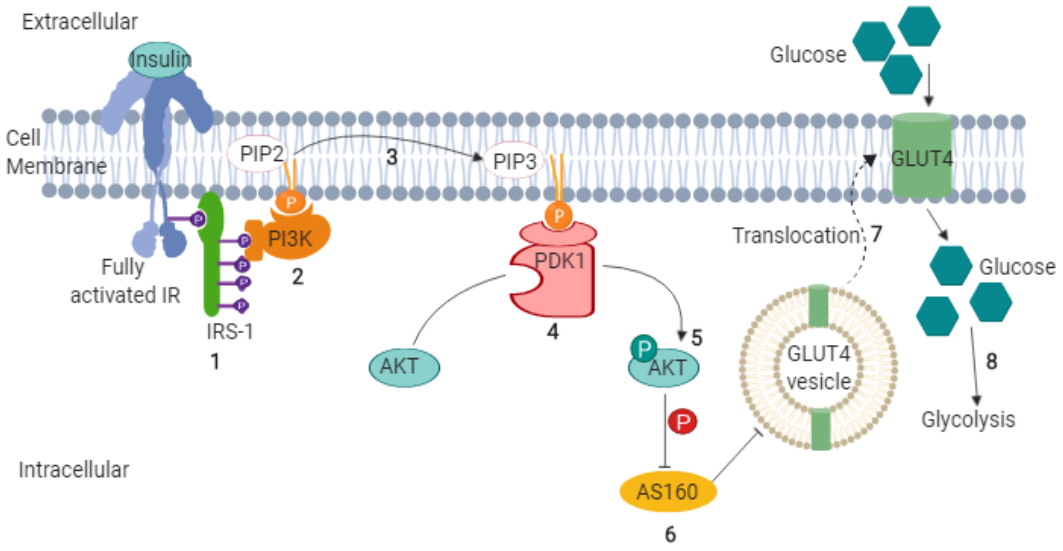

Figure 3-2: Summary of Insulin stimulates PI3K/AKT signalling pathway: (1) Phosphorylated IRS-1 leading to activation of PI3K (2), resulting in the formation of PIP3 (3) as a second messenger. (4) PDK1 is then activated, subsequently leading to activation of AKT to its phosphorylated form (5), which leads to the phosphorylation of AS160 (6), causing translocation of GLUT4 vesicle to the cell membrane (7). GLUT4 facilitates the influx of glucose, leading to glycolysis (8). (Adapted from JJ Medicine 2017)

The PI3K/AKT pathway starts when one of the phosphorylated tyrosine kinase residues of the IR attracts the IRS-1. This adaptor protein IRS-1 is one of major substrates of the IR along with IRS-2 and IRS-4, usually described as a platform for the signalling complex. Upon binding, the IRS-1 is phosphorylated by the insulin receptor kinase. The phosphorylated IRS-1 now acts as an attachment point for PI3K, a lipid kinase. Once the regulatory region of PI3K attached to the phosphorylated residues of IRS-1, it causes the active site of PI3K to move in close proximately to the membrane where phosphatidylinositol 4,5- diphosphate (PIP2) is found. Here, the active PI3K attaches a phosphate group from an ATP molecule onto PIP2, creating phosphatidylinositol 3, 4, 5 triphosphates (PIP3) – the second messenger. This PIP3 travels along the membrane to activate the 3-phosphoinositide-dependent protein kinase 1 (PDK1). This activated PDK1 subsequently activates AKT (also known as protein kinase B or PKB) via two mechanisms: PDK1 can directly phosphorylate AKT at Threonine 308 phosphorylation site or it can indirectly activate mTOR complex, which then can phosphorylate AKT at Serine 473 phosphorylation site. The activated AKT then consequentially leads to phosphorylation of AS160 (AKT substrate of 160kDa). Under normal physiology without insulin stimulation, AS160 substrate protein acts as an inhibitor of GLUT4 translocation, preventing its localisation to the membrane. However once phosphorylation of AS160 occurs, translocation of GLUT4 from the cytoplasmic vesicles onto the cell membrane surface will be stimulated (Khorami, Movahedi and Sokhini, 2015; Huang et al., 2018; Sugiyama, Fairn and Antonescu, 2019). The resultant GLUT4 translocation to the cell membrane thereby increases the insulin-dependent transport of glucose into the cell, leading to glycolysis.

One important point to consider is that under normal physiology, both receptor tyrosine kinase and G-Protein coupled receptor can lead to the activation of AKT (Law, White and Hunzicker-Dunn, 2016; Sugiyama, Fairn and Antonescu, 2019; New et al., 2007). AKT is a well-known target for multiple pathways however under basal conditions, AKT activation is relatively low therefore it is of interest to investigate the enhanced AKT activation in the presence of insulin. Beside AS160 substrate protein, the activated AKT also plays a vital role in the

cell signalling mechanisms that regulate the activity of many other major proteins (such as mTOR, FOXO) for cell metabolism, cell survival and proliferation (Nitulescu et al., 2018; Revathidevi and Munirajan, 2019). Noting that these responses from activated AKT were not illustrated in **Figure 3-2** since the key focus is to simplify the insulin signalling cascade leading to AKT phosphorylation only. However, to facilitate the study behind the biological activity of fluorescently labelled insulin candidates, the insulin action on GLUT4 translocation will be detailed in the following section.

3.1.3 Insulin regulation of glucose transporters

Glucose is an essential carbohydrate and primary energy resource within most cells, especially mammalian cells. Since most living cells use glucose for their energy production, glucose transport across the cell membrane is therefore critical for life. However, because of its relatively large size and polar nature, glucose molecules cannot cross the cell membrane by simple diffusion due to the impermeable property of the lipid bilayer to polar carbohydrate. Instead, the entry and exit of glucose molecules across the cells are mainly achieved by glucose transporters (Stringer, Zahradka and Taylor, 2015; Yaribeygi et al., 2019; Navale and Paranjape, 2016). Under basal conditions, the initial supply of energy is from the breakdown of endogenous glycogens which are stored in the liver for whole-body usage. These stores are replenished by glucose from diet. Following carbohydrate digestion and glucose absorption in the circulation, insulin secretion from the pancreatic β-cells is stimulated, leading to the distribution of glucose among various tissues in the body (Gonzalez and Betts, 2019b; Chadt and Al-Hasani, 2020). In order to achieve rapid uptake of glucose, the brain, muscle and adipose tissues have to adapt with highly specialised glucose- transport system (Chadt and Al-Hasani, 2020; Wasik and Lehtonen, 2018; Koepsell, 2020). This system is not only crucial for insulin-dependent glucose storage in muscle and adipose tissues after a meal to maintain normal blood glucose levels consistently but also particularly important during exercise to meet rapidly high metabolic requirements of skeletal muscles (Sayem et al., 2018). Meanwhile, although the brain is also highly equipped with specialised-

glucose transporters, it is understood that glucose uptake in most brain cells is not dependent on insulin (Gray, Meijer and Barrett, 2014; Koepsell, 2020).

Glucose distribution throughout the body is performed by a family of glucose transporter proteins which act as vehicles to carry glucose across the cell membrane. Sodium-glucose linked transporters (SGLTs) and facilitated diffusion glucose transporters (GLUTs) are two main types of glucose transporters that have been identified. SGLTs are also known as secondary active transporters that use the sodium concentration gradient generated by the sodium-potassium ATPase as a source of chemical potential to drive glucose uptake (Mueckler and Thorens, 2013; Stringer, Zahradka and Taylor, 2015). On the other hand, GLUTs are classed as facilitative glucose transporters that transport glucose across the plasma membrane using a facilitated diffusion mechanism as its class suggested. Here, glucose molecules diffuse down their concentration gradient across the cell membrane via GLUTs protein channels to enter the cells. Both types of transport are equally essential and can be found across different tissues and organs. SGLTs express mainly on the luminal surfaces of cells lining the small intestine where they absorb glucose from diet. They are also known to facilitate the reabsorption of glucose from the glomerular filtrate and are therefore present in renal tubules. While SGLTs are responsible for reabsorption of glucose into the circulation, GLUTs are essential for the transport of glucose into the cells where it can be utilised as energy or stored as glycogen and fat. GLUTs are proteins containing 12 membrane-spanning regions with intracellularly located amino and carboxyl terminals. According to recent researchers, 14 mammalian facilitative GLUTs have been identified until now. Each of them has distinct substrate affinity, specificity, and tissue distribution (Navale and Paranjape, 2016; Long and Cheeseman, 2015; Klip, McGraw and James, 2019). They are subdivided into three classes based on their protein sequences and structural similarity as summarised in **Table 3-1.** The information listed below is mainly collected from reviews by Calvo et al., 2010 and Navale and Paranjape, 2016.

Table 3-1: Major sites of expression and roles of different GLUTs

GLUTs classes	GLUTs isoforms	Tissue distribution	Function
Class I	GLUT1	Red blood cells present in all human tissue, blood-brain barrier, heart (lesser extent)	Insulin independent- primary vehicle for transport of glucose from the blood into the brain as well as across other blood and tissue barriers to ensure that both brain and RBC receive the appropriate level of glucose.
	GLUT2	Beta cells of the pancreas, liver and kidney.	Insulin-independent Act as glucose sensor of the insulin-secreting β-cells
	GLUT3 (GLUT14)	Brain, Neurons	Insulin-independent Transfer glucose into the cells that have a higher requirement of glucose
	GLUT4	Heart, brain, skeletal muscle, adipose tissue	Insulin-dependent Increase glucose uptake into the cells from circulation.
Class II	GLUT5	Cells of the small intestine, testes and kidney	Primary transporter of fructose
	GLUT7	Cells of the small intestine, colon, testis and prostate	High-affinity transporter for glucose and fructose
	GLUT9	The proximal tubule of the kidney, in the liver and placenta	major transporter for uric acid reabsorption by the kidney
	GLUT11	Heart, placenta, skeletal muscle, kidney and pancreas cells, adipose tissue	Facilitate the transport of both glucose and fructose
Class III	GLUT6	Brain, spleen cells and peripheral leukocytes	low-affinity glucose transporter
	GLUT8	Brain and testis cells	Not regulated by insulin, facilitate glucose transport through the intracellular membrane such as mitochondria membrane
	GLUT10	Heart, brain, placenta, skeletal muscle, lung, kidney, liver and pancreas cells	maintaining redox homeostasis
	GLUT12	Adipose tissue, small intestine, skeletal muscle, pancreas.	Insulin-dependent but influenced by protons. Facilitate transport of glucose in a similar mechanism as GLUT4
	GLUT13	Brain, Blood-brain barrier, Adipose tissue	specific transporter for myoinositol

As emphasised on the fundamental role of insulin in maintaining glucose homeostasis, GLUT4 also plays a vital role as the only source of insulin-sensitive glucose transport. It is expressed mainly in skeletal muscle and adipose tissues and to a smaller extent in heart tissues. (Klip, McGraw and James, 2019; Chadt and Al-Hasani, 2020) Under basal state, GLUT4 resides in intracellular cytoplasmic vesicles called GLUT4 storage vesicles (GVS). In response to increased BG level, insulin stimulates glucose uptake via GLUT4 by efficiently deposing of glucose bulk from the circulation into skeletal muscle and other target tissues. Upon insulin stimulation, GLUT4 vesicles would undergo exocytosis to enable GLUT4 translocation to the plasma membranes. GLUT4 exocytosis can be described as a process involving the generation of GLUT4 vesicles moving from the trans-Golgi network region to the plasma membrane and finally fusion of these vesicles to the plasma membrane (Hou and Pessin, 2007; Stöckli, Fazakerley and James, 2011; Vargas and Carrillo Sepulveda, 2019), refer to **Figure 3-3**. Here, GLUT4 acts as a protein channel allowing the influx of glucose across the plasma membrane into the cells. After uptake, glucose can either be stored as glycogen or undergo oxidation in the mitochondria for energy conversion (Bahari et al., 2020; Son and Wu, 2019)

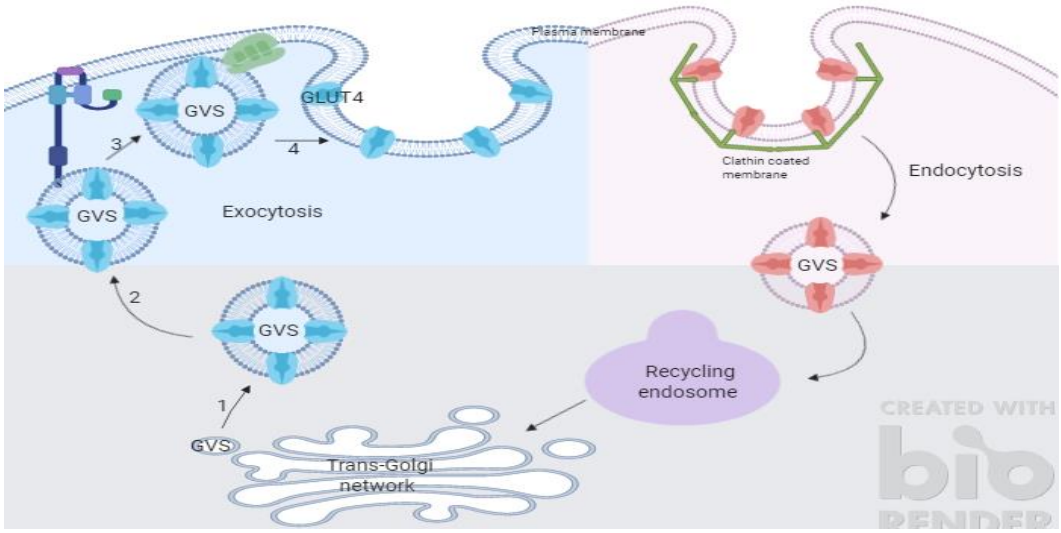

Figure 3-3: Trafficking of GLUT4 exocytosis:(1) Movement of GVS from the Trans-Golgi network toward the plasma membrane (2) Tethering;(3) Docking and (4) Fusion of GVS with the membrane then recycled via endocytosis (Adapted from Larance et al. 2008)

Another model of GLUT4 exocytosis is understood to involve the initial approach of GVS by specialised microtubules on the cell membrane, followed by tethering of these vesicles mediated by large multi-subunit complexes. Further docking and fusion of GLUT4 vesicles to the cell membrane allow GLUT4 to exert its action. This sophisticated model falls beyond the objective of this biological activity study to be discussed in detail. In fact, the underlying process involving tethering, docking and fusion of the GLUT4 vesicles to the plasma cell membrane is only partially understood to involve complex interactions between various proteins and several regulatory factors (Stöckli, Fazakerley and James, 2011; Jaldin-Fincati et al., 2017; Vargas, Podder and Sepulveda, 2019)

Over the past few decades, more information has become available from the extensive study of GLUT4 trafficking to establish that GLUT4 is a continuously recycling membrane protein. This cycling process of GLUT4 involves its exocytosis movement from the endosomal origin towards the plasma membrane and its endocytosis movement from the membrane back to the endosomal sorting system (Jaldin-Fincati et al., 2017; Tunduguru and Thurmond, 2017; Klip, McGraw and James, 2019). Endocytosis of GLUT4 involves the budding of clathrin-coated vesicles of GLUT4 on the plasma membrane then upon internalisation, GLUT4 becomes a part of the early endosomes and re-sorted back into intracellular vesicles (**Figure 3-3**) (Hou and Pessin, 2007; Vargas, Podder and Sepulveda, 2019). A detailed process of GLUT4 vesicles budding and internalisation will not be illustrated here. However, reviews by Hou and Pessin, 2007 and Antonescu et al., 2009 have discribed the activity of some protein complexes contributing to GLUT4 endocytosis. Nevertheless, GLUT4 exocytosis has been studied to a larger extent because insulin is well established to rapidly stimulate the rate of GLUT4 exocytosis in adipose and skeletal muscle cells while there is inadequate literature to support the regulation of GLUT4 endocytosis by insulin (Jaldin-Fincati et al., 2017; Elhassan et al., 2018; Brewer et al., 2014; Watson and Pessin, 2007). Interestingly, as suggested by Gonzalez and McGraw, 2006 the

primary regulator of GLUT4 exocytosis, which is AKT, is not required for insulin regulation of GLUT4 endocytosis.

PI3K/AKT pathway is a major insulin signalling that leads to GLUT4 translocation, through phosphorylation of the AS160 substrate as described in the previous section. AS160 is a GTPase-activating protein that when phosphorylated activates small G proteins called Rabs, which are important for the organisation of intracellular membrane trafficking (Tan et al., 2012; Homma, Hiragi and Fukuda, 2020). The switching between the active form by GTP loading and inactive forms via GTP hydrolysis of Rabs is catalysed by guanine nucleotide exchange factors (GEFs) and GTPase-accelerating proteins (GAPs). Here, during unstimulated conditions, Rabs are maintained in their GDP-loaded inactive form by the active AS160, retaining GLUT4 stored as GSVs within the intracellular space. Once insulin stimulates phosphorylation of AS160 via activated AKT, the activity of AS160 is inhibited. The overall effect leads to the activation of a Rab protein which then regulates docking and fusion of GSVs with the plasma membrane hence resulting in GLUT4 translocation (Jaldin-Fincati et al., 2017; Brewer et al., 2014). It was evidenced that insulin-stimulated GLUT4 translocation could be inhibited by the expression of mutant AS160 that missing AKT-specific phosphorylation site or the knockdown of AS160 in specific tissues (Tan et al., 2012; Sano et al., 2003).

Meanwhile, other pieces of evidence also suggested that the proto-oncoprotein c-Cb1 tyrosine phosphorylation is also stimulated by insulin, initiating another signalling cascade which is independent of the PI3K pathway. Although this cascade of events has not been studied extensively, the key finding is that this insulin-dependent stimulation process would also subsequently lead to GLUT4 translocation to the plasma membrane (Liu et al., 2009; Vargas and Carrillo Sepulveda, 2019) .

Besides insulin, exercise and physical activity causing muscle contractions also stimulates glucose transport via GLUT4 translocation in skeletal muscle through an AMK -dependent mechanism, which is independent of the insulin-stimulated pathway. Skeletal muscle contraction triggered by membrane depolarisation

results in increased intracellular calcium ion (Ca2+) and reduced intracellular ATP concentrations. This change, in turn, leads to activation of 5'-AMP-activated protein kinase (AMPK) which is believed to contribute to exercise-responsive GLUT4 vesicles translocation to the plasma membrane. Here, GLUT4 mediate glucose transport into the cells to meet the increased energy demands of skeletal muscle during exercise (Knudsen et al., 2020; Sylow et al., 2016; Richter and Hargreaves, 2013)

Many recent reviews related to insulin activity and signalling pathways have a rise in complexity and cascade of events in addition to increasing number of protein complexes involved and other chemicals contributing to the accomplishment of insulin functions. Understanding many intricate steps in GLUT4 translocation is essential to investigate the nature of defects in insulin resistance so that improved strategies and specialised treatment choices can be designed to tackle complications of diseases affected by insulin resistance. However, it is beyond the scope of this study to discuss in detail, the overall objective of this review is to assist a basic understanding of insulin signalling pathways yet simplify the key regulation of insulin biological activity involved in the phosphorylation of AKT and GLUT4 translocation to the plasma membrane, thus the consequence effect in maintaining glucose homeostasis as described in section 1.1.1.

3.1.4 The Role of Insulin signalling in Human Endothelial Cells.

In addition to its metabolic roles, insulin also has vasodilator actions in the production of NO from the vascular endothelium (Luse et al., 2020; Walsh et al., 2019). Functional insulin receptors are also expressed on endothelial cells, thus enabling intracellular signalling responses to insulin stimulation (Kolluru, Bir and Kevil, 2012; Escudero et al., 2017). Many studies have demonstrated that insulin induces this vasodilator response via the PI3K-AKT pathway (Mammi et al., 2011; Jiang et al., 2014; Muniyappa et al., 2020). Following insulin stimulation as detailed in section 3.1.2, the Serine/Threonine protein kinase AKT will be activated which leads to the enhancement of endothelial nitric oxide

synthase (eNOS) phosphorylation, resulting in NO production. NO is one of the most important signalling molecules in endothelial cells due to its potent vasodilator action as well as a powerful anti-platelet activity, preventing platelets from sticking to vessel walls and anti-leukocyte factor to reduce inflammation. Production of NO is essential for mediating dilation and improve blood flow hence ensuring sufficient nutrient supply to tissue (Janus et al., 2016; Strembitska et al., 2018; Luse et al., 2020). More importantly, it has been reported that inhibition of insulin via the PI3K/AKT pathway could lead to impaired NO availability and loss of NO function, which is one of the earliest indicators or markers of CVD(Zeng et al., 2000; Jiang et al., 2014; Ormazabal et al., 2018). Additionally, a decrease in NO bioavailability is well observed in patients with type 1 and type 2 diabetes and also in cardiovascular disorders such as hypertension and atherosclerosis associated with insulin resistance (Salt et al., 2003; Tessari et al., 2010; Assmann et al., 2016).

Generally, HUVECs which originate from the vein of the umbilical cord, are one of the most popular model systems used to study the regulation of endothelial cell function *in-vitro* because of their relatively high availability compared to other types of blood vessels. Their common applications in physiological and pharmacological investigations include macromolecule transport, blood coagulation, angiogenesis, and fibrinolysis (Cao et al., 2017). In addition, there are many important endothelial markers such as selectins expressed in HUVECs, as well as signalling molecules associated with vascular physiology like NO (Caniuguir et al., 2016; Choi et al., 2018).HUVECs, like other ECs, could produce NO through the activity of eNOS to regulate the function of blood vessels (Karbach et al., 2014; Gimbrone Jr and García-Cardeña, 2016). Although there is still a lack of evidence for the expression of GLUT4 in HUVECs, some studies suggested that mainly GLUT1, GLUT3 and GLUT4 are expressed in endothelial cells. However, GLUT1 is said to more predominant (Al Mamun et al., 2020; Li, J. et al., 2020; Yazdani et al., 2019). It is of interest to investigate the translocation of GLUT4 in response to insulin stimulation in HUVECs since GLUT1 is independent of insulin as detailed in **Table 3-1**.

There have been several studies examining the effects of insulin stimulation using HUVEC, none of which explicitly investigates the GLUT4 translocation. However, it is well established that insulin resistance is one of the key contributors to many complications of CVD and HUVECs have been used as an endothelial model to investigate the treatments of insulin resistance. In particular, Mammi et al., 2011 used HUVECs to study the effect of sildenafil, a phosphodiesterase 5 (PDE5) inhibitors, in insulin resistance conditions. Here, HUVECs were treated with insulin in the presence of glucose 30 mM and glucosamine 10 mM with or without sildenafil. In insulin resistance conditions, the activation of AKT and eNOS was found to be impaired to a certain extent depending on the level of resistance, leading to reduced vascular functions in patients with diabetes. AKT phosphorylation is one of the most crucial steps within insulin signalling cascade for the regulation of glucose homeostasis, glycogenesis, lipogenesis and protein synthesis. In the case of HUVEC, pAKT l enhances the activation of eNOS, leading to NO production. The level of AKT phosphorylation and NO production were the two main measurements in Mammi's study to assess the potential therapeutic use of sildenafil in restoring the activation of AKT and eNOS in insulin resistance conditions. Promisingly, the data has indicated that sildenafil might help restore the level of AKT and eNOS activation in insulin resistance conditions (Mammi et al., 2011).

Another study by Yang et al., 2016 also used HUVECs to evaluate the effect of atorvastatin- a vessel protective drug that is used to reduce blood cholesterol on insulin resistance-associated endothelial dysfunction. In Yang's study, HUVECs were pre-treated with different glucose concentrations with, or without insulin for 24 h, following treatment with atorvastatin. Interestingly, a wide range of phosphorylation products derived from the insulin signalling pathways were all assessed during this experimental study. These measurements included the tyrosine phosphorylation of IR and IRS-1, the production NO, the activity and phosphorylation level of eNOS on serine1177 although not the phosphorylation level of AKT. This study not only illustrated certain key steps within the insulin signalling pathways using HUVECs but also demonstrated that high

concentrations of glucose and insulin for 24 h would result in an insulin signalling impairment and lead to endothelial dysfunction. The data also showed promising result of atorvastatin used in a dose-dependent manner under insulin resistance state to enhance the protein expression of phosphorylated IR, IRS-1 and eNOS as well as increased activity of eNOS and the production of NO primarily via the PI3K/AKT/eNOS pathway (Yang et al., 2016).

Many other studies have also investigated HUVEC response to insulin primarily via the IRS/PI3K/AKT/eNOS pathways and mostly analysed by the level of IRS or AKT phosphorylation; the activity of eNOS or the production of NO. These studies are designed either by inhibition of insulin signalling or mimicking insulin resistance state in order to investigate the potential therapeutic use of certain medicines or chemicals in CVD related to insulin resistance (Maeno et al., 2012; De Nigris et al., 1; Choi et al., 2018).The use of HUVEC is therefore supported in this particular study to investigate the insulin signalling pathway of PI3K/AKT in response to both insulin and its FITC-labelled conjugates stimulation.

Meanwhile, it is without question that skeletal muscle is one of the major target tissues for insulin activity and plays an essential role in insulin-induced glucose uptake since most studies used skeletal muscle or adipose tissue as a model for *in-vitro* testing to investigate the GLUT4 translocation response to insulin stimulation (Brewer et al., 2014; Coughlan et al., 2016; Vazirani et al., 2016). Nevertheless, evidence is still lacking in supporting GLUT4 translocation in response to insulin stimulation in HUVEC; therefore, this specific study design will make a novel contribution to this field. The objective of this study is to confirm if our Mono-labelled FITC-insulin conjugate synthesised inhouse is as biological active as native insulin based on the levels of AKT phosphorylation and GLUT4 translocation as the key criteria in the insulin signalling pathway.

3.2 Materials and Methods

3.2.1 Chemicals and Reagents

Table 3-2 includes chemicals and reagents used in this biological activity study.

Table 3-2: List of chemicals and reagents used

Chemical and Reagents	Origin
HUVEC	Sigma-Aldrich (UK)
Gibco^{TM} Medium 200 and Medium DMEM	Fisher (Loughborough UK)
Sterilised phosphate buffer (PBS)	Fisher (Loughborough UK)
Fetal bovine serum (FBS)	Fisher (Loughborough UK)
Gibco^{TM} Low Serum Growth Supplement (LSGS)	Fisher (Loughborough UK)
Semi-skimmed milk powder	Tesco
Rabbit Phospho-AKT (Ser473) (193H12) primary antibodies	Abcam (UK)
Goat AKT primary antibodies	Abcam (UK)
Anti-goat (IgG) secondary antibodies	Abcam (UK)
Anti-rabbit (IgG) secondary antibodies	Abcam (UK)
Rabbit GLUT-4 primary antibodies (ab654)	Abcam (UK)
Alexa Fluor 546 goat anti-rabbit IgG (H+L)	Fisher (Loughborough UK)
Protein marker	Sigma-Aldrich (UK)
HPLC graded Methanol	Fisher (Loughborough UK)
Sodium orthovanadate	Sigma-Aldrich (UK)
Dithiothreitol (DTT)	Sigma-Aldrich (UK)
Acrylamide/Bis-acrylamide (Acry/Bis), 30%	Fisher (Loughborough UK)
EDTA	Sigma-Aldrich (UK)
Bromophenol blue	Sigma-Aldrich (UK)
Sodium Dodecyl Sulphate (SDS)	Sigma-Aldrich (UK)
Ammonium persulfate (APS)	Sigma-Aldrich (UK)
N, N, N′, N′-Tetramethyl ethylenediamine **(**TEMED)	Sigma-Aldrich (UK)
Tris base	Sigma-Aldrich (UK)
NaCl	Sigma-Aldrich (UK)
Bovine Serum Albumin (BSA)	Fisher (Loughborough UK)
Triton-X100	Sigma-Aldrich (UK)
p-coumaric acid	MP Biomedicals (Solon,USA)
Luminol	Sigma-Aldrich (UK)
DMSO	Sigma-Aldrich (UK)
Hydrogen peroxide	Sigma-Aldrich (UK)
FITC-Actrapid® conjugates	Produced in house
Stripping buffer(10X)	Sigma-Aldrich (UK)

C2C12 skeletal muscle cells were kindly donated to us from Loughborough University, UK. Milli-Q water was used throughout for all HPLC analysis and FITC- Actrapid® conjugates preparation. Distilled water was used for all other preparative processes such as the making of buffers. 0.1-1M NaOH and 0.1-1M HCl were used for pH adjustment.

3.2.2 Preparation of FITC-insulin conjugate for cell stimulation

Four species of FITC-insulin produced inhouse were used in this study to investigate the resultant level of phosphorylated AKT in HUVEC compared to insulin stimulation. However, as discussed in chapter 2, certain reaction conditions will affect the degree of labelling; therefore, three batches of FTIC-insulin conjugates from different reaction conditions were further purified by HPLC to isolate each species as summarised in **Table 3-3**

Table 3-3: Four species of FTIC-insulin produced from different reaction conditions and isolated by HPLC.

Species of FITC- insulin	Reaction conditions	Isolated peaks
Mono-labelled FITC-insulin at the A1 position (MonoA1)	1h reaction time at pH8.4 and 2:1 molar ratio	Sample elutes at 21.3min RT
Mono-labelled FITC-insulin at the B1 position (MonoB1)	18h reaction time at pH7 and 2:1 molar ratio	Sample elutes at 21.9min RT
Di-labelled FITC- insulin (Di)	72h reaction time at pH7 and 3:1 molar ratio	Sample elutes at 22.6min RT
Tri-labelled FITC- insulin (Tri)	72h reaction time at pH7 and 3:1 molar ratio	Sample elutes at 23.7min RT

Once separated, each species was lyophilised then confirmed by HPLC and MS analysis as detailed in chapter 2. Prior to cell stimulation, four stock concentrations of each FITC- insulin species were prepared by diluting 3.5mg of its lyophilised powder (equivalent to 100Unit per mL insulin injection) in 1mL of Milli-Q water, pH7.

3.2.3 Passage of HUVEC from Frozen (P_0)

HUVEC (P_0) were cultured in T-75 flash using Medium 200 (Fisher), containing 5% FBS and 1% LSGS at 37°C in humidified 5% CO2 air. Media was changed every two days until the cells were fully confluent (80-100%) for passaging. Cells from P_4 were used throughout this study.

Once cells from P_4 reached confluency as observed in **Figure 3-4**, they would be transferred to 6-wells plate and incubated for 24h in serum-free media before stimulation.

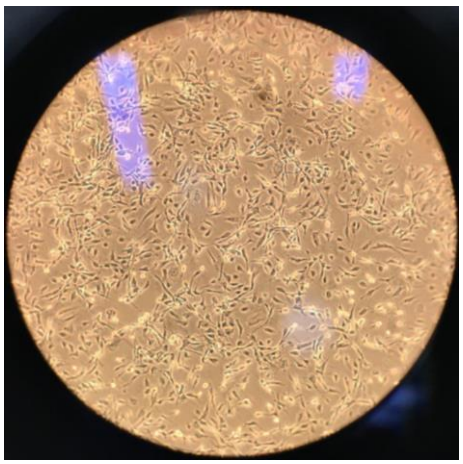

Figure 3-4: Microscopic image of 80-100% confluent HUVEC P4

3.2.4 The stimulation of HUVEC by Actrapid® and the fluorescently labelled Actrapid® conjugates.

To investigate the activity of the insulin variants, HUVEC were stimulated with or without Actrapid® and its FITC-labelled conjugates. Prior to stimulation, HUVEC were starved with serum-free media for 24h.The stimuli stocks of 100Unit /mL Actrapid®, four species of FITC-Actrapid® conjugate and FITC (3.5mg/ml) were added to each well accordingly in 1:1000 dilution (~0.1Unit of insulin), then left to incubate for 15mins at 37°C.

After 15min of stimulation, media was removed and cells washed with cold PBS, and cells lysed with 60µL of Laemmli buffer (62.5mM Tris buffer pH6.8; 87.6mM SDS;10% Glycerol; 5mM EDTA pH6.8; 0.004% Bromophenol blue; 3%w/v DTT and 8mM Sodium orthovanadate). The adherent cells were then scraped off, then transferred to mini centrifuge tubes labelled accordingly to each stimulus. The samples then underwent processes of sonication for 15 seconds then heating for 5 minutes at 95°C and finally centrifugation for 1 minute at 179xg.

Each experiment set was triplicated using cells from different batches.

3.2.5 Electrophoresis of protein lysates.

Formulation for preparing 10% SDS-PAGE is shown in **Table 3-4**

Table 3-4: The preparation of two 10% SDS-PAGE gels

Reagents	Volume added for resolving gel	Volume added for stacking gel
30% Acry/Bis	6.7 mL	3.3 mL
2M Tris pH 8.8	3.7 mL	2.5 mL
Distilled water	9.6 mL	13.7 mL
10% SDS	200 µL	200 µL
10% APS	134 µL	200 µL
TEMED	14 µL	20 µL

Standard protein marker and protein lysate samples were loaded on 10% SDS-PAGE gel and electrophoresed in electrophoresis buffer (190mM Glycine; 25mM Tris-base; 0.1%w/v SDS). Gels were electrophoresed at 120V for 1.5h The blotting cassettes were prepared according to **Figure 3-5**. The assembled cassettes were then placed in blotting tank and electrophoresed for 1.5h at 70V in blotting buffer (190mM Glycine; 25mM Tris-base; 20%v/v Methanol)

Figure 3-5: Preparation of stack for Western blot analysis

The visual appearance of protein standards as shown in **Figure 3-6**, confirmed the transfer of proteins to the nitrocellulose membrane was successful.

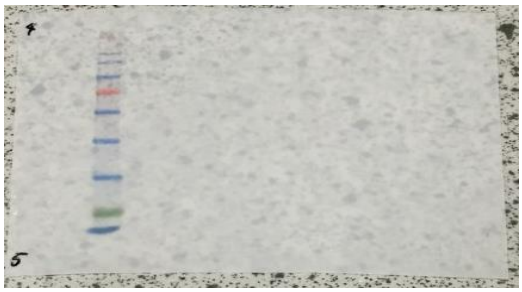

Figure 3-6: Illustration of proteins transferred to the nitrocellulose membrane.

Proteins transferred on to nitrocellulose membrane were blocked in blocking solution (5% w/v semi-skimmed milk powder in TBST (25mM Tris; 15mM NaCl ;0.1%v/v Triton-X, pH7.5)) for 1h.

5ml of primary antibody (phospho-AKT) prepared in **Table 3-5**, was then added to one blot and incubated overnight at 4°C.

Table 3-5: Preparation of phosphor-AKT primary antibody solution.

Reagents	Final concentration or volume
BSA	5% w/v
Rabbit Phospho-AKT primary antibody	1 in 1000
TBST	5 mL

After 24h, the pAKT antibody solution was removed, and the blots were washed three times with TBST before adding the secondary antibody as prepared in **Table 3-6**

Table 3-6: Preparation of secondary antibody solution.

Reagents	Final concentration or volume
Semi-skimmed milk powder	5% w/v
Anti-rabbit or goat IgG secondary antibody	1 in 2000
TBST	5 mL

The secondary antibody was added to the washed blot for 1h at room temperature. Agitation was also applied to ensure adequate homogenous covering of the membrane and prevent uneven binding. The washing process was further repeated. Once completed, the blot was emerged in ECL solution as prepared in **Table 3-7,** then analysed using the GeneGnome Chemiluminescence imaging from Syngene (discontinued model).

Table 3-7: Preparation of ECL solution used in processing for acquiring the image

Reagents	Amount added
1M Tris-HCl pH8.5	1 mL
Distilled water	9 mL
90mM p-coumaric acid in DMSO	22 µL
250mM Luminol in DMSO	50 µL
Hydrogen peroxide	3 µL

Once imaged, the blot could be stripped for 15 minutes using a stripping buffer to remove the antibodies.

After stripping, the blot was briefly rinsed with TBST, and the blocking solution was applied and the whole process begun again for total AKT antibody as prepared in **Table 3-8**.

Table 3-8: Preparation of AKT primary antibody solution

Reagents	Final concentration or volume
Semi-skimmed milk powder	5% w/v
Goat AKT primary antibody	1 in 1000
TBST	5 mL

Similarly, the secondary antibody was added then the images were acquired.

3.2.6 The immunofluorescence of GLUT4 translocation

Cells were stimulated with insulin or Mono as described in section 3.2.4
Once the course of stimulation was completed and cells washed with PBS (pH7.4), the fixation process was applied by incubating the cells in freshly prepared 4% paraformaldehyde in PBS at room temperature for 15 mins, following three washes with PBS for 2 mins each.
Permeablisation of the cell membrane was applied using Tris-buffered saline pH7.5 (TBS)-0.5% TritonX at room temperature for 15mins then cells rinsed in TBS-0.1% TX (3 changes in 3-5 mins).
Blocking in 2% BSA prepared with TBS-0.1% TritonX (blocking solution) for 1h at room temperature, was necessary to reduce the background fluorescence. 1mL of 1:200 GLUT4 primary antibody (ab654) prepared in blocking solution was then added to each well except for one blank well of the two controlled wells and incubated for 90 mins at room temperature. Once the incubation period was completed, cells were then washed at least five times in TBS-0.1%TX.
The AlexaFluor 546 labelled secondary antibody (1:500) was prepared in blocking solution and applied to each corresponding well for an incubation of 60 mins, following repeat washes with TBS-0.1%TritonX. Before imaging, cells were rinsed with PBS before serum-free media was added to each well.
Images were captured using the EVOS cells imaging system (Thermo Fisher Scientific) by RFT (red) light cube.

3.2.7 Data analysis

The intensity of pAKT and AKT level for each blot and the integrated density of GLUT4 cell membrane level for fluorescence images corresponding to each experimental set were quantified using ImageJ software. Data were obtained from the average of three readings for each set of samples then used to calculate the ratio of pAKT/AKT. The mean value of pAKT/AKT from three experimental sets would be presented as the final result. A paired T-test was performed across two sets of result to establish the difference in activity for each FITC-Actrapid® conjugates compared to native Actrapid®.

3.3 Results and Discussions

3.3.1 Determination of AKT phosphorylation and GLUT4 translocation in HUVEC stimulated by insulin and its fluorescently labelled conjugates

The initial investigation into the biological activity of FITC-insulin conjugate synthesised in-house was to determine the level of phospho-AKT (pAKT), which is a central signalling mediator in the insulin stimulated cascade. AKT phosphorylation then leads to GLUT4 translocation to the plasma membrane to facilitate glucose influx, thus maintaining homeostasis.

Figure 3-7 and **Figure 3-8** present the western blot analysis of pAKT; AKT, and the corresponding ratio of pAKT/AKT respectively, in relation to the basal state of HUVEC and each stimulation with insulin, MonoA1, MonoB1, Di, Tri and FITC. The graph shows the mean ratio of pAKT/AKT calculated from three repeats and the p-value calculated from the paired t-test for each FITC-insulin species compared to native insulin.

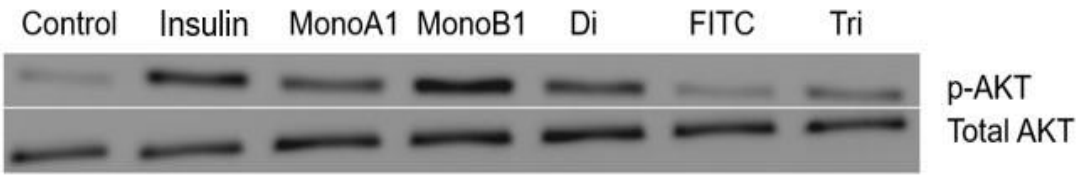

Figure 3-7: Western Blot analysis of AKT phosphorylation observed in HUVEC after 15mins at 38°C during basal state (control) and stimulation by Insulin, MonoA1; MonoB1; Di: FITC and Tri

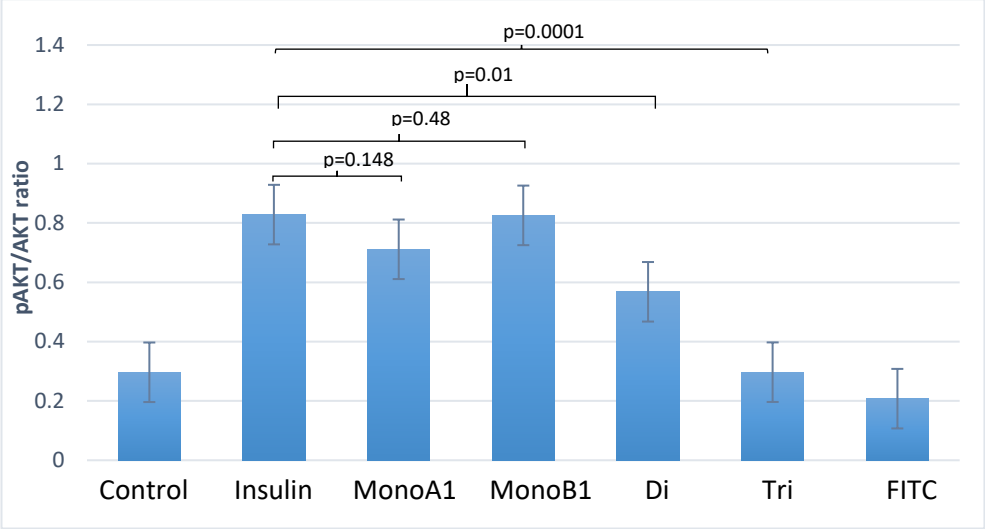

Figure 3-8:The ratio of phospho-AKT (pAKT) and total AKT levels as the mean of three repeats observed in HUVEC after 15min at basal state (control) and stimulation by insulin, four species of FITC-insulin conjugate and FITC. Noting the p-value of <0.05 for each conjugate compared to insulin indicates a significant difference in pAKT level.

The paired t-test reveals that upon 15mins stimulation, there was no significant difference in the level of pAKT (pAKT/AKT) observed in insulin and its FITC single label at A1 and B1 (MonoA1 and MonoB1) while Di and Tri showed considerably reduced levels. Notably, the pAKT/AKT ratio of ~ 0.3 was equally observed under basal cell activity and in those stimulated by Tri, which could indicate that there was no further cellular response from Tri stimulation. Meanwhile, cell stimulation by MonoA1 and Di has resulted in ~ 14% and 31% reduction in pAKT level respectively compared to the activity observed by insulin and MonoB1 stimulations, which resulted in the same level of pAKT.

Figure 3-9 presents the biological activity percentage of the four FITC-insulin species compared to native insulin calculated from the ratio of pAKT and total AKT levels taken into account the basal activity

Figure 3-8:The ratio of phospho-AKT (pAKT) and total AKT levels as the mean of three repeats observed in HUVEC after 15min at basal state (control) and stimulation by insulin, four species of FITC-insulin conjugate and FITC. Noting the p-value of <0.05 for each conjugate compared to insulin indicates a significant difference in pAKT level.

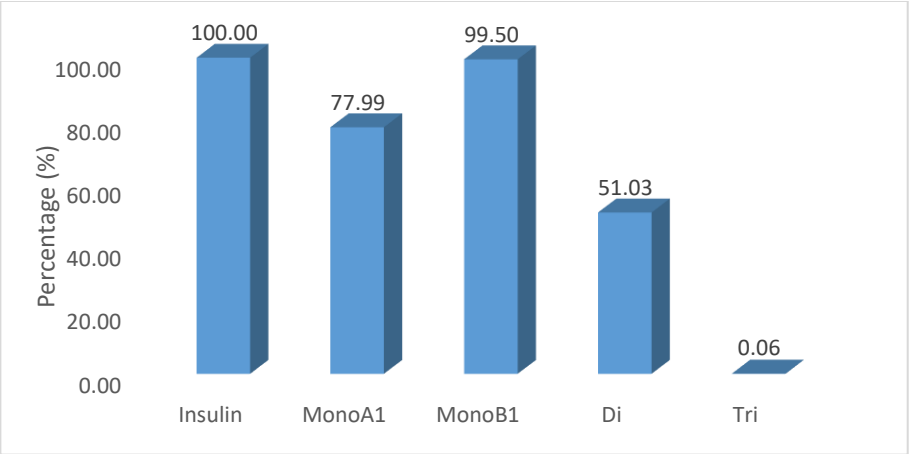

Figure 3-9: The biological activity percentage of insulin compared to its conjugates with FITC.

Overall, the biological activity of insulin was best preserved ranking from MonoB1> MonoA1> Di > Tri. This trend is in broad agreement with previous data reported by Hentz et al., 1997, where the biological activity of four FITC-insulin derivates were measured by a TK phosphorylation assay. Their results revealed that the B1 derivative was as biologically active as unlabelled human and pork insulin standards while the highest reduction in activity was observed in Tri. Notably, the decrease in biological activity observed in MonoA1 and Di has suggested that the A1 position may play an important role in the binding and IR activation dynamics. Meanwhile, the equivalent measurements in the biological activity of insulin and MonoB1 would indicate that the B1 position is less likely to involve in the insulin-IR binding. However, the dramatic decrease in biological effect of Tri suggested that the B29 position could play a key role for the binding of insulin to its IR and multiple substitutions on the insulin molecule could mean that three FITC molecules on the insulin are sufficiently big enough to cause a change in the 3D structure of insulin in such a way that the receptor-binding site of the insulin molecule is no longer recognisable by its IR. This observation was also supported by Pullen et al., 1976 and SchÄffer, 1994 who reported that the B29 residual was found to be near the secondary

binding site of insulin toward its receptor. Their studies suggested that the degree (number of substitution) and position of insulin modification with FITC could significantly alter the structural conformation of the fluorescently labelled insulin. The overall changes would then influence the binding of insulin to its receptor and therefore affecting its biological activity to a certain extent ranging from fully active as observed in MonoB1 (99.5%) down to having a significantly low biological effect as reported in Tri (0.06%). This study agrees with other published data to highlight the important of A1 and B29 residues for the binding of insulin to IR, modifications to these positions would result in alterations to the IR binding site, thus affecting insulin biological activity. Meanwhile, B1 residue is not crucial for IR binding, therefore, FITC labelling at the B1 position would not affect the receptor binding site of insulin molecule thus maintain insulin biological activity.

3.3.2 The immunofluorescence study of GLUT4 translocation in response to insulin stimulation using C2C12 skeletal muscle cells

In order to confirm the biological activity of the most active FITC-insulin candidate (MonoB1), the cellular response from the insulin signalling pathway that finally results in GLUT4 translocation was further investigated. Unfortunately, GLUT4, which is the only type of insulin-dependent transport, could not be found in HUVEC from the pre-scanning western blot analysis and immunofluorescence study. Although the presence of other GLUT types would be essential for glucose transport in HUVEC, the lack of GLUT4 expression in HUVEC could indicate that intracellular uptake of glucose in HUVEC is not regulated by insulin. Because GLUT4 was not found in HUVEC, C2C12 skeletal muscle cells were chosen as the well-known model for GLUT4 expression. C2C12 was stimulated with MonoB1 and insulin to examine the biological response that further results in GLUT4 translocation. Similar GLUT4 translocation levels resulting from both stimulations observed by fluorescent image would confirm that the biological activity of this most active form of FITC-insulin is equivalent to native insulin. **Figure** presents the immunofluorescence

images of GLUT4 obtained at 20x magnification after 15min stimulation with/without insulin and MonoB1 stimulation in C2C12.

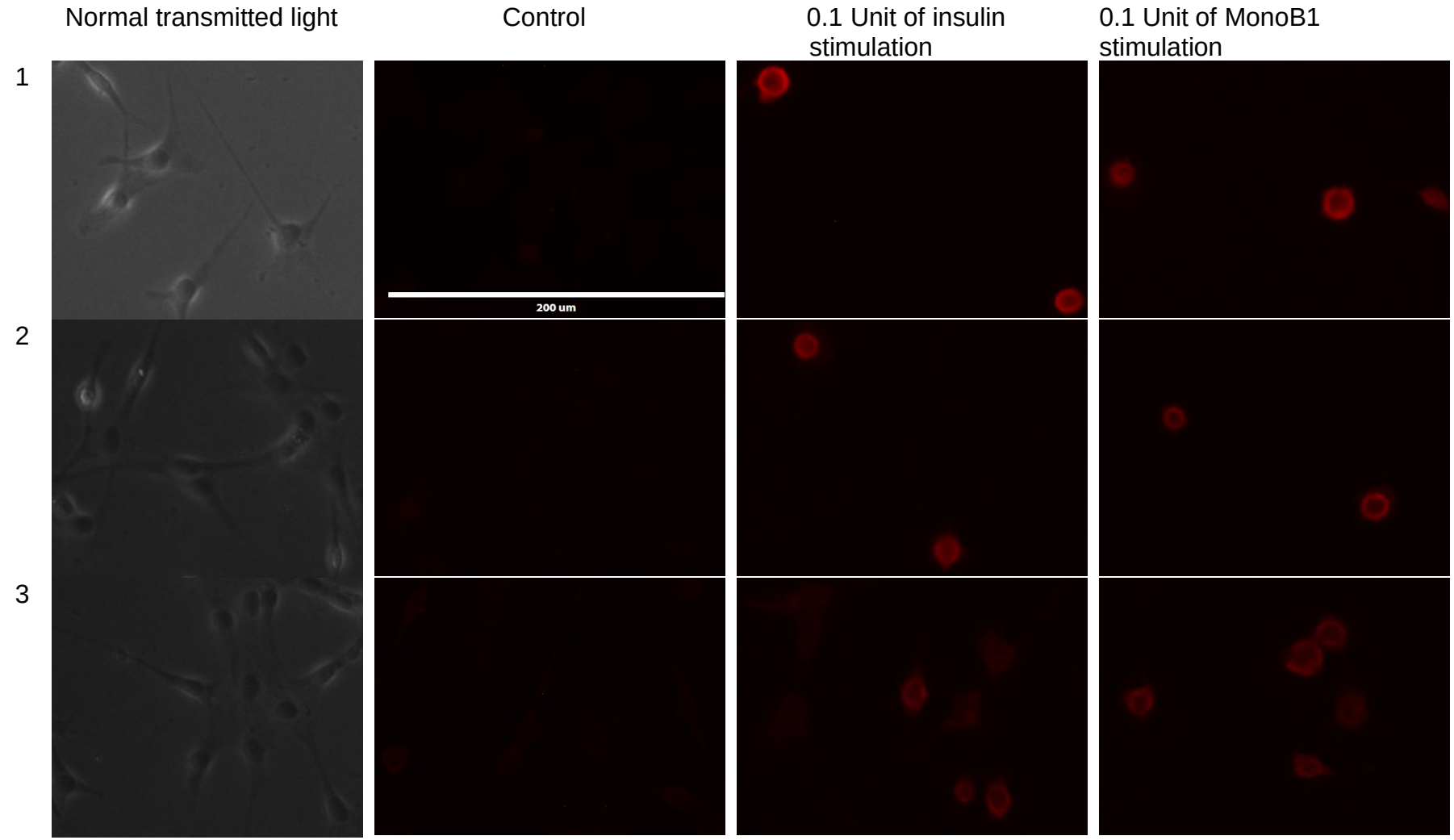

Figure 3-10: The resultant fluorescence images of GLUT4 (red) captured under RFT light at 200μm after 15min stimulation in C2C12 with/without insulin and MonoB1

Figure 3-10 above shows very few cells surface level of GLUT4 captured in the control while the expression GLUT4 were fluorescently visualised all around the cell membrane of those stimulated by insulin and MonoB1. The overall observation was also consistent for all three repeats.

Figure 3-11 presents the integrated density and the correct total cell fluorescence (CTCF) quantified using ImageJ as the mean of three readings from each of the above fluorescence images that were further presented in each bar-chart by the mean from 3 repeats. Additionally, the p-values obtained from the paired t-test of the integrated density and corresponding CTCF for insulin and MonoB1 were also indicated.

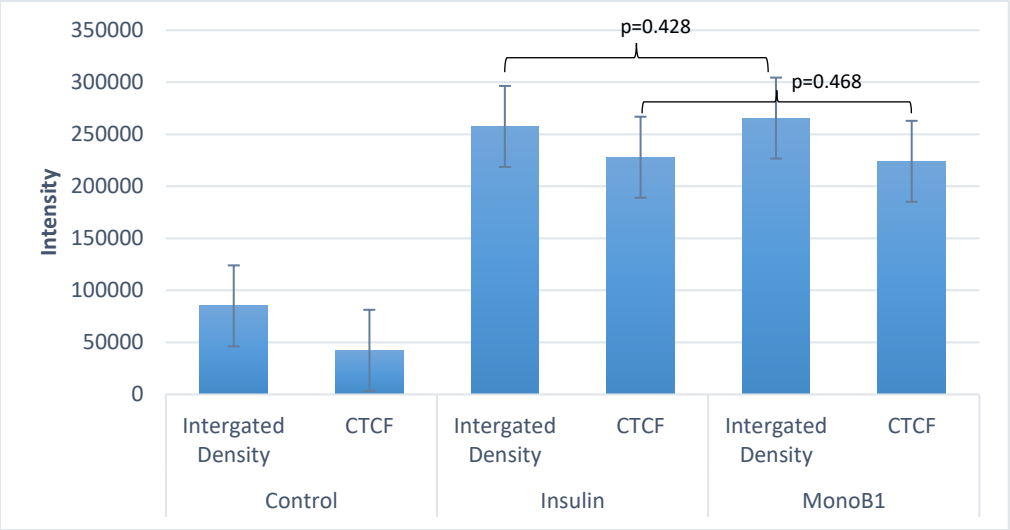

Figure 3-11: The integrated density and CTCF quantified for the GLUT4 immunofluorescence observed in C2C12 after 15min stimulation with/without Actrapid® and MonoB1 showing the p-value of >0.05 for both data comparing insulin and MonoB1.
(CTCF=Integrated density- (Area of selected cells*Mean fluorescence of background readings))

The present study reveals that the level of GLUT4 translocation in C2C12 as a result of Actrapid® and MonoB1 stimulations is considerably higher with more than 80% increase in CTCF than the limited cell surface level of GLUT4 under the basal state. Notably, the integrated density quantified for each fluorescence image shows a significant difference (p=0.006) in the cell surface level of GLUT4 visualised under the basal state comparing to the stimulated conditions, which have a similar observation of GLUT4 translocation for both insulin and MonoB1. The increased level of cell surface GLUT4 observed after insulin stimulation suggested that the

cellular response to insulin occurred via the activation of PI3K/AKT signalling pathway. Once the IRs have been activated, a cascade of events would occur inside the cell resulting in phosphorylation of AKT. The resultant pAKT then leads to the phosphorylation of AS160, which then allow the translocation of GLUT4 from the cytoplasmic vesicles onto the cell membrane surface for glucose intake, hence the observed increase in GLUT4 cell surface level.

There was no significant difference ($p=0.47$) in the increased cell surface GLUT4 levels after stimulation by insulin and Mono B1, suggesting that their biological activity would be equivalent. Besides, the additional data of pAKT levels quantified from western blot analysis as reported in section 3.3.1 for insulin and MonoB1 revealed the similarity in activation dynamics of the insulin signalling pathway.

3.4 Chapter summary

Four different species of FITC-insulin conjugates including MonoA1, MonoB1, Di and Tri were synthesised inhouse, isolated and confirmed by RP-HPLC and MS. The biological activity of each species in comparison to native insulin was assessed in HUVECs and C2C12 skeletal muscle cells via the insulin signalling pathway by examining the levels of pAKT and cell surface GLUT4. It is understood that once the IR is activated as a result of insulin binding to its receptor site, there would follow a cascade of events causing the phosphorylation of AKT. The resultant increase in pAKT level consequently leads to the translocation of GLUT4 from the cytoplasmic vesicles onto the cell membrane via the phosphorylation of AS160, thus allow the insulin-dependent transport of glucose into the cell.

The main findings are summarised as follow:

- Fully confluent HUVECs in 6-wells plate were subjected to 15mins stimulation with 0.1 Unit of insulin and its FITC-labelled conjugates including MonoA1, MonoB1, Di and Tri. The level of pAKT was measured by Western Blot analysis to compare the cellular effects of each stimulus. The most prominent finding to emerge from this study is that the biological activity of native insulin was best preserved with MonoB1 while the rest had a reduced effect of exhibiting 78% down to 51% of the insulin activity with MonoA1 and di-labelled species respectively. The significantly low activity (0.06%) observed with Tri highly indicated a complete loss of biological activity possibly due to

the inability of IR to recognise the receptor-binding site of this tri-labelled insulin.

- The screening test for GLUT4 translocation in HUVEC could not confirm the presence of GLUT4, indicating that the intracellular uptake of glucose in HUVEC would occur via other types of GLUT which is independent from insulin stimulation such as GLUT1.

- The use of C2C12 skeletal muscle cells to further confirm the biological effect of the most active FITC-insulin conjugate (MonoB1) on GLUT4 translocation by immunofluorescent showed no significant difference in the GLUT4 cell surface level, suggesting that the singly labelled FITC-insulin at B1 produced inhouse is as biologically active as insulin and could potentially be used for future biomedical applications.

Chapter 4. Stability and solubility profiles of FITC-insulin conjugate

4.1 Introduction

The work presented in this chapter reviews some aspects of insulin stability and solubility to investigate the effect of FITC labelling on the stability and solubility profiles of fluorescently labelled insulin (Actrapid® and Novorapid®) conjugates. Like many proteins, the stability of insulin is primarily affected by changes in pH and temperature that might result in physical and chemical saturation of the insulin structure, thus affecting its biological activity. Pharmaceutical insulin preparations clinically used as injections or MDI have a well-established stable shelf-life providing their storage conditions are within the recommended temperature range typically at 2-8°C with the addition of stabilising excipients. The solubility of insulin is one of the key parameters in determining its rate of absorption and therefore, its ability to exert a biological effect. As FITC labelling on certain sites (A1 and B29) of the insulin molecule has been found to affect its biological activity, it is also of interest to find out if the FITC-insulin conjugates would share similar properties of insulin stability and solubility. Although fluorescently labelled insulin conjugates have been widely used in various applications, very few has focused on investigating their long-term stability and solubility profiles. The objective of this study is to examine the stability and solubility profiles of FITC-insulin conjugates prepared in their working dilutions with or without excipients which are typically found in most insulin formulations.

4.1.1 Stability of insulin

Generally, the stability aspect of insulin typically refers to its stability in pharmaceutical formulations in terms of biological potency. In fact, according to Brange 1994, many studies into the influence of different storage conditions on insulin stability for many years were based on the estimation of its biological activity. The initial study on the biological stability of insulin carried out by

(Pingel and Volund, 1972) examined a whole range of acid and neutral insulin formulations from rapid-, intermediate- to long-acting preparations during storage at various temperatures. The result after five years of storage at 4°C showed that all preparations retained virtually full biological activity, thus exhibiting a remarkably high biological stability within the recommended storage conditions. Notably, the biological potency of insulin dropped dramatically for every 10°C increase in temperature above 25°C. It was also reported that neutral insulin preparations are generally more stable than those prepared in acidic solution probably due to the enhanced stability effect by insulin hexamers (Brange, 1994; Landreh et al., 2012; Ohno et al., 2019).

Principally, in order for therapeutic insulin to exert its biological effect, it is essential to maintain the structural integrity of insulin and thus its stability within the pharmaceutical formulation. Insulin stability is critically dependent on the conformational flexibility within the insulin molecules itself, and the resultant dimeric and hexameric formation. However, it is equally important to note that only the insulin monomer can exert the biological activity of insulin (Nagel et al., 2019; Fu, R Gilbert and Liu, 2013; Mukherjee et al., 2018b). The structural alterations of insulin during storage and usage are usually classified by changes in the conformation of secondary to quaternary structure (physical instability) or covalent modification of the primary structure leading to bond formation or cleavage (chemical instability). The overall changes have a mutual influence on the susceptibility of the molecule for chemical attack or vice versa (Manning et al., 2010; Brange et al., 1997).

The physical modifications of insulin's primary and secondary structure involve denaturation, adsorption, precipitation, fibrillation, and aggregation. Denaturation (unfolding) is the loss of the physical native three-dimensional or globular structure without alteration to their chemical composition, owing to changes in temperature or binding of chaotropes (such as urea and guanidinium hydrochloride). Insulin adsorption either to the materials within its container or by the presence of 0.1-1% albumin, can both result in insulin loss. This effect is inversely proportional to insulin concentration (negligible for higher concentrations than 5 Unit/mL) and varies with materials being more prone to

adsorption by hydrophobic than hydrophilic surfaces. Formation of amorphous or crystalline precipitates in insulin solution results from pH changes within its isoelectric precipitation zone of pH 4.5-6.5 or introduction of zinc ions (or other divalent metal ions), leading to a reduction in insulin solubility (Brange et al., 1997; Landreh et al., 2012; Gradel et al., 2018a). Meanwhile, under the influence of high temperature and exposure to hydrophobic surfaces, insulin tends to undergo dissociation of its hexameric structure and conformational changes of monomers, resulting in successive linear aggregation and insoluble insulin fibrils formation. Notably, insulin fibrillation has been one of the most extensively studied phenomena concerning insulin stability. It was well established that there is a robust reverse relationship between the fibrillating tendency of insulin and its content of insulin-related impurities, including covalent insulin dimer and proinsulin. Importantly, neutral solutions containing low concentrations of hexameric insulin are more prone to fibrillation. However, this effect is less problematic since all clinically used insulin pharmaceutical preparations are at a high concentration with the addition of zinc ions, which together can improve the physical stability of insulin (Akbarian et al., 2020; Phillips et al., 2012; Brange et al., 1997).

In contrast to the changes from physical instability, changes in amino acid sequences (primary structure) from chemical modifications or covalent alteration in insulin structure are irreversible and may result in the formation of insulin derivatives with less activity and potential immunogenicity (Yang et al., 2017; Akbarian et al., 2018). In addition to the enzymatic degradation, various chemical reactions can also degrade proteins in general and insulin in particular. Deterioration of pharmaceutical insulin preparations during storage is mainly due to hydrolysis and insulin intermolecular transformation reactions. These two categories of chemical reactions usually lead to the production of higher molecular weight transformation (HMWT). Predominantly, hydrolysis reactions of insulin involve deamination of Asn residues which occur at the A21 position in acidic solution and the B3 position in a neutral and alkaline environment. On the other hand, intermolecular aminolysis between the N-terminal amine (B1) and an amide side chain in the insulin A-chain (A18 or A21)

mainly leads to the formation of covalent insulin dimers (CID). Also, intermolecular disulphide exchange between different insulin molecules can result in the formation of covalent insulin oligomers (CIO) and polymers, observed during the storage of neutral insulin solutions as well as preparations containing amorphous insulin at ambient and higher temperatures (Brange, 1994; Akbarian et al., 2018; Jacob, 2015). Furthermore, changes in pH can also influence the chemical instability of insulin. Optimisation of CID and oligomers formation was reported around pH 4, whist the deamination of Asparagine residues due to different hydrolysis reactions was minimised at around pH 6.5. Meanwhile, in alkaline solution, the formation of CIO and polymers due to intermolecular disulphide interactions was mainly observed with increased pH> 9. Other types of insulin formulations also exhibited similar chemical stability profiles, however formation of B3 residues deamination products was more predominant in neutral and slightly alkaline pH (Brange, 1994; Manning et al., 2010; Hjorth et al., 2016b).

In summary, the stability of insulin in pharmaceutical preparations is highly complex and dependent on the formulation of each product. However, the need to understand insulin stability is critically important for designing an insulin formulation as well as producing its fluorescently labelled conjugates to maintain their efficacy. The rate of spontaneous structural transformation within the insulin molecule is determined mainly by its conformational and segmental flexibility, thus playing a crucial role in insulin stability. Notably, the combinations of physical and chemical factors contributing to the instability of insulin during storage are numerous and governed by the capacity of the B-chain terminals to undergo the structural changes that allow physical interactions and chemical reactions to take place. In current insulin pharmaceutical preparations formulated at neutral pH, there must be less than 10% transformation and degradation products formed during their shelf life if stored as recommended at 2-8°C, while the formation of the covalent HMWT which are potentially immunogenic must be less than 2% (Ohno et al., 2019; Donner and Sarkar, 2019b; Brange, 1994). Currently, isotonicity-adjusting substances and preservatives formulated in all modern pharmaceutical products

can affect the stability of insulin preparations by their influence on deamination and covalent insulin dimers. It was investigated among preservatives that the stabilising effect gradually increases from methylparaben to m-cresol to phenol. For isotonicity agents from glucose to glycerol to NaCl, most are present in clinically used insulin preparations. Notably, the addition of glycerol and some polysaccharides can significantly increase the physical stability of insulin solutions. However, the chemical and biological stability will considerably decrease with these agents since the rate of CID formation was reported to be faster in glycerol-containing preparations (Brange, 1994; Jacob et al., 2019; Modi et al., 2019). Therefore, the need for compromise composition of these agents within each insulin formulation is equally important.

4.1.2 Insulin solubility

Principally, the solubility of a compound/ drug in water or organic solvents is equally essential for critical decisions throughout the entire process from the initial drug discovery stage to development and final formulation. The solubility of a drug is generally considered as one of the most important parameters in achieving the desired concentration of drug reaching the systemic circulation for the anticipated pharmacological response. Because water is well established as the solvent in all body fluids and for any drug to be absorbed, it must be present in the form of an aqueous solution at the site of absorption. Therefore, all drugs must exhibit at least limited aqueous solubility for therapeutic efficiency regardless of their administration methods (Magbool et al., 2017; Cantrill et al., 2020). For instance, in all pharmaceutical insulin preparations, the rate-limiting step of insulin activity is indeed its absorption into the bloodstream after SC administration. Insulin glargine in Lantus® formulation is less soluble at neutral pH than HI in Actrapid® thus, it precipitates in the SC tissue post-injection, slowing its absorption and extending its duration of action for up to 24h; whereas short-acting Actrapid® is formulated in neutral pH solution, enabling rapid absorption and therefore exhibiting quick onset of action within 30mins. In general, several factors can govern the solubility of insulin, including pH, temperature, the nature of a solvent used, zinc ion content, and the

concentration of divalent metal ions and salts. Additionally, the species, purity of insulin, and the nature of its surface in contact with the solvent environment could also affect its solubility. Principally, the solubility of insulin refers to the maximum amount of crystalline insulin (solute) that can be dissolved in a given amount of solvent at specified conditions to achieve a homogeneous system. The extent of solubility can range widely, from very soluble in which less than one part of solvent is required per part of solute to give homogenous system, to practically insoluble in which more than ten thousand parts of solvent requiring per part of solute (McPherson and Gavira, 2014; Landreh et al., 2012; Gradel et al., 2018b). According to Frederiq and Neurath 1950, insulin is practically insoluble in water at its isoelectric point of pH 5.4, but it is easily soluble at pH lower than 4. Notably, insulin tends to precipitate at a pH interval of pH5.3-5.4 in an aqueous medium, and this precipitation zone is broadened towards higher pH values with increasing zinc ions concentration. Practically, insulin can be well solubilised at 2 mg/mL in dilute acetic or hydrochloric acid, pH 2–3. Although insulin is usually less soluble in neutral pH and alkaline conditions, the solubility is strongly dependent on the concentration of zinc ions and the species of insulin. Insulin is also soluble in homogenous mixtures of water and organic solvents, for instance, in 50-70% (v/v) ethanol. Depending on the solvent type, temperature, pH, and salt content, the solubility of insulin tends to decrease with a high content of the organic solvent in the mixture (Zhou et al., 2012; Pitt et al., 2020; Magbool et al., 2017).

Generally, soluble HI comprises different oligomers, including insulin monomers, dimers, and hexamers in chemical equilibrium. It is well-established that insulin monomers and dimers are readily absorbed by blood capillaries post- SC injection whereas, insulin hexamers are not well absorbed into the capillaries but can to some extent be absorbed by the lymphatic system due to their larger size. The rate of insulin absorption found to be fastest for monomers followed by dimers and hexamers respectively is therefore determined by its oligomeric equilibrium (Gast et al., 2017b; Pitt et al., 2020; Gradel et al., 2018). For all clinically used insulin preparations nowadays, in addition to the insulin type and excipients added to the formulation, which aids the formation of insulin

hexamers, the association state/ oligomeric equilibrium of soluble insulin is also dependent on its concentration. High insulin concentration can shift the oligomeric equilibrium towards hexamer formation while dilution will favour monomers and dimers state. Furthermore, upon SC administration, the subsequent dissociation rate of insulin hexamers into dimers and monomers before trans-capillary transport is dependent on the dispersion of lipophilic excipients such as phenol or meta-cresol as well as zinc from the insulin SC depot into the adipose tissue, thus contributing to faster absorption (Brange and Volund, 1999; Donner and Sarkar, 2019; Akbarian et al., 2018). Nowadays pharmaceutical insulin products are formulated at relatively high concentrations (100-500Unit/mL) for storage purpose, and therefore mainly exist as insulin hexamers in a clear, colourless solution at a specified, usually neutral pH range, except for Lantus® at pH4. Depending on their mechanism of action ranging from rapid-, intermediate and long-acting, these insulin analogues have chemical modifications to their amino acid sequences, in which for long-acting insulin analogues, insulin will precipitate in the SC tissue post-injection to achieve a slow rate of absorption. Rapid-acting insulin analogues have minor alterations in their amino acid sequence relative to HI so that in the absence of zinc and phenol or meta-cresol, these modifications reduce self-association of insulin monomers into dimers and hexamers compared with HI; therefore, a more significant fraction of insulin monomers would generate in the SC tissue. The resultant event leads to more rapid absorption from the SC tissue with a faster onset of action than HI (Savjani, Gajjar and Savjani, 2012; Gradel et al., 2018; Brange and Volund, 1999).

4.1.3 Studies on the stability and solubility profiles of fluorescently labelled insulin conjugates

Fluorescently labelled insulin preparations have been widely used for several decades to support numerous studies into the activity of insulin, its interaction with receptors, its existence and localisation at cellular levels as well as its release profiles in drug development both *in-vitro* and *in-vivo*. However, the data available for their stability profiles during long-term storage, especially in

aqueous solution and at specified conditions is limited.

Experimental data to establish the solubility of FITC-insulin conjugates at specified conditions such as at controlled temperature and pH are still not understood. Unlike all pharmaceutical insulin preparations whose stability profiles during long-term storage have been well-established in relation to their biological activity as well as physical and chemical instability, the stability aspects of fluorescently labelled insulin preparations would also be dependent on the properties of the fluorescent label itself. There are several factors to consider for the stability determination of the conjugated products such as whether the dyes remain conjugated in the solution or even in lyophilised powder form during long-term storage and the rate of photobleaching during the experimental procedure (Natarajan, Northrop and Yamamoto, 2017; Wakankar et al., 2010; Uchio et al., 1999). Theoretically, a fluorophore can repeatedly undergo the fluorescence process and emit light, but long-time exposure to high-intensity illumination can cause structural changes to the fluorophore, making it no longer fluoresce, a process known as photobleaching. For instance, a recent study by Williams et al., 2018 has examined the photostability of HI labelled with AlexaFluor 647 (INS-647) and according to their experimental imaging conditions, ~ 5-8% minimal loss in INS-647 fluorescent intensity during an experiment was due to photobleaching. Their results indicate that after 30min in circulation, 90% of the fluorescent dye remained conjugated to insulin. However, this study did not exclusively indicate beyond what point photodamage may be detected, and all the dye would become un-conjugated from insulin. The observation seemed to suggest that the course of their experiment lasted for no more than 30mins which is usually sufficient for insulin transport studies. Another study by Yang et al., 2017 also supported this time course in their stability test using BSA labelled with RBITC for injection into rabbits. The study highlighted the use of BSA-RBITC conjugates as a tracer molecule for the study of protein transportation and vascular permeability based on the findings that they are highly specific, sensitive, and stable during 30min *in-vivo* experiment. Similar to FITC, RBITC has the ITC reactive group that directly combines with lysine group of the proteins via a phosphoryl reaction to

form a dye-protein complex. Another study established that dextran products labelled with FITC are stable at 37°C in rabbit plasma, muscle homogenate, liver homogenate and urine for at least three days during which there was no significant data indicating changes in the molecular weight or the release of FSC moieties. Previous reports also concluded that FITC-dextran are stable for at least one day at physiological conditions. Using 6% trichloroacetic acid also enhanced the stability of FITC-dextran at room temperature for three days. Although FITC-dextran was found to be stable at pH 4 for over one month at 35°C, there was a considerable loss of up to 24% in fluorescence at pH 9. Overall, the stability of FITC-dextran *in-vitro* and *in-vivo* is considered as excellent; however, there is a risk for hydrolysis of the FSC label only at elevated pH (>9) and high temperatures (>50) (De Belder and Granath, 1973; Kurtzhals, Larsen and Johansen, 1989; Wu et al., 2020; Thorball, 1981).

Principally, to measure the solubility of a compound, there are several requirements, including accurate control of temperature and composition in the liquid and solid phase, preferably with the capability to collect a vast amount of data in a short time. A widely accepted and accurate method for measuring the solubility is through equilibration of a suspension, followed by concentration determination of the solution and assessing its composition. The method involves establishing a known concentration calibration curve for the tested compound in a given solvent at specified conditions and sampling from highly concentrated solution over a period of time followed by filtration to remove the solids then measuring the concentration using a gravimetric, spectroscopic or a chromatographic method like HPLC. This test enables the determination of the maximum solute amount that is soluble in a defined amount of solvent at specified conditions. However, one disadvantage is that this simplified Equilibrium Concentration (EqC) or the shake-flask method can be quite laborious and time-consuming. Alternative approaches for determining solubility include the Temperature Variation (TV) method and the Solvent Addition (SA) method, in which respectively the temperature of the suspension and the composition of the suspension are gradually changed until achieving a complete dissolution of all crystals. In order to determine the temperature-dependent

solubility line of a compound in a solvent, performing the TV method is the most suitable. Whereas SA is usually the method of choice for solubility data required at a constant temperature as in the case for multicomponent mixtures whose solubility is not strongly dependent on temperature. Although these methods have shown to achieve reliable and reproducible data in a short time, they require specialised instruments with built-in particle viewer cameras to monitor the presence or disappearing of crystals formed (Alsenz and Kansy, 2007; Di, Fish and Mano, 2012; Savjani, Gajjar and Savjani, 2012). Based on the intended testing conditions and the availability of validated HPLC method for detecting fluorescently labelled insulin, the shake-flask method offers the most suitability and reproducibility for the determination of FITC-insulin solubility.
To date, there are no studies that investigate the stability and solubility profiles of insulin labelled with FITC product, especially in their working dilutions. The objective of this study is to investigate the effect of phenol, m-cresol and diluting fluid (containing m-cresol, glycerol and zinc oxide) on the stability profiles of FITC-insulin conjugate formulated in solution subjected to a change in temperature over time. In particular, the degree of de-conjugation (the presence of free FITC) which could interfere with fluorescent data in diffusion studies of FITC-insulin conjugate will be analysed by HPLC. The solubility profiles of FITC-Actrapid® conjugate will be assessed using the shake-flask method. Here, HPLC is the chosen analytical method to determine the maximum concentration of FITC-Actrapid® conjugate at neutral pH and ambient temperature to produce a homogeneous system.

4.2. Materials and Methods

4.2.1 Materials

Mono-labelled FITC-Novorapid® and FITC-Actrapid® conjugates (both refer to as Mono) produced in house as described in chapter 2. HPLC grade ACN, HPLC grade acetone and TFA, 0.1M NaOH, NaH_2PO_4, Na_2HPO_4, 0.1M HCl and buffer salts were purchased from Fisher Chemicals (Loughborough, UK). Ethylenediaminetetraacetic acid (EDTA) disodium salt was from Hopkins & Williams. M-cresol, glycerol, zinc oxide and crystallised phenol are from Sigma-

Aldrich Chemical Company Ltd (UK). Milli-Q water obtained from a Milli-Q UF Plus water purification system were used throughout.

4.2.2 Preparation of FITC-Novorapid® and FITC-Actrapid® solutions in Milli-Q water for the stability test

5mL stock solutions of 100 Unit/mL Mono were prepared by dissolving 17.5mg of lyophilised FITC-Novorapid® and FITC-Actrapid® individually in 5mL with Milli-Q water adjusted to pH7.

Figure 4-1 shows 0.1mL of each stock solution added to individual chromatography vials and marked accordingly to the day of HPLC analysis in the first five consecutive days then several weeks after storing at specified temperatures (2-8°C, 20°C and 37 °C)

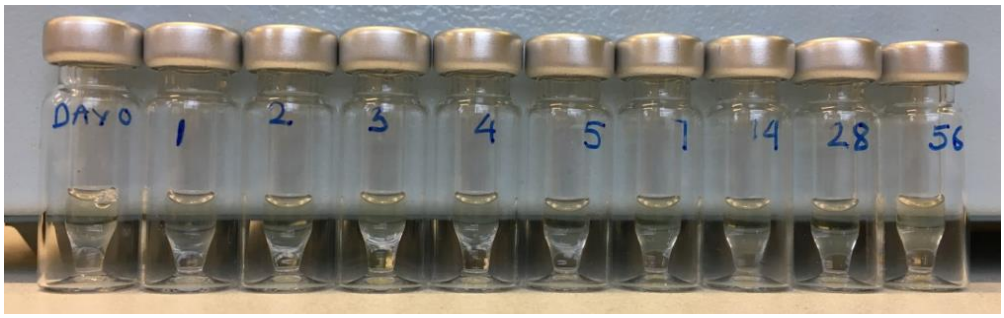

Figure 4-1: Serial samples from 100 Unit/mL FITC-Actrapid® stock solution for stability test allocated by day of HPLC analysis over 56 days period.

4.2.3 Preparation of FITC-Actrapid® serial dilutions for the solubility test

1mL stock solution of 3,000 Unit/mL Mono was prepared by dissolving 105mg of FITC-Actrapid® powder in 1mL diluting fluid (0.0005%w/v zinc oxide;1.6%w/v glycerol; 0.25%w/v m-cresol; pH7.0).

3mL of 300 Unit/mL Mono solution was made by diluting 0.3mL of 3,000Unit/mL Mono stock solution with 2.7mL of diluting fluid.

The resultant dilution of 300 Unit/ml Mono was used to prepare five further dilutions as set out in **Table 4-1**

Table 4-1: Preparation of FITC-Actrapid® serial dilutions

Concentrations of FITC-Actrapid®	Volume from FITC-Actrapid® stock solution of 300 Unit/mL (mL)	Diluting fluid (mL)
50 Unit/mL	0.167	0.833
100 Unit/mL	0.333	0.666
150 Unit/mL	0.500	0.500
200 Unit/mL	0.667	0.333
250 Unit/mL	0.833	0.167

A standard calibration graph was constructed in the range of 50Unit-3000 Unit/ml for FITC-Actrapid® (n=2)

4.2.4 Preparation of 100Unit/mL FITC-Novorapid® solution in 0.2% phenol and 0.25% m-cresol for the stability test

Two solutions of 100Unit/mL Mono in 0.2% phenol and 0.25% m-cresol was prepared by dissolving each 35 mg of lyophilised FITC-Novorapid® in freshly prepared 0.2%w/v phenol and 0.25%w/v m-cresol, pH adjusted to 7 respectively and made up to 10mL volumetrically.

4.2.5 Preparation of 100Unit/mL FITC-Actrapid® solution in diluting fluid for the stability test

35mg of lyophilised FITC-Actrapid® was dissolved in freshly prepared diluting fluid (0.0005%w/v Zinc Oxide;1.6%w/v glycerol; 0.25%w/v M-cresol; pH7.0) and made up to 10 mL volumetrically.

4.2.6 Preparation of 100Unit/mL Mono solution in buffers for the pH-dependent study

Table 4-2 shows the preparation of buffers (pH4-9) used to dissolve Mono

Table 4-2: Preparation of Acid/Base buffers pH ranging 4.0-9.0 (DeLloyd, 2000)

pH	Salt	Addition of acid or base
4	1.021g potassium hydrogen phthalate	0.1mL of 0.1M HCl
5	1.021g potassium hydrogen phthalate	2.26mL of 0.1M NaOH
6	0.681g potassium dihydrogen phosphate	5.6mL of 0.1M NaOH
7	0.681g potassium dihydrogen phosphate	2.91mL of 0.1M NaOH
8	0.681g potassium dihydrogen phosphate	4.67mL of 0.1M NaOH
9	0.477 sodium tetraborate (Borax)	4.6mL of 0.1M HCl

10mL of 100Unit/mL FITC-Actrapid® solutions were freshly prepared by dissolving 35mg of lyophilised mono-labelled FITC-Actrapid® in each buffer at pH ranging from 4 to 9 and made up to 10 mL volumetrically.

4.2.7 Solubility test of Mono by Shake-flask method

Method for the solubility equilibrium determination of FITC-Actrapid® was set out following eight basic steps as illustrated below:

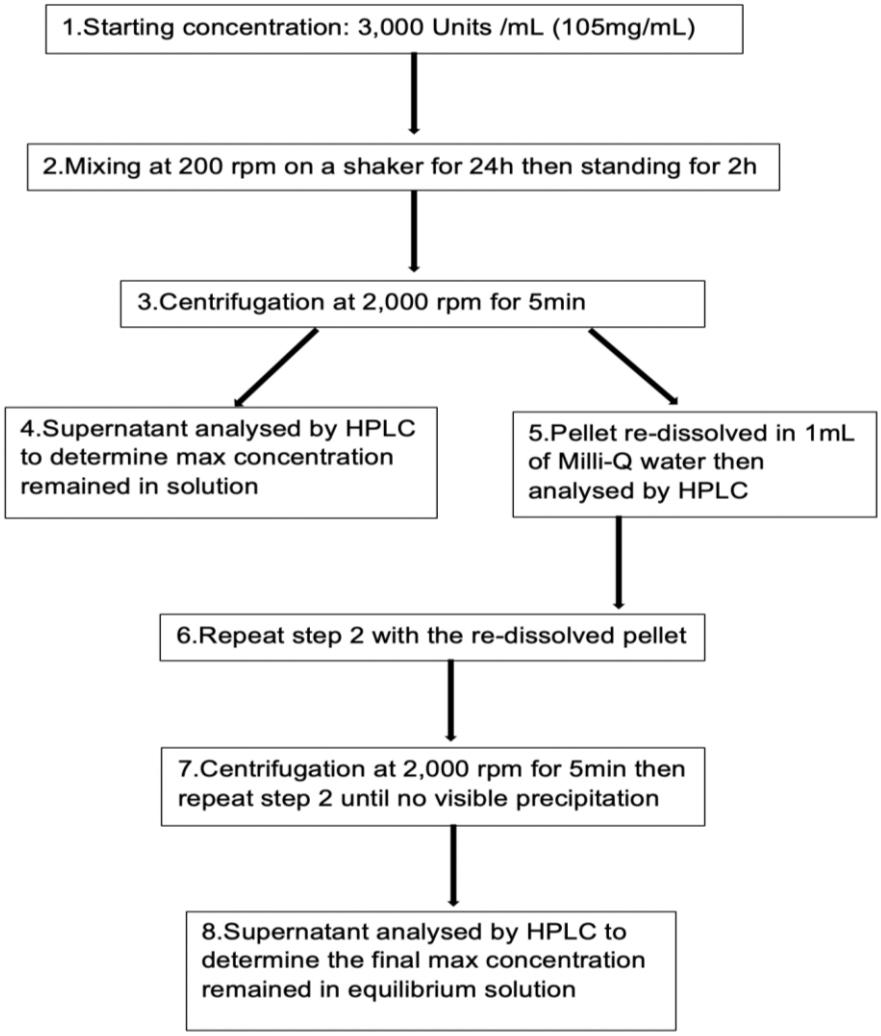

4.2.8 Analysis by RP-HPLC methods

Serial dilutions of fluorescently labelled insulin analogues prepared in different solvents subjecting to storage at specified temperature were then analysed by RP-HPLC method as described in section 2.2.4.

4.2.9 Fluorescence intensity measurement for the pH-dependent study

A fluorescence plate reader (SpectraMAX, model GeminiEM) was used to determine the fluorescence intensity of Mono conjugates prepared at different pH ranging from 4-9.

The excitation and emission wavelengths were set at 494 and 518 nm, respectively and the fluorescence intensity was recorded as the mean of three readings from different samples.

4.3 Results and discussions

4.3.1 The effect of phenol and m-cresol on the stability of FITC-insulin in solution during storage at different temperatures

The need to understand the stability profiles of fluorescently labelled insulin conjugates at 37°C is essential for the application of any *in-vivo* or *in-vitro* experiment especially where the course of studies may last over 24h. Generally, it may not always be practical to freshly prepare samples before the experimental start-up, therefore fluorescent conjugates sometimes need to be made up in solution and stored at specified temperatures. In addition to their role as anti-microbial preservatives, phenolic compounds are commonly used in insulin pharmaceutical formulation as allosteric effectors owing to their well-established stabilising effect on the hexamer conformation of insulin. It is therefore of most interest to investigate the stability enhancement effects of phenol and m-cresol on fluorescently labelled insulin formulated in solution during storage at 4°C, 20°C and 37°C. Generally, unlike insulin whose stability usually refers to its biological activity in relating to its structural transformation resulting from physical and chemical alterations, the stability aspects of its fluorescently labelled conjugate are typically discussed in relation to the maintenance of fluorescent dye conjugated to insulin throughout the experimental process. Depending on the method of analysis, the degree of FITC remaining conjugated to insulin can be quantified by the presence of free dye cleaving off the insulin molecules or the amount of native insulin formed. Moreover, the formation of other conjugated derivatives or degradation products

could also affect the experimental outcome, especially for biological activity study and therefore should be taken into consideration when investigating the stability of FITC-insulin conjugates.

Figure 4-2 shows a reduction in the percentage AUP representing Mono conjugate analysed by RP-HPLC for 21 days period with respect to increased temperature from 20°C (A) to 37°C (B).

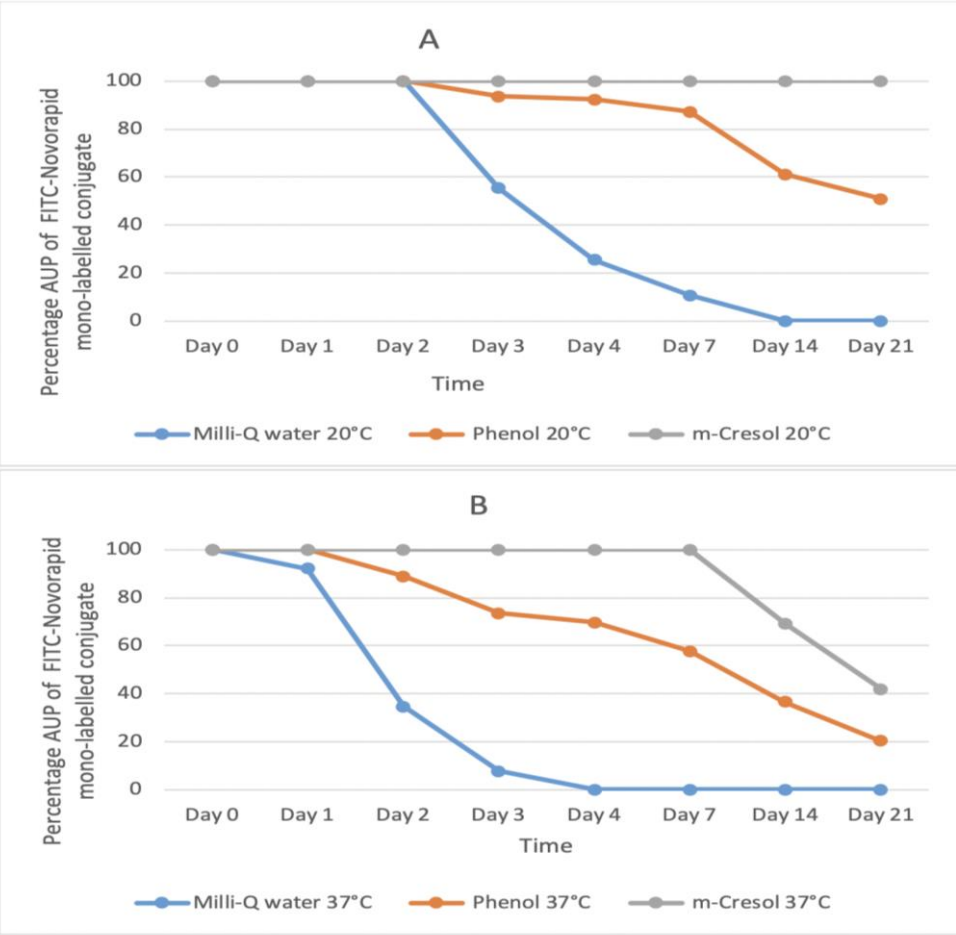

Figure 4-2: Changes observed for the original FITC-Novorapid® conjugate formulated in solution during storage at 20°C (A) and 37°C (B) showing the stability-enhancing effect of phenol and m-cresol.

The stability-enhancing effect of phenol and m-cresol was illustrated by a much slower loss in the percentage of the original Mono conjugate comparing to water alone at both 20°C and 37°C. During storage at 20°C, there was a rapid reduction of ~50% Mono formulated in *water* after two days and down to 0% by day 21. Meanwhile, the reduction rate was much slower for phenol in which during the first 7 days, there was ~90% of the original conjugate remained and

dropped down to 50% by day 21. Notably, the Mono formulated in m-cresol was maintained at 100% throughout 21 days observation at 20°C. Previous studies have established that the rate of degradation will increase with elevated temperature. However, unlike FITC-dextran which was reported to be stable for at least one day at physiological conditions (Natarajan, Northrop and Yamamoto, 2017), only 10% of Mono was lost after one-day storing at 37°C using Milli-Q water as a solvent. The reduction occurred quite rapidly after 4 days when there was no conjugate detected from HPLC analysis. In the presence of phenol, the original conjugate was stable for one day then gradually reduced by more than 10% to 40% from day 2 to day 7, and by day 21 there was only 20% of Mono remained, thus suggesting that phenol can enhance the stability of Mono but only to a certain extent. Notably, the original conjugate (100%) was maintained for up to seven days in m-cresol then reducing to ~70% on day 14 with a further 30% loss by day 21.

Meanwhile, the original Mono samples also contained a trace amount of unlabelled insulin identified by a peak at 20.4min RT from the PDA detector at 215mn as detailed in section 2.3.3. The HPLC method used to analyse FITC-insulin conjugates is unfortunately not compatible with identifying any degraded products such as insulin deamination from insulin itself. However, it is questionable that any of the denatured insulin products (if any) throughout this study would fluoresce since the appearing of other unidentifiable peaks were detected in the fluorescent mode, prompting that these other peaks could be the degradable products from FITC itself or the conjugate.

More importantly, the data collected from RP-HPLC analysis did not only demonstrate the percentage loss in the original Mono but also identified the amount of free FITC cleaving off as well as the formation of other conjugated species such as Di and Tri. **Table 4-3** and **Table 4-4** present different species identified by RP-HPLC other than the original conjugate owing to the stability changes of Mono during storage at 20°C and 37°C, respectively.

Table 4-3: Species identified by RP-HPLC showing the changes of FITC-Novorapid® conjugate formulated in Millipore water, Phenol and m-Cresol during storage at 20°C

	Time	Unlabelled Novorapid® (PDA 20.4min RT)	Mono-labelled FITC-Novorapid® (21.9 min RT)	Di-labelled FITC-Novorapid® (22.6 min RT)	Tri-labelled FITC-Novorapid® (23.4 min RT)	Free FITC (13 min RT; 16 min RT and 28 min RT)	Others
In milli-Q water	Day 0-2	Trace	100%	None	None	None	None
	Day 3	Trace	55.36%	20.13%	24.51%	None	Trace
	Day 4	Trace	25.39%	25.63%	48.98%	Trace	Multiple peaks/Trace
	Day 7	Lost	10.72%	10.78%	78.50%	Trace	Multiple peaks/Trace
	Day14	Lost	Trace	Trace	41.23%	36.81%	Multiple peaks/Trace
	Day 21	Lost	Trace	Trace	20.93%	79.07%	Multiple peaks/Trace
In 0.2% Phenol	Day 0-2	Trace	100%	None	None	None	None
	Day 3	Trace	93.62%	6.38%	None	None	None
	Day 4	Trace	92.27%	7.73%	None	None	None
	Day 7	Trace	87.18%	12.82%	None	Trace	Trace
	Day14	Lost	61.10%	Trace	None	38.91%	Trace
	Day 21	Lost	50.90	Trace	None	49.10%	Trace
In 0.25% m-Cresol	Day 0-7	Trace	100%	100%	None	None	None
	Day 14	Trace	100%	Trace	None	Trace	None
	Day 21	Trace	100%	Trace	None	Trace	None

Table 4-4: Species identified by RP-HPLC showing the changes of FITC-Novorapid® conjugate formulated in Millipore water, Phenol and m-Cresol during storage at 37°C

	Time	Unlabelled Novorapid® (PDA 20.4min RT)	Mono-labelled FITC-Novorapid® (21.9min RT)	Di-labelled FITC-Novorapid® (22.6min RT)	Tri-labelled FITC-Novorapid® (23.4min RT)	Free FITC (13min RT; 16min RT and 28min RT)	Others
In milli-Q water	Day 0	Trace	100%	None	None	None	None
	Day 1	Trace	92.24%	7.76%	None	None	None
	Day 2	Trace	34.67%	13.25%	51.83%	None	Trace
	Day 3	Trace	7.82%	Trace	92.18%	None	Trace
	Day 4	Lost	Trace	Trace	100%	Trace	Multiple peaks/Trace
	Day 7	Lost	Trace	10.09%	17.10%	67.10%	Multiple peaks/5.71%
	Day14	Lost	Trace	12.98%	13.40%	70.09%	Multiple peaks/3.53%
	Day 21	Lost	Trace	5.0%	7.97%	87.03%	Multiple peaks/Trace
In 0.2% Phenol	Day 0-1	Trace	100%	None	None	None	None
	Day 2	Trace	88.93%	11.07%	None	None	None
	Day 3	Trace	73.43%	26.57%	None	None	None
	Day 4	Trace	69.58	30.42%	None	None	None
	Day 7	Trace	57.66%	42.34%	None	Trace	Trace
	Day14	Lost	36.59%	42.57%	6.72%	14.12%	Multiple peaks /Trace
	Day 21	Lost	20.28%	36.10%	9.46%	34.16%	Multiple peaks /Trace
In 0.25% m-Cresol	Day 0-7	Trace	100%	None	None	None	None
	Day 14	Lost	69.19%	16.55%	None	14.26%	Trace
	Day 21	Lost	41.96%	30.07%	None	27.97%	Trace

During three weeks of storage at 20°C, the stability of Mono was best enhanced in m-cresol then phenol and least in water. Based on the preservation of 100% of the original conjugate, it was therefore concluded that the presence of m-cresol could enhance the stability of Mono in a solution for up to three weeks. The appearance of Di and free FITC peaks observed in day 14 indicated that change in the original conjugate may have started but occurred at a much slower rate. However, the considerably low amount of these products did not reach concentrations suitable for quantification by HPLC analysis and therefore was marked as trace. Interestingly, the loss of original conjugate in water from day 3 to day 7 was correlated to the formation of Di and Tri rather than free FITC. By day 14, deconjugation also occurred as there was ~ 40% of free FITC detected, which was further increased to 80% after 21 days as more FITC was released. It was anticipated that a complete deconjugation of Mono in water would have occurred after 28 days storage at 20°C. Meanwhile, changes in the original conjugate occurred at a much slower rate in phenol as there was only ~ 13% of Di formed without any Tri detected in day 7. Unlike the case in water, the increased loss of Mono observed in day 14 and 21 using phenol was directly correlated to FITC cleaving off. This result suggested that in the presence of phenol although the loss of Mono occurred at a much slower rate than in water, it would lead to the appearance free FITC rather than the formation of Di and Tri.

As anticipated, an elevated temperature of 37°C had a higher impact on the stability of Mono. The formation of Di, Tri and denatured products also occurred at a faster rate than compared to storage at 20°C. Especially, the fast forming of Di and Tri observed in water seemed to result in the rapid appearance of free FITC and other degraded products. After one day, there was nearly 10% reduction of Mono in water and rapidly by day 4, further Mono loss resulted in the complete formation of Tri. As deconjugation started to occur, there was nearly 70% of free FITC detected by day 7, which comparing to the deconjugation rate at 20°C was much faster. In the presence of phenol, Mono loss occurred at a slower rate than in water with a slower formation of Di and Tri. Notably, deconjugation also occurred after 14 days in phenol as free FITC

was also detected but at a much lower amount than in water. Although similar rate of deconjugation also occurred using m-cresol after 14 days, its ability to preserve 100% Mono for up to seven days at 37°C comparing to almost 50% lost by day 7 using phenol indicated that m-cresol was the most suitable solvent for enhancing the stability of FITC- insulin conjugates in solution during storage at high temperature (37°C).

Overall, the stability of lyophilised Mono conjugates in solution is best enhanced using 0.25% m-cresol for all conditions ranking best at 2-8°C for more than 8 weeks > 20°C for up to 4 weeks > 37°C for seven days. Even though the data was only collected until week eight, it is possible that the Mono samples prepared in m-cresol could have been stable for more than eight weeks if stored at 2-8°C. It is, therefore, necessary to determine at which time point insulin will start losing their fluorescent label to avoid storing samples in their working dilution for longer than needed. Notably, the stability of Mono conjugates in solution remained unchanged regardless of the solvent used for up to seven weeks if stored at 2-8°C. This study showed which conditions FITC-insulin conjugates can be formulated and stored until it is no longer suitable to use. The most appropriate solvent was also necessary to prepare FITC-insulin solution in the INsmart device for diffusion study set at room temperature and run at 37°C for several days.

3.3.2 The stability enhancement effect of diluting fluid on FITC-insulin during storage at 2-8°C, 20°C and 37°C

It is of interest to know whether the hexamer structure of insulin can be reformed after conjugation with FITC since during the labelling the process, the insulin-zinc hexameric structure was altered by the addition of chelating agent EDTA. Although the removing of zinc content was not necessary, it may be lost during the purification process owing to the disappearing of the phenolic content observed from FITC-insulin product. It is, therefore, necessary to investigate the labelling effect of FITC on the stability of insulin and the use of diluting fluid containing m-cresol, glycerol and zinc oxide as formulated in pharmaceutical insulin products for their stability-enhancing effect on FITC-insulin. According to

Brange 1987, at a concentration equal to or higher than 2mM, the hexamer can be formed at neutral pH without the assistance of zinc ions. The standard concentrations formulated in most pharmaceutical insulin preparation is 100Unit/mL which is equivalent to 0.6mM; therefore, it is proposed that the addition of zinc oxide to both pharmaceutical insulin preparations and their fluorescently labelled conjugates is still necessary for the formation of insulin hexamer to enhance their stability.

Figure 4-3 illustrates the changes in percentage AUP of Mono in diluting fluid analysed by RP-HPLC during storage at 20°C and 37°C

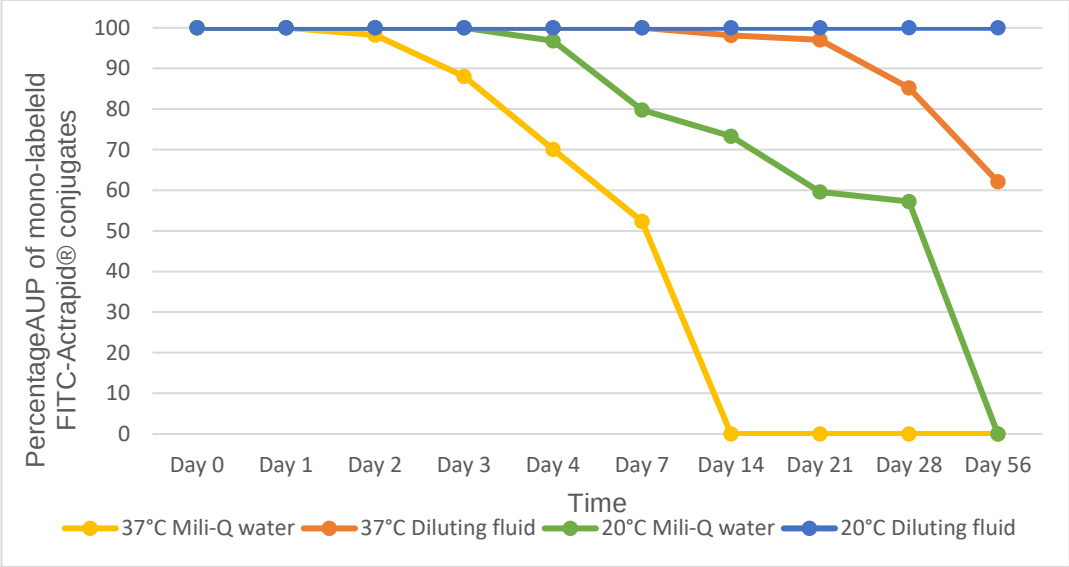

Figure 4-3: Changes in the original FITC-Actrapid® conjugate during storage at 20°C and 37°C for 56 days period showing the stability-enhancing effect of diluting fluid.

As expected, the stability of Mono was better enhanced at 20°C than at elevated temperature of 37°C. In the presence of both zinc and phenolic compound, the original conjugate was well preserved even at high temperature since the percentage AUP of Mono was maintained for up to seven days at 37°C and 56 days at 20°C. Whereas by day 7, the percentage AUP of Mono has dropped down to 80% and almost 50% at 20°C and 37°C respectively in water alone. Unlike FITC-Novorapid® samples, the purer form of FITC-Actrapid® conjugate without any unlabelled insulin maintained the original conjugate for one day longer in water at both temperatures. A complete loss of

Mono in water was not observed until day 14 at 37°C and day 56 at 20°C whereas in the case of FITC-Novorapid® this loss was observed by day 4 and 14 respectively. Notably, the presence of zinc oxide did not seem to enhance the stability of Mono for any longer than seven days at 37°C as observed using m-cresol alone. However almost 60% of the original conjugate in m-cresol has been lost by day 21. Meanwhile, in the case for diluting fluid containing zinc oxide, Mono loss at 37°C was much slower in which 97% of the original conjugate was still maintained by day 21, and there was more than 60% of Mono remained after 56 days. This observation suggested that the stability of Mono can be best enhanced using diluting fluid containing m-cresol, glycerol and zinc oxide as formulated in pharmaceutical insulin products.

Table 4-5 and **Table 4-6** summarise different species identified by RP- HPLC other than the original conjugate as a result of changes in FITC-Actrapid® stability during storage at 20°C and 37°C respectively for 56 days.

Table 4-5: Species identified by RP-HPLC showing the changes of FITC-Actrapid® conjugate formulated in diluting fluid during storage at 20°C

	Time	Mono-labelled FITC-Actrapid® (21.9min RT)	Di-labelled FITC-Actrapid® (22.6min RT)	Tri-labelled FITC-Actrapid® (23.4min RT)	Free FITC (13min RT; 16min RT and 28min RT)	Others
In milli-Q water	Day 0-3	100%	None	None	None	None
	Day 4	96.80%	None	None	None	3.20%
	Day 7	79.75%	None	None	20.25%	Trace
	Day 14	73.31%	Trace	None	20.34%	6.35%
	Day 21	59.59%	Trace	None	40.41%	Trace
	Day 28	57.25%	Trace	Trace	42.75%	Trace
	Day 56	None	None	None	100%	None
In diluting fluid	Day 0-28	100%	None	None	None	None
	Day 56	100%	None	None	Trace	None
	Day 70	85.2%	None	None	14.8%	None

Table 4-6: Species identified by RP-HPLC showing the changes of FITC-Actrapid® conjugate formulated in diluting fluid during storage at 37°C

	Time	Mono-labelled FITC-Actrapid® (21.9min RT)	Di-labelled FITC-Actrapid® (22.6min RT)	Tri-labelled FITC-Actrapid® (23.4min RT)	Free FITC (13min RT; 16min RT and 28min RT)	Others
In milli-Q water	Day 0-1	100%	None	None	None	None
	Day 2	98.2%	None	None	1.8%	None
	Day 3	88.01%	None	None	11.99%	None
	Day 4	70.03%	None	None	29.97%	None
	Day 7	52.31%	None	None	47.69%	Trace
	Day 14	None	None	None	100%	Trace
	Day 21-56	None	None	None	None	Multiple peaks-100%
In diluting fluid	Day 0-7	100%	None	None	None	None
	Day 14	98.09%	Trace	None	None	1.91%
	Day 21	97.05%	Trace	None	None	2.95%
	Day 28	85.20%	Trace	None	None	14.80%
	Day 56	62.09%	Trace	None	8.18%	29.73%
	Day 70	None	None	None	100%	Multiple peaks- trace

During storage at 20°C, the initial detection of other degradants was thought to be accountable for more than 3% loss of the original conjugate formulated in water after four days. The majority of Mono loss in water seemed to correlate with FITC cleaving off insulin molecule rather than the formation of other labelled species as observed in FITC-Novorapid® conjugate. However, it is possible that the presence of unlabelled insulin in FITC-Novorapid® samples may have contributed to the formation of Di and Tri while FITC-Actrapid® samples contain no unlabelled insulin owing to further HPLC purification. As free FITC was detected by day 7 in FITC-Actrapid® samples, it was also of interest whether unlabelled insulin would be present. However, since there was no observation of any insulin peak, it is concluded that despite losing its FITC labels as observed by an increase in free FITC from 20% to 100% detected by day 7 to day 56 respectively, the deconjugated insulin molecules cannot be restored to their native insulin form. In the presence of unlabelled insulin as in the case for FITC-Novorapid®, the loss of original conjugate resulted from the formation of Di and Tri would occur at a faster rate within three days in water. Unlike for FITC-Actrapid® the loss due to FITC cleaving off was much slower as free FITC was gradually released over seven weeks. The results suggest that unlabelled insulin remained in the conjugated product may lead to a quicker formation of other FITC-insulin species during storage in their working formulations rather than the deconjugation process of breaking the covalent bonds between FITC and insulin molecules. Notably, compared to the effect of m-cresol alone, the diluting fluid illustrated better enhancement effects on the stability of FITC-insulin, which was stable for up to 56 days at 20°C.

On the other hand, during storage at 37°C, loss of the original conjugate formulated in water by day 2 was found to correlate with the rapid formation of free FITC which reached nearly 50% by day 7 and 100% by day 14. After 21 days, the samples became completely degraded owing to the presence of multiple peaks which were not identified previously from their fluorescence chromatogram. In contrast, in diluting fluid this loss seemed to relate to the slower formation of other fluorescently degradant products, which were observed from day 14 to 56, accounting for 2%-30% respectively of the total

fluorescent peaks. It was not until nearly 40% of the original conjugate was lost that almost 10% of free FITC was detected in day 56, suggesting that the presence of diluting fluid had slowed down the deconjugation process for at least 28 days even at high temperature of 37°C. However, the conjugates are still prone to degradation at high temperature. Rapidly after further observation of 14 days (day 70) a complete loss of Mono was seen in diluting fluid with the detection of 100% free FITC and a trace amount of other fluorescently degraded products.

Overall, there is the capability of diluting fluid to maintain 100% of the original conjugate for up to 56 days (although peaks for free FITC also started to appear) at 20°C. It is, therefore, the solvent of choice for the preparation of FITC-insulin in its working formulations. However, at 37°C, daily analysis between day 7 to day 14 may be necessary to conclusively confirm at which day the loss of original conjugate starts because there was only 2% reduction of Mono by day 14, suggesting that the sample could last longer than seven days. Meanwhile, the stability of Mono in water and diluting fluid was best maintained during storage at 2-8°C for up to three months and six months respectively after which the 100% yields of original conjugates started to reduce owing to the formation of free FITC and other fluorescently degraded products. However, the complete loss of Mono has not been observed (Chromatograms for storage at 2-8°C are shown in the appendix).

In conclusion, the stability of FITC-insulin formulated in solution is best enhanced using diluting fluid containing m-cresol, glycerol and zinc oxide at 2-8°C for six months > 20°C for two months> 37°C for seven days. Although the original conjugate was best maintained in diluting fluid for all studied temperatures the results also highlighted the impact of unlabelled insulin remained in the conjugated products that likely results in the formation of other conjugated species.

4.3.3 The fluorescence stability profiles of FITC-insulin with respect to pH changes.

Figure 4-4 represents an increase in the fluorescence intensity of Mono in response to increased pH from 5 to 8 at which maximum fluorescence was recorded then reduced by 20% at pH 9. Furthermore, after seven days of storage in its working formulations at room temperature, there was a shift in fluorescence profile. However, the trend of increased fluorescence intensity with respect to increased pH has remained unchanged despite the shift.

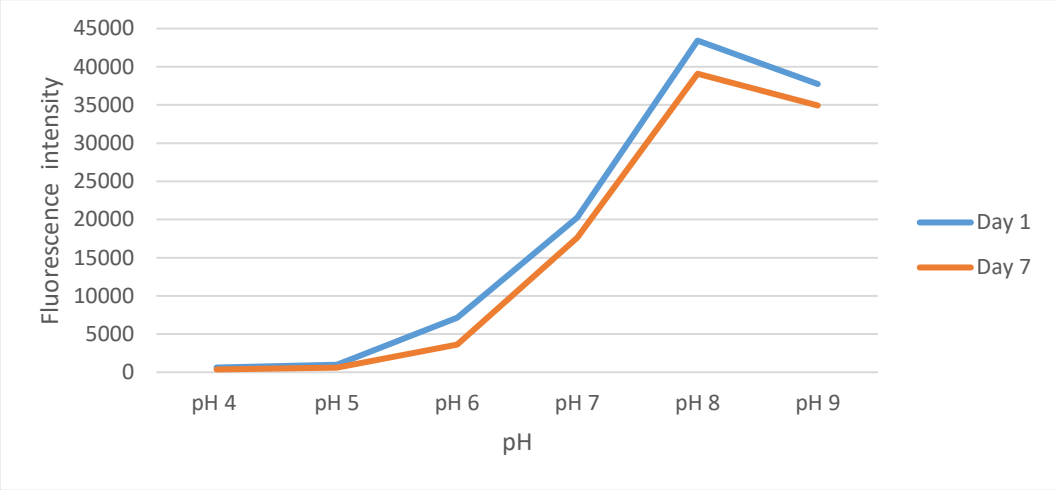

Figure 4-4: Fluorescence intensity (Emission 519mm) of FITC-insulin in the range pH 4-9 prepared in water, measured in day 1 (blue) and day 7 (orange), showing a fluorescence maximum at pH8.0 and fluorescence intensity best preserved at pH4-5

Notably, upon 24 hours standing, Mono solution formed a suspension at pH 4, 5 and 6 as illustrated in **Figure 4-5** however after thorough shaking the suspension re-dissolved to form a clear solution.

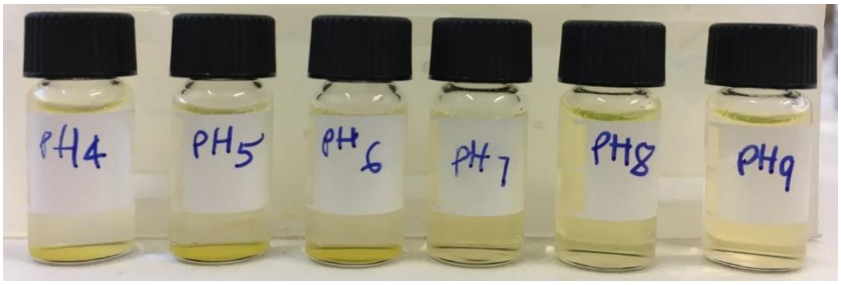

Figure 4-5: Observation of FITC-Actrapid® conjugate in solution after 24h showing Mono suspension forming at pH 4, pH 5 and pH 6 upon standing at room temperature.

Principally, FITC is well established to be highly sensitive to pH and therefore has been used as a pH indicator in biological material for intracellular and extracellular pH measurement. According to a study by (Breen, Raverdeau and Voorheis, 2016), the response to changes in pH observed from the fluorescence intensity of FITC demonstrates that the FSC moiety of FITC itself irreversibly loses fluorescence at elevated pH above 7, while FITC-methylamine exhibits reversible loss of fluorescence at high and low pH and has a fluorescence maximum at pH 8.0. Similarly, FITC-insulin sample manufactured and used in this study also demonstrated a fluorescence maximum at pH 8 (**Figure 4-4**). However, it is uncertain that FITC-insulin could exhibit best detection capacity at pH 7-8 if formulated in water for an extended period at room temperature. Notably from the previous stability test, FITC-insulin was reported to be stable in water for only four days at 20°C. Therefore, the decrease in fluorescence measured in this pH study could be due to the free FITC detaching from insulin after seven days storage at 20°C. Meanwhile, it was also well established that insulin can precipitate out in solutions due to pH changes within its isoelectric precipitation zone of pH 4.5-6.5; therefore, the precipitations of Mono observed at pH 4, 5 and 6 after 24h were expected. In general, fluorescently labelled insulin should be best formulated at pH 7-8 and ideally avoiding pH ≥9.

4.3.4 The equilibrium solubility of FITC-insulin using the shake-flask method

It is understood that FITC-insulin conjugates are more soluble than native insulin in water. This could be due to the effect of FITC modification on the hexameric structure of insulin, making it easily dissolvable but the actual reasons are beyond the scope of this study. From a practical point of view, 1,000Unit/mL (35mg/mL) of FITC-insulin could be easily formulated in water (pH7) without forming any precipitation for several weeks storing at 2-8°C. It is proposed that a starting concentration of 3,000 Unit/mL could be used to determine the maximum concentration of FITC-insulin for its working formulation. From the previous findings, it was noted that FITC-insulin could precipitate in aqueous solution at pH6 and below. Besides, the need to observe the solution for several days suggests that the use of diluting fluid (pH7) to

ensure its stability would be more appropriate for this study. Initially, 1mL of the starting concentration of 3,000 Unit/mL FITC-insulin was prepared in a 1.5mL Eppendorf tube as described in 4.2.7. Within a few seconds of gentle mixing a uniform solution was achievable however it appeared opaque as illustrated in **Figure 4-6**, suggesting that compete dissolution might not be achieved at 3,000 Unit/mL.

Figure 4-6: An opaque solution of 3,000 Unit/mL FITC-insulin observed immediately after gentle mixing in diluting fluid.

The resultant mixture was then left mixing for 24h at 200 rpm followed by 2h standing at room temperature, after which there was visible precipitation formed as showed in **Figure 4-7**

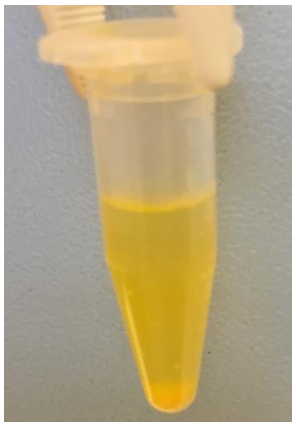

Figure 4-7: The precipitation of 3000 Unit/mL FITC-Actrapid® conjugate observed after a cycle of 24h mixing and 2h standing at room temperature.

From the calibration curve (R^2=0.999) constructed directly using the HPLC analysis software (LC lab solution), the concentration of the first supernatant was determined at ~ 490 Unit/mL, as illustrated in **Figure 4-8**

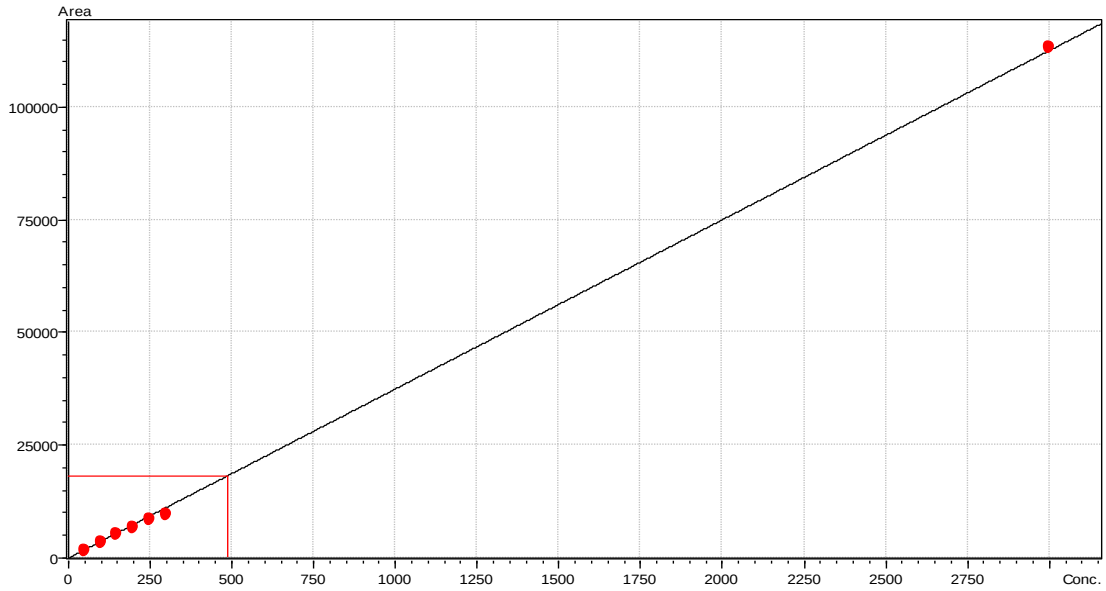

Figure 4-8: Mono concentration determined by HPLC at 490Unit/mL for the first supernatant collected from 3,000Unit/ml starting concentration.

Notably, this EqC of FITC-insulin is half the preliminary data observed for 1,000Unit/mL but is equivalent to the highest concentration in commercially available insulin injections One possible explanation for this could be due to the small volume of diluting fluid (1mL) used to dissolve such a large amount of lyophilised FITC-insulin (105mg). Principally, the surface area of any solute that can come into contact with its solvent to achieve a complete dissolution is affected by the volume of solvent available and the size of solute. The smaller amount of solute will enable more surface area contact with the same volume of solvent used than any bigger amount where contact will be considerably limited by the large particle sizes. In another way, like many other solutes, the smaller amount of lyophilised FITC-insulin (35mg) will have a higher chance of achieving complete dissolution.

Meanwhile, the resultant pellet resuspended in 1mL of diluting fluid had a concentration of ~ 2,470Unit/mL as showed in **Figure 4-9**.

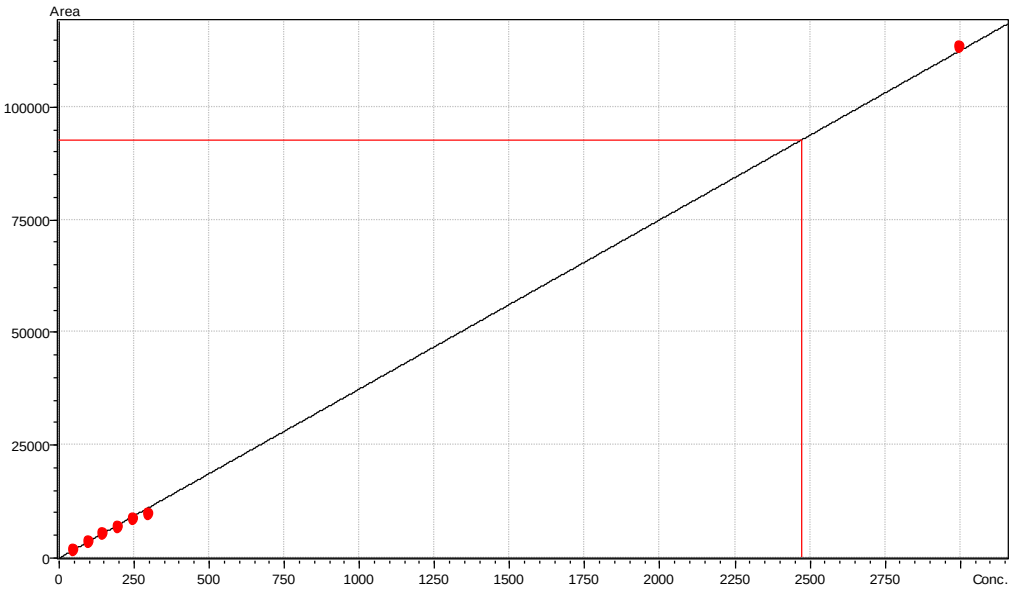

Figure 4-9: Mono concentration determined by HPLC at 2,470 Unit/mL for the first collected pellet of 3,000Unit/mL staring concentration after centrifugation then being resuspended in 1mL diluting fluid.

Interestingly, **Figure 4-10** shows that the resuspended pellet has remained in equilibrium as a clear solution for another cycle of 24h mixing.

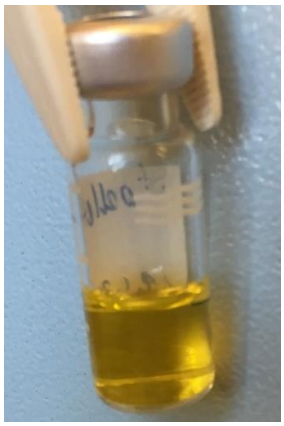

Figure 4-10: A clear solution of the resuspended pellet (determined at 2,470Unit/mL) observed after a further cycle of 24h mixing.

This observation suggested that the maximum concentration of FITC-insulin at equilibrium solubility can be as high as 2,400Unit/mL. However, it could be understood that the resultant pellet from 3,000Unit/mL FITC-insulin solute was pre-dissolved and exposed to diluting fluid for more than 24h subject to being resuspended in another mL of diluting fluid thus there is a higher chance for this

pre-wetted pellet to remain in dissolution compared to the equivalent amount of lyophilised sample. In fact, a starting concentration of 2,000Unit/mL FITC-insulin was similarly tested. However, precipitation still occurred after 24h-mixing cycle, suggesting that the amount of FITC-insulin was still too high to be completely dissolved. To further determine the maximum concentration of FITC-insulin in diluting fluid (pH>7) that would remain in equilibrium, another starting concentration of 1,500 Unit/ml was similarly tested as described in section 4.2.7.

Figure 4-11 shows a clear yellow solution of 1500 Unit/mL FITC-insulin formulated in diluting fluid after two cycle of 24h mixing and 2h standing.

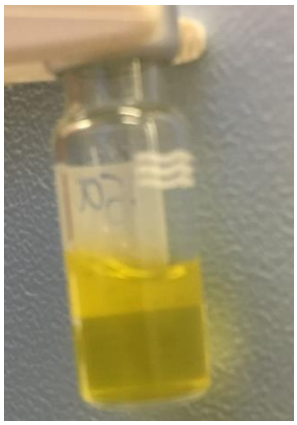

Figure 4-11: A clear solution observed after 24hour mixing then centrifugation at room temperature of the freshly prepared FITC-insulin at 1500Unit/mL.

Based on the observation of a clear uniform solution without any precipitation following two cycle of 24h mixing then centrifugation, it is therefore concluded that the equilibrium solubility for FITC-insulin formulated in diluting fluid (pH7) is at a maximum concentration of 1,500Unit/mL. Unlike fluorescently labelled insulin, the preparation of recombinant HI solution would require it to be solubilised at 1-10 mg/mL in dilute acetic (1%) or hydrochloric acid, pH 2-3. Although the labelling of FITC to insulin has increased its solubility at neutral pH since lyophilised FITC-insulin can be formulated in water and diluting fluid at pH7, it is questionable that the equilibrium solubility of FITC-insulin could be further improved in acidic pH.

Although it has been successful in determining the solubility of FITC-insulin using the equilibrium solubility test, the overall process was quite time-consuming and requires a considerably high amount of sample. Moreover, other factors influencing the solubility of FITC-insulin such as temperature, stirring speed, solvent type, the content of zinc ion have not yet been fully investigated. Nevertheless, the capability of FITC-insulin to be readily formulated in diluting fluid (pH7) at 1,500Unit/mL (3x higher than any commercially available insulin) is highly advantageous to produce a concentrated insulin depot for the *in-vitro* diffusion study to investigate the delivery of FITC-insulin from the closed-looped insulin delivery device.

4.4 Chapter summary

The study has investigated the effect of phenol, m-cresol and diluting fluid (containing m-cresol, glycerol and zinc oxide) on the stability profiles of FITC-insulin (Actrapid®/Novorapid®) conjugates in solution when subjected to change in temperature over time. These stability profiles were examined based on the degree of deconjugation (the presence of free FITC) and formation of other FITC-labelled species which exhibit reduced biological activity. The fluorescence intensity of FITC-insulin was also determined as a function of pH to determine its best pH working range. Furthermore, the equilibrium solubility of FITC-insulin was examined using the EqC (shake-flask) method to determine its maximum concentration that can remain in a homogeneous system as formulated in diluting fluid at pH7. The overall results have highlighted some key finding as follows:

- The presence of unlabelled insulin in the conjugated product will likely contribute to the formation of other labelling species which can affect the biological activity of the original conjugate being investigated. The finding suggested that there should be an absence of unlabelled insulin in its fluorescently labelled products, especially in those experiments where the biological activity of insulin is paramount. For example, for a study investigating the insulin signalling pathways where its biological activity would need to be measured or determined for an extended period then

ideally batch to batch variations in the use of fluorescently labelled insulin in the presence of unlabelled insulin are undesirable.

- Although water can be the solvent of choice for preparing most products of fluorescently labelled insulin conjugates, depending on the experimental design and objective, their working formulation should be freshly prepared and used within 24 hours for all *in-vivo* and *in-vitro* studies setting at 37°C or three days at ambient temperature. Notably, pre-formulated solution of FITC-insulin is also possible, providing that it should be used within three months of preparation, and the samples are kept at 2-8°C with protection from light.
- The use of diluting fluid as formulated in many commercially available insulin injections has successfully enhanced the stability of FITC-insulin for up to seven days, even at a high temperature of 37°C. For experiments performed at ambient temperature, the solution of FITC-insulin were found to stable for up to two months after being made in its diluting fluid. Besides, the shelf-life for this pre-made stock solution would expect to last for up to 6 months if storing at 2-8°C with protection from light. Furthermore, lyophilised FITC- insulin would expect to remain conjugated for several years and so far, Mono sample synthesised after four years has remained unchanged.
- Similar to FITC, its conjugate with insulin is also sensitive to pH changes and exhibited the best fluorescence intensity at pH8 while precipitated at pH4-6. However, after a week of storage at room temperature, the fluorescence intensity loss was least observed at pH7 (~5%) while ~ four times this lost was observed at pH 6,8 and 9. Although it is always advisable to only use a freshly prepared solution of FITC-insulin, their best working pH range should also be kept within pH7.
- The maximum concentration of lyophilised FITC-insulin that can dissolve in 1mL of diluting fluid containing m-cresol, glycerol and zinc oxide at pH7 was at 52mg/mL (equivalent to 1,500 Unit/mL) after 48h based on the equilibrium solubility test. This concentration is significantly higher

than any clinically used insulin preparations in which the highest is formulated at 500 Unit/mL.

- The labelling of FITC to insulin must have altered the structural configuration of insulin to a certain extent that can improve its solubility at neutral pH since 52mg/mL FITC-insulin can be freely solubilised in diluting fluid at pH7, while the preparation of insulin solution would require solubilising in acid at pH2-3.
- Further testing is necessary to investigate the effect of zinc oxide content alone on the stability of FITC-insulin since the presence of zinc ion would facilitate the formation of hexameric insulin, which is less prone to aggregation, therefore can keep insulin stable in its working dilution.

Chapter 5: Drug delivery mechanism and diffusion kinetics of FITC-insulin from the INsmart device.

5.1 Introduction

Understanding the capability and performance of the INsmart device (a closed-loop insulin delivery system) is fundamentally important in developing an artificial pancreas that is capable of delivering the required daily correct insulin dose in response to changing blood glucose levels. It is well understood that the best therapy for diabetes is one that mimics the physiological process of normal glucose control which operates by a negative biochemical feedback. The human pancreas behaves as a self-regulated or closed-loop insulin delivery system in the body. It operates automatically and continuously according to changes in blood glucose levels that trigger appropriate responses by releasing insulin or glucagon to maintain homeostasis as detailed in section 1.1.1. The potential benefits of an implantable INsmart device include the capability of keeping glucose levels under control to minimise diabetes-associated complications which are common in most current treatments of diabetes. Consequently, it could improve the quality of life for people with diabetes and increase longevity. Minimising diabetes complications also means that it could save expensive treatment costs from renal failure and cardiovascular diseases relating to diabetes, which represent nearly 10% of the annual NHS expenditure. In this chapter concepts of molecular transport in solutions across barriers by mean of simple diffusion will be discussed to aid the understanding of insulin release mechanisms from the INsmart device. Additionally, the diffusion kinetics of FITC-Actrapid® conjugate in the glucose responsive gel will be studied to establish the release profiles of insulin diffusing through the INsmart device in response to glucose triggers.

5.1.1 Diffusion

Diffusion is the basic mechanism of transport for molecules in living organisms. It is defined as a physical process of mass transfer or net movement of individual molecules from an area of high concentration to another one of low concentration by random movements in solution. Diffusion in living organisms, especially the human body is essentially the key mode for the absorption of digested nutrients, gas exchange, transportation of hormones such as oestrogens and metabolites towards their target organs and most importantly for nearly every event in embryonic development (Cocucci et al., 2017; Basak, Sengupta and Chattopadhyay, 2019; Schavemaker, Boersma and Poolman, 2018). Generally, there are two main types of diffusion namely simple diffusion and facilitated diffusion. As their names suggest, simple or passive diffusion is merely the movement of molecules down their concentration gradients whereas facilitated diffusion is a carrier-mediated transport system that allows molecules to move along a concentration gradient. Examples of simple diffusion include the spreading of perfume or smells in the air; movement of oxygen molecules through the capillary membrane into cells and carbon dioxide removal from cells to enter the bloodstream. In most biological systems, diffusion occurs across a lipid bilayer known as a semi-permeable membrane that has pores and openings to allow the passage of specific molecules. Facilitated diffusion is necessary for the movement of large or polar molecules like carbohydrates or nucleic acids across the hydrophobic lipid bilayer via pores or channels made of transmembrane proteins (facilitators) (Robertson, 2018; Möller et al., 2019; Rea, De Angelis and Baschetti, 2019; Gaur, Mishra and Gupta, 2014).

The study of molecular transport across artificial or biological barriers and movement of drug substances in solutions is considerably important in understanding the context of drug delivery. Principally, simple diffusion is the basic transmembrane process for many small drugs (Mabrouk et al., 2019; Dahlgren and Lennernäs, 2019; Zhang et al., 2019; Brodin, Steffansen and Nielsen, 2010). It applies to several important processes in drug delivery including dissolution of drugs from granules, powders or tablets; drug release from suppository or ointment bases; permeation and distribution of drug

substances in living cell. It also forms the basis of other drug manufacturing processes such as lyophilisation; ultrafiltration; passage of water vapour, gases, drugs and additives through coatings, packaging, films (Jacob, 2015; Albisa et al., 2018; Tona et al., 2019).

Generally, the flux of a solute is defined as the mass or number of molecules moving through a given cross-sectional area during a given period of time, thus presenting measurement of molecular transport across a barrier or mass transport of molecules in a solution. Transport investigations of drug or prodrug candidates across a barrier tissue like small intestinal cell culture models or tissue models are the most common biopharmaceutical use of flux studies. An experimental setup for flux studies typically includes a donor compartment with a defined initial concentration and volume of compound, a barrier structure with a well-defined thickness and cross-sectional area, and a receiver compartment with a defined initial concentration and volume. Furthermore, diffusion flux is also useful in establishing selection criteria and screening for candidate drug compound or to predict in-vivo bioavailability of a given drug substance (Jacob, 2015; Stewart et al., 2017; Gadgil et al., 2019; Uhl and Liu, 2019).

The need to understand the mass transfer behaviour of insulin through the glucose-responsive gel is fundamental for the optimisation and application of the INsmart device. This is because of the variable diffusional characteristic in the gel that control the diffusion. The ultimate aim of the device is to mimic the real-time response to changing glucose levels from the human pancreas. Providing that the device performance is at its optimum (no leak or blockage, correct gel thickness and content, appropriate surface area and sufficient insulin in reservoir), the response of the gel to changing glucose levels is the main factor affecting insulin delivery from the device (as detailed in section 5.1.2). This emphasised the importance of understanding the insulin release kinetics from the device to establish the mechanism behind getting the correct insulin dose for each glucose challenge. It also helps determine the service intervals at which the insulin solution in the reservoir needs refilling or when the gel might have lost its potency and would need to be replaced (Jacob, 2015). Ideally, the

profile of insulin release from the device should follow the natural pattern of basal and bolus insulin release from a normal human pancreas.

5.1.2 Glucose-responsive gel

The development of a novel glucose-responsive gel material has formed the basis of the closed-loop insulin delivery system. This smart gel exhibits a fast gel-sol transition that responds reversibly to glucose triggers. Upon interaction with glucose, the viscosity of this gel material can be lowered. The gel is a hydrophilic, viscoelastic material which is formed by an interaction between dextran (a branched glucose polymer produced by *Leuconostoc mesenteroides*) and the lectin concanavalin A (con A) from *Canavalia ensiformis* (Jack bean, Type VI) with glucose-specific receptors (refer to Error! R eference source not found.) (Tanna,Taylor et al.2006; Tanna, Sahota et al.2006; Jacob 2015).

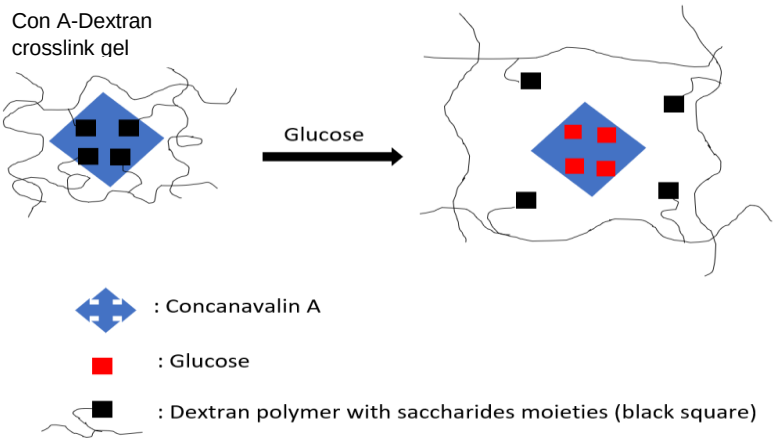

Figure 5-1:Illustration of the Con A-dextran crosslink gel structure and the displacement of saccharides moieties by free glucose (Adapted from Taylor 2020).

Notably, lectin con A is a protein that exists as a dimer at pH below 5.8 and as a tetramer at physiological pH. Each identical component of its dimeric and tetrameric structures has a binding subunit for the cooperative accommodation of divalent metal ions and appropriate configuration of carbohydrates with terminal glucose, fructose or mannose. **Figure 5-2** shows the scheme of lectin con A configurations from monomer, canonical dimer in which the two monomers associate adjacently to form a long β-sheet of 12 strands and

tetramer with binding sites for metal ions and glucose (Cavada et al., 2019; Jacob, 2015).

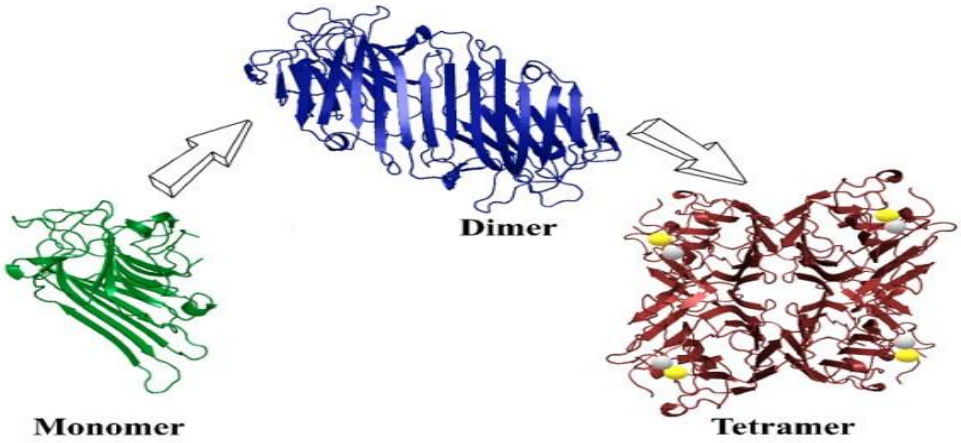

Figure 5-2: 3D structures of lectin Con A oligomerisation showing the binding sites of metal ions (silver) and glucose (yellow) in the tetramer (adapted from Cavada et al., 2019)

The mechanism for gel-sol transition of the smart gel depends on a competitive displacement of a glucose-bearing polysaccharide from the lectin receptors by free glucose molecules, thus dismantling the three-dimensional gel network. As a result, the gel viscosity falls in the presence of glucose but reforms after glucose removal. The glucose responsiveness of this smartly designed gel network implies that insulin can be delivered through a gel layer whose viscosity reversibly changes in response to glucose content. Therefore, in the presence of glucose, insulin stored in the core material of the gel is released more rapidly than when glucose is absent (Tanna, Sahota et al.2006).

In a further evolution of the smart gel design, the gel material forming part of the implantable closed-loop insulin delivery device used in the *in-vivo* pig studies was a partially polymerised product of dextran methacrylate (dex-MA) and con A methacrylamide (con A-MA). The product creates large molecular structures by a limited distribution of covalent bonds but not a solid hydrogel. Notably, both the polymerised counterpart and simple mixture of dextran and con A form glucose-sensitive gels that exhibit a reversible change in viscosity on contact with glucose to modulate insulin transport, thus acting as a self-regulated system.

Figure 5-3 presents an overview of the glucose responsiveness of the gel material contained in the insulin delivery device.

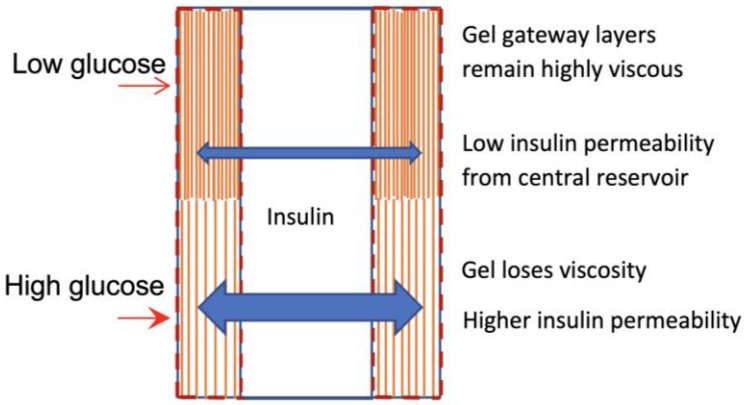

Figure 5-3: An overview of the gel action contained in insulin delivery device. (Adapted from Jacob 2015)

5.1.3 Design of the INsmart device

Open-loop insulin delivery systems

A modified open-loop insulin delivery system using a conventional externally sighted pump combines continuous subcutaneous insulin infusions (CSII) from an external insulin pump with continuous monitoring of glucose levels via a SC sensor. The latter communicates glucose readings to the pump using radio transmitter. The insulin pump delivers basal insulin into the abdominal SC tissue at an appropriate rate for the patient but mealtime bolus insulin doses need to be triggered manually. This is because the automated system cannot yet be trusted not to produce severe hypoglycaemia due to insulin overdose, thus highlighting the inability of pumps to safely deliver the higher insulin dose (Farmer Jr, Edgar and Peppas, 2008b; Karges et al., 2017; Bally et al., 2017). CSII has a number of advantages over the conventional insulin therapy with multiple daily injections (MDI) such as modest reduction in insulin dose, providing better glycaemic control as measures by HbA1c, having higher patient compliance and satisfaction (Skyler 2010; Jacob 2015). However, there are some disadvantages including higher therapy costs, risk of incidents of non-delivery and diabetic ketoacidosis due to potential pump failures, sensor

connection errors, and the need to be attached to the system. One of the major drawbacks of the open-loop is its lag time between SC blood glucose levels detected by CSII system and the real-time BG level from the vascular when BG changes rapidly i.e. during exercise, resulting in a delayed response of up to 20mins (Basu et al., 2014; Zaharieva et al., 2019). This means that a falling BG level in the vascular may not be detected immediately from the interstitial space where the SC sensor detects glucose and a large insulin dose may be delivered inappropriately.

Closed-loop insulin delivery systems

A closed-loop insulin delivery system monitors the change in glucose levels automatically and dispenses an accurate dose of insulin accordingly, both of which occur continuously in real time, which solves most of the lag time issues experienced by CSII system. The main concept of a closed system is based on its many capabilities including the maintenance of near normal glycaemic levels in real-time, prevention of long-term hyperglycaemic effects caused by the lag time, lowering the healthcare costs especially those associated with diabetes complications and improving the quality of life for patients (Jacob 2015). Ideally, a closed-loop delivery system should closely mimic the physiological release of insulin from normal pancreatic beta cells. The ideal system should accomplish several criteria including being glucose-specific and able to transmit variable insulin release rates to plasma in real-time; responding to changing glucose levels in an acceptable timescale and in a dose-related rate manner. There is also a requirement to operate long term without leak of insulin and components or creation of non-biocompatible interactions within the body after implant. Another key criterion for this system is that it should deliver readily available insulin or analogues without the need of specific conjugates such as glycosylated forms; and should not introduce increased need (down regulation) (Taylor, Sahota 2013).

The design of an implantable INsmart device (artificial pancreas) for the management of diabetes is based on the instant changes occurring in the glucose responsive gel in response to changing glucose levels and thereby

modulating the release of insulin through a rigid casing, which forms a gateway to the insulin reservoir. As mentioned above, this smart gel containing diffusing insulin from the reservoir should exhibit a fast gel-sol transition with a primary response specifically to glucose. The device, which is designed to be implanted in the peritoneal cavity works on a rapid feedback mechanism of the smart gel to control insulin release. This mechanism (refer to **Figure 5-4**) based on the fast exchanges between the peritoneal fluid and blood to mimic a normal pancreas action and therefore may overcome inherent problems faced by current biologically or electronically based closed-loop systems to maintain normal BG levels.

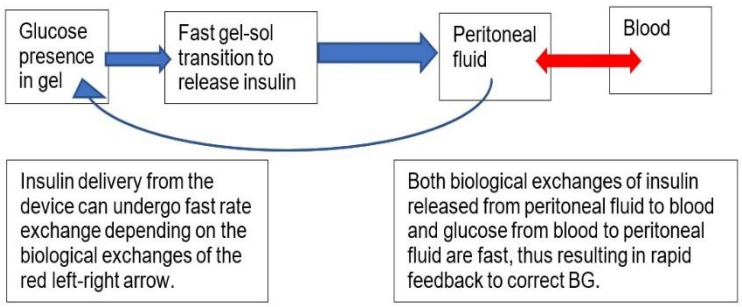

Figure 5-4: Rapid feedback mechanism of the smart gel device.

Figure 5-5 shows the working prototypes of the implantable artificial pancreas designed and manufactures by Renfrew International (Leicester, UK).

Figure 5-5: A presentation of the implantable closed-loop insulin delivery device with refill needle ports.

One of the many advantages of this device is that it provides a closed-loop insulin delivery system with accurate dose rate based on a glucose-specific chemical response. It also removes the need to inject insulin manually without electronic or moving parts like other types of artificial pancreas. Furthermore, it is simple to implant without the need for immunosuppressive drugs like transplant treatments and easily refillable. It is also aesthetically preferable to external portable pumps which is visible on the surface of skin.

Error! Reference source not found. presents components of the INsmart device i n sequential arrangements of membranes, gel spacer and grids.

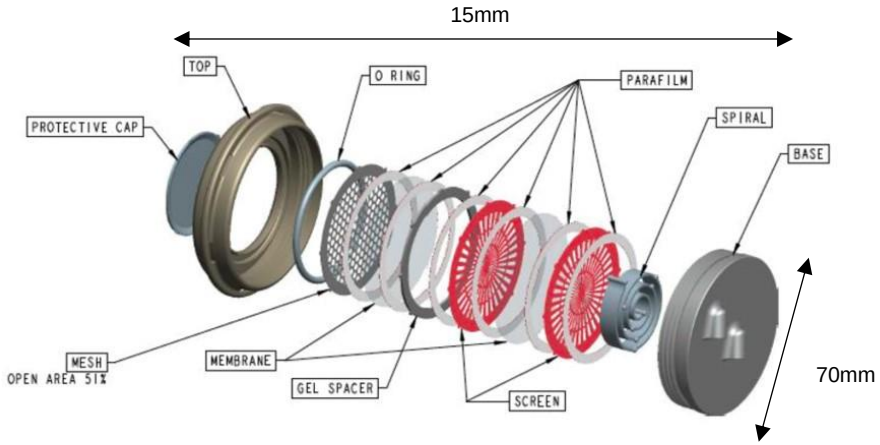

Figure 5-6: A developmental model of the INsmart device showing individual component arrangement (Taken from Jacob 2015).

The device is designed to prevent any internal swelling of the gel and distortion of the semipermeable membranes by confining the gel in the tight construction. The working model parts are made of stainless steel, polycarbonate and resin which could be replaced with polyurethane in future designs or making them entirely with polycarbonate to make these parts lighter. In order to achieve biocompatibility, the refill plumbing circuits have tubing made of polyethylene-lined polyurethane that connects the luer connections from the device to the fill ports under the skin. This tubing material manufactured by SAI strategic applications incorporated also makes it compatible with insulin and therefore minimising risk of interactions and systemic errors. Furthermore, all device parts of the experimental model can simply be removed and cleaned.

5.2 Materials and Methods

5.2.1 Materials and equipment

Con A-Methacylamide (Con A-MA) was synthesised in house with DS 40-60% lysines methacrylated (Biomaterials 2006), M-cresol, glycerol and zinc oxide were purchased from Sigma-Aldrich Chemical Company Ltd (UK). Igracure 2959 was from Ciba Geigy (UK). Parafilm was from Brand R (UK). Metal perforated disk (50% surface area) was custom made by Renfew limited (Loughborough, UK). Silicone gaskets were purchased from Fisher (Loughborough, UK). 0.2μm and 0.025μm filters were from Whatman (UK). Visking tubing was ordered from SpectroPor (UK). Diluting fluid (0.0005%w/v Zinc Oxide;1.6%w/v glycerol; 0.25%w/v M-cresol; pH7.5), synthesised FITC-insulin (section 2.2.4). Dextran methacylate (Dex-MA) was also synthesised inhouse with DS 2.6%. Milli-Q water with pH adjusted to 8 was used throughout. Peristaltic pumps used for the experimental flow setting include Watson Marlow 101U (Pump A) and Watson Marlow (Pump B). Other equipment includes Grant water bath (UK), Fisher scientific heater plate (Loughborough, UK), Perkin Elmer Precisely LS55 Luminescence Spectrometer interfaced with FL Winlab software (UK).

5.2.2 *In-vitro* diffusion test rig set-up

The diffusion test rig custom built for the purposes of this work contains various individual components which were assembled as shown in **Figure 5-7**

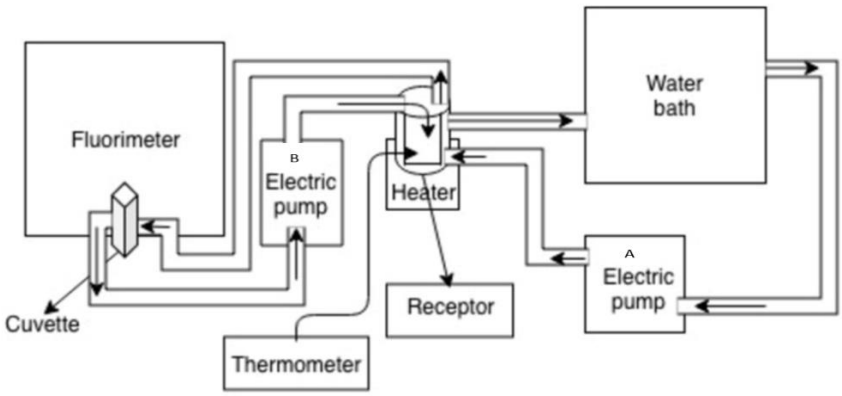

Figure 5-7: Schematic drawing of the experimental rig set-up with black arrows displaying the direction of flow within compartments.

The receptor compartment which houses the INsmart device was filled with 600mL of milli-Q water (pH adjusted to 8) to ensure the device was fully submerged and any air bubbles present in the tubing were eliminated by purging the lines. The receptor compartment was continuously stirred throughout the experiment with the magnetic stirrer bar placed directly beneath the device to circulate any bubbles on the device surface. Two separate water baths were used, the first being to maintain the temperature in the receptor compartment at 37ºC and was placed below the receptor. The second provided warm bath to the jacket of the receptor via pump A by maintaining a continuous flow of warm water from the heating water bath to the exterior surrounding of the receptor compartment to compensate the heat lost during experimental process. Pump B enables real time diffusion measurements by providing a continuous flow of the receptor solution to a quartz fluorimeter flow cell (cuvette) and the FITC-Actrapid® released was recorded every 2 mins from the fluorimeter software. The presence of any air bubbles in the cuvette was regularly checked to ensure no flawed results. The fluorimeter was pre-set with excitation and emission of 494nm and 518nm respectively and the slit width maintained at 2.5nm.

5.2.3 Preparation of the smart gel

200mg of con A-MA was dissolved in 2g of diluting fluid (0.0005%w/v zinc oxide;1.6%w/v glycerol; 0.25%w/v m-cresol; pH8) with the addition of a 20μL photoinitiator, Irgacure 2959 (0.8%w/v) and then mixed with 200mg of dex-MA. The mixture was continuously stirred until becoming homogenous to from a viscous solution which was covered in foil and allowed to stand for an hour at room temperature. After that, the mixture was poured between two glass plates separated by a 60μm thick gasket. Once the mixture has spread uniformly between plates, it was then irradiated under UV light (356nm,10mJcm^{-2}) for 5mins to allow the crosslinking process of the gel to occur. The slightly opaque partially cross-linked gel of ConA-MA and dex-MA was removed from the plates and stored at 4ºC for at least 24h prior to testing.

5.2.4 Preparation of 1000Unit/mL FITC-insulin formulation for the reservoir.

Chapter 2 has detailed the synthesis of FITC-insulin conjugates which were used in this diffusion study to investigate the release profiles of insulin from the INsmart device.

35mg of FITC-insulin powder was dissolved in 1mL of diluting fluid (as detailed in section 5.2.3) to achieve a final concentration of 1000 Unit/mL. The solution was either used immediately to fill the device reservoir prior to experimental work or stored at 4ºC until further use.

5.2.5 Assembly of the INsmart device

The INsmart device used here was an experimental, one sided, small scale one made out of polycarbonate without plumping. It was used to develop the *in-vitro* and *in-vivo* (rodent) systems. There is a number of different components forming parts of this experimental device as listed in **Table 5-1**

Table 5-1: Lists of components used in device assembly

Individual components	Numbers used
Parafilm gaskets in multiple layers	5
0.4mm Millipore gaskets	3
Metal perforated plates	2
Filtered membranes	2
Base	1
Top	1

The device was carefully assembled from the base up towards the top. **Figure 5-8** shows the order for individual components of the device assembly.

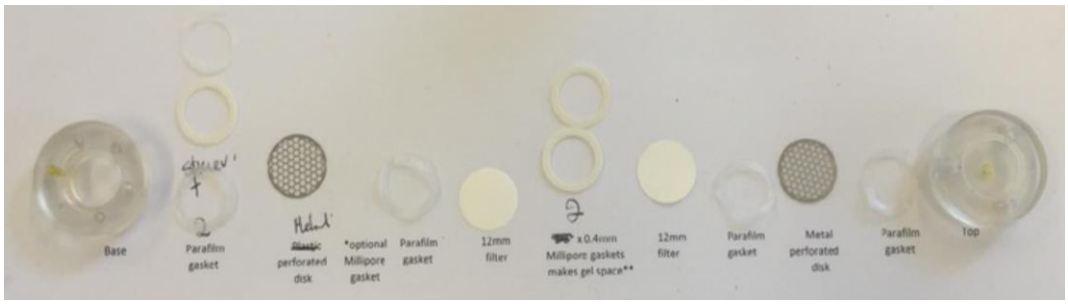

Figure 5-8: An illustration of the device components assembled in order from left (Base) to right (Top).

The assembly of the device was as follows:

1. A parafilm gasket was greased and added to the base followed by a 0.4mm Millipore gasket which was topped by another greased parafilm gasket.
2. The first metal perforated disk 1 of 2 was added, followed by the third greased parafilm gasket then topped with a 12mm membrane (0.2 - 0.025μm pore size or 100kDa Visking tubing cut into 12mm disks)
3. Two 0.4mm Millipore gaskets creating the gel space were placed on top of the membrane before adding the smart gel into it. Ideally, the gel must form a flat layer in line with the 0.4mm Millipore gaskets with fully occupied gel space to be appropriately packed. Improper addition of gel in excess or too little can cause possible leakage, leading to false results.
4. Once the gel has been added, another 12mm filter was carefully placed on top of the gel followed by a greased parafilm gasket.
5. The second metal perforated disk was then added, topping with the last parafilm gasket.
6. Finally, the top component of the device, whose rims were greased, was placed on with care taken to ensure that the whole device was airtight, reducing chances of leakage. Once the device has been aligned, greased screws were fitted to lock the entire device together.
7. 0.5mL FITC-insulin stock was then filled from the central hole on the top shell of the device using a 1mL syringe. Extra care was taken while filling the device to ensure no air bubble resided within the reservoir. A final screw then closed the central hole on the top shell entirely for the complete assembly of the device as shown in **Figure 5-9**.
8. The INsmart device was immersed in distilled water and placed at 4°C overnight prior to be used in experiments. This was to allow the gel to swell osmotically and also to see if any visible dye was leaking from the device via the rims or front. The metal perforated plates should allow minimal excess swelling (no bulge), thus preserve the flat gel surface but with enough swelling to fill the device space. Noting that the space is

limited and thus the physical strength of the plates, screw threads must balance the osmotic force.

Figure 5-9: Complete assembly of the INsmart device containing FITC-insulin reservoir showing no leaks after assembling and 24h storage in water.

5.2.6 Experimental test.

For each diffusion experiment, the receptor was topped up with Milli-Q water (pH adjusted to 8) to the 600mL mark if required and a baseline reading was obtained by running the experimental system in water for 60mins. The INsmart device containing FITC-insulin reservoir was then placed into the jacketed jar of the receptor compartment circuit with constant magnetic stirring, directly underneath it to ensure that any diffused drug from the front and no bubbles built up on the metal grid face. The system was left running for another 60 mins to obtain a baseline reading for the basal insulin release profile. After this time, glucose triggers at different concentrations (0.1%,0.2% and 0.5% w/v) were applied to the system either in single trigger or multiple triggers to assess the release profiles of FITC-insulin reservoir. These triggers were conducted by introducing powdered glucose of appropriate weight for the 600mL receptor. Once the chosen trigger time has elapsed, the receptor was fully emptied and replaced with fresh Milli-Q water (pH8) until the next glucose trigger.

5.3 Results and Discussions

5.3.1 The effect of long glucose triggers (0.1%, 0.2% and 0.5% w/v) and performance optimisation of the INsmart device.

The long release profiles of FITC-insulin in response to a single trigger of physiologically relevant glucose concentrations (0.1%,0.2% and 0.5% w/v) was investigated by challenging the smart gel in the device with glucose added to the receptor solution at the same single timepoint in separate experiments.

Figure 5-10 shows a change in FITC-insulin gradient values from the device baseline (basal FITC-insulin level) and the glucose challenge in response to 0.1%w/v glucose trigger.

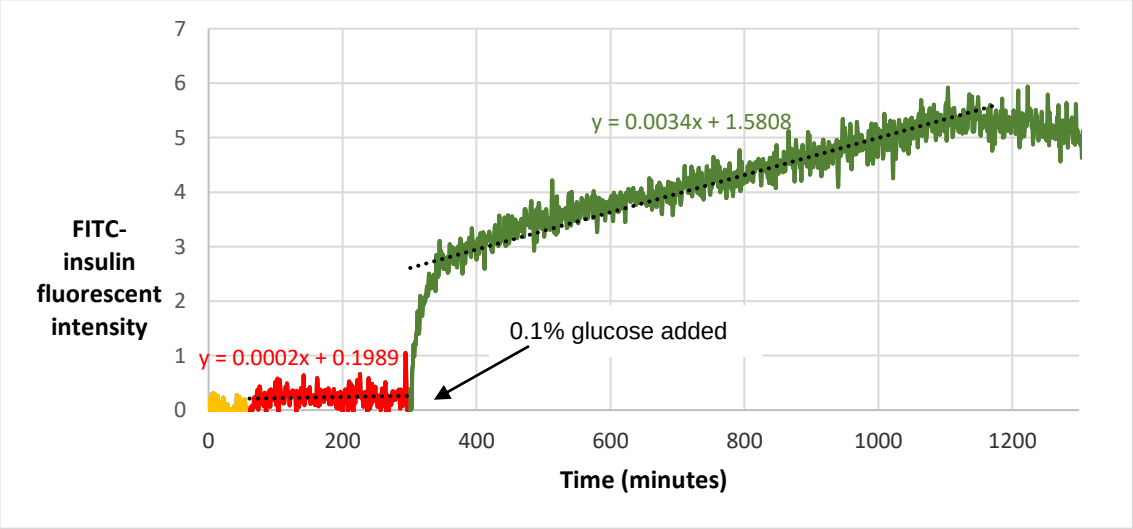

Figure 5-10: FITC-insulin release profiles at 0.1% w/v glucose trigger showing the water baseline in yellow, the device baseline (FITC-insulin basal level) in red and during glucose trigger in green.

In the first 60 mins of the experiment, water (pH8) was run through the apparatus to ascertain a stable blank and to establish a baseline level for water (yellow line). After this time, the INsmart device containing 500 Unit of FITC-insulin reservoir and smart gel as described in section 5.2.5 was added to the receptor compartment. The FITC-insulin basal release (red line) was measured for the next 240 mins. At 300 mins 0.1%w/v glucose was added to the receptor solution and the release profile of FITC-insulin (green line) was monitored for ~ 22h (overnight). Immediately after the addition of glucose, there was a surge of FITC-insulin released into the receptor solution lasting for ~ 45 mins as showed from the increased fluorescence intensity from 300-345 mins. This observation suggested that there has been an immediate response from the device as

glucose came into contact with the smart gel, leading to a fall in the smart gel viscosity. This resulted in an increase in the gradient as FITC-insulin diffused out of the gel layer into the receptor solution. This increased rate of FITC-insulin release was observed from 345 mins to 1200 mins. After reaching the peak release at 1178 mins, the diffusion rate of FITC-insulin showed a linear phase as the drug concentration remained unchanged from 1200-1300 mins. This suggested that FITC-insulin is no longer being released from the reservoir into the receptor. Since the glucose level remained stable in the receptor compartment, the low viscosity of the gel should also remain constant, allowing the constant enhanced rate of FITC-insulin release. The degree of FITC-insulin release was determined by the activation ratio (=17) of the gradient obtained during glucose trigger (0.0034) over FITC-insulin basal release (0.0002).

Figure 5-11 presents a change in gradient from FITC-insulin diffusion experiments in response to 0.2%w/v glucose trigger.

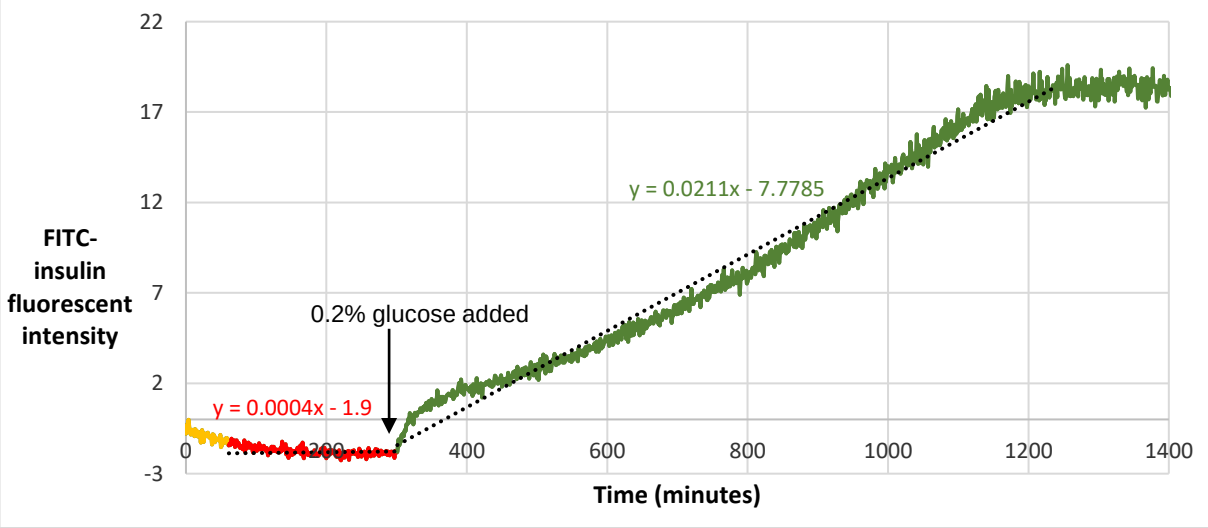

Figure 5-11: FITC-insulin release profiles at 0.2% w/v glucose trigger showing the water baseline in yellow, the FITC-insulin basal level in red and during glucose trigger in green.

As before, a basal release profile in the receptor solution was established between 60-300 mins (red line). 0.2%w/v glucose was then added to the receptor solution at 300 mins and as with 0.1% w/v glucose trigger, there was an immediate surge of FITC-insulin release for the first 15 mins of the glucose challenge. This was followed by a gradually increased release over 15h (green

line) until reaching a linear phase (plateau) (from 1200 mins to 1400 mins) as observed in the 0.1% w/v glucose trigger. Although 0.2%w/v glucose stimulated a much higher rate of FITC-insulin release, the initial burst seems much lower than the 0.1% w/v glucose trigger. However, its release degree as determined by the activation ratio (=53) of the gradient during glucose trigger (0.0211) over FITC-insulin basal gradient (0.0004) was three time higher than the activation ratio calculated from 0.1%w/v trigger. This result suggests that although there was an immediate response from the device to both glucose challenges, the degree of FITC-insulin release varies with different glucose concentrations. However, since the same gel used in the 0.1%w/v trigger also responded to 0.2% glucose trigger as seen by the boost FITC-insulin release, it is still of interest to establish when the fast gel-sol transition become irreversible meaning that glucose level is no longer the rate determining step for FITC-insulin release from the reservoir.

Figure 5-12 displays changes in gradient values during the device baseline measure and glucose challenge showing the release of FITC-insulin from the device in response to 0.5%w/v glucose trigger.

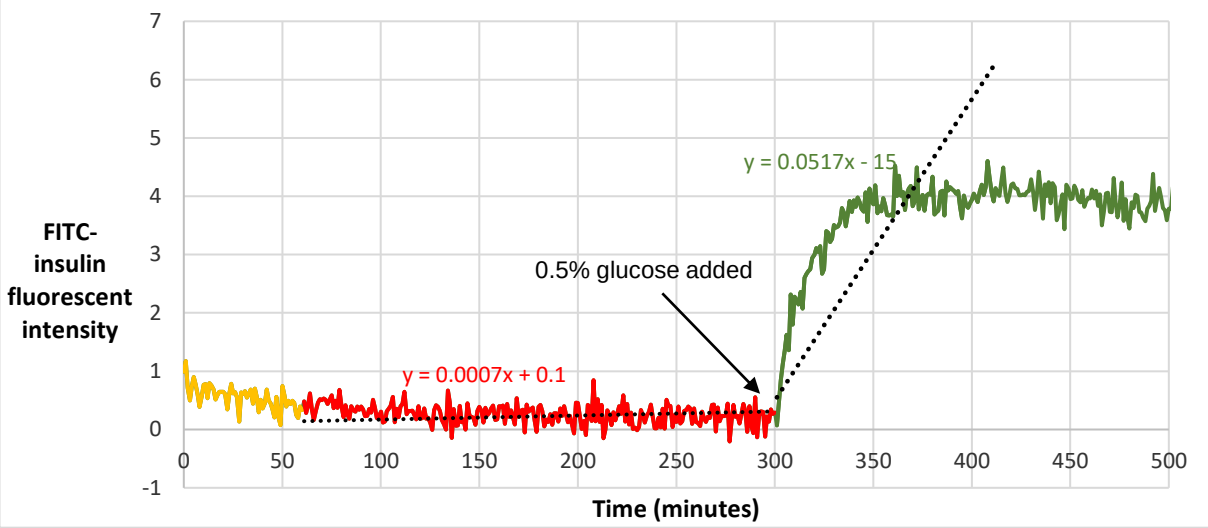

Figure 5-12:FITC-insulin release profiles at 0.5% w/v glucose trigger showing the water baseline in yellow, the FITC-insulin basal level in red and during glucose trigger in green.

Similar to previous experiments, the device baseline measurements were obtained during 60-300 mins (red line). Upon the addition of 0.5%w/w glucose

to the receptor solution, there was a much higher surge of FITC-insulin release seen in the first 15 mins of trigger, after which the release continued to increase gradually over the next 35 mins. Unlike the lower glucose triggers, the peak release of FITC-insulin from the 0.5%w/w glucose trigger was rapidly achieved within 50 mins. However, after reaching the peak release, the dose rate also remained constant as similarly observed in the 0.1% and 0.2% w/v glucose triggers. Not only showing a much more rapid response, the activation ratio calculated for 0.5%w/v glucose trigger (74) was also the highest compared to lower values of 0.1% (17) and 0.2% w/v glucose triggers (53). Once the experiment was terminated, the INsmart device was examined and the gel disappeared completely. It is therefore concluded that repeatedly (three times) prolonged glucose triggers over 24h period would result in irreversible gel-sol transition, thus retaining the gel in it liquified state. As a result, the gel components could have escaped from the device through the large pore size filter and over time the gel would become more diluted to the point that it has turned into a low viscosity solution mixture and completely lost its potency. This would certainly prevent glucose being the driving force for the rate of FITC-insulin release, which at this point is believed to be by mean of simple diffusion down its concentration gradient.

The overall observations suggest that the smart gel exhibits fast gel-sol transition upon glucose triggers, followed by a continuous increased rate of FITC-insulin release, thus showing zero order release kinetics (drug release rate is independent of the drug concentrations). However, once the peak release is reached, the dose rate of FITC-insulin would become plateaued regardless of the prolonged effect of constant glucose present. This could be due to a combination of factors. When the gel is in prolonged contact to glucose it will osmotically swell and occupy any micro-voids within the device resulting from assembly. The porosity of the membranes is important as dex-MA is polydisperse and the polymerisation process may have produced polymeric structures which are not large enough to be retained by the membrane pore size. This is especially relevant given that we have a lightly polymerised gel (irradiation of 5 mins). This short irradiation time is used because we want to

maintain the competitive glucose binding part of the gel mechanism and a longer irradiation time would produce a more rigid gel (Tanna et al., 2006) which may be retained by the membrane pore but at the expense of competitive displacement and a reduced insulin release rate. The chosen irradiation times is a fine compromise. When the devices were examined after each of the glucose triggers the gel layer had been compromised. This suggests that over prolonged period in glucose, the gel components could escape from the large pore membranes to the exterior. It should be mentioned however in reality such prolonged high glucose challenges would be unlikely.

In a real time scenario, the negative feedback loop would respond quickly to changes in glucose level to maintain normal glycaemia and therefore only the initial rapid surge of FITC-insulin release as observed with 0.5%w/v glucose trigger should occur, following by an increased steady state diffusion as compared to basal diffusion rate. The chosen glucose concentrations (0.1%; 0.2% and 0.5% w/v) correlate to the therapeutic range of plasma glucose (5.6mmol/L; 11.1mmol/L and 27.8mmol/L respectively) that would stimulate increased insulin release therefore it is expected that the INsmart device would respond to these glucose triggers in similar way compared to the physiological response.

5.3.2 The effect of different membrane pore size used in the INsmart device

The selection of a suitable membrane is important in designing the device not only to enable a flat gel surface for simple diffusion of FITC-insulin in response to changing glucose levels but also to prevent the gel materials leaking out of the device, which can affect the gel integrity as previously reported during the long release tests.

Figure 5-13 shows the effect of using 0.2μm membrane within the device on the release profiles of FITC-insulin subjecting to sequential 0.1%,0.2% and 0.5% w/v glucose multi-trigger at different timepoints.

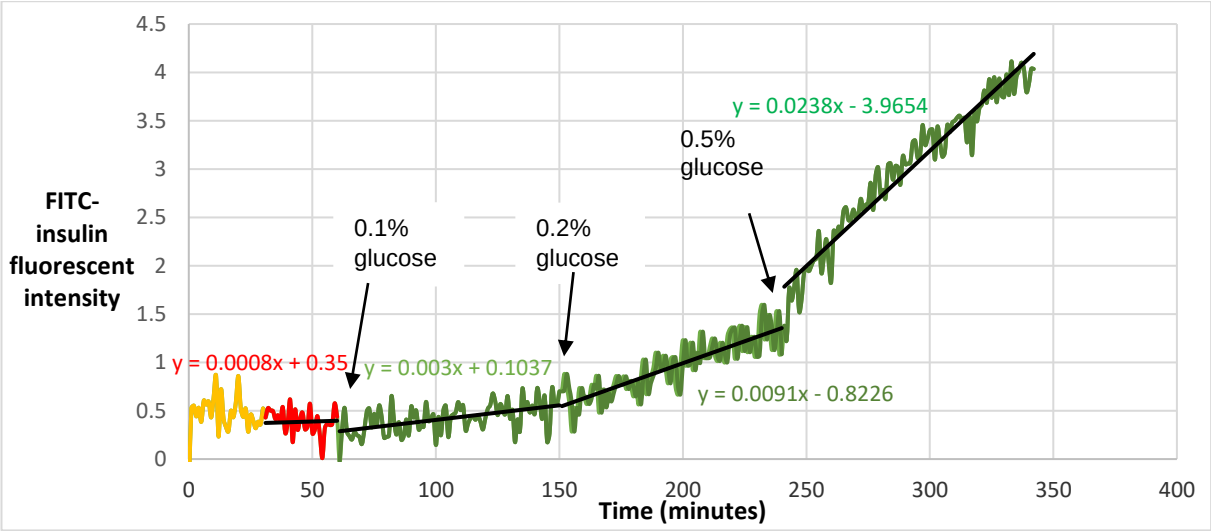

Figure 5-13:FITC-insulin release profiles through the device using 0.2μm membrane in response to sequential 0.1%,0.2% and 0.5% w/v glucose multi-trigger showing the water baseline in yellow, FITC-insulin basal level in red and during glucose challenges (0.1%;0.2% and 0.5%) at three different timepoints in green

As anticipated, there are three distinct gradient changes seen at each glucose trigger with the initial activation ratio calculated for the first 0.1% glucose trigger to be 3.8, which increased by 3 with 0.2% glucose trigger and reaching 30 at 0.5% glucose trigger. The staggered approach with multiple glucose triggers showed that the device could respond to multi-triggers of glucose as seen by a continuous increased rate of FITC-insulin release during the 5h delivery test. However, the degree of FITC-insulin release was much less than observed for single trigger tests at any timepoint. Furthermore, the release rate was much steadier and there was no burst of initial FITC-insulin release upon the addition of glucose as would be the ideal pattern in real case scenarios as it would better mimic normal pancreatic activity. This observation could be because as a smaller filer sized membrane was used, insulin deposited at the outermost layer of the gel would not burst out of the membrane as fast as observed for the larger filter sized membrane once the gel liquefied after glucose trigger This indicated that multiple glucose triggers at shorter time would allow a much apparent linear release of FITC-insulin. In the previous experiment with prolonged glucose trigger, the FITC-insulin deposited at the outermost layer of the gel would burst out of the device through large membrane pore size

immediately after the glucose triggers kicked in to reduce the gel viscosity, resulting in the surge release. However, this was not observed in the sequential glucose multi-trigger at different timepoints using the same membrane pore size.

Figure 5-14 presents the effect of using 0.025μm filter within the device on the release profiles of FITC-insulin subjecting to sequential 0.1%,0.2% and 0.5% w/v glucose multi-trigger at different timepoints.

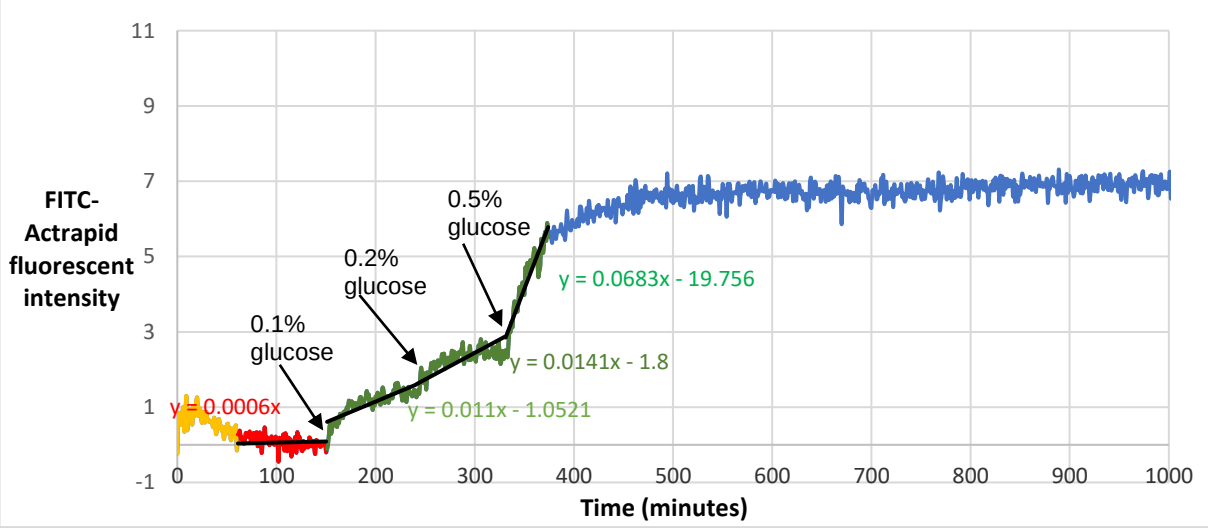

Figure 5-14: FITC-insulin release profiles through the device using 0.025 μm membrane in response to sequential 0.1%,0.2% and 0.5% w/v glucose multi-trigger showing the water baseline in yellow, the FITC-insulin basal measurements in red and during glucose challenges (0.1%;0.2% and 0.5%) at three different timepoints in green, with effect thereafter in blue.

The use of smaller pore size membrane resulted in much better FITC-insulin release profiles that follow similar pattern expected in real case scenarios. There was an initial increased rate in FITC-insulin release in response to each addition of 0.1%,0.2% and 0.5% w/v glucose, reaching its peak release after ~ 5h from initial trigger, after which a steady state remained for another 7h. The total activation ratio indicating the degree of FITC-insulin release was four times higher than reported using the bigger pore size (0.2 μm) membrane. The result suggested that fitting the gel within 0.025μm pore size membrane will improve the overall performance of the device to achieve physiologically relevant FITC-insulin release profiles.

Figure 5-15 displays the effect of using Visking MWCO100kDa membrane within the device on the release profiles of FITC-insulin subjecting to consequential 0.1%,0.2% and 0.5% w/v glucose multi-trigger at various timepoints.

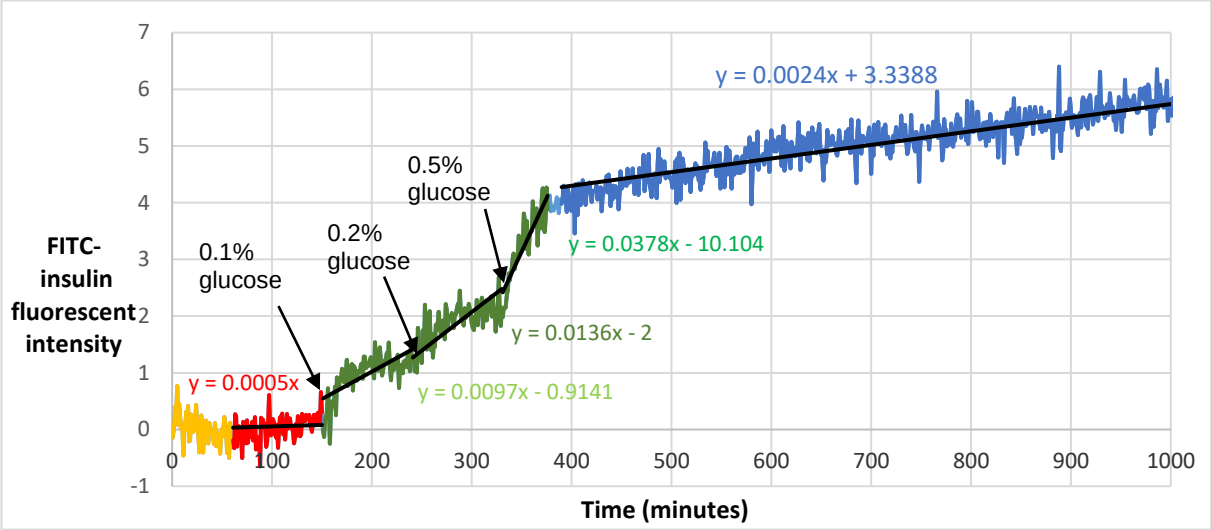

Figure 5-15: FITC-insulin release profiles through the device using Visking MWCO 100kDa in response to 0.1%,0.2% and 0.5% w/v glucose multi-trigger showing the water baseline in red, the device baseline in yellow, during glucose challenge at three different timepoints in green and the effect thereafter in blue.

The increased rate of FITC-insulin release profiles observed with the device test using Visking MWCO100kDa membrane followed a similar trend to the 0.025µm membrane. The difference is that Visking membrane acts as a barrier to prevent passage of large molecular weight molecules over 100kDa while 0.025µm membrane works on pore size of around 300kDa. Notably, there were four distinct changes in gradient values following each 0.1%,0.2% and 0.5% w/v glucose trigger and the continued effect of 0.5% (blue line), whereas using the 0.025µm membrane the effect thereafter remained plateau. Although the total activation ration calculated (75.6) was not as high as compared to using 0.025µm membrane (113), the continued increase release of FITC-insulin in response to prolonged 0.5% w/v glucose trigger seen with Visking membrane suggested that the glucose effect on the gel performance would not wear off after multiple triggers. This is because the molecular mass of Con A as tetramers at pH8 is 110Da, which would be retained within the membrane inside

the device. As the gel components are not escaping through the membranes, it is unlikely that the gel will dismantle after prolonged multi-glucose triggers and could remain rate determining in response to glucose present.

Overall, both 0.025μm and Visking membranes showed better device performances in FITC-insulin release, thus are viable parts for the device. However, Visking membrane provides a definitive cut of point at which only molecules <100kDa i.e. insulin can pass through, hence making it more reliable in retaining the gel integrity, yet still allowing adequate insulin diffusion.

5.3.3 The effect of galactose (control) on the insulin release mechanism of the glucose-responsive gel.

Experimental tests with single and multiple glucose triggers showed promising results of the smart gel delivery of FITC-insulin. In order to confirm that the gel only has specificity for glucose, an experiment was conducted using galactose which is identical to glucose in molecular weight and similarly structured. The specificity of the smart gel for glucose should be confirmed if galactose did not provoke a viscosity change in the smart gel to release FITC-insulin.

Figure 5-16 shows the effect of galactose on the gel responsiveness to release FITC-insulin subjecting to 0.1%,0.2% and 0.5% w/v galactose multi-trigger at different timepoints.

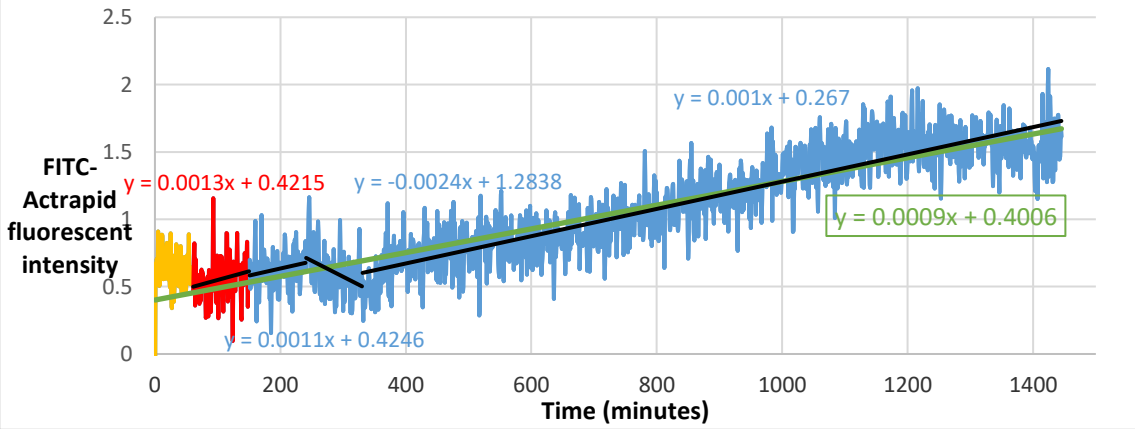

Figure 5-16: FITC-insulin release profiles in response to 0.1%,0.2% and 0.5% w/v galactose multi-trigger showing the water baseline (yellow), basal FITC-insulin level (red) and during galactose challenges (blue) at three different timepoints

Although there was still a basal release of insulin from the device throughout the experimental course of galactose triggers, minimal change in gradient was observed at any timepoint possibly due to the inability of galactose to alter the gel-sol transition as seen with glucose triggers. The total activation ratio calculated was less than 1 and the overall gradient value (in green) obtained from the galactose multi-trigger on reservoir depletion was similar to the basal level of FITC-insulin. The results show that the addition of galactose did not trigger the same response as seen for glucose. Generally, glucose and galactose share a simple structure of a six-carbon ring, making them almost identical. However, galactose differs slightly in the orientation of the hydroxyl group (OH) at the fourth carbon atom as illustrated in **Figure 5-19**. As a result, the OH group of its second carbon atom is in the axial position rather than the equatorial position, which is crucial site for Con A binding.

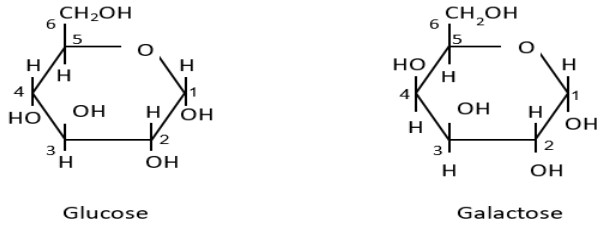

Figure 5-17: Structures of glucose and galactose.

The slight change in galactose stereochemistry causes its lack of affinity, preventing it from fitting into the lectin receptors to change the three-dimensional gel network. Because there was no galactose binding to con A, the smart gel viscosity remains unchanged and therefore resulting in no release of insulin. Although there is still need to test the gel specificity to other sugar types, this experiment shows that galactose with similar structure to glucose does not provoke a viscosity response in the smart gel.

5.3.4 The effect of continuous triggers with glucose and other inert sugars on the device release mechanism of the glucose-responsive gel.

Figure 5-18 shows an extended experiment where the INsmart device has been set up and triggered multiple times with glucose and other dietary saccharides which act as controls to show the specificity of the gel to glucose

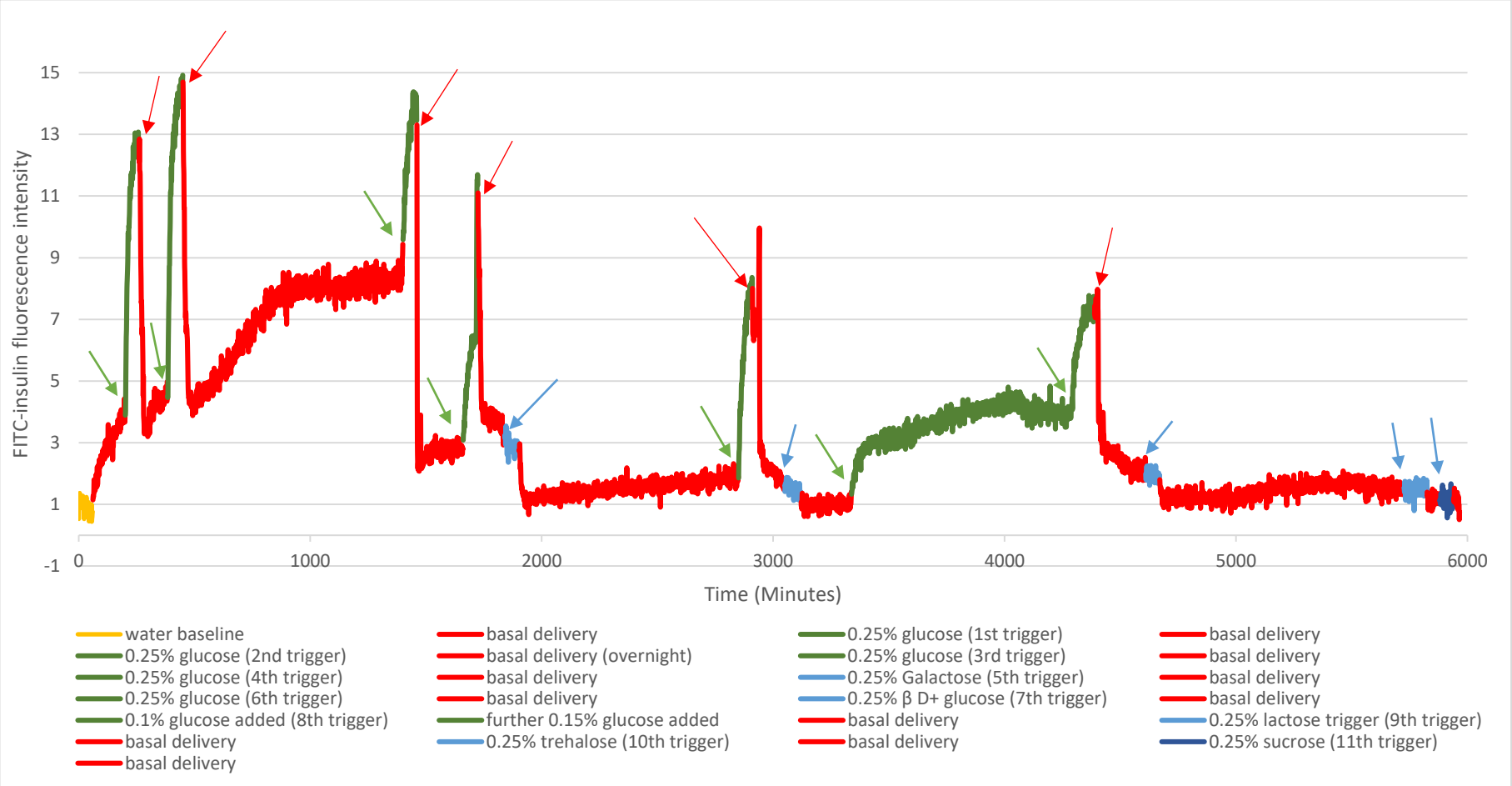

Figure 5-18: FITC-insulin release profiles in response to multiple glucose triggers (6) in green and other inert sugars (galactose, βD + glucose, lactose, trehalose, sucrose) in blue showing the basal delivery in red and the water baseline in yellow. Noting green arrows indicate glucose trigger points, red arrows show glucose trigger removal points and blue arrows for other inert sugars trigger point

Briefly this device was set up as described in section 6.2.5 with some modifications. The membrane used in device comprised dialysis membrane with a MWCO of 100kDa which should retain both the dextran-MA (average MW of 500kDa) and con A-MA (MW of 110kDa). This is because con A-MA is most likely in its tetrameric form as the gel was formulated in diluting fluid at pH 8 and the receptor was in the pH range 8-8.2 for all the glucose and control challenges as well as for the water baseline after each challenge. The 500 Unit FITC-insulin reservoir was also formulated in diluting fluid (pH8). After the device had been assembled with the FITC-insulin reservoir it was left immersed for 6 days at 4ºC in diluting fluid (pH 8). This served two purposes, the first is to assess if any of the yellow FITC-insulin had escaped the device via a gross leak and the second was to allow the gel to osmotically swell to occupy all the micro spaces with the gel thickness so that a surge release did not occur in the first few hours of the experiment. After each trigger whether it be glucose or a control the receptor was washed through twice with Milli-Q water adjusted to pH 8-8.2 to remove all practical remains of the trigger material and to ensure that a lower gradient water baseline was obtained. The smart gel in the experiment was D500-MA (DS2.7%) – con A-MA which had been irradiated for 5 mins in diluting fluid (pH 8). This is almost an identical gel to that used in the *in-vivo* diabetic pig experiments previously which resulted in near normoglycemia over an extended period (Taylor et al., 2016). The only difference being that it is formulated in diluting fluid (pH 8) which is an important further improvement on device design. The insulin used in the *in-vivo* experiments (Humulin R®) is formulated in diluting fluid. When the device was surgically implanted in the diabetic pigs, the reservoir was filled with diluting fluid for the first two days (Up to this point the pigs still had functioning pancreas). This was because the diabetic state in the pigs was streptozotocin induced after a few days recovery from implantation. The diluting fluid in the reservoir of the device would have equilibrated with smart gel during this time as the gel was formulated in distilled water for that study. It was therefore thought that in these experiments we would formulate the smart gel in diluting fluid from the beginning to avoid this step. Also, because FITC-insulin is formulated in diluting fluid it is beneficial that

the gel is primed for solvent and pH to avoid any pH differences that may cause FITC-insulin to precipitate since it is pH dependent as observed in the stability study (Chapter 4).

The experiment was run continuously for a total of 5940 mins which equates to ~4.125 days. During this period, the gel was subjected to 6 glucose triggers and 5 control triggers lasting for ~ 60 mins each except for the 8th trigger which was overnight. Five of the glucose triggers were of 0.25% w/v concentration corresponding to a 13.9mmol/L which would be a hyperglycaemic state and a typical uncorrected BG after a meal in diabetic patients (Heinemann et al., 2018). In the 8th trigger, the gel was left in 0.1%w/v glucose overnight corresponding to 5.6mmol/L, which is what the gel would be exposed to for the majority of the time in normoglycemia of diabetic patients to check if the device was able to deal with glucose surges like the 13.9mmol/L by outputting more insulin. After this long glucose trigger the gel was triggered with an additional 0.15% (total 0.25%) to show it was still able to allow an increased output of FITC-insulin There was an instant response of the device to each glucose trigger as seen from the increased output of FITC-insulin (green line) but not in the control triggers (blue line). This result emphasised that the smart gel not only responds differently to glucose concentration increases, but also responds specifically to glucose rather than other saccharides. **Figure 5-19** presents the structures of lactose, sucrose, trehalose and β-D+glucose showing the different rotation of the hydroxyl groups at positions C-3, C-4 and C-6 which are most critical for Con A binding of glucose (refer to **Figure 5-17)**

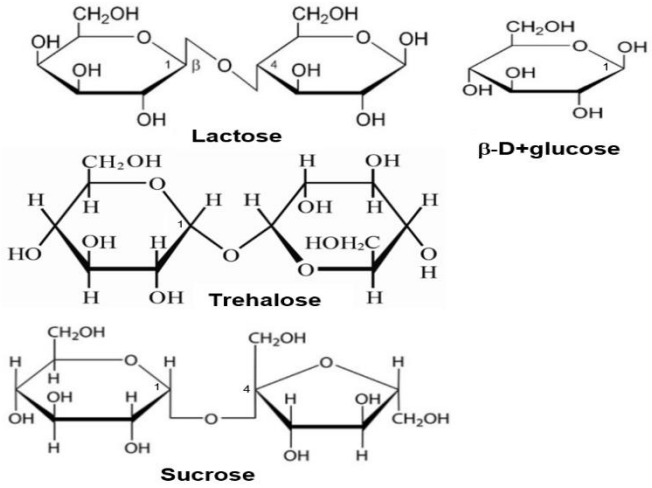

Figure 5-19: Different structures of other saccharides used as control trigger.

The glucose-responsive behaviour of polysaccharide-con A based material has been well-established in various studies of biosensors and drug delivery (Yin et al., 2019; Lin et al., 2019; Cavada et al., 2019), therefore it is anticipated that glucose would be the only relevant sugar for the application of this smart gel in the artificial pancreas. Error! Reference source not found. shows the activation r atios calculated from the gradient of each trigger in relation to baseline gradient where only a basal dose of FITC-insulin is output.

Table 5-2: Activation ratios corresponding to each glucose trigger for the extended experiment over 4 days.

Triggers	Baseline gradient	Trigger gradient	Activation ratio
1st (0.25%w/v glucose)	0.0142	0.1165	8.2
2nd (0.25%w/v glucose)	0.0126	0.1234	9.8
3rd (0.25%w/v glucose)	0.0044	0.0719	16.3
4th (0.25%w/v glucose)	0.0016	0.0868	54.3
5th (0.25%w/v galactose)	0.0068	0.006	0.9
6th (0.25%w/v glucose)	0.0008	0.0938	117.3
7th (0.25%w/v β-D+glucose)	0.0064	0.0043	0.7
8th (0.1%+0.15% w/v glucose)	0.0003	0.0292	97.3
9th (0.25%w/v lactose)	0.005	0.0012	0.2
10th (0.25%w/v trehalose)	0.0005	0.0002	0.4
11th (0.25%w/v sucrose)	0.0002	0.0003	1.5

It is noted that the basal delivery period recorded before each trigger (glucose and control) varied between 2h (daytime) to 15h (overnight) due to time availability, therefore showing different values of baseline gradient. As a result, the activation ratio of FITC-insulin output for each glucose trigger also varied despite having equal glucose concentrations. It is anticipated that the FITC-insulin output (thus the activation ratio) would not be identical for each glucose trigger of the same concentration due to the different driving forces of FITC-insulin diffusion as more FITC-insulin is released from the reservoir after each response. However, it is emphasised that the gel still remains rate-determining in response to glucose present as demonstrated by the release from 6th long glucose trigger (overnight 0.1%w/v glucose and the consequential 0.15 %w/v glucose added).

Figure 5-20 shows another extended experiment similar to the last experiment where an artificial pancreas has been set up and triggered multiple times with glucose and two controls (lactose and galactose). This device was set up in the same way as the previous extended experiment except that the smart gel was from a different batch of crosslinked gel. This experiment serves to confirm that long multi-trigger study shows reproducible results.

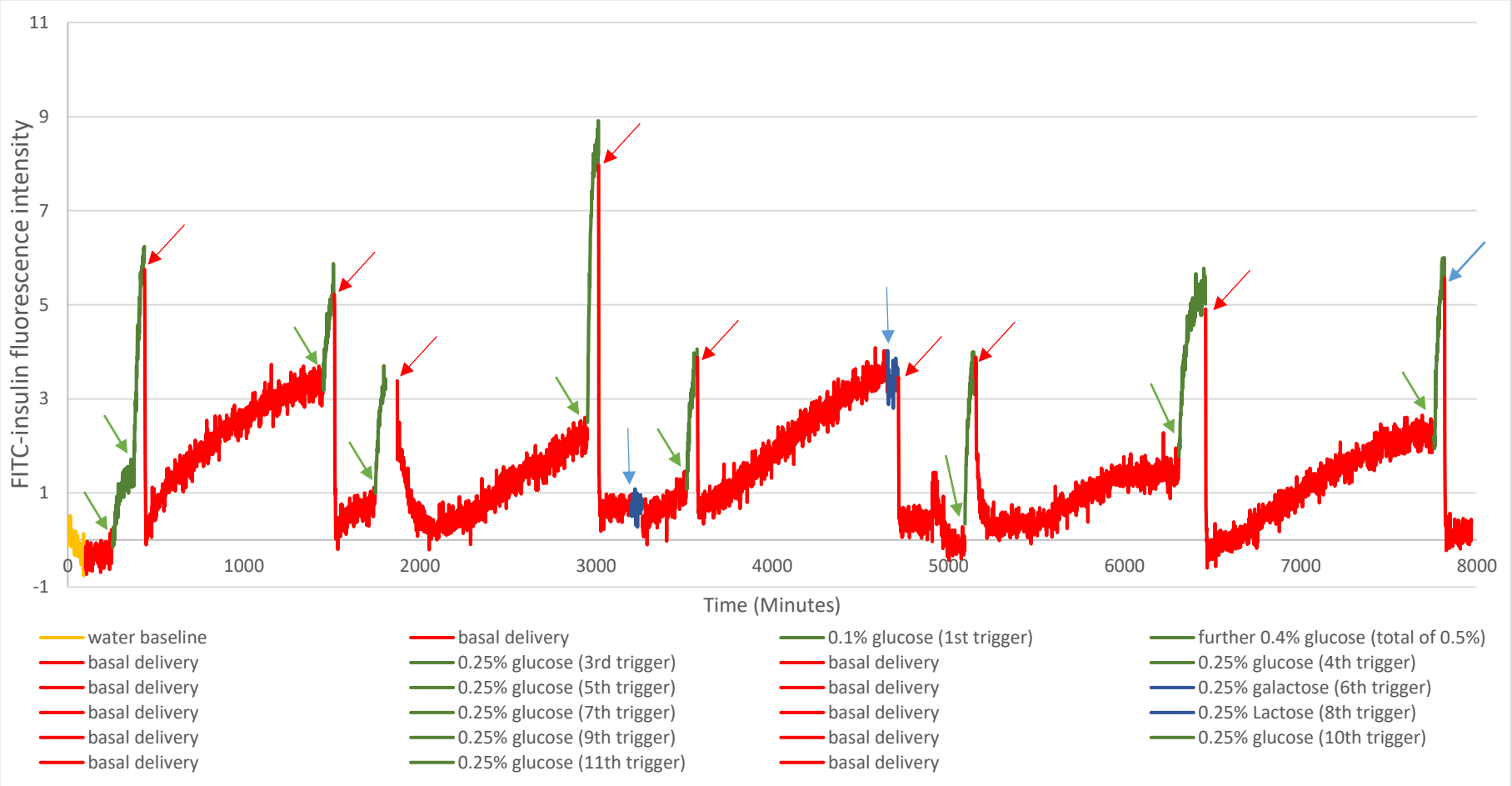

Figure 5-20: FITC-insulin release profiles in response to multiple glucose triggers (8) in green and other inert sugars (galactose, lactose) in blue showing the basal delivery in red and the water baseline in yellow. Noting green arrows indicate glucose trigger points, red arrows show glucose trigger removal points and blue arrows for other inert sugars trigger points.

The initial setting was similar to the previous extended experiment, only that this longer experiment was run continuously for a total of 8000 mins which equates to ~5.556 days. During this period, the gel was subjected to 8 glucose triggers and 2 control triggers lasting for ~ 60 mins each except for the 1st trigger with 0.1% w/v glucose overnight and the consequential 0.4% w/v glucose addition. The overall FITC-insulin output in response to multiple triggers followed similar releasing pattern observed in **Figure 5-18**. The ability of the smart gel to increase FITC-insulin output during 60 mins of glucose trigger and then switch off immediately after glucose removal in both experiments indicated that they are reproducible. The content of FITC-insulin remaining in the reservoir after the termination of the experiment was also analysed by HPLC showing 310 Unit of insulin (basal+bolus) has been released over 5.6 days from the INsmart device that initially hold 500 Unit. This showed an average of 55 Unit per day, which is within the range (35-70 Unit/day) of a typical total daily insulin requirement for an adult (70kg) with T1DM (Li and Hussain, 2020).

Table 5-3 shows the activation ratios calculated from the gradient of each trigger when compared to baseline gradient where only a basal dose of FITC-insulin is output.

Table 5-3: Activation ratios of each trigger for the extended experiment over 5 days.

Triggers	Basal gradient	Trigger gradient	Activation ratio
1st (0.1% w/v glucose)	0.0009	0.0118	13.1
2nd (+0.4% w/v glucose=0.5% in total)	0.0009	0.0742	82.4
3rd (0.25%w/v glucose)	0.0028	0.0321	11.5
4th (0.25%w/v glucose)	0.0024	0.038	15.8
5th (0.25%w/v glucose)	0.0023	0.0792	34.4
6th (0.25%w/v galactose)	0.0009	0.0002	0.007
7th (0.25%w/v glucose)	0.003	0.04	13.7
8th (0.25%w/v lactose)	0.0029	0.002	0.7
9th (0.25%w/v glucose)	0.0015	0.0494	32.9
10th (0.25%w/v glucose)	0.0013	0.0183	14.1
11th (0.25%w/v glucose)	0.0021	0.069	32.9

Apart from the first three triggers, the activation ratios show a distinct pattern of FITC-insulin output for each glucose trigger after the daytime basal delivery (2h) compared to overnight basal delivery (16h). For instance, there was more than twice higher activation ratio (33-34) for glucose triggers right after long basal deliveries

compared to the output (14-15) for the same amount of glucose trigger after the short basal deliveries. The result indicated that the INsmart device is capable of delivering the required daily correct dose rate of insulin in response to changing blood glucose levels. Providing that other factors (gel thickness and surface area, membrane pore size...) affecting the diffusion of FITC-insulin have been addressed accordingly, the overall release pattern of insulin from the device in response to change in glucose level is highly achievable using FITC-insulin However, for further testing on the device performance, glucose triggers corresponding to three mealtimes daily should be applied to further assess the correct dose rate for bolus insulin delivery from the device.

5.4 Chapter summary

Formulating the smart gel in diluting fluid at pH 8 was an important further improvement on the smart gel (D500-MA (DS2.7%) – con A-MA) previously used in the *in-vivo* diabetic pig experiments, which resulted in near normoglycemia over an extended period (Taylor et al., 2016). The performance of the artificial pancreas device from this improved smart gel formulation was assessed *in-vitro* using a custom-built diffusion test rig. The following are the key findings from the *in-vitro* experiments:

- It was highlighted that the gel potency could be lost following prolonged glucose trigger (over 24h) when using large pore membrane (0.2μm). This is highly due to the loss of gel components to both the inside device space and the exterior due to large pore membranes after prolonged liquefying. Different membrane pore sizes have been used to investigate if the gel components could be retained within the membrane inside the device to maintain its potency as the rate determining for insulin release in response to glucose present. 0.025μm and Visking MWCO100kDa pore size membranes showed better device performance and therefore are viable membrane parts for the device. However, Visking is more practical and reliable owing to its ability to provide a definitive cut of point at which only molecules with molecular weight of less than 100kDa i.e. insulin can pass through.

- Improvement in the smart gel formulation and the use of correct membrane pore size have showed promising and reproducible results in the extended experiments where an artificial pancreas has been set up and triggered multiple times with glucose and other dietary saccharides which act as controls to show the specificity of the gel to glucose challenges. These extended experiments have not been set up in any previous *in-vitro* studies of the INsmart device performance. The overall result indicated that the artificial pancreas device is capable of delivering the required daily correct dose rate for insulin in response to changing BG levels.
- Providing that other controllable factors (gel thickness and surface area, membrane pore size...) in the device design affecting the diffusion of insulin have been addressed accordingly, the overall delivery of insulin in response to glucose triggers, thus the performance of the artificial pancreas is highly predictable using FITC-insulin conjugate.

Chapter 6: Synthesis and Identification of Eosin-5-Isothiocyanate-insulin conjugates and Rhodamine B Isothiocyanate-insulin conjugates

6.1 Introduction

Nowadays, the availability of a robust variety of fluorescent derivatives has enabled researchers to tailor conjugations to specific needs for uses in a wide variety of *in-vitro* or *in-vivo* fluorescence-based assays. The addition of a fluorescent label to targeted molecules has improved the detection capabilities that they themselves are unlikely to possess, emphasising the versatility, sensitivity and quantitative characteristics of many fluorescent probes. Moreover, the use of various fluorescent dye also enables the detection of multiple targets spontaneously within the same assays (Warrier and Kharkar, 2014; Fu and Finney, 2018).

In this chapter, the labelling of insulin with EITC and RBITC will be performed using analogous synthesis method for FITC-insulin conjugate. This practical extension is to assess the production of fluorescently labelled insulin using different but related dye molecules. Initially, the structural differences of these dyes will be discussed followed by some highlights in their applications. Similar analytical methods including RP-HPLC and MS will be used to identify and characterise promising conjugates. By using different molecular weight dyes, the selective production of the desired mono-labelled conjugate can also be investigated and optimised for wider application ranges. Furthermore, the different fluorescent characteristics exhibited by these dyes would enable visible differentiation of their conjugate, which could be highly applicable for the detection of multiple targets spontaneously.

6.1.1 EITC

Similar to FITC, EITC is also a derivative of FSC dye, which belongs to the xanthine families that are the most widely utilised fluorophores in biological assay. FSC is a classic for its ability to exhibit high quantum yields and its derivatives are useful fluorescent probes for labelling peptides and proteins to enable visualisation of these biomolecules inside living cells. FSC and eosin share a multi-ring aromatic xanthene

core structure that contributes to their fluorescent character. The presence of the oxygen bridge between the upper phenyl rings of this fused three-ring structure helps create the rigid aromatic system that constricts the molecule to a planar shape, thus conferring luminescent qualities (Hermanson, 2013).

FSC derivatives usually have modifications in their phenyl ring to provide reactivity toward particular functional groups in biomolecules, thus allowing rapid labelling of proteins and nucleic acids. For instance, FITC is also known as an ITC derivative of FSC that has its ring modified at the 5- or 6-carbon positions by the addition of the ITC reactive group. Generally, ITC reacts with nucleophiles such as amines, sulfhydryl, and the phenolate ion of tyrosine side chains. However, the only stable product is with primary amine groups, therefore ITC is almost entirely selective for modifying N-terminal amines in proteins (Holmes and Lantz, 2009; Dufour, Stahl and Baysse, 2015).

Meanwhile, EITC is structurally analogous to FITC, the difference being the addition of four bromine atoms. It is also referred to as the tetrabromo-5-ITC derivative of FSC. Similar to FITC, EITC has two anionic sites, which are the oxyanion at the xanthene skeleton and the carboxyl anion at the phenyl ring in the pH 5 to 10 region (Chiba, Sato and Suzuki, 1987; Lilly et al., 2018) as shown in Error! Reference s ource not found..

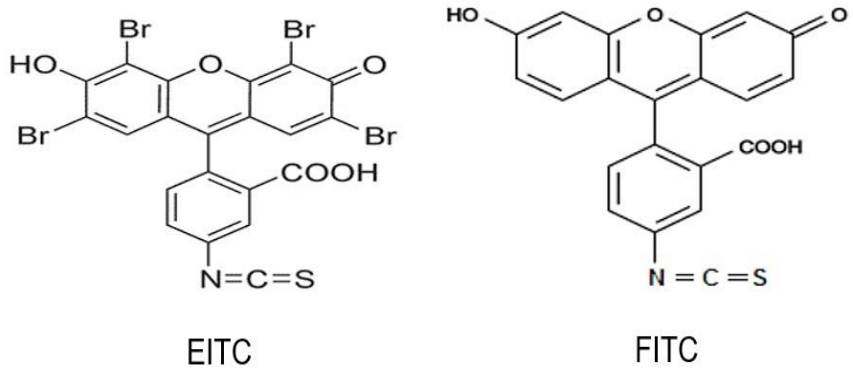

Figure 6-1: Structures of Eosin isothiocyanate (EITC) and Fluorescein isothiocyanate (FITC).

The ITC group at the phenyl ring in both FITC and EITC is a covalent binding site. Owing to the addition of four bromine atoms, EITC has a higher molecular mass of 705Da than 389Da of FITC. The fluorescent properties of FITC include an absorption maximum at about 495 nm and an emission wavelength of 520 nm, whereas EITC

exhibits phosphorescence with an emission maximum at ~680nm. Interestingly, EITC exhibits not only the properties of an organo-bromine compound but also an FSC and an ITC. Although EITC is better known as an excellent photosensitiser rather than selective labelling to amines, its labelling to insulin via the ITC reactive group would be similar to FITC. Other applications for EITC include its use as a reversible inhibitor of the erythrocyte calcium pump and as an effective phosphorescent probe in protein rotational studies (Garland and Moore, 1979; Gatto and Milanick, 1993; Cockrell et al., 2015).

6.1.2 RBITC

RBITC is a derivative of rhodamine dye which also belongs to the xanthine families because it has an aromatic xanthene core structure. The structural difference of RBITC (**Figure 6-2**) compared to FSC is the substitution of nitrogen atoms to replace the oxygen atoms which form part of the alcohol and carbonyl functional groups in FITC and EITC. Each substituted nitrogen atom also links to two ethyl groups, and in the presence of chloride ions at lower pH (in diluted HCl), the nitrogen atom replacing the carbonyl functional groups also exhibits a positive charge (Tripathi, 2013).

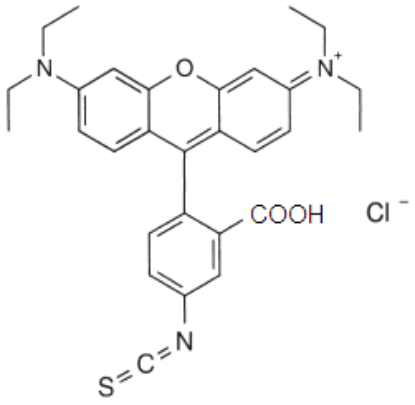

Figure 6-2: Structure of Rhodamine B Isothiocyanate (RBITC).

Although at neutral pH, RBITC exhibits lower quantum yield than FITC in aqueous solutions, the main advantage of RBITC is its better stability to photo-bleaching (Mugica et al., 2016). It has a molecular weight of 536.08 Da and an absorption maximum at 555nm. However, unlike FITC, RBITC exists as an inseparable mixture of 5- and 6-isocyanate isomers.

Rhodamine and its derivatives are popular fluorescent probes for labelling all types of biomolecules such as chitosan, cyclodextrins and bovine serum albumin (BSA). In particular, RBITC-BSA conjugate has been found to be highly specific, sensitive, and stable in vitro, thus is useful as a tracer molecule for vascular permeability and protein transportation studies (Yang et al., 2017). Other delivery studies also used RBITC-insulin conjugates to investigate the *in-vitro* release and *in-vivo* insulin absorption in rats from aminated gelatin microspheres (Wang, Tabata and Morimoto, 2006). However, in this study, a full detail of the synthesis process and the confirmation of RBITC-insulin conjugate remained unclear. It was only highlighted that there is a need to maintain the pH of the reaction using carbonate buffer (pH 9.4) while the synthesis was conducted at 4°C for 10h, and unreacted dye was removed by dialysis. Further synthesis testing is therefore necessary to further confirm the production of RBITC-insulin conjugate. Other applications of RBITC include its use as an anterograde and retrograde marker of retinal neurons in the adult rat (Thanos, Vidal-Sanz and Aguayo, 1987) . It has also been used to label type I collagen (C1) and pathogenic bacterum *Staphylococcus aureus* (Sun et al., 2015; Depke et al., 2014).

These fluorescence probes exhibit distinctively different fluorescence characteristics that are useful for multiple detections spontaneously. Furthermore, by sharing the same amine-reactive group (ITC) it is of interest to investigate if their labelling to insulin would produce fluorescently labelled insulin derivatives at the same target binding site on the insulin molecule.

6.2 Materials and Methods

6.2.1 Chemicals and Reagents

EITC (Pcode: 102159311; CAS: 60520-47-0) and RBITC in mixed isomers (PCode:100245687; CAS: 36877-69-7) were purchased from Sigma-Aldrich (UK). Actrapid® (HI) was manufactured by Novo Nordisk. $NaH_2PO_4.2H_2O$ and $Na_2HPO_4.2H_2O$; HPLC grade acetone, acetonitrile and trifluoroacetic acid were purchased from Fischer Chemicals (Loughborough, UK). EDTA was from Hopkins & Williams. Milli-Q water was used throughout for all HPLC analysis while the use of

distilled water was for other preparation processes such as the making of buffers;0.1M and 1M NaOH and 0.1M and 1M HCl were used for pH adjustment.

6.2.2 Preparation of 0.1M Sodium Phosphate buffer pH 5.4 and pH7.0

1L of phosphate buffer pH5.4 was prepared by dissolving 13.13g of $NaH_2PO_4.2H_2O$ and 1.3g of $Na_2HPO_4.2H_2O$ in ~ 500mL of distilled water. After dissolution, the solution was made up to 1L in a volumetric flask with distilled water and pH was adjusted to 5.4 with 1M NaOH and 1M HCl.

1L of phosphate buffer pH7 was prepared by dissolving 6.6g of $NaH_2PO_4.2H_2O$ and 10.27g $Na_2HPO_4.2H_2O$ in ~ 500mL of distilled water. After dissolution, the solution was made up to 1L in a volumetric flask with distilled water and pH was adjusted to 7.0 with 1M NaOH and 1M HCl.

6.2.3 Synthesis of EITC-insulin conjugate

Preparation of EITC solution

5mg/ml of EITC solution was freshly prepared before the conjugation process by weighing 5mg of EITC on an analytical balance then dissolving it in 1mL of Acetone, and storing in the dark at 4°C until further use.

Synthesis of EITC-insulin conjugate

5ml of Actrapid® solution (equivalent to 17.5mg HI) was measured and transferred into a clean glass jar with the addition of 0.44mg EDTA. For a 2:1 molar ratio of EITC: insulin 0.850mL of 5mg/mL EITC solution was added to the solution mixture then the pH was adjusted to 7 with 0.1M NaOH. The conjugate was left to react in the dark and magnetically stirred for the allocated reaction time of 2h and 18h.

Purification of EITC-insulin conjugate produced

The purification process by GPC followed the same method for FITC as previously described in section 2.2.3

6.2.4 Synthesis of RBITC-insulin conjugate

Preparation of RBITC solution

5mg/ml of RBITC solution was freshly prepared and stored in the dark at 4°C until further use by weighting 5mg of RBITC on an analytical balance then dissolving it in 1mL of methanol.

Synthesis of RBITC-insulin conjugate

For each conjugation, 5ml of Actrapid® solution (equivalent to 17.5mg HI) was measured and transferred into a cleaned glass jar with the addition of 0.44mg EDTA. For a 2:1 molar ratio of RBITC: insulin 0.643 mL of 5mg/mL RBITC stock solution was added to the solution mixture then the pH was adjusted to 7 with 0.1M NaOH. The conjugate was left to react in the dark and magnetically stirred for the allocated reaction time of 2h and 20h.

For a 1:1 molar ratio of RBITC: insulin 0.323mL of 5mg/mL RBITC stock solution was added to the solution mixture then the pH was adjusted to 7 and 8.5 for two separated reaction conditions with 0.1M NaOH. The conjugate was left to react in the dark and magnetically stirred for 24h.

Purification of RBITC-insulin conjugate produced

After reaction for the allocated time, the conjugation of insulin with RBITC was stopped by dropping the pH down to the isoelectric zone of insulin around pH5.3-5.4 to introduce precipitation. The resultant mixture was then centrifuged for five minutes at 2000 rpn, the supernatant was then removed and the pellet washed twice using pH5.4 buffer before dissolving in phosphate buffer pH7 (as prepared in section 7.2.2). The conjugated mixture was then subjected to another cycle of precipitation at pH5.3-5.4 and re-centrifugation to remove any unreacted RBITC further. The re-washed pellet was also dissolved in phosphate buffer pH7 then dialysed for 48h using 1000 Da molecular weight cut off membrane to ensure the final conjugated product was free from unreacted RBITC.

6.2.5 Analytical procedures for the identification of EITC-insulin and RBITC-insulin conjugates produced.

RP-HPLC analyses

The conjugated products from the synthesis of EITC-insulin and RBITC-insulin after purification were analysed using RP-HPLC to identify the species produced and confirm the absence of any unreacted EITC and RBITC. The same HPLC system and setting as detailed in section 2.2.4 was used except for the following chromatographic conditions as shown in **Table 6-1** according to each fluorescently labelled insulin sample.

Table 6-1:Different RP-HPLC conditions used for the detection of fluorescently labelled insulin conjugates with EITC and RBITC.

Samples detected	RP-HPLC methods	Fluorescence detection
EITC-insulin conjugate	0-15 min (85% to 55%A), 15-25 min (55% to 25%A), and 25-32 min (25% to 35%A) where A and B are mobile phases as shown below; **Mobile Phase A**: 0.1% Trifluoroacetic acid (TFA) in Milli-Q water. **Mobile Phase B**: 90% Acetonitrile/ 10% Milli-Q Water/0.1% TFA	the excitation and emission wavelengths were set at 490 and 540nm, respectively to monitor fluorescence data
RITC-insulin conjugate	0–10min (90% to 60% A), 10–25 min (60%to 30% A), and 25–35 min (35% A) where A and B are mobile phases as shown below; **Mobile Phase A**: 20mmol Ammonium acetate in Milli-Q water, pH 6.5 and **Mobile Phase B**: 95% Acetonitrile.	the excitation and emission wavelengths were set at 556 and 576nm, respectively to monitor fluorescence data

MS analyses

MS to determine the mass of the EITC-insulin conjugate produced was performed using a Thermofisher LTQ Orbitrap XL (a high-resolution instrument giving accurate mass measurement over the mass range: m/z 50–2000 or m/z 200–4000) using the nanospray ionisation mode (NSI) at the EPSRC National Mass Spectrometry Facility, Swansea University. The solvent used for sample preparation was a mixture of water/1:1 water: methanol + 0.1% formic acid. Samples were infused into the source of the mass spectrometer using a syringe pump at a flow rate of 10 µL/min. Analyses were performed in the positive ion detection mode. Scans were acquired over a range of m/z 50–2000 or m/z 200–4000.

6.2.6 Fluorescently labelled insulin conjugate storage conditions and lyophilisation process

All fresh labelled conjugates were taken for HPLC analysis immediately after being collected from the GPC. The rest of the products would be protected from light and kept at -20°C for lyophilisation no later than a week after being synthesised. The samples for drying were placed inside a round bottom flask and frozen using liquid nitrogen. The frozen flask was then placed on the Heto drywinner for ~ 48h to ensure no aqueous solution remained in the flask. An orange-pink powder and a dark pink powder remained consisting of the EITC-insulin and RBITC-insulin conjugate respectively which were then stored at 4°C until further uses.

6.3 Results and Discussion

6.3.1 Synthesis and Identification of EITC-insulin conjugate

Before identifying which species of EITC-insulin conjugates are being produced using RP-HPLC system; it was necessary to confirm complete removal of unreacted EITC by GPC as well as the presence of any unlabelled insulin from the final products. The detection of peaks at RT of 26.6min; 27.7min,29.1min, 29.9min and 32.1min illustrated in **Figure 6-3** would indicate that the conjugated products also contain unreacted EITC thus, requiring further purification.

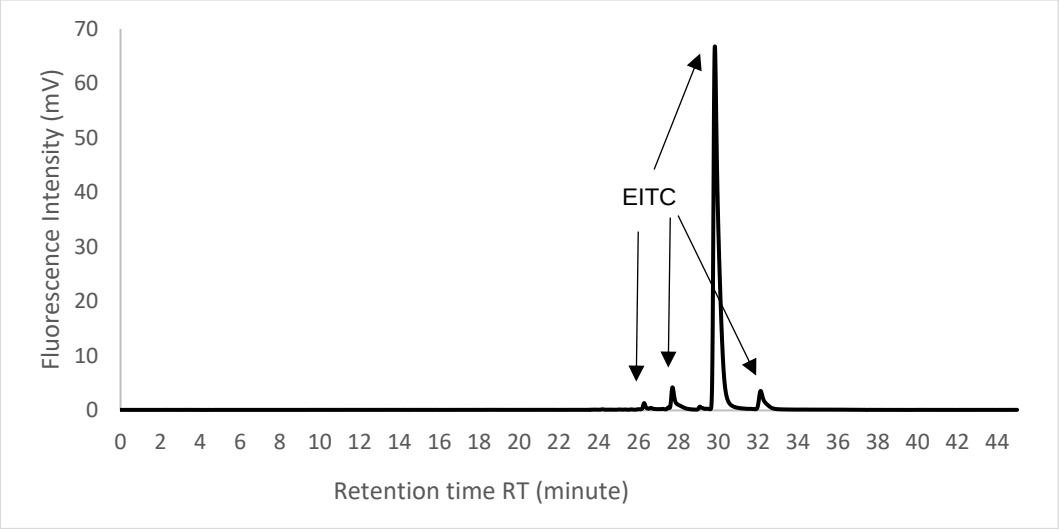

Figure 6-3: RP-HPLC fluorescence chromatogram of EITC in acetone showing peaks at RT 26.6min;27.7min;29.1min;29.9min;32.1min

Figure 6-4. presents the PDA UV chromatogram detected at 215nm for Actrapid® alone to confirm the presence of any unlabelled insulin in the conjugated products.

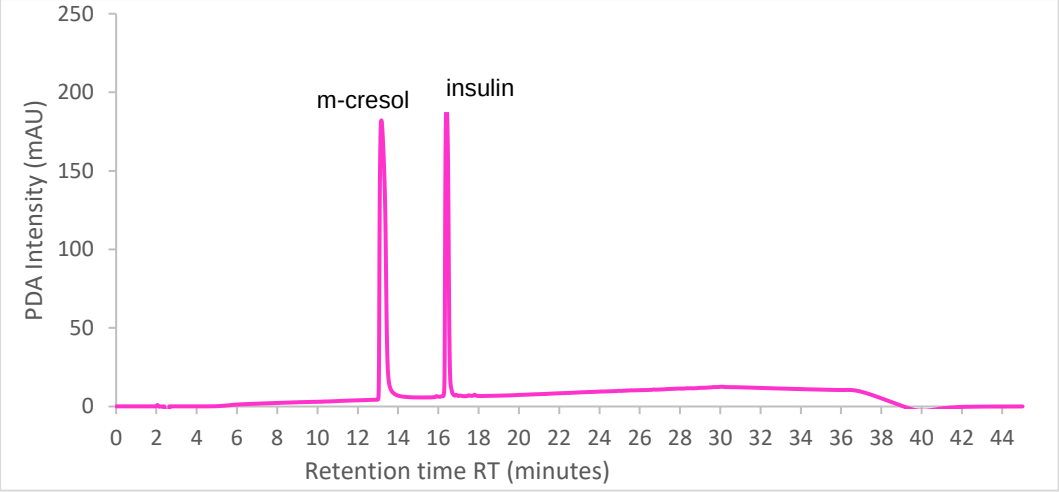

Figure 6-4: PDA UV chromatogram of Actrapid® presenting peaks at RT of 13.2 min for m-cresol and 16.4 min for native human insulin in Actrapid®.

The peaks observed at RT of 13.2 min and 16.4 min are corresponding to m-cresol and native HI respectively, noting the shift in RT compared to the previous chromatogram obtained from FITC-insulin method was due to the different composition of mobile phase used. The PDA peak detected at 16.4 min RT for any conjugated product would indicate the presence of unlabelled insulin.

Figure 6-5 shows the combined fluorescence chromatograms for EITC-insulin conjugated produced at two reaction times of 2h and 18h.

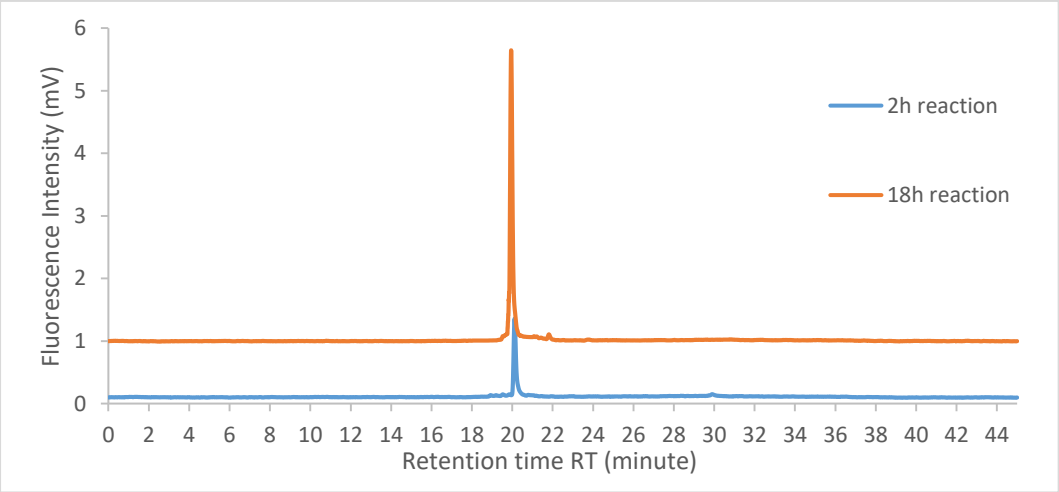

Figure 6-5: Fluorescence chromatogram of EITC-insulin conjugate synthesised after 2h and 18h presenting peak at 20.1minRT for Mono.

The single fluorescence peak detected at a RT of 20.1min indicates that the EITC-insulin conjugate synthesised was mono-labelled. The production of Mono from a 2:1

molar ratio (EITC/insulin) using the same synthesis method as FITC-insulin suggested that their conjugation process is transferable despite the different molecular mass dye. According to their percentage AUP, the fluorescence peak at 20.1minRT obtained from their HPLC analysis yielded 100% Mono. However, the conjugates also contain unlabelled insulin detected from their PDA data at peak 16.4minRT. Furthermore, 18h reaction time showed a considerably lower amount of unlabelled insulin and a higher yield of Mono. Notably, the fluorescence data obtained after 18h reaction also showed a minor peak at 22minRt, which could indicate di-labelled species yet not at relevant concentrations for HPLC detection. Their MS data (**Figure 6-6**) also confirmed unlabelled insulin present (peak at 5807.7 m/z). The observed data $[6511+H]^+$ indicate only Mono present with no observed mass of 7216 for di-labelled species. Notably, the two units shift from the theoretical [6513+H] + for Mono could be due to the reduction of a disulphide bond.

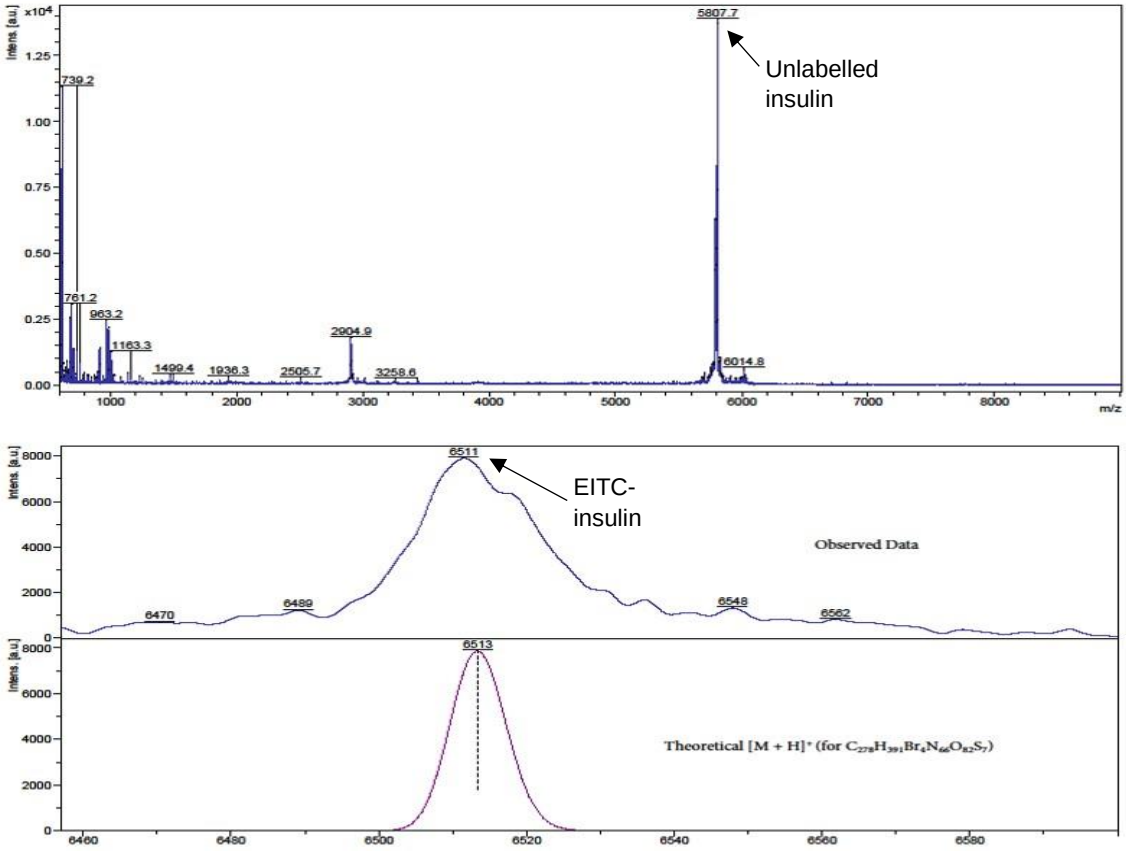

Figure 6-6: Mass spectra for EITC-insulin conjugate synthesised after 18h reaction at pH7 using 2:1 molar ratio (EITC/insulin) showing peak at 5807.7m/z corresponding to unlabelled insulin and the observed mass at $[5611+H]^+$ indicating Mono.

By adapting the same reaction conditions that produce only the desire Mono with FITC, the synthesis of EITC-insulin conjugate also yielded 100% Mono. However, further purification by HPLC may be necessary to remove all unlabelled insulin from the conjugated product. It is possible that the larger molecular mass of EITC (705Da) from the addition of four bromine atoms might limit EITC navigation around the insulin molecule to bind to its target site to some extent. This could be seen from the relatively higher production of FITC-insulin conjugate (refer to section 2.3) than EITC-insulin conjugate from the same amounts of materials used. Optimal reaction conditions may require further adjustment for EITC-insulin synthesis. Binding to the IR sites might also be affected by the large size of EITC and the biological activity of EITC-insulin conjugate also needs further investigation.

6.3.2 Synthesis and Identifications RBITC-insulin conjugate

Figure 6-7 represents the fluorescence chromatogram obtained for the rhodamine analogue in methanol showing multiple peaks of RBITC mixed isomer with the most abundant peaks at RT of 21.8min; 22.8min; 24.1min and 25.3min. The detection of these RBITC peaks in the product of RBITC-insulin conjugate would indicate the presence of unreacted RBITC which requires further purification.

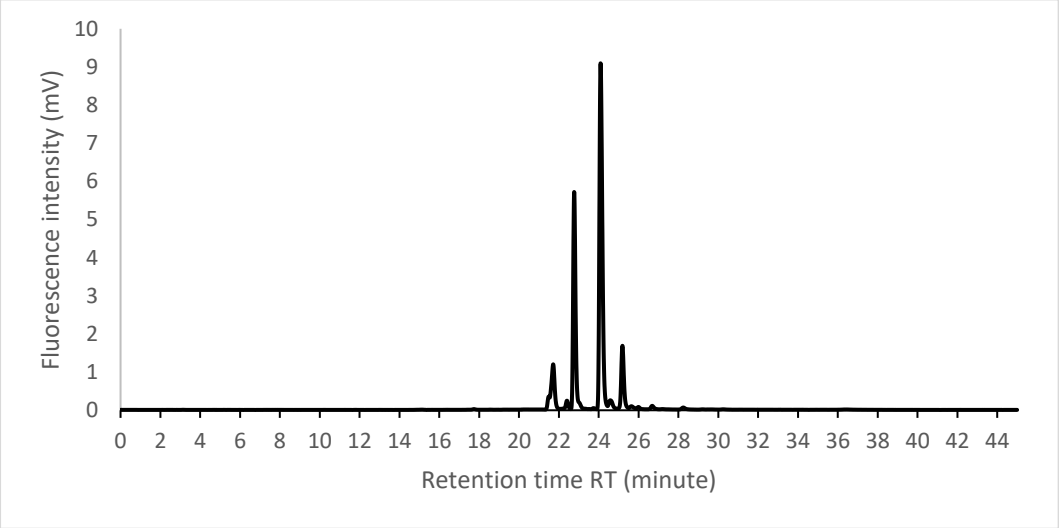

Figure 6-7:RP-HPLC fluorescence chromatogram of RBITC in methanol showing multiple peaks of mixed isomer at RT 21.8min;22.5min;22.8min;24.1min;24.4min;25.3min; 26,8min and 28.3min.

Figure 6-8 shows the PDA UV chromatogram of Actrapid® detected at 215nm for insulin present with peaks observed at RT of 12.3min and 14.5min corresponding to m-cresol and native HI respectively.

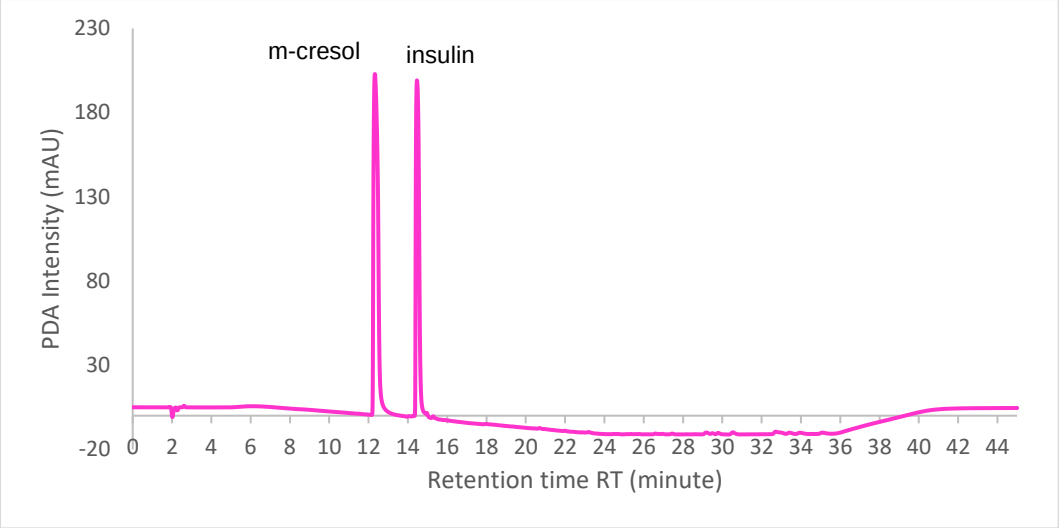

Figure 6-8:PDA UV chromatogram of Actrapid® presenting peaks at RT 12.3 min for m-cresol and 14.5 min for native HI in Actrapid®

The difference in RT of Actrapid® sample compared to previous chromatogram obtained from FITC-insulin method was also due to different mobile phases used. The PDA peak detected at 14.5 min RT in this particular method for any EITC-insulin conjugate would indicate the presence of unlabelled insulin.

Unlike FITC and EITC, purification by GPC resulted in weak recovery and separation of RBITC-insulin conjugate with excess RBITC as the Sephadex column remained pink throughout the GPC process. The strong adsorption of RBITC to the matrix in the Sephadex column could be due to the highly hydrophilic properties of RBITC. Meanwhile, Sephadex is prepared by cross-linking dextran with epichlorohydrin. These highly cross-linked porous particles with covalent bonds provide the matrix with a great hydrophilic environment for RBITC to remain in, thus resulting in poor separation. The initial attempt to separate unreacted RBITC from its conjugated product with insulin using GPC was unsuccessful; therefore, dialysis was another purification method of choice to remove unreacted RBITC.

The synthesis of RBITC-insulin conjugate from 2:1 molar ratio (RBITC/insulin) at pH7 produced a mixture of two conjugated species with considerably higher amount of unlabelled insulin at both short (2h) and long (20h) reaction time compared to labelling with FITC and EITC. Besides, unreacted RBITC was the most abundant product detected by HPLC with a significantly lower yield of RBITC-insulin conjugate (~30.1%AUP) even at long reaction time as showed in **Figure 6-9**.

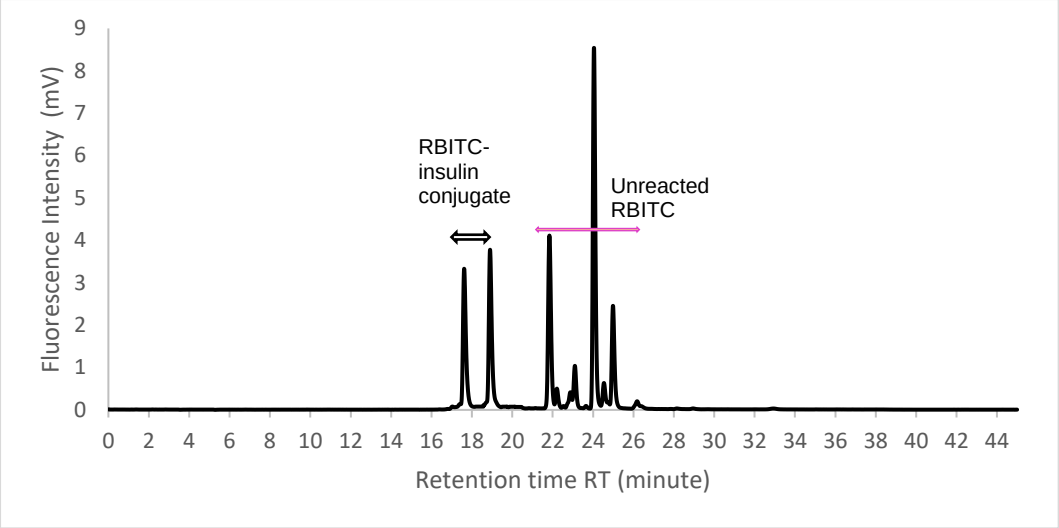

Figure 6-9:RP-HPLC fluorescent chromatogram of RBITC-insulin conjugate synthesised from 2:1 molar ratio at pH7 after 20h reaction, showing two peaks corresponding to RBITC-insulin conjugate indicated by the black double- arrow and multiple peaks corresponding to unreacted RBITC marked by the pink double-arrow.

The observed lower yield of RBITC-Actrapid® conjugate for the same reaction conditions could be due to the overall positive charge of RBITC compared to the neutral FITC and EITC, making it more difficult for labelling to insulin to occur. Besides, the structure of RBITC is considerably different from FITC and EITC despite having the same amine-reactive group (ITC), therefore could also result in significantly less labelling. A further modification to the reaction condition was necessary in order to improve conjugation and minimise having excessively unwanted dye that may require more extended dialysis time for complete removal from the conjugated product. Furthermore, due to the high polarity of RBITC, its complete removal from the conjugated product could also be more challenging. Although there have been several compounds of interest labelled with RBITC such as chitosan and BSA, very little information was available for the removal of the unreacted dye from its conjugated product, or how these conjugates were identified. Meanwhile, the difficulty encountered while removing unreacted RBITC from the conjugated products owing to the high lipophilicity of RBITC was also reported in the synthesis of ATPase labelled with RBITC (Papp, Pikula and Martonosi, 1987).

In order to maximise the synthesis of RBITC-insulin conjugate, a 1:1 molar ratio (RBITC/Actrapid®) for 24h at both pH7 and pH8.5 was employed. The hypothesis was that by minimising the amount of available dye for conjugation and increasing

the reaction time, there would be more conjugate formed with very little unreacted dye left to remove. An increased pH might also facilitate better binding of the ITC reactive group with the primary amine of insulin. Furthermore, the literature also suggests that reaction conditions at pH9-9.5 were usually required for conjugation to aliphatic amine as described in the synthesis of RBITC with BSA, chitosan and insulin (Yang et al., 2017; Ma et al., 2008; Wang, Tabata and Morimoto, 2006). However, due to the high rate of hydrolysis at the high pH>9 and the low yield of conjugation observed with FITC, pH 8.5 was deemed a better choice. **Figure 6-10** presents the combined fluorescence chromatograms for RBITC-insulin conjugate synthesised at pH7 and pH8.5, in which the conjugated peaks were highlighted by the black double-arrow from RT of 17.7min to 20.1min while the pink double-arrow marked peaks from RT 21.8min to 26.4 min corresponding to unreacted RBITC.

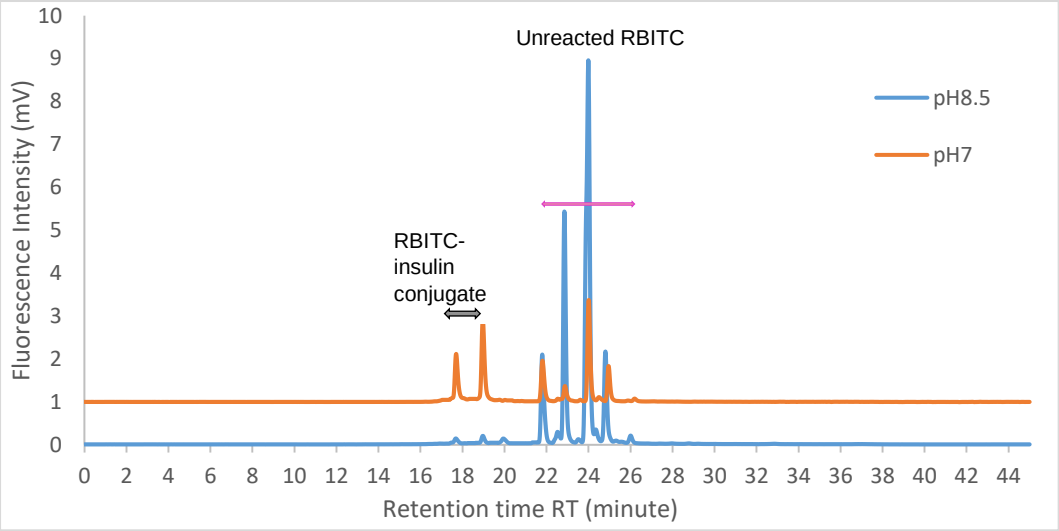

Figure 6-10: Combined fluorescence chromatograms of RBITC-insulin conjugate synthesised after 24h at pH7 (Orange) and pH8.5 (Blue) from 1:1 molar ratio, showing peaks corresponding to RBITC-insulin conjugate indicated by the black double-arrow and multiple peaks corresponding to unreacted RBITC marked by the pink double-arrow.

The chromatographic data show that the increased pH resulted in the production of three conjugated species, although at a significantly lower yield than the synthesis at pH7. This suggests that pH >7 may not be ideal for labelling as similarly observed from the conjugation with FITC (section 2.3. 5). Reducing the amount of RBITC in excess clearly indicated that less unreacted RBITC was present in the conjugated product while still producing ~ 50% RBITC-insulin conjugate at pH7. However, all

conjugates synthesised so far with RBITC always contain unlabelled insulin and a considerably high amount of unreacted dye, none of which is ideal.

In conclusion, despite trying several purification steps of precipitation and dialysis, the final rhodamine conjugation always contains a high amount of unreacted dye. This highlights the extreme difficulty encountered for the removal of unreacted RBITC. Moreover, the extended dialysis that required for over one week despite being kept at 2-8°C might result in deconjugation of RBITC from the insulin molecule, thus causing more release of unreacted dye. Overall, the synthesis of RBITC-insulin conjugate would yield at least two conjugated species regardless of short or long reaction time, and the best reaction conditions (1:1 molar ratio; pH7 and 24h reaction) tried so far would yield 50% RBITC-Actrapid® conjugate owing to the difficulty in the removal of unreacted dye. Although further purification of the two RBITC-insulin conjugates synthesised could be achievable by HPLC, the low yield, high risk and cost of damaging the column suggest that further variation method in the synthesis of RBITC-insulin conjugate is necessary.

6.4. Chapter summary

The present study was designed to investigate the synthesis of fluorescently labelled insulin derivatives with EITC and RBITC via the same binding site as FITC. These fluorescent candidates share the same amine-reactive group (ITC), which would form a strong thiourea linkage with the primary amine of insulin molecules to produce covalently labelled fluorescence conjugate. The ability to synthesis other fluorescently labelled insulin derivatives could be highly advantageous in a wide range of bioanalytical applications, especially for the detection of multiple targets spontaneously as well as in advanced drug delivery.

The main findings are summarised as follow:

- The synthesis of EITC-insulin from 2:1 molar ratio (EITC/insulin) at pH7 after 2 and 18hours also yield 100% singly labelled species with a lower amount of unlabelled insulin observed after 18h reaction. The RP-HPLC method has identified conjugate synthesised was mono-labelled EITC-insulin however the product also contains a trace amount of unlabelled insulin, both of which were further confirmed by MS. Owing to the structural similarity of FITC and EITC, it is highly anticipated that their conjugation with insulin would be equally the

same. However, further purification by HPLC may be necessary to remove all unlabelled insulin from the conjugated product. Alternatively, longer reaction time may be necessary to ensure the complete labelling of all insulin molecule but may also lead to Di production. To conclusively confirm the use of the EITC-insulin conjugate produced inhouse, further studies to investigate its stability profile and biological activity may be necessary.

- Although RBITC also has the same amine-reactive group as FITC and EITC, its labelling to insulin using similar reaction conditions to FITC and EITC showed a significant reduction in the production of RBITC-insulin conjugate. Owing to the availability as mixed isomers, there would always be at least two species of RBITC-insulin conjugate being produced regardless of short or long reaction time. The most distinct structural of RBITC compared to other dyes is its overall positive charge that results in the high polarity of RBITC as well as its conjugation. However, the difficulty encountered when removing unreacted RBITC from its conjugated product in addition to the considerably lower yield suggest that further development in the synthesis method is necessary.

Chapter 7 : Overall conclusions and future work

7.1 Overall conclusions

Diabetes mellitus, commonly known as diabetes, is a lifelong endocrine disorder that is on the rise, affecting 4.7 million people in the UK, of whom 90% have T2DM (Whicher, O'Neill and Holt, 2020; Magliano et al., 2019). It is characterised by a prolonged high blood glucose level that is due to either the pancreas inability to produce insulin (T1DM), or not enough insulin production and the cells of the body not responding properly to the insulin produced (insulin resistant T2DM). Insulin is an essential hormone that regulates glucose homeostasis. T1DM patients are dependent on lifelong administration of exogenous insulin for survival. For patients with T2DM, apart from taking antidiabetic drugs, many of them will eventually require exogenous insulin to maintain good glycaemic control as the disease progresses. Insulin replacement therapy therefore plays an indispensable role in fulfilling the treatment goal for all T1DM patients and many more patients with T2DM. It is expected that from 2018 to 2030, there will be more than 20% increase in insulin users with T2DM (Basu et al., 2019). There have been various approaches into different routes of insulin delivery including oral, intranasal, transdermal and inhaler to reduce the burden of SC insulin administration. Newer generation of insulin analogues serving as insulin bolus and basal to mimic the normal physiological activity of endogenous insulin have also been developed. However, the risk of hypoglycaemia associated with insulin use remains the most challenging obstacle for the evolution of insulin therapy to overcome. One of the most cutting-edge technology is the development of insulin replacement therapy via an artificial pancreas which is capable of determining the insulin requirement in real-time and delivering an accurate insulin dose. In particular, the implantable artificial pancreas developed within our research group is based on a principle that insulin can be delivered through a novel glucose-sensitive smart gel as a function of changing glucose environment.

In advanced drug development and delivery, fluorescence studies have enabled the understanding of many cellular level activities such as biodistribution and metabolism with respect to the complexities imposed by the biological systems. Fluorescently labelled insulin has been widely used to investigate the advanced delivery of insulin

through various routes including oral, intranasal, transdermal and implanted artificial pancreas (Lee, Sang Hoon et al., 2020; Lochhead et al., 2019; Chen, Shyu and Chen, 2018; Jacob, 2015). However, there are very few studies addressing the quality and characterisation of the fluorescent-labelled insulin being used. The main objective of this study was to synthesis a FITC-insulin conjugate that was as biologically active as native insulin. Secondly, the stability and solubility profiles of FITC-insulin in solution was also examined for long-term storage and future application in both *in-vitro* and *in-vivo* testing. Thirdly, the performance and kinetics of insulin delivery from an implantable artificial pancreas with respect to multiple glucose triggers were investigated using FITC-insulin. Lastly, EITC and RBITC were assessed as labelling candidates to produce other fluorescent insulin derivatives. The following conclusions summaries key findings from this current study:

- Fluorescently labelled insulin was chosen as an improved analytical tool to aid detection and quantification of insulin delivery *in-vitro* from an artificial pancreas. This is partly because fluorescence detection offers highly sensitive and specific quantification at significantly lower concentration compared to UV. In addition, UV detection of insulin could be compromised by the protein absorbance from the smart gel components in the device.
- Several reaction times of less than 18h at pH7 using a molar ratio (FITC: insulin) of 2:1 are capable of producing the desired mono-labelled FITC-insulin conjugate. However, the conjugated product always contains some unlabelled insulin. As the reaction time was increased over 20h, no unlabelled insulin was present but 5% undesirable Di was also produced. The quantities switch from Mono to Di productions were observed between 19h to 20h reaction and at pH$\geq$8.
- Adjusting the pH of the reaction close to the pK_a of the individual amino acid FITC binding sites at A1 (pK_a of 8.4); B1(pK_a of 7.1) and B29 (pK_a>9.8) could not selectively target labelling to a specific site. However, reaction at pH≥8 showed some degree of selective labelling at both A1 and B1 positions, resulting in the production of two mono-labelled species and 3% Di even at a short reaction time of 2h. Reaction at pH≥9 resulted in a mixture of FITC-insulin conjugates including Mono, Di and Tri. Meanwhile, only the reactions at pH7 and pH7.5 (using 2:1 molar ratio) have successfully produced only one

mono-labelled species, which was found to be at the B1 position. However, unlabelled insulin was also present due to the short reaction time.

- Further purification of the FITC-Actrapid® conjugate (produced at 2:1 molar ratio, pH 7 after 18h reaction) by HPLC has successfully removed any unlabelled insulin to achieve 100% pure Mono conjugate which was confirmed by RP-HPLC and MS. Fragmentation of this species by electrospray MS has confirmed FITC label at the B1 position.
- The biological activity of four FITC-insulin species (MonoA1, MonoB1, Di and Tri) was assessed in HUVEC and C2C12 skeletal muscle cells via the insulin signalling pathway by examining the levels of pAKT and cell surface GLUT4. These markers were chosen because AKT is a key signal transduction mediator for GLUT4 synthesis and translocation to the cell membrane, thus allow the insulin-dependent transport of glucose into the cell. Different levels of pAKT obtained from Western Blot analysis indicated that the insulin molecule labelled at the B1 position behaved most similarly to native insulin while Di and Tri as well as MonoA1 significantly reduced the insulin signalling pathway by virtue of AKT activation. Other conjugates showed reduced effects from 78% down to 51% of the native insulin activity with MonoA1 and Di respectively. The significantly low activity (0.06%) observed with Tri would indicate a complete loss of biological activity due to the inability of IR to recognise the receptor-binding site of this tri-substituted insulin.
- The preliminary test for GLUT4 translocation in HUVEC could not confirm the presence of GLUT4, indicating that the intracellular uptakes of glucose in HUVEC occur via other types of GLUT which is insulin-independent such as GLUT1. The use of C2C12 skeletal muscle cells to further confirm the biological effect of the most active FITC-insulin conjugate (MonoB1) on GLUT4 translocation by immunofluorescent showed no significant difference in the GLUT4 cell surface level compared to native insulin. This observation suggests that the mono-labelled FITC-insulin conjugate at B1 produced inhouse was as biologically active as native insulin.
- The stability of FITC-insulin in solution can be enhanced for all three temperatures studied (2-8°C,20°C and 37°C) using diluting fluid (0.0005%w/v Zinc Oxide;1.6%w/v glycerol; 0.25%w/v m-cresol; pH7.0), which is typically used in most pharmaceutical insulin preparations. It is advantageous to

formulate FITC-insulin diluting fluid for use in all *in-vivo* and *in-vitro* studies setting at 37°C as this formulation showed stability for up to seven days. FITC-insulin formulated in diluting fluid can last for up to 2 months at ambient temperature and up to 6 months if storing at 2-8°C with protection from light.

- FITC-insulin exhibited the best fluorescence intensity at pH8 but precipitated at pH4-6. However, after a week of storage at room temperature, the fluorescence intensity loss was least observed at pH7 (~5%) while ~ four times this loss was observed at pH 6,8 and 9. Although it is always advisable to use a freshly prepared FITC-insulin solutions, their best working pH range should also be kept within pH7.
- The maximum concentration of lyophilised FITC-insulin that can dissolve in 1mL of diluting fluid (pH7) was at 52mg/mL (equivalent to 1,500Unit/mL) based on the equilibrium solubility test. This concentration is significantly higher than any clinically used insulin preparations maximising at 500Unit/mL. It is reported that the B1 substitution with FITC could improve the solubility of insulin at neutral pH because the unchanged form of human insulin powder would require solubilising in acidic condition at pH2-3.
- It was highlighted in the *in-vitro* diffusion study that the gel components could be lost following prolonged glucose trigger (over 20h) when using large pore size membrane (0.2μm) in the INsmart device. This is highly due to the gel components diffusing out of the device through the membrane pores after prolonged liquifying, thus affecting the gel potency. Different membrane pore sizes have been used to investigate if the gel components could be retained within the membranes inside the device to maintain its potency as the rate determining for insulin release in response to changing glucose. 0.025μm pore size and Visking MWCO100kDa membranes showed better device performance and therefore are viable parts for the device. However, Visking membrane is more practical and reliable owing to its ability to provide a definitive cut of point at which only molecules with molecular weight of less than 100kDa can pass through.
- Improvement in the smart gel formulation prepared in diluting fluid and the use of correct membrane pore size for the INsmart device have showed promising and reproducible results in the extended experiments. These were

where the device has been set up and triggered multiple times with glucose and other dietary saccharides acting as controls to show the specificity of the smart gel to glucose challenges. These extended experiments have not been set up in any previous *in-vitro* studies of the INsmart device performance. The overall result indicated that the INsmart device is capable of delivering the required daily bolus insulin dose which can be boosted in response to multiple increases in glucose levels.

- The synthesis of EITC-insulin using 2:1 molar ratio (EITC/insulin) at pH7 after a reaction time of 18h has successfully produced Mono but unlabelled insulin was also present. The labelling position and biological activity of this conjugate have not yet been confirmed. Although EITC conjugation with insulin using the same synthesis method as FITC-insulin could be reproducible, further removal of unlabelled insulin using HPLC is necessary. Alternatively, longer reaction time may be necessary to ensure complete labelling but may also lead to the production of Di and Tri as observed in the synthesis of FITC-insulin.
- Although RBITC also share the same amine-reactive group as FITC and EITC, its labelling to insulin using the same synthesis method showed a considerably low production of RBITC-insulin conjugate. Owing to the availability as mixed isomers, it is understood that at least two species of RBITC-insulin will be produced regardless of the reaction conditions. The overall positive charge of RBITC that is distinctively different to other dyes might have make it more difficult for ITC reaction with insulin. The resultant positive charge of RBITC-insulin has been found to be advantageous for its transportation across the plasma membrane; however, the difficulty encountered when removing unreacted RBITC from its conjugation in addition to the considerably lower yield suggested that further development in the synthetic method is necessary.

7.2 Future work plans

Keys findings from this research suggest several courses of action for further study as follow:

- It was highly anticipated that during the conjugation with FITC, insulin exists in its hexameric form, thus limiting the binding of FITC molecule to various sites

on the insulin. Further research would be useful to investigate the effect of zinc removal to facilitate insulin monomer formation by using various concentrations of EDTA (higher than 200mM) on the production of FITC-insulin conjugate.

- FITC is partially soluble in water while insulin is insoluble in water however the findings of this study indicated that their conjugation is freely soluble in water at 50mg/mL. Further work is needed to fully understand the implication of FITC labelling to insulin solubility in which the lyophilised FITC-Insulin conjugate can be readily dissolve in water without the need to use acidic diluent as required for powder insulin.
- Most excipients in diluting fluid also help enhance the stability of insulin in pharmaceutical preparations by facilitating the formation of insulin hexamer. The results from the stability study also support the idea that FITC-Insulin conjugate can also be formulated in diluting fluid for better shelf-life protection, especially for experiments carried out at 37°C over an extended period. A greater focus on the stabilising effect of individual excipients in diluting fluid or in different combination could produce interesting findings that account more for the formation of FITC-Insulin monomer, dimer or hexamer.
- EITC can potentially be used as an alternate fluorescent probe for insulin labelling. Further investigation into the biological activity of EITC-Insulin could shed more light on the application of multiple fluorescent labels of insulin for advanced delivery research and biological response of insulin spontaneously.
- The stability enhancement effect of diluting fluid has made it possible to use FITC-Insulin for the *in-vitro* diffusion study at 37°C over an extended period of 7 days to examine the performance and kinetics of insulin delivery from the INsmart device. Further diffusion experiment with multiple glucose triggers at three different time points corresponding to three meals intake per day could also be conducted to confirm the potential use of the INsmart device for future clinical use.

References:

AARTHY, R. et al. (2020) Clinical features, complications and treatment of rarer forms of maturity-onset diabetes of the young (MODY)-A review*. Journal of Diabetes and its Complications,* pp. 107640.

ACERBI, F. et al. (2018) Fluorescein-Guided Surgery for Resection of High-Grade Gliomas: A Multicentric Prospective Phase II Study (FLUOGLIO)*. Clinical Cancer Research: An Official Journal of the American Association for Cancer Research,* 24 (1), pp. 52-61.

ADERINTO, S.O. (2020) Fluorescent, colourimetric, and ratiometric probes based on diverse fluorophore motifs for mercuric (II) ion (Hg2) sensing: highlights from 2011 to 2019*. Chemicke Zvesti,* pp. 1.

AJMERA, I. et al. (2013) The impact of mathematical modeling on the understanding of diabetes and related complications*. CPT: Pharmacometrics & Systems Pharmacology,* 2 (7), pp. 1-14.

AKBARIAN, M. et al. (2018) Chemical modifications of insulin: Finding a compromise between stability and pharmaceutical performance*. International Journal of Pharmaceutics,* 547 (1-2), pp. 450-468.

AKBARIAN, M. et al. (2020) Insulin fibrillation: toward strategies for attenuating the process*. Chemical Communications,* 56 (77), pp. 11354-11373.

AL MAMUN, A. et al. (2020) Hypoxia induces the translocation of glucose transporter 1 to the plasma membrane in vascular endothelial cells*. The Journal of Physiological Sciences,* 70 (1), pp. 1-15.

ALAM, M.W., VEDAEI, S.S. and WAHID, K.A. (2020) A Fluorescence-Based Wireless Capsule Endoscopy System for Detecting Colorectal Cancer*. Cancers,* 12 (4), pp. 890.

ALBISA, A. et al. (2018) Sustainable production of drug-loaded particles by membrane emulsification*. ACS Sustainable Chemistry & Engineering,* 6 (5), pp. 6663-6674.

ALSENZ, J. and KANSY, M. (2007) High throughput solubility measurement in drug discovery and development*. Advanced Drug Delivery Reviews,* 59 (7), pp. 546-567.

AMERICAN DIABETES ASSOCIATION (2020) 2. Classification and Diagnosis of Diabetes: Standards of Medical Care in Diabetes-2020. *Diabetes Care,* 43 (Suppl 1), pp. S14.

AMORIM, R.G. et al. (2019) Kidney Disease in Diabetes Mellitus: Cross-Linking between Hyperglycemia, Redox Imbalance and Inflammation*. Arquivos Brasileiros De Cardiologia,* 112 (5), pp. 577-587.

ANDERS, H. et al. (2018) CKD in diabetes: diabetic kidney disease versus nondiabetic kidney disease*. Nature Reviews Nephrology,* 14 (6), pp. 361-377.

ANDERSSON-HALL, U.K. et al. (2019) Maternal obesity and gestational diabetes mellitus affect body composition through infancy: the PONCH study*. Pediatric Research,* 85 (3), pp. 369-377.

ARONOFF, S.L. et al. (2004) Glucose metabolism and regulation: beyond insulin and glucagon*. Diabetes Spectrum,* 17 (3), pp. 183-190.

ARTASENSI, A. et al. (2020) Type 2 Diabetes Mellitus: A Review of Multi-Target Drugs*. Molecules,* 25 (8), pp. 1987.

ASSMANN, T.S. et al. (2016) Nitric oxide levels in patients with diabetes mellitus: A systematic review and meta-analysis*. Nitric Oxide,* 61, pp. 1-9.

ASTHANA, S. et al. (2019) Insulin adsorption onto zinc oxide nanoparticle mediates conformational rearrangement into amyloid-prone structure with enhanced cytotoxic propensity*. Biochimica Et Biophysica Acta (BBA)-General Subjects,* 1863 (1), pp. 153-166.

BAESHEN, N.A. et al. (2014) Cell factories for insulin production*. Microbial Cell Factories,* 13 (1), pp. 141.

BAHADORAN, Z., MIRMIRAN, P. and GHASEMI, A. (2020) Role of nitric oxide in insulin secretion and glucose metabolism*. Trends in Endocrinology & Metabolism,* 31 (2), pp. 118-130.

BAHARI, M. et al. (2020) Oxidation efficiency of glucose using viologen mediators for glucose fuel cell applications with non-precious anodes*. Applied Energy,* 261, pp. 114382.

BALLY, L. et al. (2017) Day-and-night glycaemic control with closed-loop insulin delivery versus conventional insulin pump therapy in free-living adults with well controlled type 1 diabetes: an open-label, randomised, crossover study*. The Lancet Diabetes & Endocrinology,* 5 (4), pp. 261-270.

BANERJEE, P., MONDAL, S. and BAGCHI, B. (2018) Insulin dimer dissociation in aqueous solution: A computational study of free energy landscape and evolving microscopic structure along the reaction pathway*. The Journal of Chemical Physics,* 149 (11), pp. 114902.

BANKIR, L. et al. (2018) Glucagon revisited: Coordinated actions on the liver and kidney*. Diabetes Research and Clinical Practice,* 146, pp. 119-129.

BASAK, S., SENGUPTA, S. and CHATTOPADHYAY, K. (2019) Understanding biochemical processes in the presence of sub-diffusive behavior of biomolecules in solution and living cells*. Biophysical Reviews,* pp. 1-22.

BASU, A. et al. (2014) Time lag of glucose from intravascular to interstitial compartment in type 1 diabetes. *Journal of Diabetes Science and Technology,* 9 (1), pp. 63-68.

BERCHTOLD, H. and HILGENFELD, R. (1999) Binding of phenol to R6 insulin hexamers. *Peptide Science,* 51 (2), pp. 165-172.

BERENSON, D.F. et al. (2011) Insulin analogs for the treatment of diabetes mellitus: therapeutic applications of protein engineering. *Annals of the New York Academy of Sciences,* 1243, pp. E40.

BERNARD VALEUR and MARIO BERBERAN-SANTOS (2012) Characteristics of Fluorescence Emission. In: *Molecular Fluorescence*: John Wiley & Sons, Ltd, pp. 53-74.

BORDIN, P. et al. (2020) Gestational diabetes mellitus yesterday, today and tomorrow: A 13 year italian cohort study. *Diabetes Research and Clinical Practice,* 167, pp. 108360.

BOUGHTON, C.K. and HOVORKA, R. (2019) Is an artificial pancreas (closed-loop system) for Type 1 diabetes effective?. *Diabetic Medicine,* 36 (3), pp. 279-286.

BRANGE, J. (1994) *Stability of insulin*. 1st ed. Lancaster: Kluwer Academic.

BRANGE, J. et al. (1997) Toward Understanding Insulin Fibrillation. *Journal of Pharmaceutical Sciences,* 86 (5), pp. 517-525.

BRANGE, J. and VOLUND, A. (1999) Insulin analogs with improved pharmacokinetic profiles. *Advanced Drug Delivery Reviews,* 35 (2), pp. 307-335.

BRANNICK, B. and DAGOGO-JACK, S. (2018) Prediabetes and cardiovascular disease: pathophysiology and interventions for prevention and risk reduction. *Endocrinology and Metabolism Clinics,* 47 (1), pp. 33-50.

BRAUN, M. et al. (2010) γ-Aminobutyric acid (GABA) is an autocrine excitatory transmitter in human pancreatic β-cells. *Diabetes,* 59 (7), pp. 1694-1701.

BRAUNWALD, E. (2019) Diabetes, heart failure, and renal dysfunction: The vicious circles. *Progress in Cardiovascular Diseases,* 62 (4), pp. 298-302.

BREWER, P.D. et al. (2014) Insulin-regulated Glut4 Translocation MEMBRANE PROTEIN TRAFFICKING WITH SIX DISTINCTIVE STEPS. *Journal of Biological Chemistry,* 289 (25), pp. 17280-17298.

BRIANT, L. et al. (2016) Glucagon secretion from pancreatic α-cells. *Upsala Journal of Medical Sciences,* 121 (2), pp. 113-119.

BROADWATER, D. et al. (2019) Modulating cellular cytotoxicity and phototoxicity of fluorescent organic salts through counterion pairing. *Scientific Reports,* 9 (1), pp. 1-11.

BRODIN, B., STEFFANSEN, B. and NIELSEN, C.U. (2010) Passive diffusion of drug substances: the concepts of flux and permeability*. Molecular Biopharmaceutics,* pp. 135-152.

BROWN, E.C. et al. (2020) Effects of single bout resistance exercise on glucose levels, insulin action, and cardiovascular risk in type 2 diabetes: A narrative review*. Journal of Diabetes and its Complications,* pp. 107610.

CANIUGUIR, A. et al. (2016) Markers of early endothelial dysfunction in intrauterine growth restriction-derived human umbilical vein endothelial cells revealed by 2D-DIGE and mass spectrometry analyses*. Placenta,* 41, pp. 14-26.

CANTRILL, C. et al. (2020) Fundamental aspects of DMPK optimization of targeted protein degraders*. Drug Discovery Today,*.

CAO, Y. et al. (2017) The use of human umbilical vein endothelial cells (HUVECs) as an in vitro model to assess the toxicity of nanoparticles to endothelium: a review*. Journal of Applied Toxicology,* 37 (12), pp. 1359-1369.

CAPRIFICO, A.E. et al. (2020) Fluorescein isothiocyanate chitosan nanoparticles in oral drug delivery studies*. Trends in Pharmacological Sciences,* 41 (10), pp. 686-689.

CASU, A. et al. (2020) Characteristics of adult-compared to childhood-onset type 1 diabetes*. Diabetic Medicine,*.

CAVADA, B.S. et al. (2019) ConA-like lectins: high similarity proteins as models to study structure/biological activities relationships*. International Journal of Molecular Sciences,* 20 (1), pp. 30.

CHADT, A. and AL-HASANI, H. (2020) Glucose transporters in adipose tissue, liver, and skeletal muscle in metabolic health and disease*. Pflügers Archiv-European Journal of Physiology,* pp. 1-26.

CHAWLA, A., CHAWLA, R. and JAGGI, S. (2016) Microvasular and macrovascular complications in diabetes mellitus: distinct or continuum?*. Indian Journal of Endocrinology and Metabolism,* 20 (4), pp. 546.

CHEN, C., SHYU, V.B. and CHEN, C. (2018) Dissolving microneedle patches for transdermal insulin delivery in diabetic mice: potential for clinical applications*. Materials,* 11 (9), pp. 1625.

CHIBA, T., SATO, Y. and SUZUKI, Y. (1987) Characterization of eosin 5-isothiocyanate binding site in band 3 protein of the human erythrocyte*. Biochimica Et Biophysica Acta (BBA)-Biomembranes,* 897 (1), pp. 14-24.

CHOI, E.S. et al. (2018) Ligustilide attenuates vascular inflammation and activates Nrf2/HO-1 induction and, NO synthesis in HUVECs*. Phytomedicine,* 38, pp. 12-23.

COCKRELL, G.M. et al. (2015) Photoinduced aggregation of a model antibody–drug conjugate*. Molecular Pharmaceutics,* 12 (6), pp. 1784-1797.

COCUCCI, E. et al. (2017) Role of Passive Diffusion, Transporters, and Membrane Trafficking-Mediated Processes in Cellular Drug Transport*. Clinical Pharmacology & Therapeutics,* 101 (1), pp. 121-129.

COUGHLAN, K.A. et al. (2016) PKD1 inhibits AMPKα2 through phosphorylation of serine 491 and impairs insulin signaling in skeletal muscle cells*. Journal of Biological Chemistry,* 291 (11), pp. 5664-5675.

CRIVAT, G. and TARASKA, J.W. (2012) Imaging proteins inside cells with fluorescent tags*. Trends in Biotechnology,* 30 (1), pp. 8-16.

CRYER, P.E. (2012) Minireview: Glucagon in the pathogenesis of hypoglycemia and hyperglycemia in diabetes*. Endocrinology,* 153 (3), pp. 1039-1048.

CUI, C., SHU, W. and LI, P. (2016) Fluorescence in situ hybridization: cell-based genetic diagnostic and research applications*. Frontiers in Cell and Developmental Biology,* 4, pp. 89.

DAHL, A. and KUMAR, S. (2020) Recent Advances in Neonatal Diabetes*. Diabetes, Metabolic Syndrome and Obesity: Targets and Therapy,* 13, pp. 355.

DAHLGREN, D. and LENNERNÄS, H. (2019) Intestinal permeability and drug absorption: Predictive experimental, computational and in vivo approaches*. Pharmaceutics,* 11 (8), pp. 411.

DAI, C. et al. (2013) Pancreatic Islet Vasculature Adapts to Insulin Resistance Through Dilation and Not Angiogenesis*. Diabetes (New York, N.Y.),* 62 (12), pp. 4144-4153.

DAL CANTO, E. et al. (2019) Diabetes as a cardiovascular risk factor: An overview of global trends of macro and micro vascular complications*. European Journal of Preventive Cardiology,* 26 (2_suppl), pp. 25-32.

DANNE, T., HEINEMANN, L. and BOLINDER, J. (2019) New insulins, biosimilars, and insulin therapy*. Diabetes Technology & Therapeutics,* 21 (S1), pp. S-78.

DAS, P.N. et al. (2020) Delay in ATP-dependent calcium inflow may affect insulin secretion from pancreatic beta-cell*. Applied Mathematical Modelling,*.

DASHORA, U. et al. (2016) Clinical use of Humulin R U-500 insulin in the UK: results of the first Association of British Clinical Diabetologists' U-500 audit*. British Journal of Diabetes,* 16 (4), pp. 185-187.

DAVIS, A., KURIAKOSE, J. and CLEMENTS, J.N. (2019) Faster insulin aspart: a new bolus option for diabetes mellitus*. Clinical Pharmacokinetics,* 58 (4), pp. 421-430.

DE BELDER, A.N. and GRANATH, K. (1973) Preparation and properties of fluorescein-labelled dextrans. *Carbohydrate Research,* 30 (2), pp. 375-378.

DE MEYTS, P. (2016) The insulin receptor and its signal transduction network. In: *Endotext [Internet]*: MDText. com, Inc.

DE MEYTS, P. (2015) Insulin/receptor binding: the last piece of the puzzle? What recent progress on the structure of the insulin/receptor complex tells us (or not) about negative cooperativity and activation. *Bioessays,* 37 (4), pp. 389-397.

DE NIGRIS, V. et al. (1) Short-term high glucose exposure impairs insulin signaling in endothelial cells. *Cardiovascular Diabetology,* 14 (1).

DEPAOLI, M.R. et al. (2019) Live cell imaging of signaling and metabolic activities. *Pharmacology & Therapeutics,* 202, pp. 98-119.

DEPKE, M. et al. (2014) Labeling of the pathogenic bacterium Staphylococcus aureus with gold or ferric oxideâ€• core nanoparticles highlights new capabilities for investigation of hostâ€“pathogen interactions. *Cytometry Part A,* 85 (2), pp. 140-150.

DEREWENDA, U. et al. (1989) Phenol stabilizes more helix in a new symmetrical zinc insulin hexamer. *Nature,* 338 (6216), pp. 594.

DI, L., FISH, P.V. and MANO, T. (2012) Bridging solubility between drug discovery and development. *Drug Discovery Today,* 17 (9-10), pp. 486-495.

DIDANGELOS, T. (2011) Insulin: from its discovery to its role in state-of-the-art management of diabetes mellitus Introduction. *Diabetes Research and Clinical Practice,* 93, pp. S1.

DIWANJI, D., THAKER, T. and JURA, N. (2019) More than the sum of the parts: Toward full-length receptor tyrosine kinase structures. *IUBMB Life,* 71 (6), pp. 706-720.

DOLIBA, N.M. et al. (2012) Glucokinase activation repairs defective bioenergetics of islets of Langerhans isolated from type 2 diabetics. *American Journal of Physiology-Endocrinology and Metabolism,* 302 (1), pp. E87-E102.

DONG, X. et al. (2020) Dual fluorescence imaging-guided programmed delivery of doxorubicin and CpG nanoparticles to modulate tumor microenvironment for effective chemo-immunotherapy. *Biomaterials,* 230, pp. 119659.

DONNER, T. (2015) Insulin–pharmacology, therapeutic regimens and principles of intensive insulin therapy. In: *Endotext [Internet]*: MDText. com, Inc.

DONNER, T. and SARKAR, S. (2019a) Insulin–pharmacology, therapeutic regimens, and principles of intensive insulin therapy. In: *Endotext [Internet]*: MDText. com, Inc.

DONNER, T. and SARKAR, S. (2019b) Insulin–pharmacology, therapeutic regimens, and principles of intensive insulin therapy. In: *Endotext [Internet]*: MDText. com, Inc.

DUCA, L.M. et al. (2019) Diabetic ketoacidosis at diagnosis of type 1 diabetes and glycemic control over time: the SEARCH for Diabetes in Youth study. *Pediatric Diabetes,* 20 (2), pp. 172-179.

DUFOUR, V., STAHL, M. and BAYSSE, C. (2015) The antibacterial properties of isothiocyanates. *Microbiology,* 161 (2), pp. 229-243.

DUNN, J. and GRIDER, M.H. (2020) Physiology, Adenosine Triphosphate (ATP).

EGAN, A.M., DOW, M.L. and VELLA, A. (2020) A Review of the Pathophysiology and Management of Diabetes in Pregnancy. In: *Mayo Clinic Proceedings*: Elsevier.

ELHASSAN, S.A.M. et al. (2018) Autophagy and GLUT4: The missing pieces. *Diabetes & Metabolic Syndrome: Clinical Research & Reviews,* 12 (6), pp. 1109-1116.

ELIASCHEWITZ, F.G. and BARRETO, T. (2016) Concepts and clinical use of ultra-long basal insulin. *Diabetology & Metabolic Syndrome,* 8 (1), pp. 2.

ESCUDERO, C.A. et al. (2017) Pro-angiogenic Role of Insulin: From Physiology to Pathology. *Frontiers in Physiology,* 8, pp. 204.

FARMER JR, T.G., EDGAR, T.F. and PEPPAS, N.A. (2008a) The future of open and closed loop insulin delivery systems. *Journal of Pharmacy and Pharmacology,* 60 (1), pp. 1-13.

FARMER JR, T.G., EDGAR, T.F. and PEPPAS, N.A. (2008b) The future of open-and closed-loop insulin delivery systems. *Journal of Pharmacy and Pharmacology,* 60 (1), pp. 1-13.

FEINGOLD, K.R. (2020) Oral and Injectable (Non-insulin) Pharmacological Agents for Type 2 Diabetes. *Endotext [Internet],*.

FERRARA, D. et al. (2019) Impact of different ectopic fat depots on cardiovascular and metabolic diseases. *Journal of Cellular Physiology,* 234 (12), pp. 21630-21641.

FERRI, G. et al. (2019) Insulin secretory granules labelled with phogrin-fluorescent proteins show alterations in size, mobility and responsiveness to glucose stimulation in living β-cells. *Scientific Reports,* 9 (1), pp. 1-12.

FILI, S. et al. (2015) Human insulin polymorphism upon ligand binding and pH variation: the case of 4-ethylresorcinol. *IUCrJ,* 2 (5), pp. 534-544.

FLIER, J.S. (2019) Starvation in the Midst of Plenty: Reflections on the History and Biology of Insulin and Leptin. *Endocrine Reviews,* 40 (1), pp. 1-16.

FORBES, J.M. and COOPER, M.E. (2013) Mechanisms of diabetic complications. *Physiological Reviews,* 93 (1), pp. 137-188.

FOWLER, M.J. (2008) Microvascular and macrovascular complications of diabetes. *Clinical Diabetes,* 26 (2), pp. 77-82.

FU, Y. and FINNEY, N.S. (2018) Small-molecule fluorescent probes and their design. *RSC Advances,* 8 (51), pp. 29051-29061.

FU, Z., R GILBERT, E. and LIU, D. (2013) Regulation of insulin synthesis and secretion and pancreatic Beta-cell dysfunction in diabetes. *Current Diabetes Reviews,* 9 (1), pp. 25-53.

GADGIL, P. et al. (2019) Assessing the utility of in vitro screening tools for predicting bio-performance of oral peptide delivery. *Pharmaceutical Research,* 36 (10), pp. 151.

GAISANO, H., MACDONALD, P.E. and VRANIC, M. (2012) Glucagon secretion and signaling in the development of diabetes. *Frontiers in Physiology,* 3, pp. 349.

GAN, Y. et al. (2020) A novel fluorescent probe for selective imaging of cellular cysteine with large Stokes shift and high quantum yield. *Talanta,* 210, pp. 120612.

GARLAND, P.B. and MOORE, C.H. (1979) Phosphorescence of protein-bound eosin and erythrosin. A possible probe for measurements of slow rotational mobility. *Biochemical Journal,* 183 (3), pp. 561-572.

GAST, K. et al. (2017a) Rapid-acting and human insulins: hexamer dissociation kinetics upon dilution of the pharmaceutical formulation. *Pharmaceutical Research,* 34 (11), pp. 2270-2286.

GAST, K. et al. (2017b) Rapid-acting and human insulins: hexamer dissociation kinetics upon dilution of the pharmaceutical formulation. *Pharmaceutical Research,* 34 (11), pp. 2270-2286.

GATTO, C. and MILANICK, M.A. (1993) Inhibition of the red blood cell calcium pump by eosin and other fluorescein analogues. *American Journal of Physiology-Cell Physiology,* 264 (6), pp. C1577-C1586.

GAUR, R., MISHRA, L. and GUPTA, S.K.S. (2014) Diffusion and transport of molecules in living cells. In: *Modelling and Simulation of Diffusive Processes*: Springer, pp. 27-49.

GERICH, J.E. (1993) Control of glycaemia. *Bailliere's Clinical Endocrinology and Metabolism,* 7 (3), pp. 551-586.

GILON, P. (2020) The Role of α-Cells in Islet Function and Glucose Homeostasis in Health and Type 2 Diabetes. *Journal of Molecular Biology,* 432 (5), pp. 1367-1394.

GIMBRONE JR, M.A. and GARCÍA-CARDEÑA, G. (2016) Endothelial cell dysfunction and the pathobiology of atherosclerosis. *Circulation Research,* 118 (4), pp. 620-636.

GIRI, B. et al. (2018) Chronic hyperglycemia mediated physiological alteration and metabolic distortion leads to organ dysfunction, infection, cancer progression and other pathophysiological consequences: an update on glucose toxicity*. Biomedicine & Pharmacotherapy,* 107, pp. 306-328.

GLOVACI, D., FAN, W. and WONG, N.D. (2019) Epidemiology of diabetes mellitus and cardiovascular disease*. Current Cardiology Reports,* 21 (4), pp. 21.

GONZALEZ, J.T. and BETTS, J.A. (2019a) Dietary sugars, exercise and hepatic carbohydrate metabolism*. Proceedings of the Nutrition Society,* 78 (2), pp. 246-256.

GONZALEZ, J.T. and BETTS, J.A. (2019b) Dietary sugars, exercise and hepatic carbohydrate metabolism*. Proceedings of the Nutrition Society,* 78 (2), pp. 246-256.

GRADEL, A.K.J. et al. (2018a) Factors affecting the absorption of subcutaneously administered insulin: effect on variability*. Journal of Diabetes Research,* 2018.

GRADEL, A.K.J. et al. (2018b) Factors affecting the absorption of subcutaneously administered insulin: effect on variability*. Journal of Diabetes Research,* 2018.

GRAY, S.M., MEIJER, R.I. and BARRETT, E.J. (2014) Insulin regulates brain function, but how does it get there?*. Diabetes,* 63 (12), pp. 3992-3997.

GROMADA, J., CHABOSSEAU, P. and RUTTER, G.A. (2018) The α-cell in diabetes mellitus*. Nature Reviews Endocrinology,* 14 (12), pp. 694-704.

GRUBELNIK, V. et al. (2020) Modelling of dysregulated glucagon secretion in type 2 diabetes by considering mitochondrial alterations in pancreatic α-cells*. Royal Society Open Science,* 7 (1), pp. 191171.

GUILHERME, A. et al. (2019) Molecular pathways linking adipose innervation to insulin action in obesity and diabetes mellitus*. Nature Reviews Endocrinology,* 15 (4), pp. 207-225.

GUO, S. (2014) Insulin Signaling, Resistance, and the Metabolic Syndrome: Insights from Mouse Models to Disease Mechanisms*. The Journal of Endocrinology,* 220 (2), pp. T1-T23.

GYLFE, E. and GILON, P. (2014) Glucose regulation of glucagon secretion*. Diabetes Research and Clinical Practice,* 103 (1), pp. 1-10.

HABEB, A.M. et al. (2020) Diagnosis and management of neonatal diabetes mellitus: A survey of physicians' perceptions and practices in ASPED countries*. Diabetes Research and Clinical Practice,* 159, pp. 107975.

HALL, C., YU, H. and CHOI, E. (2020) Insulin receptor endocytosis in the pathophysiology of insulin resistance*. Experimental & Molecular Medicine,* 52 (6), pp. 911-920.

HATTING, M. et al. (2018) Insulin regulation of gluconeogenesis*. Annals of the New York Academy of Sciences,* 1411 (1), pp. 21.

HAUGLAND, R.P. (2002) *Handbook of fluorescent probes and research products*. 9th ed. Eugene: Molecular Probes.

HEINEMANN, L. et al. (2019) Concentrated insulins: history and critical reappraisal*. Journal of Diabetes,* 11 (4), pp. 292-300.

HEINEMANN, L. et al. (2018) Real-time continuous glucose monitoring in adults with type 1 diabetes and impaired hypoglycaemia awareness or severe hypoglycaemia treated with multiple daily insulin injections (HypoDE): a multicentre, randomised controlled trial*. The Lancet,* 391 (10128), pp. 1367-1377.

HEMMINGSEN, B., RICHTER, B. and METZENDORF, M. (2019) (Ultra-) long-acting insulin analogues for people with type 1 diabetes mellitus*. Cochrane Database of Systematic Reviews,* (12).

HENQUIN, J., DUFRANE, D. and NENQUIN, M. (2006) Nutrient control of insulin secretion in isolated normal human islets*. Diabetes,* 55 (12), pp. 3470-3477.

HENTZ, N.G. et al. (1997) Synthesis and characterization of insulin− fluorescein derivatives for bioanalytical applications*. Analytical Chemistry,* 69 (24), pp. 4994-5000.

HERMANSON, G.T. (2013) Fluorescent probes*. Bioconjugate Techniques (Third Edition) Chapter,* 10 (1), pp. 395-463.

HILGENFELD, R. et al. (2014) The evolution of insulin glargine and its continuing contribution to diabetes care*. Drugs,* 74 (8), pp. 911-927.

HIPPISLEY-COX, J. and COUPLAND, C. (2016) Diabetes treatments and risk of amputation, blindness, severe kidney failure, hyperglycaemia, and hypoglycaemia: open cohort study in primary care*. Bmj,* 352.

HJORTH, C.F. et al. (2016a) Structure, aggregation, and activity of a covalent insulin dimer formed during storage of neutral formulation of human insulin*. Journal of Pharmaceutical Sciences,* 105 (4), pp. 1376-1386.

HJORTH, C.F. et al. (2016b) Structure, aggregation, and activity of a covalent insulin dimer formed during storage of neutral formulation of human insulin*. Journal of Pharmaceutical Sciences,* 105 (4), pp. 1376-1386.

HOLMES, K. and LANTZ, L. (2009) Protein labeling with fluorescent probes. In: WEIMBS THOMAS (ed.)*Essential cytometry methods*. 1st ed. United State: Academic Press, pp. 185-204.

HOME, P.D. (2015) Plasma insulin profiles after subcutaneous injection: how close can we get to physiology in people with diabetes?*. Diabetes, Obesity and Metabolism,* 17 (11), pp. 1011-1020.

HOME, P.D. (2012) The pharmacokinetics and pharmacodynamics of rapid-acting insulin analogues and their clinical consequences. *Diabetes, Obesity and Metabolism,* 14 (9), pp. 780-788.

HOMMA, Y., HIRAGI, S. and FUKUDA, M. (2020) Rab family of small GTPases: An updated view on their regulation and functions. *The FEBS Journal,*.

HOU, J.C. and PESSIN, J.E. (2007) Ins (endocytosis) and outs (exocytosis) of GLUT4 trafficking. *Current Opinion in Cell Biology,* 19 (4), pp. 466-473.

HUA, Q. et al. (1996) Mapping the functional surface of insulin by design: structure and function of a novel A-chain analogue. *Journal of Molecular Biology,* 264 (2), pp. 390-403.

HUANG, X. et al. (2018) The PI3K/AKT pathway in obesity and type 2 diabetes. *International Journal of Biological Sciences,* 14 (11), pp. 1483-1496.

IANNUZZI, C. et al. (2017) Insights into insulin fibril assembly at physiological and acidic pH and related amyloid intrinsic fluorescence. *International Journal of Molecular Sciences,* 18 (12), pp. 2551.

ICHA, J. et al. (2017) Phototoxicity in live fluorescence microscopy, and how to avoid it. *Bioessays,* 39 (8), pp. 1700003.

IKENO, T., NAGANO, T. and HANAOKA, K. (2017) Silicon-substituted Xanthene Dyes and Their Unique Photophysical Properties for Fluorescent Probes. *Chemistry–An Asian Journal,* 12 (13), pp. 1435-1446.

JACOB, D. (2015) *Investigation into reliability and performance of an implantable closed-loop insulin delivery device*, De Montfort University.

JACOB, D. et al. (2019) Insulin Solution Stability and Biocompatibility with Materials Used for an Implantable Insulin Delivery Device Using Reverse Phase HPLC Methods. *Applied Sciences,* 9 (22), pp. 4794.

JACOB, D. et al. (2016) Synthesis and identification of FITC-insulin conjugates produced using human insulin and insulin analogues for biomedical applications. *Journal of Fluorescence,* 26 (2), pp. 617-629.

JALDIN-FINCATI, J.R. et al. (2017) Update on GLUT4 vesicle traffic: a cornerstone of insulin action. *Trends in Endocrinology & Metabolism,* 28 (8), pp. 597-611.

JAMESON, D.M. (2014) *Introduction to fluorescence*. 1st ed. Oxfordshire,UK: Taylor & Francis.

JANUS, A. et al. (2016) Insulin resistance and endothelial dysfunction constitute a common therapeutic target in cardiometabolic disorders. *Mediators of Inflammation,* 2016.

JEAN-BAPTISTE, V.S. et al. (2017) Type 1 diabetes and type 1 interferonopathies: localization of a type 1 common thread of virus infection in the pancreas. *EBioMedicine,* 22, pp. 10-17.

JENSEN, E.C. (2012) Use of fluorescent probes: their effect on cell biology and limitations. *The Anatomical Record: Advances in Integrative Anatomy and Evolutionary Biology,* 295 (12), pp. 2031-2036.

JIANG, H. et al. (2014) Dietary nitrite improves insulin signaling through GLUT4 translocation. *Free Radical Biology and Medicine,* 67, pp. 51-57.

JOHNS, E.C. et al. (2018) Gestational diabetes mellitus: mechanisms, treatment, and complications. *Trends in Endocrinology & Metabolism,* 29 (11), pp. 743-754.

JOHNSON, M. (2019) FITC/Fluorescein. *Materials and Methods,*.

JONES, B. et al. (2018) Control of insulin secretion by GLP-1. *Peptides,* 100, pp. 75-84.

KACHIKIS, A. et al. (2017) Gestational diabetes mellitus: Case definition & guidelines for data collection, analysis, and presentation of immunization safety data. *Vaccine,* 35 (48Part A), pp. 6555.

KAHN, S.E., COOPER, M.E. and DEL PRATO, S. (2014) Pathophysiology and treatment of type 2 diabetes: perspectives on the past, present, and future. *The Lancet,* 383 (9922), pp. 1068-1083.

KARAMITSOS, D.T. (2011) The story of insulin discovery. *Diabetes Research and Clinical Practice,* 93 (1), pp. S2 - S8.

KARBACH, S. et al. (2014) eNOS uncoupling in cardiovascular diseases-the role of oxidative stress and inflammation. *Current Pharmaceutical Design,* 20 (22), pp. 3579-3594.

KARGES, B. et al. (2017) Association of insulin pump therapy vs insulin injection therapy with severe hypoglycemia, ketoacidosis, and glycemic control among children, adolescents, and young adults with type 1 diabetes. *Jama,* 318 (14), pp. 1358-1366.

KE, C. et al. (2020) Development and validation of algorithms to classify type 1 and 2 diabetes according to age at diagnosis using electronic health records. *BMC Medical Research Methodology,* 20 (1), pp. 1-15.

KERRU, N. et al. (2018) Current anti-diabetic agents and their molecular targets: a review. *European Journal of Medicinal Chemistry,* 152, pp. 436-488.

KHAN, B.K., FORTUNATO, L. and LEIKNES, T. (2019) Early biofouling detection using fluorescence-based extracellular enzyme activity. *Enzyme and Microbial Technology,* 120, pp. 43-51.

KHAN, S. et al. (2016) Role of recombinant DNA technology to improve life. *International Journal of Genomics,* 2016.

KHARDORI, R. and GRIFFING, G.T. (2017) Type 1 diabetes mellitus treatment & management. *Available: Type,* 2.

KHARROUBI, A.T. and DARWISH, H.M. (2015) Diabetes mellitus: The epidemic of the century. *World Journal of Diabetes,* 6 (6), pp. 850.

KHORAMI, S.A.H., MOVAHEDI, A. and SOKHINI, A.M.M. (2015) Review Article; PI3K/AKT pathway in modulating glucose homeostasis and its alteration in Diabetes. *Annals of Medical and Biomedical Sciences,* 1 (2).

KHURSHEED, R. et al. (2019) Treatment strategies against diabetes: Success so far and challenges ahead. *European Journal of Pharmacology,* 862, pp. 172625.

KIRIYAMA, Y. and NOCHI, H. (2018) Role and cytotoxicity of amylin and protection of pancreatic islet β-cells from amylin cytotoxicity. *Cells,* 7 (8), pp. 95.

KLIP, A., MCGRAW, T.E. and JAMES, D.E. (2019) Thirty sweet years of GLUT4. *Journal of Biological Chemistry,* 294 (30), pp. 11369-11381.

KNUDSEN, J.R. et al. (2020) Prior exercise in humans redistributes intramuscular GLUT4 and enhances insulin-stimulated sarcolemmal and endosomal GLUT4 translocation. *Molecular Metabolism,* pp. 100998.

KOBAYASHI, H. et al. (2009) New strategies for fluorescent probe design in medical diagnostic imaging. *Chemical Reviews,* 110 (5), pp. 2620-2640.

KOEPSELL, H. (2020) Glucose transporters in brain in health and disease. *Pflügers Archiv-European Journal of Physiology,* pp. 1-45.

KOLB, H. et al. (2020) Insulin: too much of a good thing is bad. *BMC Medicine,* 18 (1), pp. 1-12.

KOLLURU, G.K., BIR, S.C. and KEVIL, C.G. (2012) Endothelial dysfunction and diabetes: effects on angiogenesis, vascular remodeling, and wound healing. *International Journal of Vascular Medicine,* 2012.

KOSINOVÁ, L. et al. (2014) Insight into the structural and biological relevance of the T/R transition of the N-terminus of the B-chain in human insulin. *Biochemistry,* 53 (21), pp. 3392-3402.

KOVATCHEV, B. (2019) A century of diabetes technology: signals, models, and artificial pancreas control. *Trends in Endocrinology & Metabolism,* 30 (7), pp. 432-444.

KREIDER, K.E. (2018) Updates in the management of diabetic ketoacidosis. *The Journal for Nurse Practitioners,* 14 (8), pp. 591-597.

KURTZHALS, P., LARSEN, C. and JOHANSEN, M. (1989) High-performance size-exclusion chromatographic procedure for the determination of fluoresceinyl isothiocyanate dextrans of various molecular masses in biological media. *Journal of Chromatography B: Biomedical Sciences and Applications,* 491, pp. 117-127.

LAKOWICZ, J.R. (2013) *Principles of fluorescence spectroscopy*. 2nd ed. Berlin: Springer science & business media.

LANDREH, M. et al. (2012) Insulin solubility transitions by pH-dependent interactions with proinsulin C-peptide. *The FEBS Journal,* 279 (24), pp. 4589-4597.

LAREDO-AGUILERA, J.A. et al. (2020) Physical Activity Programs during Pregnancy Are Effective for the Control of Gestational Diabetes Mellitus. *International Journal of Environmental Research and Public Health,* 17 (17), pp. 6151.

LAVAUD, J. et al. (2020) Noninvasive monitoring of liver metastasis development via combined multispectral photoacoustic imaging and fluorescence diffuse optical tomography. *International Journal of Biological Sciences,* 16 (9), pp. 1616.

LAW, N.C., WHITE, M.F. and HUNZICKER-DUNN, M.E. (2016) G protein-coupled receptors (GPCRs) that signal via protein kinase A (PKA) cross-talk at insulin receptor substrate 1 (IRS1) to activate the phosphatidylinositol 3-kinase (PI3K)/AKT pathway. *Journal of Biological Chemistry,* 291 (53), pp. 27160-27169.

LEE, S.H. et al. (2020) Enhanced oral delivery of insulin via the colon-targeted nanocomposite system of organoclay/glycol chitosan/Eudragit® S100. *Journal of Nanobiotechnology,* 18 (1), pp. 1-10.

LEE, S.H. et al. (2019) A bright blue fluorescent dextran for two-photon in vivo imaging of blood vessels. *Bioorganic Chemistry,* 89, pp. 103019.

LEPORE, D. et al. (2018) Follow-up to Age 4 Years of Treatment of Type 1 Retinopathy of Prematurity Intravitreal Bevacizumab Injection versus Laser: Fluorescein Angiographic Findings. *Ophthalmology,* 125 (2), pp. 218-226.

LI, A. and HUSSAIN, S. (2020) Diabetes technologies–what the general physician needs to know. *Clinical Medicine,* 20 (5), pp. 469.

LI, C., TEBO, A.G. and GAUTIER, A. (2017) Fluorogenic labeling strategies for biological imaging. *International Journal of Molecular Sciences,* 18 (7), pp. 1473.

LI, J. et al. (2020) LC-MS analysis of Myrica rubra extract and its hypotensive effects via the inhibition of GLUT 1 and activation of the NO/Akt/eNOS signaling pathway. *RSC Advances,* 10 (9), pp. 5371-5384.

LI, M. et al. (2020) Rhodamine B-based fluorescent probes for molecular mechanism study of the anti-influenza activity of pentacyclic triterpenes. *European Journal of Medicinal Chemistry,* 205, pp. 112664.

LI, S. et al. (2020) Different intracellular signalling sensitivity and cell behaviour of porcine insulin with aging. *Peptides,* 127, pp. 170278.

LI, Y. et al. (2020) Maternal age and the risk of gestational diabetes mellitus: a systematic review and meta-analysis of over 120 million participants. *Diabetes Research and Clinical Practice,* 162, pp. 108044.

LILLY, J.L. et al. (2018) Comparison of eosin and fluorescein conjugates for the photoinitiation of cell-compatible polymer coatings. *PloS One,* 13 (1), pp. e0190880.

LIMPOUCHOVÁ, Z. and PROCHÁZKA, K. (2016) Theoretical principles of fluorescence spectroscopy. In: *Fluorescence Studies of Polymer Containing Systems*: Springer, pp. 91-149.

LIN, K. et al. (2019) Glucose-sensitive hydrogels from covalently modified carboxylated pullulan and concanavalin A for smart controlled release of insulin. *Reactive and Functional Polymers,* 139, pp. 112-119.

LIU, F. et al. (2009) Development of a novel GLUT4 translocation assay for identifying potential novel therapeutic targets for insulin sensitization. *Biochemical Journal,* 418 (2), pp. 413-420.

LIU, M. et al. (2018) Biosynthesis, structure, and folding of the insulin precursor protein. *Diabetes, Obesity and Metabolism,* 20, pp. 28-50.

LIU, M. et al. (2014) Proinsulin entry and transit through the endoplasmic reticulum in pancreatic beta cells. In: *Vitamins & Hormones*: Elsevier, pp. 35-62.

LOCHHEAD, J.J. et al. (2019) Distribution of insulin in trigeminal nerve and brain after intranasal administration. *Scientific Reports,* 9 (1), pp. 1-9.

LONG, W. and CHEESEMAN, C.I. (2015) Structure of, and functional insight into the GLUT family of membrane transporters. *Cell Health and Cytoskeleton,* 7, pp. 167.

LONGO, M. et al. (2019) Adipose Tissue Dysfunction as Determinant of Obesity-Associated Metabolic Complications. *International Journal of Molecular Sciences,* 20 (9).

LOPES-NUNES, J. et al. (2020) Biological studies of an ICG-tagged aptamer as drug delivery system for malignant melanoma. *European Journal of Pharmaceutics and Biopharmaceutics,* 154, pp. 228-235.

LOTFY, M. et al. (2017a) Chronic complications of diabetes mellitus: a mini review. *Current Diabetes Reviews,* 13 (1), pp. 3-10.

LOTFY, M. et al. (2017b) Chronic complications of diabetes mellitus: a mini review. *Current Diabetes Reviews,* 13 (1), pp. 3-10.

LUCIER, J. and WEINSTOCK, R.S. (2020) Diabetes mellitus type 1. *StatPearls [Internet],*.

LUSE, M.A. et al. (2020) Cellular and Functional Effects of Insulin Based Therapies and Exercise on Endothelium. *Current Pharmaceutical Design,* 26 (30), pp. 3760-3767.

LV, X. et al. (2020) Improving the quantum yields of fluorophores by inhibiting twisted intramolecular charge transfer using electron-withdrawing group-functionalized piperidine auxochromes. *Chemical Communications,* 56 (5), pp. 715-718.

MABROUK, M. et al. (2019) Nanoparticle-and nanoporous-membrane-mediated delivery of therapeutics. *Pharmaceutics,* 11 (6), pp. 294.

MADDALONI, E. et al. (2020) Adult-onset autoimmune diabetes in 2020: An update. *Maturitas,*.

MADHUNAPANTULA, S.V., MOSCA, P.J. and ROBERTSON, G.P. (2011) The Akt signaling pathway: an emerging therapeutic target in malignant melanoma. *Cancer Biology & Therapy,* 12 (12), pp. 1032-1049.

MAENO, Y. et al. (2012) Inhibition of insulin signaling in endothelial cells by protein kinase C-induced phosphorylation of p85 subunit of phosphatidylinositol 3-kinase (PI3K). *Journal of Biological Chemistry,* 287 (7), pp. 4518-4530.

MAGBOOL, F.A. et al. (2017) Formulation approches to enhance drug solubility_brief overview. *Eur J Pharm Med Res,* 5 (2), pp. 94-100.

MAGLIANO, D.J. et al. (2019) Trends in incidence of total or type 2 diabetes: systematic review. *Bmj,* 366, pp. l5003.

MAIKAWA, C.L. et al. (2020) Stable monomeric insulin formulations enabled by supramolecular PEGylation of insulin analogues. *Advanced Therapeutics,* 3 (1), pp. 1900094.

MAMMI, C. et al. (2011) Sildenafil Reduces Insulin-Resistance in Human Endothelial Cells. *PloS One,* 6 (1), pp. e14542.

MAN, F., GAWNE, P.J. and DE ROSALES, R.T. (2019) Nuclear imaging of liposomal drug delivery systems: A critical review of radiolabelling methods and applications in nanomedicine. *Advanced Drug Delivery Reviews,* 143, pp. 134-160.

MANIRUZZAMAN, M. et al. (2017) Comparative approaches for classification of diabetes mellitus data: Machine learning paradigm. *Computer Methods and Programs in Biomedicine,* 152, pp. 23-34.

MANNING, M.C. et al. (2010) Stability of protein pharmaceuticals: an update. *Pharmaceutical Research,* 27 (4), pp. 544-575.

MARCHETTI, P. et al. (2020) A direct look at the dysfunction and pathology of the β cells in human type 2 diabetes.

MARTY, N., DALLAPORTA, M. and THORENS, B. (2007) Brain glucose sensing, counterregulation, and energy homeostasis. *Physiology,* 22 (4), pp. 241-251.

MATHIEU, C., GILLARD, P. and BENHALIMA, K. (2017) Insulin analogues in type 1 diabetes mellitus: getting better all the time. *Nature Reviews Endocrinology,* 13 (7), pp. 385-399.

MATTEUCCI, E. et al. (2015) Insulin administration: present strategies and future directions for a noninvasive (possibly more physiological) delivery. *Drug Design, Development and Therapy,* 9, pp. 3109.

MAURICIO, D., ALONSO, N. and GRATACÒS, M. (2020) Chronic diabetes complications: the need to move beyond classical concepts. *Trends in Endocrinology & Metabolism,* 31 (4), pp. 287-295.

MCKAY, T.B., PRIYADARSINI, S. and KARAMICHOS, D. (2019) Mechanisms of collagen crosslinking in diabetes and keratoconus. *Cells,* 8 (10), pp. 1239.

MCPHERSON, A. and GAVIRA, J.A. (2014) Introduction to protein crystallization. *Acta Crystallographica Section F: Structural Biology Communications,* 70 (1), pp. 2-20.

MÉNARD, V., SOTUNDE, O.F. and WEILER, H.A. (2020) Ethnicity and Immigration Status as Risk Factors for Gestational Diabetes Mellitus, Anemia and Pregnancy Outcomes Among Food Insecure Women Attending the Montreal Diet Dispensary Program. *Canadian Journal of Diabetes,* 44 (2), pp. 139-145. e1.

MENTING, J.G. et al. (2013) How insulin engages its primary binding site on the insulin receptor. *Nature,* 493 (7431), pp. 241.

MODI, K.D. et al. (2019) Clinical challenges with excipients in insulin formulations and role of concentrated insulin. *International Journal of Basic & Clinical Pharmacology,* 8 (4), pp. 821-826.

MÖLLER, M.N. et al. (2019) Diffusion and transport of reactive species across cell membranes. In: *Bioactive Lipids in Health and Disease*: Springer, pp. 3-19.

MOON, J.S. and WON, K.C. (2015) Pancreatic α-Cell Dysfunction in Type 2 Diabetes: Old Kids on the Block. *Diabetes & Metabolism Journal,* 39 (1), pp. 1-9.

MORSE, Z.J. et al. (2020) Virus-mediated dysbiosis alters immune populations to promote type 1 diabetes onset. *The Journal of Immunology,*.

MUECKLER, M. and THORENS, B. (2013) The SLC2 (GLUT) family of membrane transporters. *Molecular Aspects of Medicine,* 34 (2-3), pp. 121-138.

MUGICA, L.C. et al. (2016) Surface functionalization of silica particles for their efficient fluorescence and stereo selective modification. *Colloids and Surfaces A: Physicochemical and Engineering Aspects,* 500 (1), pp. 79-87.

MUKHERJEE, S. et al. (2018a) What gives an insulin hexamer its unique shape and stability? Role of ten confined water molecules. *The Journal of Physical Chemistry B,* 122 (5), pp. 1631-1637.

MUKHERJEE, S. et al. (2018b) What gives an insulin hexamer its unique shape and stability? Role of ten confined water molecules. *The Journal of Physical Chemistry B,* 122 (5), pp. 1631-1637.

MUNIYAPPA, R. et al. (2020) Endothelial dysfunction due to selective insulin resistance in vascular endothelium: insights from mechanistic modeling. *American Journal of Physiology-Endocrinology and Metabolism,* 319 (3), pp. E629-E646.

MURPHY, R.M., WATT, M.J. and FEBBRAIO, M.A. (2020) Metabolic communication during exercise. *Nature Metabolism,* pp. 1-12.

NAGEL, N. et al. (2019) The quaternary structure of insulin glargine and glulisine under formulation conditions. *Biophysical Chemistry,* 253, pp. 106226.

NATARAJAN, R., NORTHROP, N. and YAMAMOTO, B. (2017) Fluorescein Isothiocyanate (FITC)-Dextran Extravasation as a Measure of Blood-Brain Barrier Permeability. *Current Protocols in Neuroscience,* 79 (1), pp. 9.58. 1-9.58. 15.

NATH, A. et al. (2018) Physiological models and control for type 1 diabetes mellitus: a brief review. *IFAC-PapersOnLine,* 51 (1), pp. 289-294.

NAVALE, A.M. and PARANJAPE, A.N. (2016) Glucose transporters: physiological and pathological roles. *Biophysical Reviews,* 8 (1), pp. 5-9.

NEUPANE, S. and EVANS, M.L. (2019) Modern strategies for management of glycaemia in type 1 diabetes. *Medicine,* 47 (1), pp. 28-31.

NEW, D.C. et al. (2007) G protein-coupled receptor-induced Akt activity in cellular proliferation and apoptosis. *The FEBS Journal,* 274 (23), pp. 6025-6036.

NICE (2015a) *Diabetes in pregnancy: management from preconception to the postnatal period*. [Online] [Accessed 30/09/2020].

NICE (2015b) Type 2 diabetes in adults: management. *NICE Guidelines [NG28] Published December,*.

NICHOLLS, D.G. (2016) The pancreatic β-cell: a bioenergetic perspective. *Physiological Reviews,*.

NISHI, K. et al. (2015) Fluorescence-based bioassays for the detection and evaluation of food materials. *Sensors,* 15 (10), pp. 25831-25867.

NITULESCU, G.M. et al. (2018) The Akt pathway in oncology therapy and beyond. *International Journal of Oncology,* 53 (6), pp. 2319-2331.

NOORDEN, B., KNOPP, J.L. and CHASE, J.G. (2019) A subcutaneous insulin pharmacokinetic model for insulin Detemir. *Computer Methods and Programs in Biomedicine,* 178, pp. 1-9.

NORRIS, J.M., JOHNSON, R.K. and STENE, L.C. (2020) Type 1 diabetes—early life origins and changing epidemiology. *The Lancet Diabetes & Endocrinology,* 8 (3), pp. 226-238.

NWANERI, C. (2015) Diabetes mellitus: A complete ancient and modern historical perspective.

O'BRIEN, C.M. et al. (2020) Regulation of Metabolic Homeostasis in Cell Culture Bioprocesses. *Trends in Biotechnology,*.

OHNO, Y. et al. (2019) Investigation of factors that cause insulin precipitation and/or amyloid formation in insulin formulations. *Journal of Pharmaceutical Health Care and Sciences,* 5 (1), pp. 1-11.

OLIVEIRA, S.C. et al. (2020) Maturity-onset diabetes of the young: From a molecular basis perspective toward the clinical phenotype and proper management. *Endocrinologia, Diabetes Y Nutricion,* 67 (2), pp. 137-147.

OLOKOBA, A.B., OBATERU, O.A. and OLOKOBA, L.B. (2012) Type 2 diabetes mellitus: a review of current trends. *Oman Medical Journal,* 27 (4), pp. 269.

ORMAZABAL, V. et al. (2018) Association between insulin resistance and the development of cardiovascular disease. *Cardiovascular Diabetology,* 17 (1), pp. 122.

OWENS, D.R. and BOLLI, G.B. (2020) The continuing quest for better subcutaneously administered prandial insulins: a review of recent developments and potential clinical implications. *Diabetes, Obesity and Metabolism,* 22 (5), pp. 743-754.

PADHI, S., NAYAK, A.K. and BEHERA, A. (2020a) Type II diabetes mellitus: a review on recent drug based therapeutics. *Biomedicine & Pharmacotherapy,* 131, pp. 110708.

PADHI, S., NAYAK, A.K. and BEHERA, A. (2020b) Type II diabetes mellitus: a review on recent drug based therapeutics. *Biomedicine & Pharmacotherapy,* 131, pp. 110708.

PALIVEC, V. et al. (2017) Computational and structural evidence for neurotransmitter-mediated modulation of the oligomeric states of human insulin in storage granules. *Journal of Biological Chemistry,* 292 (20), pp. 8342-8355.

PALMIERI, L.C. et al. (2013) A T3R3 hexamer of the human insulin variant B28Asp. *Biophysical Chemistry,* 173, pp. 1-7.

PANDEY, M. et al. (2018) Recent Updates on Novel Approaches in Insulin Drug Delivery: A Review of Challenges and Pharmaceutical Implications*. Current Drug Targets,* 19 (15), pp. 1782-1800.

PAPATHEODOROU, K. et al. (2018) Complications of diabetes 2017*. Journal of Diabetes Research,* 2018.

PARK, S. et al. (2019) Recent advances in the pathogenesis of microvascular complications in diabetes*. Archives of Pharmacal Research,* 42 (3), pp. 252-262.

PATEL, B.M. and GOYAL, R.K. (2019) Liver and insulin resistance: New wine in old bottle!!!*. European Journal of Pharmacology,* 862, pp. 172657.

PEREGO, C. et al. (2019) Cholesterol metabolism, pancreatic β-cell function and diabetes*. Biochimica Et Biophysica Acta (BBA)-Molecular Basis of Disease,* 1865 (9), pp. 2149-2156.

PHILLIPS, N.B. et al. (2012) Insulin fibrillation and protein design: topological resistance of single-chain analogs to thermal degradation with application to a pump reservoir*. Journal of Diabetes Science and Technology,* 6 (2), pp. 277-288.

PITT, J.P. et al. (2020) Factors Influencing Insulin Absorption Around Exercise in Type 1 Diabetes*. Frontiers in Endocrinology,* 11, pp. 793.

PLOWS, J.F. et al. (2018) The pathophysiology of gestational diabetes mellitus*. International Journal of Molecular Sciences,* 19 (11), pp. 3342.

PODOBNIK, B. et al. (2020) β-cells operate collectively to help maintain glucose homeostasis*. Biophysical Journal,*.

PRAKASH, A. and RAJESWARI, V.D. (2014) Applications of Analytical Instruments in Biotechnology: A Comparative Review*. American Journal of Biochemistry and Molecular Biology,* 4 (1), pp. 1-7.

PRENTICE, P.M. et al. (2019) Reduced size at birth and persisting reductions in adiposity in recent, compared with earlier, cohorts of infants born to mothers with gestational diabetes mellitus*. Diabetologia,* 62 (11), pp. 1977-1987.

PRINCIPI, N. et al. (2017) Type 1 diabetes and viral infections: What is the relationship?*. Journal of Clinical Virology,* 96, pp. 26-31.

QUIANZON, C.C. and CHEIKH, I. (2012) History of insulin*. Journal of Community Hospital Internal Medicine Perspectives,* 2 (2), pp. 18701.

RABIU, M.M. et al. (2020) Prevalence of Diabetes Mellitus and Diabetic Retinopathy in Persons 50 Years and Above in Katsina State Nigeria: A Population-based Cross-sectional Survey*. Ophthalmic Epidemiology,* pp. 1-6.

RAGHAVAN, S. et al. (2019) Diabetes Mellitus–Related All-Cause and Cardiovascular Mortality in a National Cohort of Adults. *Journal of the American Heart Association,* 8 (4), pp. e011295.

RAI, U. et al. (2019) Tetramethylpyrazine prevents diabetes by activating PI3K/Akt/GLUT-4 signalling in animal model of type-2 diabetes. *Life Sciences,* 236, pp. 116836.

RAJASEKAR, M. (2020) Recent Development in Fluorescein derivatives. *Journal of Molecular Structure,* pp. 129085.

RATNER, R.E. et al. (2013) Hypoglycaemia risk with insulin degludec compared with insulin glargine in type 2 and type 1 diabetes: a pre-planned meta-analysis of phase 3 trials. *Diabetes, Obesity and Metabolism,* 15 (2), pp. 175-184.

REA, R., DE ANGELIS, M.G. and BASCHETTI, M.G. (2019) Models for facilitated transport membranes: A review. *Membranes,* 9 (2), pp. 26.

REEVES, K.J. et al. (2012) Evaluation of fluorescent plasma markers for in vivo microscopy of the microcirculation. *Journal of Vascular Research,* 49 (2), pp. 132-143.

REGE, N.K. et al. (2018) Structure-based stabilization of insulin as a therapeutic protein assembly via enhanced aromatic–aromatic interactions. *Journal of Biological Chemistry,* 293 (28), pp. 10895-10910.

REVATHIDEVI, S. and MUNIRAJAN, A.K. (2019) Akt in cancer: mediator and more. In: *Seminars in cancer biology*: Elsevier, pp. 80-91.

RICHTER, E.A. and HARGREAVES, M. (2013) Exercise, GLUT4, and skeletal muscle glucose uptake. *Physiological Reviews,* 93 (3), pp. 993-1017.

RIDDLE, M.C. et al. (2014) New insulin glargine 300 units/mL versus glargine 100 units/mL in people with type 2 diabetes using basal and mealtime insulin: glucose control and hypoglycemia in a 6-month randomized controlled trial (EDITION 1). *Diabetes Care,* 37 (10), pp. 2755-2762.

ROBERTSON, J.L. (2018) The lipid bilayer membrane and its protein constituents. *Journal of General Physiology,* 150 (11), pp. 1472-1483.

RÖDER, P.V. et al. (2016a) Pancreatic regulation of glucose homeostasis. *Experimental & Molecular Medicine,* 48 (3), pp. e219.

RÖDER, P.V. et al. (2016b) Pancreatic regulation of glucose homeostasis. *Experimental & Molecular Medicine,* 48 (3), pp. e219.

RÖDER, P.V. et al. (2016c) Pancreatic regulation of glucose homeostasis. *Experimental & Molecular Medicine,* 48 (3), pp. e219.

RODRÍGUEZ-SÁINZ, C. et al. (2013) Flow Cytometry Analysis with a New FITC-Conjugated Monoclonal Antibody-3E12 for HLA-B*57:01 Rapid Screening in Prevention of Abacavir Hypersensitivity in HIV-1–Infected Patients*. HIV Clinical Trials,* 14 (4), pp. 160-164.

ROMA, L.P. and JONAS, J. (2020) Nutrient metabolism, subcellular redox state, and oxidative stress in pancreatic islets and β-cells*. Journal of Molecular Biology,* 432 (5), pp. 1461-1493.

RONCERO-RAMOS, I. et al. (2018) Alpha cell function interacts with diet to modulate prediabetes and Type 2 diabetes*. The Journal of Nutritional Biochemistry,* 62, pp. 247-256.

RORSMAN, P. and ASHCROFT, F.M. (2018) Pancreatic β-cell electrical activity and insulin secretion: of mice and men*. Physiological Reviews,* 98 (1), pp. 117-214.

RORSMAN, P. and BRAUN, M. (2013) Regulation of insulin secretion in human pancreatic islets*. Annual Review of Physiology,* 75, pp. 155-179.

ROSENSTOCK, J. et al. (2013) Better glycemic control and weight loss with the novel long-acting basal insulin LY2605541 compared with insulin glargine in type 1 diabetes: a randomized, crossover study*. Diabetes Care,* 36 (3), pp. 522-528.

SABNIS, R.W. (2015) *Handbook of fluorescent dyes and probes*. 1st ed. New Jersey: John Wiley & Sons.

SABOURI, S. et al. (2020) Human herpesvirus-6 is present at higher levels in the pancreatic tissues of donors with type 1 diabetes*. Journal of Autoimmunity,* 107, pp. 102378.

SAHOO, H. (2012) Fluorescent labeling techniques in biomolecules: a flashback*. Rsc Advances,* 2 (18), pp. 7017-7029.

SALARI, M. et al. (2019) Development & characterization of fluorescently tagged nanocellulose for nanotoxicological studies*. Environmental Science: Nano,* 6 (5), pp. 1516-1526.

SALEH, E. et al. (2018) Learning ensemble classifiers for diabetic retinopathy assessment*. Artificial Intelligence in Medicine,* 85, pp. 50-63.

SALT, I.P. et al. (2003) High glucose inhibits insulin-stimulated nitric oxide production without reducing endothelial nitric-oxide synthase Ser1177 phosphorylation in human aortic endothelial cells*. Journal of Biological Chemistry,* 278 (21), pp. 18791-18797.

SAMPATH KUMAR, A. et al. (2017) Exercise and insulin resistance in type 2 diabetes mellitus: A systematic review and meta-analysis*. Journal of Environmental Sciences (China),* (10), pp. 125-126.

SANO, H. et al. (2003) Insulin-stimulated phosphorylation of a Rab GTPase-activating protein regulates GLUT4 translocation. *Journal of Biological Chemistry,* 278 (17), pp. 14599-14602.

SANO, K. et al. (2012) In vivo breast cancer characterization imaging using two monoclonal antibodies activatably labeled with near infrared fluorophores. *Breast Cancer Research,* 14 (2), pp. R61.

SANTOS, M.C. et al. (2020) Molecular fluorescence spectroscopy with multi-way analysis techniques detects spectral variations distinguishing uninfected serum versus dengue or chikungunya viral infected samples. *Scientific Reports,* 10 (1), pp. 1-13.

SAVJANI, K.T., GAJJAR, A.K. and SAVJANI, J.K. (2012) Drug solubility: importance and enhancement techniques. *ISRN Pharmaceutics,* 2012.

SAYEM, A. et al. (2018) Action of phytochemicals on insulin signaling pathways accelerating glucose transporter (GLUT4) protein translocation. *Molecules,* 23 (2), pp. 258.

SCAPIN, G. et al. (2018) Structure of the insulin receptor–insulin complex by single-particle cryo-EM analysis. *Nature,* 556 (7699), pp. 122-125.

SCHAVEMAKER, P.E., BOERSMA, A.J. and POOLMAN, B. (2018) How important is protein diffusion in prokaryotes?. *Frontiers in Molecular Biosciences,* 5, pp. 93.

SEIDU, S. et al. (2020) A disease state approach to the pharmacological management of Type 2 diabetes in primary care: A position statement by Primary Care Diabetes Europe. *Primary Care Diabetes,*.

SHAH, D. et al. (2019) FITC labeling of human insulin and transport of FITC-insulin conjugates through MDCK cell monolayer. *Journal of Pharmaceutical Analysis,*.

SHAH, R.B. et al. (2016) Insulin delivery methods: Past, present and future. *International Journal of Pharmaceutical Investigation,* 6 (1), pp. 1.

SHARMA, A.K. et al. (2019) Insulin analogs: Glimpse on contemporary facts and future prospective. *Life Sciences,* 219, pp. 90-99.

SHIMODA, S. et al. (2016) A 1-year, prospective, observational study of Japanese outpatients with type 1 and type 2 diabetes switching from insulin glargine or detemir to insulin degludec in basal–bolus insulin therapy (Kumamoto Insulin Degludec Observational study). *Journal of Diabetes Investigation,* 7 (5), pp. 703-710.

SHINODA, H., SHANNON, M. and NAGAI, T. (2018) Fluorescent proteins for investigating biological events in acidic environments. *International Journal of Molecular Sciences,* 19 (6), pp. 1548.

SHIRAMOTO, M. et al. (2020) Ultra-Rapid Lispro results in accelerated insulin lispro absorption and faster early insulin action in comparison with Humalog® in Japanese patients with type 1 diabetes. *Journal of Diabetes Investigation,* 11 (3), pp. 672-680.

SIMS, E.K. and DIMEGLIO, L.A. (2019) Cause or effect? A review of clinical data demonstrating beta cell dysfunction prior to the clinical onset of type 1 diabetes. *Molecular Metabolism,* 27, pp. S129-S138.

SKELIN KLEMEN, M. et al. (2017) The triggering pathway to insulin secretion: functional similarities and differences between the human and the mouse β cells and their translational relevance. *Islets,* 9 (6), pp. 109-139.

SON, M. and WU, J. (2019) Egg white hydrolysate and peptide reverse insulin resistance associated with tumor necrosis factor-α (TNF-α) stimulated mitogen-activated protein kinase (MAPK) pathway in skeletal muscle cells. *European Journal of Nutrition,* 58 (5), pp. 1961-1969.

STACEY, T. et al. (2019) Gestational diabetes and the risk of late stillbirth: a case–control study from England, UK. *BJOG: An International Journal of Obstetrics & Gynaecology,* 126 (8), pp. 973-982.

STANDL, E. and OWEN, D.R. (2016a) New long-acting basal insulins: does benefit outweigh cost?. *Diabetes Care,* 39 (Supplement 2), pp. S172-S179.

STANDL, E. and OWEN, D.R. (2016b) New long-acting basal insulins: does benefit outweigh cost?. *Diabetes Care,* 39 (Supplement 2), pp. S172-S179.

STANDL, E. and OWEN, D.R. (2016c) New long-acting basal insulins: does benefit outweigh cost?. *Diabetes Care,* 39 (Supplement 2), pp. S172-S179.

STEWART, A.M. et al. (2017) Development of a biorelevant, material-sparing membrane flux test for rapid screening of bioavailability-enhancing drug product formulations. *Molecular Pharmaceutics,* 14 (6), pp. 2032-2046.

STÖCKLI, J., FAZAKERLEY, D.J. and JAMES, D.E. (2011) GLUT4 exocytosis. *Journal of Cell Science,* 124 (24), pp. 4147-4159.

STODDARD, A. and ROLLAND, V. (2019) I see the light! Fluorescent proteins suitable for cell wall/apoplast targeting in Nicotiana benthamiana leaves. *Plant Direct,* 3 (1), pp. e00112.

STREMBITSKA, A. et al. (2018) A769662 inhibits insulin-stimulated Akt activation in human macrovascular endothelial cells independent of AMP-activated protein kinase. *International Journal of Molecular Sciences,* 19 (12), pp. 3886.

STRINGER, D.M., ZAHRADKA, P. and TAYLOR, C.G. (2015) Glucose transporters: cellular links to hyperglycemia in insulin resistance and diabetes. *Nutrition Reviews,* 73 (3), pp. 140-154.

STUBBS, D.J., LEVY, N. and DHATARIYA, K. (2017) Diabetes medication pharmacology*. Bja Education,*.

SUBRAMANIAN, S. et al. (2016) The management of type 1 diabetes. In: *Endotext [Internet]*: MDText. com, Inc.

SUDHAKAR, S. et al. (2020) Biodistribution and pharmacokinetics of thiolated chitosan nanoparticles for oral delivery of insulin in vivo*. International Journal of Biological Macromolecules,* 150, pp. 281-288.

SUGIYAMA, M.G., FAIRN, G.D. and ANTONESCU, C.N. (2019) Akt-ing up just about everywhere: compartment-specific Akt activation and function in receptor tyrosine kinase signaling*. Frontiers in Cell and Developmental Biology,* 7, pp. 70.

SUN, W. et al. (2015) Transdermal delivery of functional collagen via polyvinylpyrrolidone microneedles*. Annals of Biomedical Engineering,* 43 (12), pp. 2978-2990.

SUZUKI, Y. and YOKOYAMA, K. (2015) Development of functional fluorescent molecular probes for the detection of biological substances*. Biosensors,* 5 (2), pp. 337-363.

SWEETING, A.N. et al. (2019) A novel early pregnancy risk prediction model for gestational diabetes mellitus*. Fetal Diagnosis and Therapy,* 45 (2), pp. 76-84.

ŚWIDERSKA, E. et al. (2018) Role of PI3K/AKT Pathway in Insulin-Mediated Glucose Uptake. In: *Glucose Transport*: IntechOpen.

SWINNEN, S.G. et al. (2010) A 24-week, randomized, treat-to-target trial comparing initiation of insulin glargine once-daily with insulin detemir twice-daily in patients with type 2 diabetes inadequately controlled on oral glucose-lowering drugs*. Diabetes Care,* 33 (6), pp. 1176-1178.

SYLOW, L. et al. (2016) Rac1 governs exercise-stimulated glucose uptake in skeletal muscle through regulation of GLUT4 translocation in mice*. The Journal of Physiology,* 594 (17), pp. 4997-5008.

SZABLEWSKI, L. (2011) Glucose homeostasis-mechanism and defects*. Diabetes-Damages and Treatments,* 2.

SZABLEWSKI, L. and SULIMA, A. (2017) The structural and functional changes of blood cells and molecular components in diabetes mellitus*. Biological Chemistry,* 398 (4), pp. 411-423.

SZMUILOWICZ, E.D., JOSEFSON, J.L. and METZGER, B.E. (2019) Gestational diabetes mellitus*. Endocrinology and Metabolism Clinics,* 48 (3), pp. 479-493.

TAMBASCIA, M.A. and ELIASCHEWITZ, F.G. (2015) Degludec: the new ultra-long insulin analogue*. Diabetology & Metabolic Syndrome,* 7 (1), pp. 57.

TAN, S. et al. (2012) The Rab GTPase-activating protein TBC1D4/AS160 contains an atypical phosphotyrosine-binding domain that interacts with plasma membrane phospholipids to facilitate GLUT4 trafficking in adipocytes. *Molecular and Cellular Biology,* 32 (24), pp. 4946-4959.

TAN, S.Y. et al. (2019) Type 1 and 2 diabetes mellitus: a review on current treatment approach and gene therapy as potential intervention. *Diabetes & Metabolic Syndrome: Clinical Research & Reviews,* 13 (1), pp. 364-372.

TANNA, S. et al. (2006) Glucose-responsive UV polymerised dextran–concanavalin A acrylic derivatised mixtures for closed-loop insulin delivery. *Biomaterials,* 27 (8), pp. 1586-1597.

TAVERNA, M.J. (2018) Epidemiology of Diabetes. In: *Dermatology and Diabetes*: Springer, pp. 1-6.

TAYLOR, M.J. et al. (2016) Closed-loop glycaemic control using an implantable artificial pancreas in diabetic domestic pig (Sus scrofa domesticus). *International Journal of Pharmaceutics,* 500 (1-2), pp. 371-378.

TAYLOR, M.J., SAHOTA, T.S. and CHAUHAN, K.P. (2019) Glucose lowering strategies with insulin. *The British Journal of Diabetes,* 19 (2), pp. 124-130.

TAYLOR, M.J., TANNA, S. and SAHOTA, T. (2010) In vivo study of a polymeric glucose-sensitive insulin delivery system using a rat model. *Journal of Pharmaceutical Sciences,* 99 (10), pp. 4215-4227.

TESSARI, P. et al. (2010) Nitric oxide synthesis is reduced in subjects with type 2 diabetes and nephropathy. *Diabetes,* 59 (9), pp. 2152-2159.

THANOS, S., VIDAL-SANZ, M. and AGUAYO, A.J. (1987) The use of rhodamine-B-isothiocyanate (RITC) as an anterograde and retrograde tracer in the adult rat visual system. *Brain Research,* 406 (1-2), pp. 317-321.

THORBALL, N. (1981) FITC-dextran tracers in microcirculatory and permeability studies using combined fluorescence stereo microscopy, fluorescence light microscopy and electron microscopy. *Histochemistry,* 71 (2), pp. 209-233.

THORN, K. (2017) Genetically encoded fluorescent tags. *Molecular Biology of the Cell,* 28 (7), pp. 848-857.

TOKARZ, V.L., MACDONALD, P.E. and KLIP, A. (2018) The cell biology of systemic insulin function. *Journal of Cell Biology,* 217 (7), pp. 2273-2289.

TONA, R.M. et al. (2019) Microfluidic droplet liquid reactors for active pharmaceutical ingredient crystallization by diffusion controlled solvent extraction. *Lab on a Chip,* 19 (12), pp. 2127-2137.

TOSELAND, C. (2013) Fluorescent labeling and modification of proteins. *Journal of Chemical Biology,* 6 (3), pp. 85-95.

TRIPATHI, N. (2013) Cationic and anionic dye adsorption by agricultural solid wastes: A comprehensive review*. Journal of Applied Chemistry,* 5, pp. 91-108.

TUNDUGURU, R. and THURMOND, D.C. (2017) Promoting glucose transporter-4 vesicle trafficking along cytoskeletal tracks: PAK-Ing them out*. Frontiers in Endocrinology,* 8, pp. 329.

UCHIKAWA, E. et al. (2019) Activation mechanism of the insulin receptor revealed by cryo-EM structure of the fully liganded receptor–ligand complex*. Elife,* 8, pp. e48630.

UCHIO, T. et al. (1999) Site-specific insulin conjugates with enhanced stability and extended action profile*. Advanced Drug Delivery Reviews,* 35 (2-3), pp. 289-306.

UHL, C.G. and LIU, Y. (2019) Microfluidic device for expedited tumor growth towards drug evaluation*. Lab on a Chip,* 19 (8), pp. 1458-1470.

URIARTE, M. et al. (2019) Evidence supporting a role for the blood-cerebrospinal fluid barrier transporting circulating ghrelin into the brain*. Molecular Neurobiology,* 56 (6), pp. 4120-4134.

VAJO, Z., FAWCETT, J. and DUCKWORTH, W.C. (2001) Recombinant DNA technology in the treatment of diabetes: insulin analogs*. Endocrine Reviews,* 22 (5), pp. 706-717.

VANDANA SAINI (2010) Molecular mechanisms of insulin resistance in type 2 diabetes mellitus*. World Journal of Diabetes,* 1 (3), pp. 68-75.

VARGAS, E. and CARRILLO SEPULVEDA, M.A. (2019) Biochemistry, Insulin Metabolic Effects. In: *StatPearls*Treasure Island (FL): StatPearls Publishing.

VARGAS, E., PODDER, V. and SEPULVEDA, M.A.C. (2019) Physiology, Glucose Transporter Type 4 (GLUT4). In: *StatPearls [Internet]*: StatPearls Publishing.

VASILJEVIĆ, J. et al. (2020) The making of insulin in health and disease*. Diabetologia,* 63 (10), pp. 1981-1989.

VAZIRANI, R.P. et al. (2016) Disruption of adipose Rab10-dependent insulin signaling causes hepatic insulin resistance*. Diabetes,* 65 (6), pp. 1577-1589.

VECCHIO, I. et al. (2018) The Discovery of Insulin: An Important Milestone in the History of Medicine*. Frontiers in Endocrinology,* 9, pp. 613.

VERMA, N. et al. (2020) Diabetic microcirculatory disturbances and pathologic erythropoiesis are provoked by deposition of amyloid-forming amylin in red blood cells and capillaries*. Kidney International,* 97 (1), pp. 143-155.

VERMA, S., SHARMA, S. and RANGARI, P. (2019) Association of Birth-Weight, Obesity and Family History in the Development of Latent Autoimmune Diabetes in Adults (LADA) and Type 2 Diabetes Mellitus*. Academia Journal of Medicine,* 2 (2).

VILLAMENA, F.A. (2017) Chapter 4 - Fluorescence Technique. In: VILLAMENA, F.A. (ed.)*Reactive Species Detection in Biology*Boston: Elsevier, pp. 87-162.

VISARIA, J. et al. (2020) Healthcare Costs of Diabetes and Microvascular and Macrovascular Disease in Individuals with Incident Type 2 Diabetes Mellitus: A Ten-Year Longitudinal Study*. ClinicoEconomics and Outcomes Research: CEOR,* 12, pp. 423.

WAKANKAR, A.A. et al. (2010) Physicochemical stability of the antibody− drug conjugate trastuzumab-DM1: changes due to modification and conjugation processes*. Bioconjugate Chemistry,* 21 (9), pp. 1588-1595.

WALKER, E., FLANNERY, O. and MACKILLOP, L. (2020) Gestational diabetes and progression to type two diabetes mellitus: missed opportunities of follow up and prevention?*. Primary Care Diabetes,*.

WALSH, L.K. et al. (2019) Increased endothelial shear stress improves insulin-stimulated vasodilatation in skeletal muscle*. The Journal of Physiology,* 597 (1), pp. 57-69.

WANG, J., TABATA, Y. and MORIMOTO, K. (2006) Aminated gelatin microspheres as a nasal delivery system for peptide drugs: evaluation of in vitro release and in vivo insulin absorption in rats*. Journal of Controlled Release,* 113 (1), pp. 31-37.

WANG, L. et al. (2019) Hybrid rhodamine fluorophores in the visible/NIR region for biological imaging*. Angewandte Chemie International Edition,* 58 (40), pp. 14026-14043.

WANG, P. et al. (2017) A novel DCM-NBD conjugate fluorescent probe for discrimination of Cys/Hcy from GSH and its bioimaging applications in living cells and animals*. Sensors and Actuators B: Chemical,* 245, pp. 297-304.

WARRIER, S. and KHARKAR, P.S. (2014) Fluorescent probes for biomedical applications (2009–2014)*. Pharmaceutical Patent Analyst,* 3 (5), pp. 543-560.

WASIK, A.A. and LEHTONEN, S. (2018) Glucose transporters in diabetic kidney disease—friends or foes?*. Frontiers in Endocrinology,* 9, pp. 155.

WASKO, J. et al. (2020) Human Serum Albumin Binds Native Insulin and Aggregable Insulin Fragments and Inhibits Their Aggregation*. Biomolecules,* 10 (10), pp. 1366.

WATSON, R.T. and PESSIN, J.E. (2007) GLUT4 translocation: the last 200 nanometers*. Cellular Signalling,* 19 (11), pp. 2209-2217.

WEIR, G.C., GAGLIA, J. and BONNER-WEIR, S. (2020) Inadequate β-cell mass is essential for the pathogenesis of type 2 diabetes*. The Lancet Diabetes & Endocrinology,* 8 (3), pp. 249-256.

WEIS, F. et al. (2018) The signalling conformation of the insulin receptor ectodomain. *Nature Communications,* 9 (1), pp. 1-10.

WEISS, M.A. (2009) The structure and function of insulin: decoding the TR transition. *Vitamins & Hormones,* 80, pp. 33-49.

WEISS, M.A. and LAWRENCE, M.C. (2018) A thing of beauty: Structure and function of insulin's “aromatic triplet”. *Diabetes, Obesity and Metabolism,* 20, pp. 51-63.

WEISS, M., STEINER, D.F. and PHILIPSON, L.H. (2014) Insulin biosynthesis, secretion, structure, and structure-activity relationships. In: *Endotext [Internet]*: MDText. com, Inc.

WERNER, C.T. et al. (2019) Circuit mechanisms of neurodegenerative diseases: a new frontier with miniature fluorescence microscopy. *Frontiers in Neuroscience,* 13.

WERNROTH, M. et al. (2020) Early Childhood Antibiotic Treatment for Otitis Media and Other Respiratory Tract Infections Is Associated With Risk of Type 1 Diabetes: A Nationwide Register-Based Study With Sibling Analysis. *Diabetes Care,* 43 (5), pp. 991-999.

WESTERMEIER, F. et al. (2019) Gluconeogenic Enzymes in β-Cells: Pharmacological Targets for Improving Insulin Secretion. *Trends in Endocrinology & Metabolism,* 30 (8), pp. 520-531.

WHICHER, C.A., O’NEILL, S. and HOLT, R.G. (2020) Diabetes in the UK: 2019. *Diabetic Medicine,* 37 (2), pp. 242-247.

WHITE, N.S. and ERRINGTON, R.J. (2005) Fluorescence techniques for drug delivery research: theory and practice. *Advanced Drug Delivery Reviews,* 57 (1), pp. 17-42.

WILLIAMS, I.M. et al. (2018) Insulin exits skeletal muscle capillaries by fluid-phase transport. *The Journal of Clinical Investigation,* 128 (2), pp. 699-714.

WOLLMER, A. et al. (1987) Phenol-promoted structural transformation of insulin in solution. *Biological Chemistry Hoppe-Seyler,* 368 (2), pp. 903-912.

WRIGHT JR, J.R. (2020) Essential contributions of pathologists and laboratory physicians leading to the discovery of insulin. *Archives of Pathology & Laboratory Medicine,* 144 (7), pp. 894-904.

WU, C. et al. (2020) One injection for one-week controlled release: In vitro and in vivo assessment of ultrasound-triggered drug release from injectable thermoresponsive biocompatible hydrogels. *Ultrasonics Sonochemistry,* 62, pp. 104875.

XIAO, Y. et al. (2017) Long-term effect of biomineralized insulin nanoparticles on type 2 diabetes treatment. *Theranostics,* 7 (17), pp. 4301.

XIONG, X. et al. (2020) Novel four-disulfide insulin analog with high aggregation stability and potency. *Chemical Science,* 11 (1), pp. 195-200.

XU, Y. et al. (2018) How ligand binds to the type 1 insulin-like growth factor receptor. *Nature Communications,* 9 (1), pp. 1-13.

YAN, F. et al. (2017) Fluorescein applications as fluorescent probes for the detection of analytes. *TrAC Trends in Analytical Chemistry,* 97, pp. 15-35.

YANG, O. et al. (2016) Atorvastatin ameliorates endothelium-specific insulin resistance induced by high glucose combined with high insulin. *Molecular Medicine Reports,* 14 (3), pp. 2791-2798.

YANG, P. et al. (2019) Advanced glycation end products: potential mechanism and therapeutic target in cardiovascular complications under diabetes. *Oxidative Medicine and Cellular Longevity,* 2019.

YANG, X. et al. (2017) Immunogenicity of insulin-producing cells derived from human umbilical cord mesenchymal stem cells. *Experimental and Therapeutic Medicine,* 13 (4), pp. 1456-1464.

YARIBEYGI, H., ATKIN, S.L. and SAHEBKAR, A. (2019) A review of the molecular mechanisms of hyperglycemia-induced free radical generation leading to oxidative stress. *Journal of Cellular Physiology,* 234 (2), pp. 1300-1312.

YARIBEYGI, H. et al. (2019a) Insulin resistance: Review of the underlying molecular mechanisms. *Journal of Cellular Physiology,* 234 (6), pp. 8152-8161.

YARIBEYGI, H. et al. (2019b) Insulin resistance: Review of the underlying molecular mechanisms. *Journal of Cellular Physiology,* 234 (6), pp. 8152-8161.

YAZDANI, S. et al. (2019) Endothelial cell barriers: transport of molecules between blood and tissues. *Traffic,* 20 (6), pp. 390-403.

YE, L. et al. (2017) Structure and dynamics of the insulin receptor: implications for receptor activation and drug discovery. *Drug Discovery Today,* 22 (7), pp. 1092-1102.

YEO, K.B. et al. (2016) Highly effective detection of inflamed cells using a modified bradykinin ligand labeled with FITC fluorescence. *Enzyme and Microbial Technology,* 82, pp. 191-196.

YIN, R. et al. (2019) Concanavalin A-sugar affinity-based system: Binding interactions, principle of glucose-responsiveness, and modulated insulin release for diabetes care. *International Journal of Biological Macromolecules,* 124, pp. 724-732.

YUE, Y. et al. (2019) Functional synthetic probes for selective targeting and multi-analyte detection and imaging. *Chemical Society Reviews,* 48 (15), pp. 4155-4177.

ZAHARIEVA, D.P. et al. (2019) Lag time remains with newer real-time continuous glucose monitoring technology during aerobic exercise in adults living with type 1 diabetes. *Diabetes Technology & Therapeutics,* 21 (6), pp. 313-321.

ZATTERALE, F. et al. (2020) Chronic adipose tissue inflammation linking obesity to insulin resistance and type 2 diabetes. *Frontiers in Physiology,* 10, pp. 1607.

ZAVVAR, T. et al. (2020) Synthesis of multimodal polymersomes for targeted drug delivery and MR/fluorescence imaging in metastatic breast cancer model. *International Journal of Pharmaceutics,* 578, pp. 119091.

ZENG, G. et al. (2000) Roles for insulin receptor, PI3-kinase, and Akt in insulin-signaling pathways related to production of nitric oxide in human vascular endothelial cells. *Circulation,* 101 (13), pp. 1539-1545.

ZHANG, R. et al. (2019) Improving cellular uptake of therapeutic entities through interaction with components of cell membrane. *Drug Delivery,* 26 (1), pp. 328-342.

ZHANG, X., ZHANG, J. and LIU, L. (2014) Fluorescence properties of twenty fluorescein derivatives: lifetime, quantum yield, absorption and emission spectra. *Journal of Fluorescence,* 24 (3), pp. 819-826.

ZHANG, Y. et al. (2018) Advances in transdermal insulin delivery. *Advanced Drug Delivery Reviews.*

ZHAO, B. and ZHENG, Z. (2017) Insulin growth factor 1 protects neural stem cells against apoptosis induced by hypoxia through Akt/mitogen-activated protein kinase/extracellular signal-regulated kinase (Akt/MAPK/ERK) pathway in hypoxia-ishchemic encephalopathy. *Medical Science Monitor: International Medical Journal of Experimental and Clinical Research,* 23, pp. 1872.

ZHENG, H. et al. (2013) Advances in modifying fluorescein and rhodamine fluorophores as fluorescent chemosensors. *Chemical Communications,* 49 (5), pp. 429-447.

ZHOU, C. et al. (2012) The preparation of a complex of insulin–phospholipids and their interaction mechanism. *Journal of Peptide Science,* 18 (9), pp. 541-548.

ZHOU, J. et al. (2020) Fluorescent Diagnostic Probes in Neurodegenerative Diseases. *Advanced Materials,* pp. 2001945.

ZHU, L., TITONE, R. and ROBERTSON, D.M. (2019) The impact of hyperglycemia on the corneal epithelium: molecular mechanisms and insight. *The Ocular Surface,* 17 (4), pp. 644-654.

ZIMMERMAN, C., FORLENZA, G. and SCHATZ, D. (2020) The Discovery and Structure of Human Insulin. *Pediatric Endocrinology Reviews: PER,* 17 (Suppl 1), pp. 131-137.

Appendix 1-Chromatogram data and Mass spectra of chapter 3

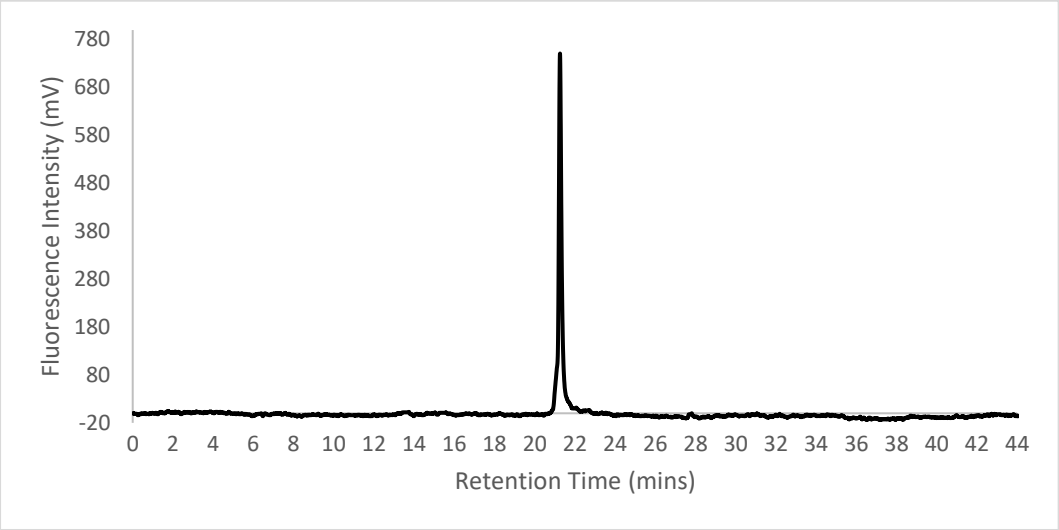

Figure A1 1: Fluorescence chromatogram for 100Unit/mL MonoA1 conjugate isolated from the FITC-insulin synthesis of 1h reaction at pH8.4 and 2:1 molar ratio (FITC/insulin) showing a single Mono peak at a RT of 21.3min

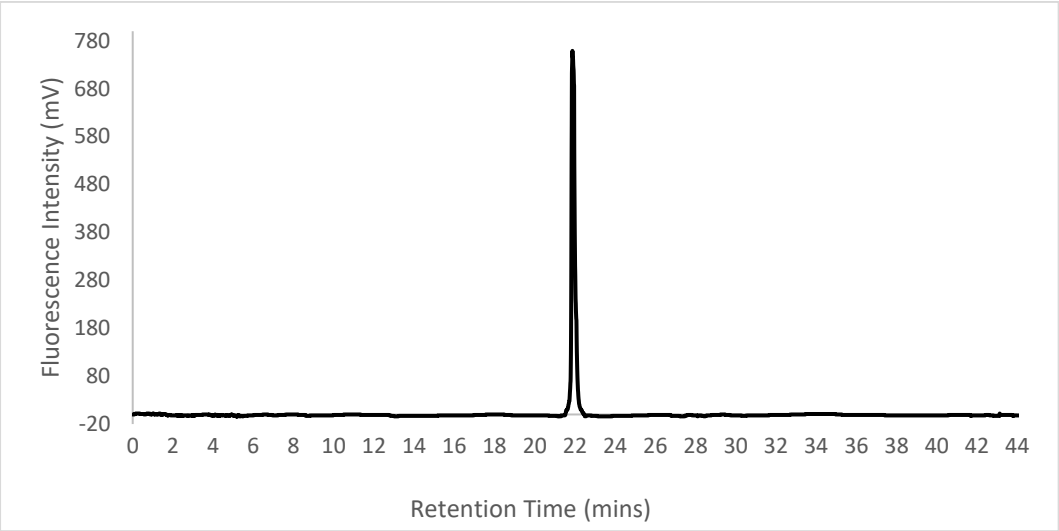

Figure A1 2: Fluorescence chromatogram for 100Unit/mL MonoB1 conjugate isolated from the FITC-insulin synthesis of 18h reaction at pH7 and 2:1 molar ratio (FITC/insulin) showing a single Mono peak at a RT of 21.9min

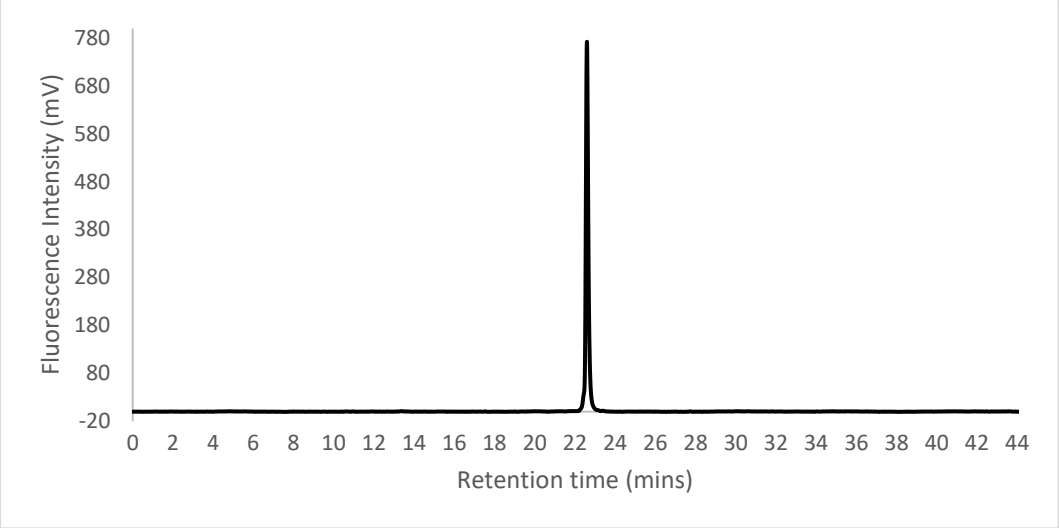

Figure A1 3: Fluorescence chromatogram for 100Unit/mL Di conjugate isolated from the FITC-insulin synthesis of 72h reaction at pH7 and 3:1 molar ratio (FITC/insulin) showing a single Di peak at a RT of 22.6min.

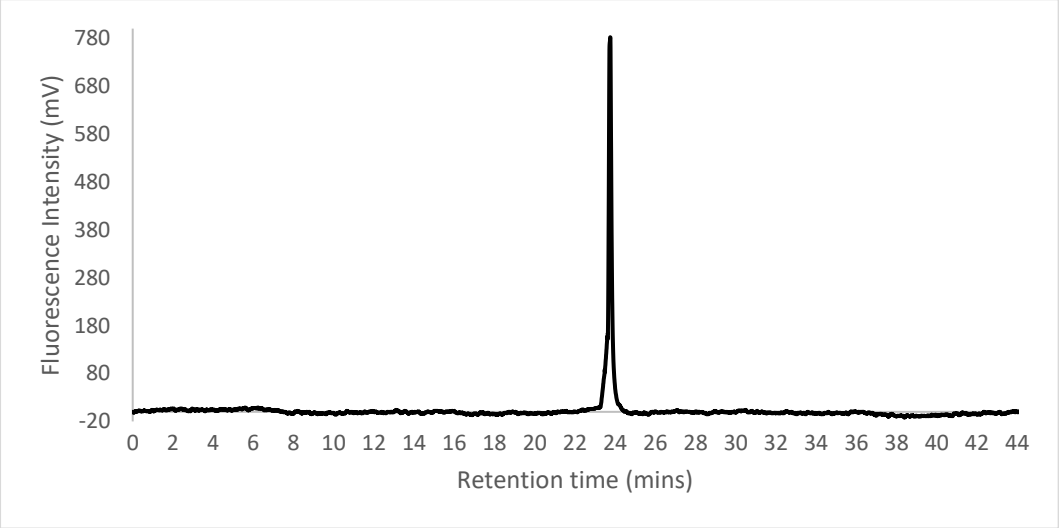

Figure A1 4: Fluorescence chromatogram for 100Unit/mL Tri conjugate isolated from the FITC-insulin synthesis of 72h reaction at pH7 and 3:1 molar ratio (FITC/insulin) showing a single Tri peak at a RT of 23.7min.

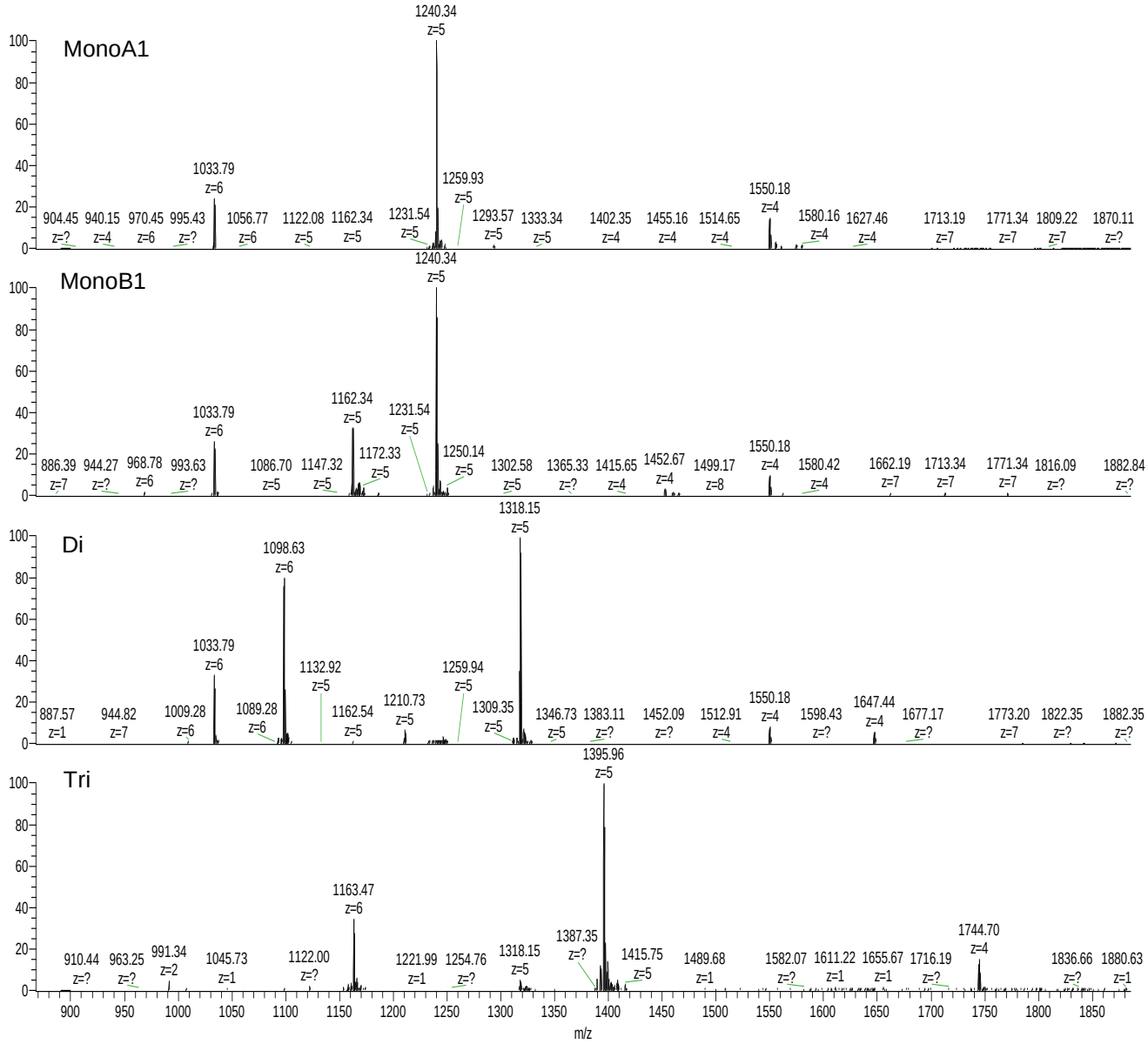

Figure A1 5: Mass spectra for MonoA1, MonoB1, Di and Tri conjugates isolated for the biological activity test (peaks present in raw data at m/z 1240.34 z5 corresponding to mono-labelled conjugates, at m/z 1318.15 z5 corresponding to di-labelled conjugates and at m/z 1395.96 z5 corresponding to tri-labelled conjugates.

Appendix 2-Chromatogram data for chapter 4

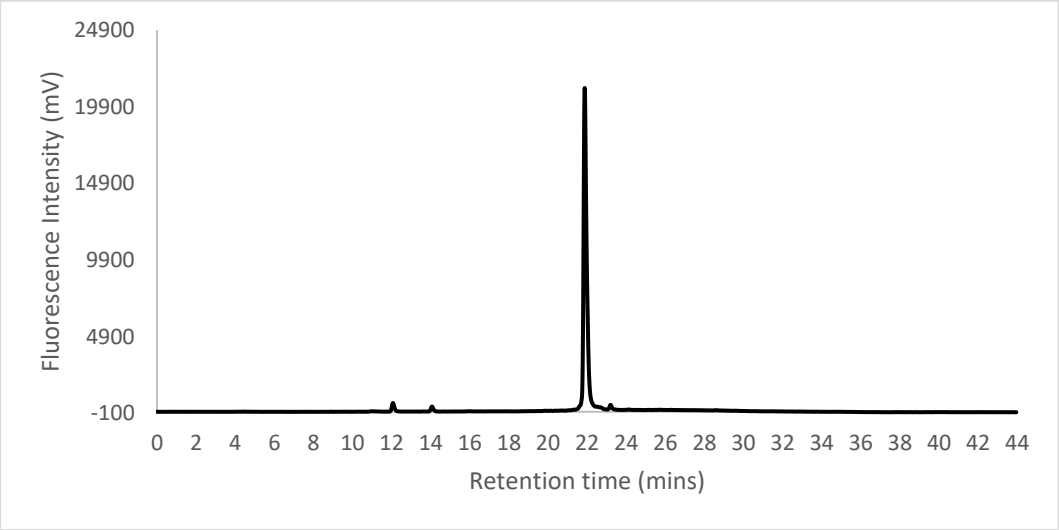

Figure A2 1: Fluorescence chromatogram of FITC-insulin conjugates formulated in water after 5 months storage at 2-8°C showing the begin loss in original Mono conjugate at a RT of 21.9min (95% AUP) and the appearance of Di conjugate at a RT of 22.6min (1.4%AUP) as well as free FITC peaks (3.6%AUP) at RT of 12min and 14min, none of which was detected in the original Mono conjugates

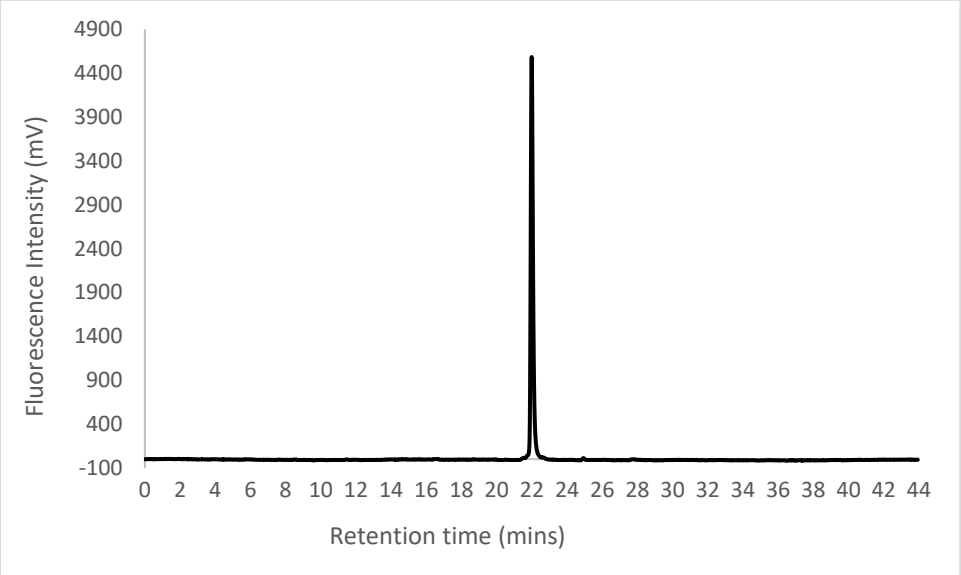

Figure A2 2: Fluorescence chromatogram of FITC-insulin conjugates formulated in diluting fluid after 6 months storage at 2-8°C showing the maintaining of the original Mono conjugate at a RT of 21.9min (100% AUP)

Abstract titled “Fluorescently labelled insulin for specialised drug delivery” for **poster presentation** at the Royal Society of Biology Postgraduate Poster Symposium 2019

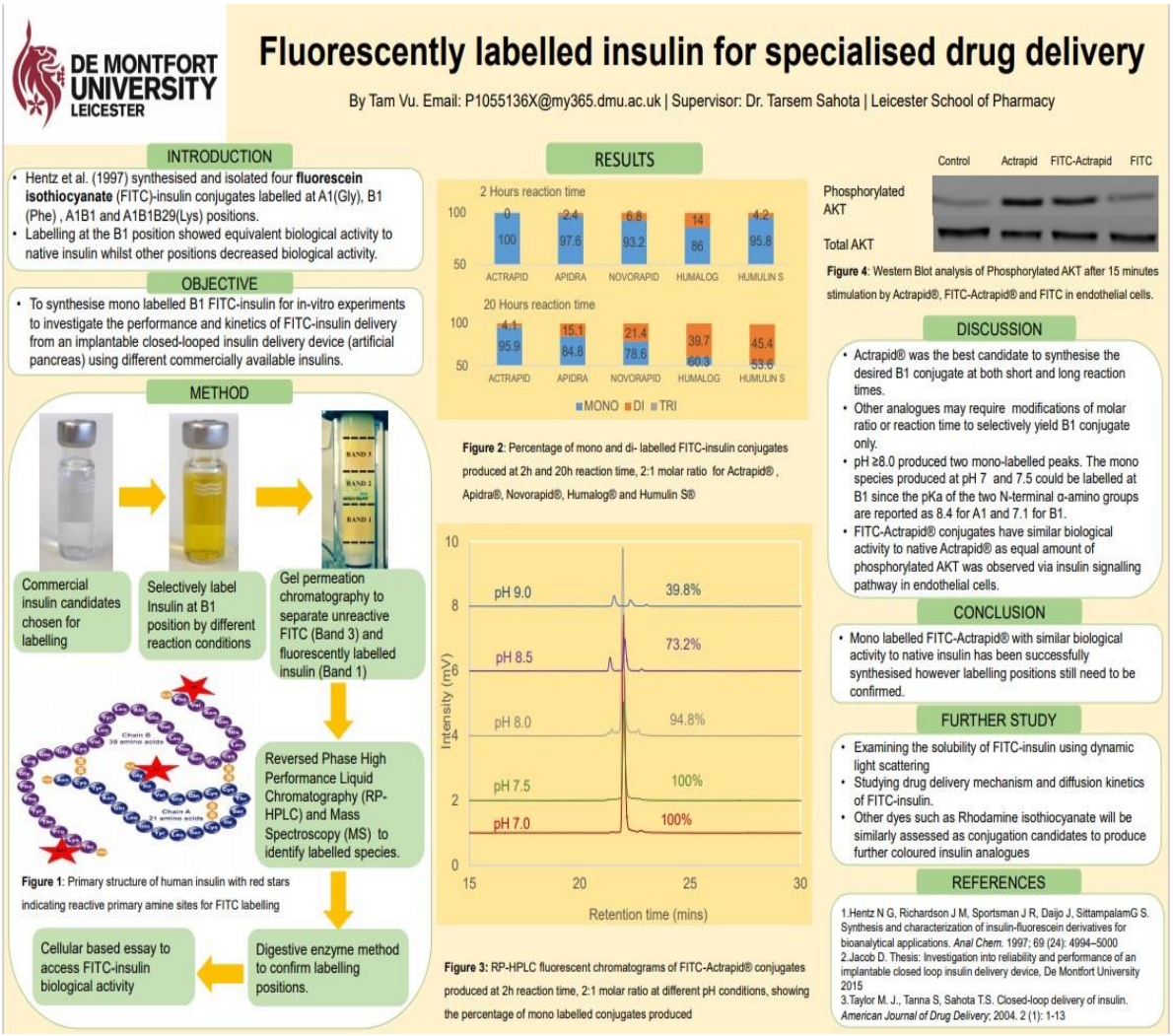

Paper titled "Synthesis and identification of mono-labelled FITC-insulin conjugate" submitted for peer review

Synthesis and identification of biologically active mono-labelled FITC-insulin conjugate

Tam Vu[1], M. Joan Taylor[1], Harprit Singh[2], Jay Bilimoria[2], Andrew Bottrill[3] and Tarsem Sahota[1*]

[1]Leicester Institute for Pharmaceutical Innovation, Faculty of Health and Life Sciences, De Montfort University, The Gateway, Leicester, LE1 9BH, United Kingdom

[2]Allied Health Sciences, Faculty of Health and Life Sciences, De Montfort University, The Gateway, Leicester, LE1 9BH, United Kingdom

[3]Proteomics, School of Life Sciences, University of Warwick, Gibbet Hill Road, Coventry, CV4 7AL; United Kingdom

Correspondence should be addressed to:

*Tarsem Sahota, Leicester Institute for Pharmaceutical Innovation, Faculty of Health and Life Sciences, De Montfort University, The Gateway, Leicester, LE1 9BH, UK.

Tel: +44 116 250 551551 (ext 6972).
E-mail: ssahota@dmu.ac.uk.

Abstract

Actrapid® was labelled with fluorescein isothiocyanate (FITC) and the synthesised conjugate was identified using reverse phase high performance liquid chromatography (RP-HPLC). Mono-labelled FITC-insulin conjugate was successfully produced with labelling at the B1 chain on insulin using a molar ratio of 2:1 (FITC: insulin) with short reaction times (up to 18h) however some trace amounts of unlabelled insulin was also present. As the reaction time was increased over 20h, no unlabelled insulin was present but 5% of FITC-insulin conjugate was di labelled (diA1B1). The quantities switch from mono-labelled to di-labelled FITC-insulin conjugate between 19h to 20h reaction time at pH>8.The exact labelling position of mono-labelled FITC- insulin was confirmed to be at the B1 amino acid by electrospray mass spectroscopy. The biological activity of four FITC-insulin conjugates in comparison to native insulin was assessed in HUVEC and C2C12 skeletal muscle cells via the insulin signalling pathway by examining the levels of pAKT and cell surface GLUT4. There was no significant difference in the GLUT4 cell surface level observed for monoB1 produced in-house compared to native insulin. Mono-labelled FITC-insulin at the B1 position showed similar biological activity as native insulin and can potentially be used for future biomedical applications.

Keywords

Insulin, Fluorescent labelling, FITC-labelled insulin, Biologically active FITC-insulin, FITC